Coupled Boussinesq equations and nonlinear waves in layered waveguides

by

Kieron Moore

A Doctoral Thesis

Submitted in partial fulfilment of the requirements for the award of
Doctor of Philosophy of Loughborough University

August 2013

Certificate of originality

This is to certify that I am responsible for the work submitted in this thesis, that the original work is my own except as specified in acknowledgments or in footnotes, and that neither the thesis nor the original work contained therein has been submitted to this or any other institution for a degree.

..... (Signed)

..... (Date)

Loughborough University

Abstract

There exists substantial applications motivating the study of nonlinear longitudinal wave propagation in layered (or laminated) elastic waveguides, in particular within areas related to non-destructive testing, where there is a demand to understand, reinforce, and improve deformation properties of such structures. It has been shown [76] that long longitudinal waves in such structures can be accurately modelled by coupled regularised Boussinesq (cRB) equations, provided the bonding between layers is sufficiently soft.

The work in this thesis firstly examines the initial-value problem (IVP) for the system of cRB equations in [76] on the infinite line, for localised or sufficiently rapidly decaying initial conditions. Using asymptotic multiple-scales expansions, a nonsecular weakly nonlinear solution of the IVP is constructed, up to the accuracy of the problem formulation. The asymptotic theory is supported with numerical simulations of the cRB equations.

The weakly nonlinear solution for the equivalent IVP for a single regularised Boussinesq equation is then constructed; constituting an extension of the classical d'Alembert's formula for the leading order wave equation. The initial conditions are also extended to allow one to separately specify an $O(1)$ and $O(\epsilon)$ part. Large classes of solutions are derived and several particular examples are explicitly analysed with numerical simulations.

The weakly nonlinear solution is then improved by considering the IVP for a single regularised Boussinesq–type equation, in order to further develop the higher order terms in the solution. More specifically, it enables one to now correctly specify the higher order term's time dependence. Numerical simulations of the IVP are compared with several examples to justify the improvement of the solution.

Finally an asymptotic procedure is developed to describe the class of radiating solitary wave solutions which exist as solutions to cRB equations under particular regimes of the parameters. The validity of the analytical solution is examined with numerical simulations of the cRB equations.

Numerical simulations throughout this work are derived and implemented via developments of several finite difference schemes and pseudo-spectral methods, explained in detail in the appendices.

Keywords: coupled regularised Boussinesq equations; regularised Boussinesq equation; regularised Boussinesq–Ostrovsky equation; initial-value problem; asymptotic multiple-scales expansions; averaging; perturbation theory; solitons; radiating solitary waves; wave packets; nonlinear waves in layered waveguides.

Acknowledgements

First and foremost, I wish to offer my sincerest gratitude to my supervisor and mentor Karima Khusnutdinova. The endless time and constant encouragement she has given me throughout my studies will never be forgotten. Her wealth of knowledge and belief in me has been inspirational.

I would like to thank all of the staff and research students in the School of Mathematics, their kind help has been invaluable to me. I must also express a special thanks to Ben Carter for many insightful discussions.

I wish to condone a huge thank you to all of my family and close friends who have been there for me, right back to my first day in Loughborough as an undergraduate. I have welcomed their many distractions from mathematics.

Last, but certainly not least, I wish to bestow my fullest gratitude to my mother and father, for without their love and support, this work would never have been possible.

Abbreviations

cKG - Coupled Klein–Gordon

cRB - Coupled regularised Boussinesq

DDE - Doubly dispersive equation

DFT - Discrete Fourier transform

FFT - Fast Fourier transform

FPU - Fermi–Pasta–Ulam

IDFT - Inverse discrete Fourier transform

IFFT - Inverse fast Fourier transform

IST - Inverse scattering transform

IVP - Initial-value problem

KdV - Korteweg–de Vries

NLS - Nonlinear Schrödinger

ODE - Ordinary differential equation

PDE - Partial differential equation

RK4 - Runge–Kutta fourth-order

Contents

1 Introduction **1**

2 Nonlinear waves in layered waveguides **5**

2.1 Derivation of coupled regularised Boussinesq equations 6

2.1.1 Simplified lattice model 6

2.1.2 Complex lattice model 9

2.2 Conservation laws 14

2.3 Classical and radiating solitary waves 16

2.4 Concluding remarks 18

3 Cauchy problem for coupled regularised Boussinesq equations **21**

3.1 Introduction 22

3.2 Weakly nonlinear solution of the initial-value problem 24

3.2.1 Strong interactions: $c - 1 = O(\epsilon)$ 25

3.2.2 Weak interactions: $c - 1 = O(1)$ 29

3.3 Numerical simulations 32

3.4 Concluding remarks 36

4 Weakly nonlinear extension of d'Alembert's formula **39**

4.1 Introduction 40

4.2 Weakly nonlinear solution 42

4.3 Numerical scheme 44

4.4 Exactly solvable initial conditions 48

4.4.1 Right-propagating initial conditions 48

4.4.2 Right- and left-propagating initial conditions 49

4.5 Examples: weakly nonlinear solution and numerical simulations 50

4.5.1 Right-propagating 1-soliton initial conditions 50
4.5.2 Right- and left-propagating 1-soliton initial conditions 53
4.5.3 Right-propagating 2-soliton initial conditions 55
4.5.4 Right- and left-propagating 2-soliton initial conditions 58
4.6 Perturbations of exactly solvable initial conditions 59
4.7 Concluding remarks 63

5 Time dependence of higher order solution 65
5.1 Weakly nonlinear solution 66
5.2 Regularised Boussinesq equation 68
5.2.1 Perturbation solution for higher order left-propagating wave . . . 69
5.2.2 Perturbation solution for higher order right-propagating wave . . 71
5.2.3 Numerical solution for higher order corrections 76
5.2.4 Numerical simulations 79
5.3 Regularised Boussinesq–Ostrovsky equation 87
5.4 Concluding remarks 88

6 Radiating solitary wave solutions of coupled Boussinesq equations 91
6.1 Weak perturbation from the symmetric case 92
6.2 Non-oscillating higher order part of the solution 93
6.3 Oscillating higher order part of the solution 94
6.3.1 Approximation to the variable coefficient term 95
6.3.2 Asymptotic solution 98
6.3.2.1 Leading order solution 99
6.3.2.2 Higher order correction terms 100
6.4 Analytical description of radiating solitary waves 107
6.5 Numerical Simulations 108
6.5.1 Simulations using the approach in Section 6.3.1 109
6.5.2 Simulations using the approach in Section 6.3.2 112
6.6 Concluding remarks 115

7 Conclusions and future work 117

Appendices 124

A Finite difference methods for Boussinesq-type equations **125**

A.1 Regularised Boussinesq equation 125

A.1.1 Periodic Boundary conditions 127

A.1.2 Local truncation error 128

A.1.3 Stability 130

A.2 Coupled regularised Boussinesq equations 132

B Pseudo-spectral methods and the Fourier transform **135**

B.1 Introduction 135

B.2 Boussinesq–Ostrovsky equation 137

B.3 Linearised Korteweg–de Vries equation 139

B.3.1 Linearised Korteweg–de Vries equation on zero background . . . 139

B.3.2 Linearised Korteweg–de Vries equation on nonzero background . 140

B.4 Ostrovsky equation 141

B.5 Linearised Ostrovsky equations 143

B.5.1 Linearised Ostrovsky equation on zero background 143

B.5.2 Linearised Ostrovsky equation on non-zero background 144

B.6 Coupled regularised Boussinesq equations 146

C Miscellaneous equations **149**

Bibliography **151**

Publications

The results of this thesis are partially summarised in the following papers:

(i) KHUSNUTDINOVA, K.R. & MOORE, K.R. (2011) Initial-value problem for coupled Boussinesq equations and a hierarchy of Ostrovsky equations. *Wave Motion*, **48**, 738-752.

(ii) KHUSNUTDINOVA, K.R. & MOORE, K.R. (2012) Weakly non-linear extension of d'Alembert's formula. *IMA J. Appl. Math.*, **77**, 361-381.

(iii) KHUSNUTDINOVA, K.R., MOORE, K.R. & PELINOVSKY, D.E. (2013) Validity of the weakly-nonlinear solution of the Cauchy problem for the Boussinesq–type equation. To appear in *Stud. Appl. Math.*

Chapter 1

Introduction

The study of nonlinear waves has been a relatively recent actively developing area of research in mathematics, with important applications in fluid and solid mechanics, nonlinear optics and mathematical biology, to name but a few (see, for example, [1, 3, 29, 48, 91, 115]). A significant part of this area of research is devoted to the study of waves exhibiting weak nonlinearity and weak dispersion, which is particularly relevant to nonlinear processes in fluids and elastic solids. The most significant feature of such problems is the possibility of a balance between nonlinearity and dispersion, resulting in the existence of stable localised solutions such as solitons and nonlinear wave packets.

The first observation of a solitary wave dates back to 1834, when John Scott Russell followed "the great wave of translation" on horseback along the Edinburgh–Glasgow canal (reported in 1844) [99]. The first mathematical models describing this observed solitary wave were derived and studied in the works of Boussinesq (1872, 1877) [15, 16], Lord Rayleigh (1876) [98] and Korteweg & de Vries (1895) [78].

The Boussinesq and Korteweg–de Vries (KdV) equations, originally derived in the context of fluids, reappeared in connection with waves in solids, in the groundbreaking work by Zabusky and Kruskal (1965) [119]. Their work was motivated from the Fermi–Pasta–Ulam (FPU) lattice model (1955) [40] where it was shown that there was an absence of equipartition of energy among the modes of the harmonic approximation. This unexplained observation motivated Zabusky and Kruskal to consider the problem in the long-wave approximation, and to rederive the Boussinesq and KdV equations in this new setting, which subsequently led to numerical studies of solutions of the KdV

equation [119]. The general concept of a 'soliton' emerged from this study: a stable localised travelling wave of permanent form.

Later work showed that the Boussinesq and KdV equations belong to the group of so-called 'integrable' models, which possess a number of remarkable mathematical properties (for example, they have infinitely many conservation laws, and can be written as a compatibility condition for a pair of linear equations known as the 'Lax pair' [81]). Perhaps most importantly, a rather general Cauchy problem for such equations can be solved using the 'inverse scattering transform' (IST). This method was initially developed by Gardner, Green, Kruskal and Miura (1967) for the KdV equation [44]. However, Zakharov and Shabat (1972) developed the method in order to solve the Nonlinear Schrödinger (NLS) equation [121], and later Ablowitz, Kaup, Newell and Segur (1974) suggested a rather general scheme, by showing that the methods for solving the KdV and NLS equations in fact applied to a large class of equations, e.g. the Sine-Gordon equation and the modified KdV equation [2]. This work has since formed a foundation for all subsequent developments in the area of integrable systems.

Lattice models of the type considered by Fermi, Pasta and Ulam, i.e. ordered, in particular periodic, discrete systems of interacting particles, are often used to model nonlinear dynamics in condensed matter physics (e.g. [7, 19, 20, 85]). Typically lattice models allow for a long-wave or continuum approximation, which links them with continuum theories. Frenkel and Kontorova (1939) used a harmonic chain of particles in the presence of an external periodic potential to model the dynamics of dislocations in metals [77]. Various extensions and generalisations of the Frenkel–Kontorova model have been applied to studies of dynamics of molecular and polymer chains, DNA, and many more areas (see [19, 107] and references there). Toda (1967) introduced a chain of particles with exponential interaction potentials, which were shown to manifest exact soliton solutions [108]. A modified Toda lattice with an external linear elastic term was used to model the dynamics of a solid waveguide on an elastic substrate in [116], establishing that stable wave packet solutions play a central role in the dynamics of such a system, instead of solitons. Coupled Klein–Gordon (cKG) chains and corresponding cKG equations were proposed as a model for long longitudinal waves in bilayers where nonlinearity comes only from the bonding material [71] (see also references therein). The model was used to study solitary waves, modulational instability of nonlinear multi-phase wave trains and energy exchange between the layers.

In [76] a lattice model was used to study nonlinear waves in layered elastic waveguides with some softer material between the layers (for example, a soft adhesive bonding). The key element of this model is the use of a complex chain of oscillating mechanical dipoles, earlier considered as a linear model in [70] (the model is a natural generalisation of the linear model considered in [7] and [60], and the nonlinear model in [69]). A system of coupled Boussinesq-type equations were derived as an accurate asymptotic model from a complex chain which has all the essential degrees of freedom of a real elastic waveguide, taking into account both geometrical and physical sources of nonlinearity.

The work contained in this thesis is devoted to the analytical and numerical studies of one-dimensional longitudinal nonlinear bulk strain waves in layered elastic waveguides with a soft bonding layer, modelled by cRB equations derived in [76]. In Chapter 2 we consider a simplified model consisting of two coupled one-dimensional FPU chains, with some soft bonding between the layers, and rederive a system of coupled Boussinesq-type equations in the continuum approximation. We also overview the derivation of the equations from the complex lattice model considered in [76]. We then briefly discuss the conservation laws for the system of cRB equations, as well as the structure of the linear dispersion relation and the difference between classical and radiating solitary wave solutions.

Chapter 3 is devoted to the construction of a weakly nonlinear solution of the Cauchy problem for the cRB equations. We consider the IVP for a system of cRB equations on the infinite line for localised or sufficiently rapidly decaying initial data, where it is assumed that the data generates sufficiently rapidly decaying right- and left-propagating waves. We study the dynamics of weakly nonlinear waves, and using asymptotic multiple-scales expansions and an averaging procedure with respect to the fast time variable, we obtain a hierarchy of asymptotically exact coupled and uncoupled Ostrovsky equations for unidirectional waves. The Ostrovsky equation is a modification of the KdV equation, which first appeared in the study of oceanic waves to include background rotation in the model [94]. We then construct a nonsecular weakly nonlinear solution of the IVP in terms of solutions of the derived Ostrovsky equations, within the accuracy of the problem formulation. We perform numerical simulations for the cRB equations to illustrate the striking difference in the behaviour of the solutions for different asymptotic regimes, obtained from the theory.

In Chapter 4 we consider a weakly nonlinear solution of the Cauchy problem for the single regularised Boussinesq equation, obtained when coupling parameters in the system of cRB equations are equal to zero. The weakly nonlinear solution of the IVP for the single Boussinesq equation is constructed in terms of solutions of the IVPs for two KdV equations, integrable by the IST. This solution constitutes an extension of the classical d'Alembert's formula for the linear wave equation. We generalise the formulation of the work in Chapter 3, to account for possible perturbations to 'exactly solvable initial conditions' and test the formula by considering several examples with both exactly solvable initial conditions and their perturbations. Explicit analytical solutions are compared with numerical simulations of the single Boussinesq equation.

In Chapter 5 we show how the accuracy of the constructed solution can be improved even further by considering higher order terms in the weakly nonlinear solution. To do this, we now view the Boussinesq-type equations studied in Chapters 3 & 4 as exact models, disregarding higher order terms in the equations in order to simplify the analysis. In this respect we can view this work as a 'toy'-problem. However, it is certainly a valid mathematical problem, and it makes sense as a first step towards the study of relevant physical problems, since the results we obtain can be extended to account for the higher order terms in the equations. The derived higher order problems in this chapter are solved numerically and for a particular configuration of the initial conditions, a perturbation approach is developed. The validity of the solutions are analysed with relevant numerical simulations of the Boussinesq-type equations.

In Chapter 6 we develop an asymptotic procedure for the construction of radiating solitary wave solutions of cRB equations for the case when the coefficients of the system are slightly perturbed from the symmetric case. The derived analytical solutions are compared directly with results of numerical simulations for the cRB equations.

The final chapter is devoted to summarising and discussing the results obtained throughout the thesis, along with a discussion on how this work can be developed in future studies.

Numerical simulations throughout this work are performed using finite difference and pseudo-spectral methods; detailed descriptions of the numerical schemes are contained in Appendices A & B respectively.

Chapter 2

Nonlinear waves in layered waveguides

Recent studies of nonlinear waves, especially solitons, have included intensive studies of longitudinal bulk strain solitary waves in nonlinear elastic waveguides (see [96, 102] and references therein). One of the first long wave models used to describe waves propagating in solid waveguides was the well-known KdV equation [35, 90, 95]. Later it was shown that long longitudinal bulk solitary waves in an elastic rod are governed by the so-called 'doubly dispersive equation' (DDE), which is an equation of Boussinesq-type with two kinds of dispersive terms [97, 101]. This result was then confirmed by experiments on the generation and observation of bulk solitary waves in optically transparent polymeric materials such as polystyrene and plexiglas [32].

Various types of layered (or laminated) waveguides are used in physics and engineering to reinforce and improve deformation properties of elastic structures. The mechanical properties of the structure depend not only on the type of bulk material, but also on the type of bonding between the layers. The nonlinear effects in a waveguide with perfect horizontal bonding (not allowing a jump in the horizontal displacement across the interface) has been studied in [75]. The theory predicts, in particular, that the result of splitting (delamination) in the layered waveguide leads to fission of an incident bulk strain solitary wave (i.e., generation of a train of secondary solitons from a single incident soliton). This prediction has been confirmed experimentally [30], and it has been suggested that this phenomenon can be used for nondestructive testing of layered structures [31].

The study of nonlinear processes in a waveguide with imperfect bonding between layers (allowing a jump in the horizontal displacement across the interface) was initiated in [76] where the following system of cRB equations:

$$\begin{aligned} u_{tt} - u_{xx} &= u_x u_{xx} + u_{ttxx} - \delta(u - w), \\ w_{tt} - c^2 w_{xx} &= \alpha w_x w_{xx} + \beta w_{ttxx} + \gamma(u - w), \end{aligned} \tag{2.1}$$

were derived as a model describing long nonlinear bulk strain waves in a two layered waveguide, with a soft intermediate bonding layer. The displacements in the upper and lower layer are described by u and w respectively and the parameters $c, \alpha, \beta, \delta, \gamma$ depend upon the physical and geometrical properties of the waveguide. In this chapter we first derive system (2.1) from a simplified model consisting of coupled one-dimensional FPU-type chains. We then overview the derivation of the system of cRB equations from the complex lattice model used in [76], and discuss some general mathematical properties of system (2.1) (also detailed in [76]).

2.1 Derivation of coupled regularised Boussinesq equations

2.1.1 Simplified lattice model

Let us consider a simplified lattice model of longitudinal waves in a layered elastic waveguide consisting of two weakly coupled one-dimensional FPU chains, as depicted in Figure 2.1 (this is an extension of the cKG chains modelled in [71]).

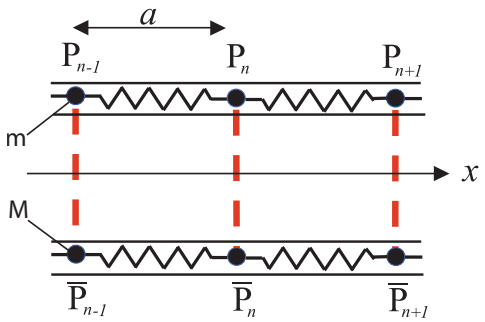

Figure 2.1: Coupled one-dimensional FPU chains of particles in equilibrium.

We denote the distance between adjacent particles in each chain when in equilibrium as a, and we allow the particles to move only along smooth horizontal tracks (i.e. not allowing for vertical displacements). We assume particles in the 'upper' and 'lower' chains have mass m and M respectively, and denote the n-th particles horizontal displacements by u_n and w_n respectively. We consider only nearest neighbour interactions, and write the Lagrangian of the system as

$$L = T - U,$$

where the kinetic energy T of the system is given by

$$T = \sum_n \frac{1}{2}(m\dot{u}_n^2 + M\dot{w}_n^2),$$

and the potential energy U of the system is of the form

$$\begin{aligned} U &= \sum_n \left[\frac{1}{2}\alpha(u_{n+1}-u_n)^2 + \frac{1}{3}\beta(u_{n+1}-u_n)^3 \right. \\ &+ \left. \frac{1}{2}A(w_{n+1}-w_n)^2 + \frac{1}{3}B(w_{n+1}-w_n)^3 + \frac{1}{2}\gamma(u_n-w_n)^2\right]. \end{aligned}$$

The potentials of interchain interactions are approximated by the first few terms of the respective Taylor expansions, where interactions between chains is assumed to be weak.

Substituting the Lagrangian of the system into each of the Euler-Lagrange equations

$$\frac{d}{dt}\left(\frac{\partial L}{\partial \dot{u}_n}\right) - \frac{\partial L}{\partial u_n} = 0, \qquad \frac{d}{dt}\left(\frac{\partial L}{\partial \dot{w}_n}\right) - \frac{\partial L}{\partial w_n} = 0, \tag{2.2}$$

we obtain the following system of difference-differential equations:

$$\begin{aligned} m\ddot{u}_n &= \alpha(u_{n+1}-2u_n+u_{n-1}) + \beta(u_{n+1}-u_{n-1})(u_{n+1}-2u_n+u_{n-1}) - \gamma(u_n-w_n), \\ M\ddot{w}_n &= A(w_{n+1}-2w_n+w_{n-1}) + B(w_{n+1}-w_{n-1})(w_{n+1}-2w_n+w_{n-1}) + \gamma(u_n-w_n). \end{aligned}$$

To study long waves, one can use the continuum approximation (e.g. [85]) in the governing equations. Hence, we approximate the terms

$$\begin{aligned} u_n(t) &= u(x,t), \\ u_{n\pm1}(t) &= u(x\pm a,t) = u(x,t) \pm a u_x(x,t) + \frac{a^2}{2}u_{xx}(x,t) \\ &\qquad \pm \frac{a^3}{6}u_{xxx}(x,t) + \frac{a^4}{24}u_{xxxx}(x,t) + \dots, \end{aligned}$$

and use equivalent approximations for the functions $w_n(t)$, to yield the following system of coupled partial differential equations (PDEs):

$$\begin{aligned} u_{tt} - \frac{\alpha}{m}\left(a^2 u_{xx} + \frac{a^4}{12}u_{xxxx}\right) - 2\frac{\beta a^3}{m}u_x u_{xx} + \frac{\gamma}{m}(u-w) + \ldots &= 0, \\ w_{tt} - \frac{A}{M}\left(a^2 w_{xx} + \frac{a^4}{12}w_{xxxx}\right) - 2\frac{Ba^3}{M}w_x w_{xx} + \frac{\gamma}{M}(w-u) + \ldots &= 0. \end{aligned} \quad (2.3)$$

Introducing the dimensionless variables

$$\widetilde{u} = \frac{u}{u_0}, \qquad \widetilde{w} = \frac{w}{w_0}, \qquad \widetilde{t} = \frac{t}{t_0}, \qquad \widetilde{x} = \frac{x}{x_0}, \quad (2.4)$$

and assuming that $x_0/t_0 \sim O(1)$, one can see that the scalings

$$\frac{u_0}{a} \sim O(\varepsilon^{\frac{1}{2}}), \quad \frac{w_0}{a} \sim O(\varepsilon^{\frac{1}{2}}), \quad \frac{a}{x_0} \sim O(\varepsilon^{\frac{1}{2}}), \quad \frac{\gamma}{\alpha} \sim O(\varepsilon^2), \quad (2.5)$$

where ϵ is assumed to be a small parameter, together with the assumptions that

$$\frac{\alpha a^2}{m} \sim O(1), \quad \frac{2\beta a^3}{m} \sim O(1), \quad \frac{Aa^2}{M} \sim O(1), \quad \frac{2Ba^3}{M} \sim O(1), \quad (2.6)$$

will yield the following system of coupled Boussinesq equations:

$$\begin{aligned} \tilde{u}_{\tilde{t}\tilde{t}} - c^2\tilde{u}_{\tilde{x}\tilde{x}} &= \varepsilon\left[D_1\tilde{u}_{\tilde{x}}\tilde{u}_{\tilde{x}\tilde{x}} + D_2\tilde{u}_{\tilde{x}\tilde{x}\tilde{x}\tilde{x}} - D_3(\tilde{u}-\tilde{w})\right] + O(\varepsilon^2), \\ \tilde{w}_{\tilde{t}\tilde{t}} - \hat{c}^2\tilde{w}_{\tilde{x}\tilde{x}} &= \varepsilon\left[\hat{D}_1\tilde{w}_{\tilde{x}}\tilde{u}_{\tilde{x}\tilde{x}} + \hat{D}_2\tilde{w}_{\tilde{x}\tilde{x}\tilde{x}\tilde{x}} - \hat{D}_3(\tilde{w}-\tilde{u})\right] + O(\varepsilon^2), \end{aligned} \quad (2.7)$$

where the coefficients $c^2, \hat{c}^2, D_i$ and $\hat{D}_i$ $(i = 1, 2, 3)$ are of order $O(1)$. Therefore to leading order we have

$$\begin{aligned} \tilde{u}_{\tilde{t}\tilde{t}} &= c^2\tilde{u}_{\tilde{x}\tilde{x}} + O(\varepsilon), \\ \tilde{w}_{\tilde{t}\tilde{t}} &= \hat{c}^2\tilde{w}_{\tilde{x}\tilde{x}} + O(\varepsilon), \end{aligned} \quad (2.8)$$

and as a result one can write system (2.7) in the asymptotically equivalent form

$$\begin{aligned} \tilde{u}_{\tilde{t}\tilde{t}} - c^2\tilde{u}_{\tilde{x}\tilde{x}} &= \varepsilon\left[D_1\tilde{u}_{\tilde{x}}\tilde{u}_{\tilde{x}\tilde{x}} + \frac{D_2}{c^2}\tilde{u}_{\tilde{t}\tilde{t}\tilde{x}\tilde{x}} - D_3(\tilde{u}-\tilde{w})\right] + O(\varepsilon^2), \\ \tilde{w}_{\tilde{t}\tilde{t}} - \hat{c}^2\tilde{w}_{\tilde{x}\tilde{x}} &= \varepsilon\left[\hat{D}_1\tilde{w}_{\tilde{x}}\tilde{u}_{\tilde{x}\tilde{x}} + \frac{\hat{D}_2}{\hat{c}^2}\tilde{w}_{\tilde{t}\tilde{t}\tilde{x}\tilde{x}} - \hat{D}_3(\tilde{w}-\tilde{u})\right] + O(\varepsilon^2). \end{aligned} \quad (2.9)$$

Truncating the $O(\varepsilon^2)$ terms and reverting back to the original dimensional form yields equations (2.9) in the form of the following cRB equations:

$$\begin{aligned} u_{tt} - c_0^2 u_{xx} &= E_1 u_x u_{xx} + E_2 u_{ttxx} - E_3(u-w), \\ w_{tt} - \hat{c}_0^2 w_{xx} &= \hat{E}_1 w_x w_{xx} + \hat{E}_2 w_{ttxx} - \hat{E}_3(w-u), \end{aligned} \quad (2.10)$$

where the coefficients in (2.10) are

$$c_0^2 = \frac{\alpha a^2}{m}, \quad E_1 = \frac{2\beta a^3}{m}, \quad E_2 = \frac{a^2}{12}, \quad E_3 = \frac{\gamma}{m},$$
$$\hat{c}_0^2 = \frac{Aa^2}{M}, \quad \hat{E}_1 = \frac{2Ba^3}{M}, \quad \hat{E}_2 = \frac{a^2}{12}, \quad \hat{E}_3 = \frac{\gamma}{M}.$$

2.1.2 Complex lattice model

In this section we overview the derivation of the cRB equations from the complex lattice model used in [76]. Although we have formulated the problem from a simplified model using coupled one-dimensional FPU chains, it should be emphasised that the complex lattice model in this derivation simulates all essential degrees of freedom of a real elastic waveguide, taking into account both physical and geometrical sources of nonlinearity. Hence it is important to consider the mathematical problem which most represents the real life problem.

A basic dipole lattice model representing a homogeneous waveguide is first considered by using two coupled FPU-type chains of interacting particles (see Figure 2.2(a)). From the approach outlined in this first model, the problem is then extended to include an intermediate layer in between two sets of two coupled FPU-type chains, thus simulating a two layered waveguide with some intermediate bonding material (the methodology can be further extended to model an N-layered waveguide with N-1 intermediate bonding layers).

In the dipole model for the homogeneous waveguide, each particle is assumed to have a mass m and to be separated horizontally in each chain by a distance a and vertically by a distance $2l$ when in equilibrium. Each pair of n-th particles situated in the upper and lower chains represent two poles of a dipole denoted P_n and $\overline{P}_n$ respectively (see Figure 2.2(a)).

The displacements of the n-th dipole are characterised by: (i) the horizontal displacement u_1^n of the geometrical centre denoted O_n; (ii) the vertical displacement u_2^n of the geometrical centre O_n; (iii) the in-plane rotation $\Delta\phi^n$ of the dipole axis; (iv) the difference in distance between the poles ($2u_4^n$). From this, the horizontal displacements of the poles of the n-th dipole are defined relative to their original position as (see Figure 2.2(b)):

$$U_1^n = u_1^n - (l + u_4^n)\sin\Delta\phi^n, \qquad \overline{U}_1^n = u_1^n + (l + u_4^n)\sin\Delta\phi^n, \tag{2.11}$$

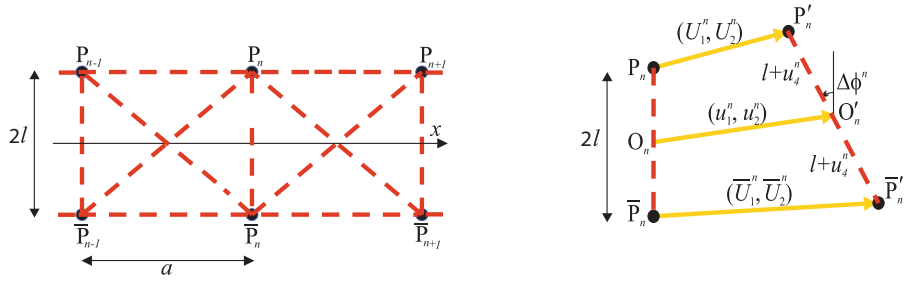

(a) (b)

Figure 2.2: (a) A dipole lattice model consisting of two coupled FPU chains and (b) displacement of the n-th dipole from equilibrium.

and similarly, the corresponding vertical displacements are

$$U_2^n = u_2^n + (l + u_4^n)\cos\Delta\phi^n - l, \qquad \overline{U}_2^n = u_2^n - (l + u_4^n)\cos\Delta\phi^n + l. \tag{2.12}$$

In subsequent derivations we denote $u_3^n = l\Delta\phi^n$ and assume $\Delta\phi^n \ll 1$ (corresponding to weak rotations), and take Taylor series expansions up to and including cubic terms.

The kinetic energy of the n-th dipole is given by

$$T_n = \frac{M}{2}\left((\dot{u}_1^n)^2 + (\dot{u}_2^n)^2 + (\dot{u}_4^n)^2 + \left(1 + \frac{u_4^n}{l}\right)^2 (\dot{u}_3^n)^2\right), \tag{2.13}$$

where $M = 2m$ is the dipole mass. The potential energy at the n-th dipole is characterised by each of the nine possible pairwise interactions of the dipoles at the n-th position (see Figure 2.2(a)), namely:

$$\begin{aligned}\Phi_n &= \Phi_{n,n+1} + \Phi_{\overline{n},\overline{n+1}} + \Phi_{n,\overline{n+1}} + \Phi_{\overline{n},n+1} + \Phi_{n-1,n} \\ &+ \Phi_{\overline{n-1},\overline{n}} + \Phi_{n-1,\overline{n}} + \Phi_{\overline{n-1},n} + \Phi_{\perp},\end{aligned} \tag{2.14}$$

where the bars above the position notations n correspond to the particles in the bottom chain, and the final term denotes the vertical interaction between the poles of the n-th dipole. Each of the individual potential energy terms in (2.14) can be written as

$$\Phi_*(\Delta r_*) = \frac{\widetilde{\beta}}{2}\Delta r_*^2 + \frac{\widetilde{\gamma}}{3}\Delta r_*^3 + \ldots, \tag{2.15}$$

where Δr_* denotes the change of distance between the two corresponding particles. The set of constants $(\widetilde{\beta}, \widetilde{\gamma})$ each correspond to one of three constants depending on

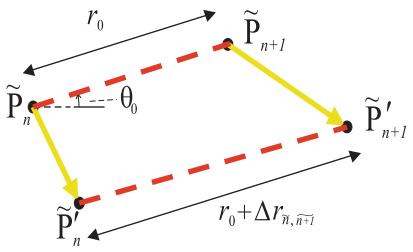

Figure 2.3: Distance between two poles at equilibrium: $\widetilde{P}_n$, $\widetilde{P}_{n+1}$ and after a displacement: $\widetilde{P}'_n$, $\widetilde{P}'_{n+1}$.

whether the pair-wise interactions are horizontal, vertical or diagonal. The distance $\Delta r_{\widetilde{n},\widetilde{n+1}}$ is explicitly defined as

$$\Delta r_{\widetilde{n},\widetilde{n+1}} = \left[(\Delta x + r_0\cos\theta_0)^2 + (\Delta y + r_0\sin\theta_0)^2\right]^{1/2} - r_0, \tag{2.16}$$

where $\Delta x = \widetilde{U}_1^{n+1} - \widetilde{U}_1^n$, $\Delta y = \widetilde{U}_2^{n+1} - \widetilde{U}_2^n$ denotes the changes in the horizontal and vertical distances respectively between any interacting pole $\widetilde{P}_n$ of the n-th dipole and any pole $\widetilde{P}_{n+1}$ of the $(n+1)$-th dipole (see Figure 2.3). Note, the change of distance between the poles both at the n-th dipole is $\Delta r_\perp = 2u_4^n$.

Assuming horizontal and vertical displacements are small, namely $\Delta x/r_0 \ll 1$, $\Delta y/r_0 \ll 1$, the change in distance of the dipoles are approximated as

$$\begin{aligned}\Delta r_{\widetilde{n},\widetilde{n+1}} &= \Delta x\cos\theta_0 + \Delta y\sin\theta_0 + \frac{1}{2r_0}(\Delta x\sin\theta_0 - \Delta y\cos\theta_0)^2 \\ &- \frac{1}{2r_0^2}(\Delta x\cos\theta_0 + \Delta y\sin\theta_0)(\Delta x\sin\theta_0 - \Delta y\cos\theta_0)^2 + \dots\,.\end{aligned} \tag{2.17}$$

Substituting the kinetic and potential energy expressions into the following Euler-Lagrange equations

$$\frac{\mathrm{d}}{\mathrm{d}t}\left(\frac{\partial T_n}{\partial \dot{u}_i^n}\right) - \frac{\partial T_n}{\partial u_i^n} + \frac{\partial \Phi_n}{\partial u_i^n} = 0, \qquad \text{for} \qquad i = 1,2,3,4, \tag{2.18}$$

yields the system of difference-differential equations

$$\begin{aligned}&M\ddot{u}_1^n + \frac{\partial\Phi_n}{\partial u_1^n} = 0, \qquad M\ddot{u}_2^n + \frac{\partial\Phi_n}{\partial u_2^n} = 0,\\ &M\left[\ddot{u}_3^n\left(1+\frac{u_4^n}{l}\right)^2 + 2\frac{\dot{u}_3^n\dot{u}_4^n}{l}\left(1+\frac{u_4^n}{l}\right)\right] + \frac{\partial\Phi_n}{\partial u_3^n} = 0,\\ &M\left[\ddot{u}_4^n - \frac{(\dot{u}_3^n)^2}{l}\left(1+\frac{u_4^n}{l}\right)\right] + \frac{\partial\Phi_n}{\partial u_4^n} = 0.\end{aligned} \tag{2.19}$$

The continuum approximation is then implemented, thus the terms in (2.19) are approximated as:

$$u_i^n(t) = u_i(x,t),$$
$$u_i^{n\pm1}(t) = u_i(x \pm a, t) = u_i(x,t) \pm a u_{i_x}(x,t) + \frac{a^2}{2} u_{i_{xx}}(x,t) \pm \frac{a^3}{6} u_{i_{xxx}}(x,t) + \frac{a^4}{24} u_{i_{xxxx}}(x,t) + ..., \qquad \text{for} \qquad i = 1,2,3,4,$$

and the four difference-differential equations (2.19) are rewritten as PDEs (see [76] for full details and the exact form of these equations).

From the subsequently derived PDEs it is noted that the equations uncouple into two subsystems involving the variables u_1, u_4 and u_2, u_3 respectively. After non-dimensionalising the equations, it is shown that from seeking predominantly longitudinal waves, one can obtain suitable scalings (analogous to the approach outlined for the simpler model in Section 2.1.1) to find that the leading order behaviour of the system is described by the subsystem for u_1 and u_4. It is then shown that u_4 can be expressed in terms of derivatives of u_1. Therefore, returning to the original dimensional form of the system and denoting $u_1 = u$, yields the following equation for long nonlinear longitudinal waves:

$$u_{tt} - c_0^2 u_{xx} = E_1 u_x u_{xx} + E_2 u_{ttxx} + E_3 u_{xxxx}, \tag{2.20}$$

where c_0, E_1, E_2, E_3 are expressed in terms of the lattice parameters (see [76] for the explicit form of these parameters). Equation (2.20) is in the form of the DDE, which as noted, is previously derived in [97, 101]. It is also shown in [76] that the solutions of the other subsystem, involving equations for the variables u_2, u_3, are determined at higher order and thus transversal and rotational motions are slaved to the longitudinal waves.

Since the parameters in the right-hand side of (2.20) are $O(\epsilon)$, one can notice $u_{tt} \sim c_0^2 u_{xx}$ and thus (2.20) is asymptotically equivalent to the integrable (via the IST) 'nonlinear string equation' (see [120]), and also the regularised Boussinesq equation:

$$u_{tt} - c_0^2 u_{xx} = E_1 u_x u_{xx} + \widetilde{E}_{23} u_{ttxx}, \tag{2.21}$$

where $\widetilde{E}_{23} = E_{23}/c_0^2$. This form of the Boussinesq equation is nonintegrable by the IST (see [3, 120]), however it is favourable from a numerical viewpoint since it obviates the

short wave instability (see [10, 14, 25]). This latter feature of the Boussinesq equation (2.21) can be realised directly by considering the linear dispersion relation, where one can find that the phase velocity is real for any wavenumber. Conversely, if one replaces the fourth order mixed derivative term in (2.21) with a fourth order spatial derivative term, one can find that for some wave numbers the phase velocity is imaginary, hence indicating the instability.

The work in [76] is then extended to consider a two layered imperfectly bonded waveguide by considering the analogue of the homogeneous problem in each layer, but now the effects of an intermediate bonding layer are introduced (see Figure 2.4).

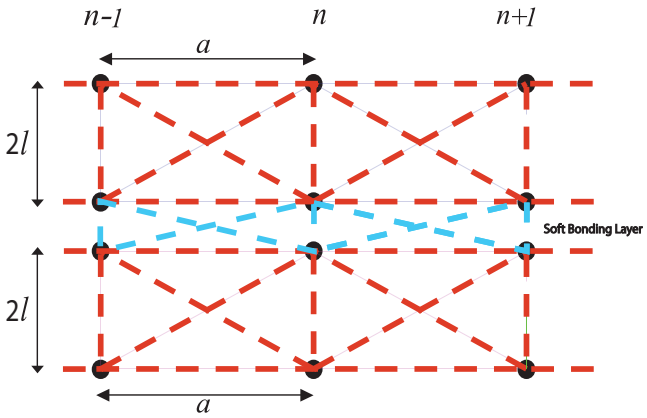

Figure 2.4: Two layered lattice model: two dipole lattices with an intermediate bonding layer.

The potential energy of an n-th lattice element is now modified to the form

$$\Phi_n^{total} = \Phi_n + \hat{\Phi}_n + \Phi_n^g, \tag{2.22}$$

where the potential energy of the n-th dipole in the upper and lower layer is denoted by Φ_n and $\hat{\Phi}_n$ respectively, and are each found similar to the approach outlined in the homogenous case (see equations (2.14)–(2.17)). The potential energy Φ_n^g models the potential energy in the interactions between the upper and lower layer where, as depicted in Figure 2.4, there are five possible interactions at the n-th element, thus

$$\Phi_n^g = \Phi^g_{\overline{n},n+1} + \Phi^g_{n,\overline{n+1}} + \Phi^g_{\overline{n-1},n} + \Phi^g_{n-1,\overline{n}} + \Phi^g_{\perp}. \tag{2.23}$$

Crucially in [76] it was found that if one assumes the bonding layer is sufficiently 'soft' (implemented by choosing the interaction constants to be sufficiently small in comparison with the constants in both layers), and subsequently following the same process as in the problem for the homogenous waveguide, with the same scalings previously derived from seeking predominantly longitudinal waves, one can asymptotically derive 'coupled doubly dispersive equations' describing the longitudinal displacement in each layer. In the form of dimensional variables, denoting $u_1 = u$ and $w_1 = w$, these equations are

$$\begin{aligned} u_{tt} - c_0^2 u_{xx} &= E_1 u_x u_{xx} + E_2 u_{ttxx} + E_3 u_{xxxx} - E_4(u - w), \\ w_{tt} - \hat{c}_0^2 w_{xx} &= \hat{E}_1 w_x w_{xx} + \hat{E}_2 w_{ttxx} + \hat{E}_3 w_{xxxx} - \hat{E}_4(w - u), \end{aligned} \tag{2.24}$$

where $c_0, \hat{c}_0, E_{1,2,3,4}$ and $\hat{E}_{1,2,3,4}$ are expressed in terms of the lattice parameters (see [76] for the exact form of these coefficients). Noting that to leading order $u_{xx} \sim c_0^2 u_{tt}$ and $w_{xx} \sim \hat{c}_0^2 w_{tt}$ (since the terms in the right-hand side of (2.24) are $O(\epsilon)$), one can write an asymptoticly equivalent form of (2.24) in the form of the following cRB equations:

$$\begin{aligned} u_{tt} - c_0^2 u_{xx} &= E_1 u_x u_{xx} + (E_2 + \frac{E_3}{c_0^2}) u_{ttxx} - E_4(u - w), \\ w_{tt} - \hat{c}_0^2 w_{xx} &= \hat{E}_1 w_x w_{xx} + (\hat{E}_2 + \frac{\hat{E}_3}{\hat{c}_0^2}) w_{ttxx} - \hat{E}_4(w - u). \end{aligned} \tag{2.25}$$

2.2 Conservation laws

We first rewrite the cRB equations (2.25) by introducing the variables

$$t \to \frac{t}{T^*}, \quad x \to \frac{x}{X^*}, \quad u \to \frac{u}{U^*}, \quad w \to \frac{w}{U^*},$$

where

$$U^* = \frac{c_0^2 X^*}{E_1}, \quad T^* = \frac{X^*}{c_0}, \quad X^* = \Big(E_2 + \frac{E_3}{c_0^2}\Big)^{1/2},$$

yielding the cRB equations (2.25) in the following nondimensional form:

$$\begin{aligned} u_{tt} - u_{xx} &= u_x u_{xx} + u_{ttxx} - \delta(u - w), \\ w_{tt} - c^2 w_{xx} &= \alpha w_x w_{xx} + \beta w_{ttxx} + \gamma(u - w). \end{aligned} \tag{2.26}$$

The coefficients in (2.26) are written in terms of the previous coefficients as

$$c^2 = \frac{\hat{c}_0^2}{c_0^2}, \quad \delta = \Big(E_2 + \frac{E_3}{c_0^2}\Big)\frac{E_4}{c_0^2}, \quad \alpha = \frac{\hat{E}_1}{E_1}, \quad \beta = \Big(\hat{E}_2 + \frac{\hat{E}_3}{\hat{c}_0^2}\Big)\Big/\Big(E_2 + \frac{E_3}{c_0^2}\Big), \quad \gamma = \frac{\delta \hat{E}_4}{E_4}.$$

It should be noted that system (2.26) is Lagrangian with the Lagrangian density

$$L = \frac{1}{2}\left[u_t^2 + \frac{\delta}{\gamma}w_t^2 - u_x^2 - \frac{\delta c^2}{\gamma}w_x^2 - \frac{1}{3}\left(u_x^3 + \frac{\alpha\delta}{\gamma}w_x^3\right) + u_{tx}^2 + \frac{\beta\delta}{\gamma}w_{tx}^2 - \delta(u-w)^2\right].$$

One can show (2.26) admits three groups of point symmetries: shifts in x and t, and a shift in u and w; all of which preserve solutions of (2.26). Using Noether's theorem (e.g., [59]), one can utilise these symmetries to derive two conservation laws, in addition to an obvious conservation law

$$\left[u_t + \frac{\delta}{\gamma}w_t\right]_t - \left[u_x + \frac{\delta c^2}{\gamma}w_x + \frac{1}{2}u_x^2 + \frac{\alpha\delta}{2\gamma}w_x^2 + u_{ttx} + \frac{\beta\delta}{\gamma}w_{ttx}\right]_x = 0,$$

(corresponding to conservation of mass) found directly by rearranging the cRB equations (2.26). The conservation laws from Noether's theorem are

$$A_t^i + B_x^i = 0, \quad \text{for} \quad i = 1, 2, \tag{2.27}$$

corresponding to conservation laws for energy and momentum respectively, where the densities and flows are of the form

$$\begin{aligned}
A^1 &= \frac{1}{2}\left[u_t^2 + \frac{\delta}{\gamma}w_t^2 + u_x^2 + \frac{\delta c^2}{\gamma}w_x^2 + \frac{1}{3}\left(u_x^3 + \frac{\alpha\delta}{\gamma}w_x^3\right) + u_{tx}^2 + \frac{\beta\delta}{\gamma}w_{tx}^2 + \delta(u-w)^2\right],\\
B^1 &= -u_t u_x - \frac{\delta c^2}{\gamma}w_t w_x - \frac{1}{2}u_t u_x^2 - \frac{\alpha\delta}{2\gamma}w_t w_x^2 - u_t u_{ttx} - \frac{\beta\delta}{\gamma}w_t w_{ttx},\\
A^2 &= u_t u_x + \frac{\delta}{\gamma}w_t w_x + u_{tx}u_{xx} + \frac{\beta\delta}{\gamma}w_{tx}w_{xx},\\
B^2 &= -\frac{1}{2}\left[u_t^2 + \frac{\delta}{\gamma}w_t^2 + u_x^2 + \frac{\delta c^2}{\gamma}w_x^2 + \frac{2}{3}\left(u_x^3 + \frac{\alpha\delta}{\gamma}w_x^3\right)\right.\\
&+ \left. u_{tx}^2 + \frac{\beta\delta}{\gamma}w_{tx}^2 - \delta(u-w)^2\right] - u_x u_{ttx} - \frac{\beta\delta}{\gamma}w_x w_{ttx}.
\end{aligned}$$

Naturally, the conservations laws defined by (2.27) can be shown to hold by virtue of the governing equations (2.26).

For the purpose of the work considered in this thesis, the main use of the conservation laws (2.27) is from the viewpoint of numerical simulations. The accuracy of derived numerical approaches for solving equations of the type (2.26) can be justified via the conservation laws.

2.3 Classical and radiating solitary waves

The system of cRB equations (2.26) generally admits kink-type solutions. In order to analyse localised solutions and subsequently utilise the well known theory of solitons, we differentiate (2.26) with respect to x, denoting $u_x = f, w_x = g$, to obtain

$$\begin{aligned} f_{tt} - f_{xx} &= \frac{1}{2}(f^2)_{xx} + f_{ttxx} - \delta(f-g), \\ g_{tt} - c^2 g_{xx} &= \frac{1}{2}\alpha(g^2)_{xx} + \beta g_{ttxx} + \gamma(f-g). \end{aligned} \tag{2.28}$$

We refer to both systems of equations (2.26) and (2.28) as cRB equations, since system (3.2) is obtained directly by differentiation of system (3.1). In the symmetric case, when $c = \alpha = \beta = 1$, system (2.28) admits a reduction $g = f$, where f satisfies the single Boussinesq equation

$$f_{tt} - f_{xx} = \frac{1}{2}(f^2)_{xx} + f_{ttxx}. \tag{2.29}$$

The Boussinesq equation (2.29) has particular solutions in the form of pure solitary waves:

$$f = A\ \mathrm{sech}^2 \frac{x - vt}{\Lambda}, \tag{2.30}$$

where $A = 3(v^2 - 1),\ \Lambda = \frac{2v}{\sqrt{v^2-1}}$. Figure 2.5 illustrates the pure solitary wave solution (2.30) for some typical parameters.

However, in the cRB system of equations (2.28) these 'pure' or 'classical' solitary wave solutions, rapidly decaying to zero in their tail regions, are structurally unstable and are replaced with 'radiating' solitary waves [76], i.e. a solitary wave radiating a co-propagating one-sided oscillatory tail, using the terminology in [9, 14, 113]. A typical illustration of radiating solitary wave solutions in each component of the cRB equations (2.28) is depicted in Figure 2.6 (the solution is obtained from a numerical approach for solving the system of cRB equations, discussed in detail later in this thesis).

There have been extensive studies of generalised and radiating solitary waves, especially in the context of fluid mechanics (e.g., [17, 41, 51, 52, 67, 83, 112]). The most commonly studied systems supporting these non-local nonlinear long waves include: perturbed KdV equations; coupled KdV systems; perturbed NLS equations and coupled NLS systems. The underlying reason for the occurrence of generalised and radiating solitary waves is due to a resonance between a long wave (with wavenumber

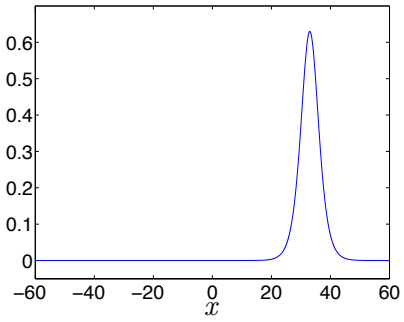

Figure 2.5: Pure solitary wave solution (2.30) at $t = 30$, with $v = 1.1$.

$k \approx 0$) and a short wave (with some finite wavenumber). Steady generalised solitary waves are necessarily symmetric (they support oscillating tails on both sides of the localised central core), however this means they usually cannot be realised physically since the group velocity of the oscillating tails is the same at both ends. In practice, one instead finds that radiating solitary waves are generated (asymmetric non-local solitary waves) with the oscillating tail appearing on the side of the central core determined by the group velocity.

In the system we consider (2.28), long-wave ripples are radiated by solitons, due to the type of coupling terms in the equations and the resulting structure of the dispersion relation. The linear dispersion relation for (2.28) was analysed in [76] by assuming that coefficients in (2.28) are perturbed compared to the symmetric case, but remain positive. The dispersion relation is of the form

$$[k^2(1-p^2) - k^4p^2 + \delta][k^2(c^2-p^2) - \beta k^4 p^2 + \gamma] = \gamma\delta,$$

where k is the wavenumber and p is the phase speed. A typical linear dispersion curve of the system of cRB equations (2.28) is shown in Figure 2.7. A significant difference with the linear dispersion curve of the reduction (2.29) consists in the appearance of the second (upper) branch, going to infinity as $k \to 0$, and approaching zero, remaining above the lower branch, as $k \to \infty$.

The classical or pure solitary waves of the single Boussinesq equation (2.29) arise as a bifurcation from wavenumber $k = 0$ of the linear wave spectrum, shown in Figure 2.7(b), when there is no possible resonance with any linear wave for any value of k. The solitary wave speed v is greater than the linear long wave speed, i.e. $v > 1$, while

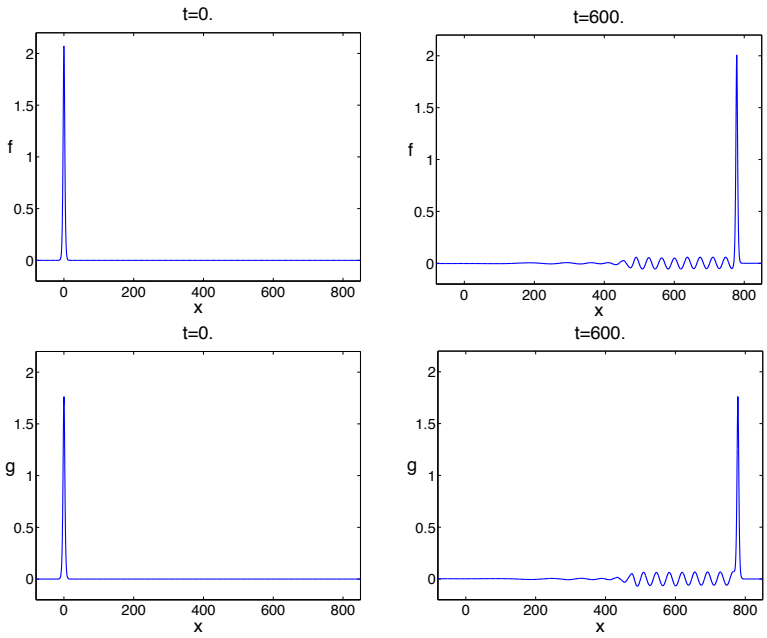

Figure 2.6: Typical generation of radiating solitary waves in the system of cRB equations (2.28), from pure solitary wave initial conditions.

the speed of a linear wave of any wavenumber is smaller, i.e. $p \leq 1$. This becomes impossible when the symmetry is broken. Instead, radiating solitary waves arise for the case when there is a possible resonance with the upper branch for some finite non-zero value of k. For example, a possible resonance is shown in Figure 2.7(a) for $v = p = 1.3$. The solitary wave solutions of (2.29), viewed as particular solutions of the coupled equations in the symmetric case, constitute a one-parameter family of so-called 'embedded' solitary waves (e.g., [21, 118]). Recently, radiating solitary waves have been experimentally observed in two- and three-layered elastic waveguides with soft bonding layers [33].

The radiating solitary wave solution depicted in Figure 2.6 is discussed in further detail in subsequent chapters.

2.4 Concluding remarks

In this chapter we have discussed the motivation for considering nonlinear wave propagation in layered elastic waveguides with an introduction to some of the key models

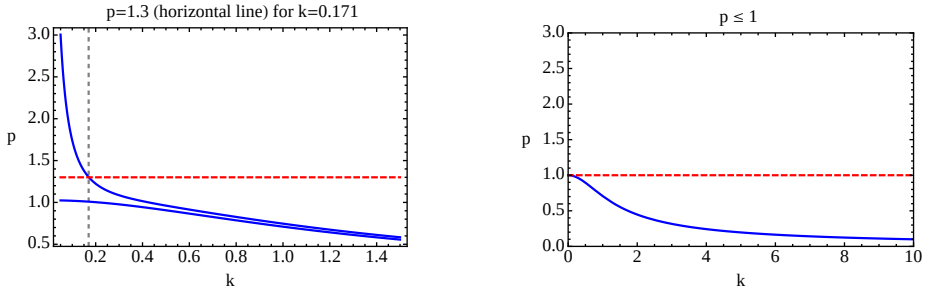

(a) (b)

Figure 2.7: (a) Two branches of the linear dispersion curve of the cRB equations (2.28) for $c = 1.05, \beta = 1, \delta = \gamma = 0.01$ and intersection with $p = 1.3$ (horizontal line) and (b) Linear dispersion curve of the reduction (2.29) in the symmetric case $c = 1, \beta = 1, \delta = \gamma = 0.01$.

which have been previously derived to mathematically simulate such processes. We have outlined the derivation of Boussinesq-type equations as nonlinear asymptotic models describing one-dimensional longitudinal displacement in layered waveguides with a soft intermediate bonding later.

Firstly, using a simple lattice model consisting of two weakly coupled one-dimensional FPU chains (extended from the cKG chains modelled in [71]) we rederived cRB equations modelling longitudinal displacement; generalising the derivation in the famous work by Zabusky and Kruskal [119] in a single FPU chain. We then overviewed the derivation in [76] where the cRB equations were derived using a complex layered lattice model from two sets of coupled FPU-type chains with all the essential degrees of freedom in a real elastic waveguide. We then finished by discussing some key features of the derived cRB equations including conservation laws, the linear dispersion relation and a brief discussion of some types of solutions which are known to exist for the cRB equations. In particular, it is noted that rather subtle changes to the parameters in the system of cRB equations yield significant qualitative changes to the solitary wave solutions of the symmetric case.

Using the derived Boussinesq-type models reviewed in this chapter, we now aim to develop some suitable methods for solving these equations, with the view to further develop the understanding of the behaviour of nonlinear waves in layered elastic waveguides, hence contributing to the many applications governed by such models.

It is interesting to ask such questions as:

- Can one develop some analytical representation of the radiating solitary waves which arise from pure solitary waves when the parameters in each layer are close to the symmetric case?
- Alternatively, what type of waves exist when the parameters in the system are sufficiently perturbed from the symmetric case? Do the pure solitary wave features of the solution still exist? If not, do any localised long wave solutions exist in such a case?
- Can one derive a general solution to describe the propagation of a wave through a layered waveguide from a given rather general initial condition?

Such natural questions and many more alike are examined and answered throughout the work contained in the subsequent chapters.

Chapter 3

Cauchy problem for coupled regularised Boussinesq equations

We consider the IVP for a system of coupled Boussinesq equations on the infinite line for localised or sufficiently rapidly decaying initial data, generating sufficiently rapidly decaying right- and left-propagating waves. We study the dynamics of weakly nonlinear waves, and using asymptotic multiple-scales expansions and averaging with respect to the fast time variable, we obtain a hierarchy of asymptotically exact coupled and uncoupled Ostrovsky equations for unidirectional waves. We then construct a weakly nonlinear solution of the IVP in terms of solutions of the derived Ostrovsky equations within the accuracy of the governing equations, and show that there are no secular terms. We also perform relevant numerical simulations of the original unapproximated system of Boussinesq equations to illustrate the difference in the behaviour of the solutions for different asymptotic regimes.

The results of this chapter are partially summarised in [72].

3.1 Introduction

The Ostrovsky equation

$$(\eta_t + \nu\eta\eta_x + \gamma\eta_{xxx})_x = \lambda\eta,$$

is a modification of the KdV equation used in the study of oceanic waves, which takes into account the effect of background rotation [94]. It is well known that rotation in the oceanographic problem ($\gamma\lambda > 0$) eliminates the solitary wave solutions of the KdV equation through the terminal radiation damping [49, 82]. The numerical simulations in [50, 56] have shown that a localised wave packet emerges as a stable dominant solution of the Ostrovsky equation. In an independent study [116], it was established that stable envelope solitons play a central role in the dynamics of a modified Toda lattice with an additional linear term, which can be related to the two-directional generalisation of the Ostrovsky equation derived in [46]. The weakly nonlinear description of the emerging wave packet for the Ostrovsky equation in terms of a higher order NLS equation has been developed in [50], linking the wavenumber of the carrier wave with the extremum of the group velocity [50, 116].

In this chapter, we are concerned with the construction of a weakly nonlinear solution of the IVP for the system of cRB equations:

$$\begin{aligned} u_{tt} - u_{xx} &= u_x u_{xx} + u_{ttxx} - \delta(u - w), \\ w_{tt} - c^2 w_{xx} &= \alpha w_x w_{xx} + \beta w_{ttxx} + \gamma(u - w), \end{aligned} \tag{3.1}$$

(see Section 2.1 for an overview of the derivation of such Boussinesq-type equations). As previously mentioned, this version of the Boussinesq equation is nonintegrable via the IST, but from the viewpoint of the subsequently developed analytical approach, we could have worked with any version of coupled Boussinesq equations. Also, within this approach, generalisation of the derivations to the case of three and more equations of this type is straightforward, and we do not discuss it in this work, although the detailed study of various physical effects is interesting. In the context of waves in solids, Boussinesq-type equations have been derived, for example, for nonlinear waves in solid waveguides [97, 101, 102] and for waves in microstructured solids [62, 96] (further references can be found in [85] and [23, 24, 25]).

Differentiating (3.1) with respect to x, and denoting $u_x = f, w_x = g$, we obtain

$$\begin{aligned} f_{tt} - f_{xx} &= \frac{1}{2}(f^2)_{xx} + f_{ttxx} - \delta(f-g), \\ g_{tt} - c^2 g_{xx} &= \frac{1}{2}\alpha(g^2)_{xx} + \beta g_{ttxx} + \gamma(f-g), \end{aligned} \tag{3.2}$$

(uncoupled equations in this form are sometimes called 'regularised long wave equations' and 'improved bad Boussinesq equations'). In what follows we will consider solutions of system (3.2) instead of the solutions of the original system (3.1). We refer to both systems (3.1) and (3.2) as cRB equations, since system (3.2) is obtained by differentiation of system (3.1).

We are interested in constructing a weakly nonlinear solution of the IVP for system (3.2) using asymptotic multiple-scales expansions of the type used in the study of oblique interaction of solitary waves in [86, 87] (see also references therein and also in [45]). Recently in [75], a scheme based on these type of asymptotic expansions were developed in order to solve a weakly nonlinear wave scattering problem, formulated in terms of a Boussinesq-type equation with piecewise-constant coefficients subject to two continuity conditions across the jump and some natural radiation conditions. In this chapter, we first use the procedure of averaging with respect to the fast time variable to obtain a hierarchy of asymptotically exact coupled and uncoupled Ostrovsky equations for the cases when the characteristic linear speeds of the two wave operators in (3.2) are close or essentially different ('strong' or 'weak' interactions in the terminology of [45, 86, 87]). More precisely, to leading order we derive four uncoupled Ostrovsky equations when $c - 1 = O(1)$, but two coupled systems of Ostrovsky equations when $c - 1 = O(\epsilon)$. We then show how to construct the weakly nonlinear solution of the IVP in terms of solutions of the derived Ostrovsky equations within the accuracy of the cRB equations (3.2). We also establish that corrections to leading order terms are nonsecular due to a special property of the solutions of the Ostrovsky equation. In the absence of coupling ($\delta = \gamma = 0$), these results yield a weakly nonlinear solution of the IVP for the Boussinesq equation in terms of solutions of the IVPs for two KdV equations; this case is examined in more detail in the following chapter. Finally, we perform numerical simulations of the original unapproximated system (3.2) to show the difference in the asymptotic behaviour of the solutions, when initial conditions are taken in the form of co-propagating solitary waves of the uncoupled equations. The numerical results support the developed theory.

The word 'hierarchy' is used here to reflect on the growing complexity of the leading order asymptotic models. In particular, generalisation to the case of N coupled Boussinesq-type equations (describing, for example, long longitudinal waves in an N-layered elastic waveguide, or waves in N coupled FPU chains), with N characteristic speeds close to each other, will lead to a system of N coupled Ostrovsky equations.

From the studies of solitary waves in [45, 86, 87] and the recent studies of the dynamics of weakly nonlinear wave packets [47] we know that the dynamics and the asymptotic models depend on the relative speeds of the waves. A question arises, to what extent does the difference between the characteristic linear speeds of the two wave operators (i.e., $c-1$) effect the dynamics of the nonlinear waves in (3.2)? In particular, if we take initial conditions in the form of the solitary wave solutions of the uncoupled Boussinesq equations, will the outcome be different for the cases $c-1=O(\epsilon)$ and $c-1=O(1)$, where ϵ is the natural small parameter of the Boussinesq model? The following analysis shows that this difference is crucial.

3.2 Weakly nonlinear solution of the initial-value problem

In this section we are concerned with unidirectional waves, which constitute the leading order terms in the asymptotic multiple-scales expansions. We use an averaging procedure which allows us to derive asymptotic reductions to simpler asymptotically exact models in the form of coupled and uncoupled Ostrovsky equations, and construct a weakly nonlinear solution of the IVP in terms of solutions of the derived Ostrovsky equations.

For these purposes we need to rewrite system (3.2) in the original unscaled form

$$\begin{aligned} f_{tt}-f_{xx} &= \epsilon\left[\frac{1}{2}(f^2)_{xx}+f_{ttxx}-\delta(f-g)\right]+O(\epsilon^2),\\ g_{tt}-c^2g_{xx} &= \epsilon\left[\frac{1}{2}\alpha(g^2)_{xx}+\beta g_{ttxx}+\gamma(f-g)\right]+O(\epsilon^2). \end{aligned} \tag{3.3}$$

The previous system of cRB equations (3.2) is obtained by truncating the cRB equations (3.3) and implementing the substitution (and also omitting the tildes)

$$\tilde{f}=\epsilon f,\quad \tilde{g}=\epsilon g,\quad t=\sqrt{\epsilon}\tilde{t},\quad x=\sqrt{\epsilon}\tilde{x},\quad \tilde{\delta},=\epsilon^2\delta\quad \tilde{\gamma}=\epsilon^2\gamma.$$

As with any Boussinesq-type model, system (3.3) appears as an approximation containing $O(1)$ and $O(\epsilon)$ terms (see [76]).

We consider the Cauchy problem for the system of cRB equations (3.3) on the infinite line, imposing the following initial conditions:

$$f|_{t=0} = F(x), \quad g|_{t=0} = G(x), \tag{3.4}$$

$$f_t|_{t=0} = V(x), \quad g_t|_{t=0} = W(x). \tag{3.5}$$

Some local existence results applicable to this problem were recently obtained in [34] (Theorem 2.4 and Remark 2.5, according to [39]). In this chapter we are concerned with the 'explicit' construction of the weakly nonlinear solution of the Cauchy problem in terms of asymptotically exact (KdV-like) models for unidirectional waves.

We assume that the initial conditions are sufficiently rapidly decaying at both infinities, so that to leading order the initial ($t = O(1)$) evolution of the Cauchy data is described by the classical d'Alembert's solution

$$f_0(t,x) = f_0^-(x-t) + f_0^+(x+t), \quad g_0(t,x) = g_0^-(x-ct) + g_0^+(x+ct),$$

where

$$f_0^\pm(x \pm t) = \frac{1}{2}\left(F(x \pm t) \pm \int_{-\infty}^{x\pm t} V(x)dx\right), \tag{3.6}$$

$$g_0^\pm(x \pm ct) = \frac{1}{2}\left(G(x \pm ct) \pm \frac{1}{c}\int_{-\infty}^{x\pm ct} W(x)dx\right). \tag{3.7}$$

In general, $f_0^\pm$ and $g_0^\pm$ are some step-like functions. In what follows we restrict the considerations to the case when these functions are sufficiently rapidly decaying 42 $\int_{-\infty}^{\infty} V(x)dx = 0$ and $\int_{-\infty}^{\infty} W(x)dx = 0$).

To describe the subsequent ($t = O(\epsilon^{-1})$) evolution of the given initial data we introduce the slow time $T = \epsilon t$ and look for the weakly nonlinear solution of the Cauchy problem (3.3)–(3.5) in the form of asymptotic multiple-scales expansions. The form of these expansions depends on the difference between the characteristic speeds of the linear wave operators in system (3.3), thus we next consider the two main cases: when $c - 1 = O(\epsilon)$ and $c - 1 = O(1)$.

3.2.1 Strong interactions: $c - 1 = O(\epsilon)$

In this case, we rewrite system (3.3) as

$$\begin{aligned} f_{tt} - f_{xx} &= \epsilon\left[\frac{1}{2}(f^2)_{xx} + f_{ttxx} - \delta(f-g)\right], \\ g_{tt} - g_{xx} &= \epsilon\left[\frac{1}{2}\alpha(g^2)_{xx} + \beta g_{ttxx} + \gamma(f-g) + \frac{c^2-1}{\epsilon}g_{xx}\right], \end{aligned} \tag{3.8}$$

where $\frac{c^2-1}{\epsilon} \sim O(1)$ since $c-1=O(\epsilon)$, and look for the solution in the form

$$\begin{aligned} f &= f^-(\xi,T) + f^+(\eta,T) + \epsilon f^1(\xi,\eta,T) + O(\epsilon^2), \\ g &= g^-(\xi,T) + g^+(\eta,T) + \epsilon g^1(\xi,\eta,T) + O(\epsilon^2). \end{aligned} \tag{3.9}$$

We define $\xi = x - t$, $\eta = x + t$, $T = \epsilon t$, and consider each wave in its own reference frame. We view the leading order approximation of the linear solution (3.6) and (3.7) (for the case $c-1=O(\epsilon)$, c is replaced with 1) as initial conditions for the functions f^-, f^+, g^-, g^+ with respect to the slow time variable T, i.e.

$$f^\pm|_{T=0} = f_0^\pm, \quad g^\pm|_{T=0} = g_0^\pm, \tag{3.10}$$

(this is later derived at leading order, when we substitute the asymptotic expansions into the initial conditions (3.4) and (3.5)).

Substituting expansions (3.9) into (3.8), we find that the equations are satisfied at leading order, while at $O(\epsilon)$ we obtain

$$\begin{aligned} -4f^1_{\xi\eta} &= (2f^-_T + f^-f^-_\xi + f^-_{\xi\xi\xi})_\xi + (-2f^+_T + f^+f^+_\eta + f^+_{\eta\eta\eta})_\eta \\ &+ 2f^-_\xi f^+_\eta + f^+f^-_{\xi\xi} + f^-f^+_{\eta\eta} - \delta(f^- + f^+ - g^- - g^+), \end{aligned} \tag{3.11}$$

$$\begin{aligned} -4g^1_{\xi\eta} &= (2g^-_T + \alpha g^-g^-_\xi + \beta g^-_{\xi\xi\xi})_\xi + (-2g^+_T + \alpha g^+g^+_\eta + \beta g^+_{\eta\eta\eta})_\eta \\ &+ \alpha(2g^-_\xi g^+_\eta + g^+g^-_{\xi\xi} + g^-g^+_{\eta\eta}) + \gamma(f^- + f^+ - g^- - g^+) \\ &+ \frac{c^2-1}{\epsilon}(g^-_{\xi\xi} + g^+_{\eta\eta}). \end{aligned} \tag{3.12}$$

We next average equations (3.11) and (3.12) with respect to the fast time variable t (see for example [8]), by taking

$$\lim_{\tau\to\infty} \frac{1}{\tau} \int_0^\tau \dots dt$$

at constant ξ or η, i.e. in the reference frame moving with the linear speed of the right- or left-propagating waves, respectively. Indeed, requiring that f^1, g^1 and their derivatives remain bounded (which is necessary to avoid the appearance of secular terms in expansions (3.9)), we see that, for example at constant ξ,

$$\lim_{\tau\to\infty} \frac{1}{\tau} \int_0^\tau f^1_{\xi\eta} dt = \lim_{\tau\to\infty} \frac{1}{2\tau} \int_\xi^{\xi+2\tau} f^1_{\xi\eta} d\eta = \lim_{\tau\to\infty} \frac{1}{2\tau} \left[f^1_\xi\right]_\xi^{\xi+2\tau} = 0.$$

We find similar results for g^1, as well as for f^1 and g^1 at constant η, showing that the averaging results in zeros in the left-hand sides of (3.11) and (3.12). Assuming that

the functions f^-, f^+, g^-, g^+ and their derivatives remain bounded and are sufficiently rapidly decaying at infinity for any fixed T (the assumptions are consistent with relevant numerical experiments), and averaging the entire equation (3.11) with respect to t at constant ξ, we obtain

$$\begin{aligned}
0 = &\left(2f_T^- + f^- f_\xi^- + f_{\xi\xi\xi}^-\right)_\xi - \delta(f^- - g^-) \\
+ &\lim_{\tau\to\infty}\frac{1}{\tau}\int_0^\tau [(-2f_T^+ + f^+ f_\eta^+ + f_{\eta\eta\eta}^+)_\eta + 2f_\xi^- f_\eta^+ + f^+ f_{\xi\xi}^- + f^- f_{\eta\eta}^+ - \delta(f^+ - g^+)]dt \\
= &\left(2f_T^- + f^- f_\xi^- + f_{\xi\xi\xi}^-\right)_\xi - \delta(f^- - g^-) + \lim_{\tau\to\infty}\frac{1}{2\tau}\int_\xi^{\xi+2\tau}\Big[(-2f_T^+ + f^+ f_\eta^+ + f_{\eta\eta\eta}^+)_\eta \\
+ &2f_\xi^- f_\eta^+ + f^+ f_{\xi\xi}^- + f^- f_{\eta\eta}^+ - \delta(f^+ - g^+)\Big]d\eta \\
= &\left(2f_T^- + f^- f_\xi^- + f_{\xi\xi\xi}^-\right)_\xi - \delta(f^- - g^-),
\end{aligned} \tag{3.13}$$

while averaging (3.12) at constant ξ results in

$$0 = \left(2g_T^- + \alpha g^- g_\xi^- + \beta g_{\xi\xi\xi}^-\right)_\xi + \gamma(f^- - g^-) + \frac{c^2-1}{\epsilon}g_{\xi\xi}^-. \tag{3.14}$$

Similarly, averaging (3.11) at constant η under the same assumptions yields

$$0 = \left(-2f_T^+ + f^+ f_\eta^+ + f_{\eta\eta\eta}^+\right)_\eta - \delta(f^+ - g^+), \tag{3.15}$$

while averaging (3.12) at constant η results in

$$0 = \left(-2g_T^+ + \alpha g^+ g_\eta^+ + \beta g_{\eta\eta\eta}^+\right)_\eta + \gamma(f^+ - g^+) + \frac{c^2-1}{\epsilon}g_{\eta\eta}^+. \tag{3.16}$$

Thus, to leading order we obtain two systems of coupled Ostrovsky equations.

Substituting equations (3.13)–(3.16) back into equations (3.11) and (3.12), we obtain the following equations for the higher order corrections:

$$f_{\xi\eta}^1 = -\frac{1}{4}\left(2f_\xi^- f_\eta^+ + f^+ f_{\xi\xi}^- + f^- f_{\eta\eta}^+\right), \quad g_{\xi\eta}^1 = -\frac{\alpha}{4}\left(2g_\xi^- g_\eta^+ + g^+ g_{\xi\xi}^- + g^- g_{\eta\eta}^+\right),$$

which imply

$$\begin{aligned}
f^1 &= -\frac{1}{4}\left(2f^- f^+ + f_\xi^-\int_{-\infty}^\eta f^+ d\tilde{\eta} + f_\eta^+\int_{-\infty}^\xi f^- d\tilde{\xi}\right) + \phi_1(\xi,T) + \psi_1(\eta,T), \\
g^1 &= -\frac{\alpha}{4}\left(2g^- g^+ + g_\xi^-\int_{-\infty}^\eta g^+ d\tilde{\eta} + g_\xi^+\int_{-\infty}^\eta g^- d\tilde{\xi}\right) + \phi_2(\xi,T) + \psi_2(\eta,T),
\end{aligned}$$

where $\phi_{1,2}$, $\psi_{1,2}$ are four arbitrary functions. The presence of four arbitrary functions allows us to satisfy not only the equations, but also the initial conditions (3.4) and

(3.5) up to $O(\epsilon^2)$, constructing therefore an accurate asymptotic solution of the IVP (within the accuracy of the problem formulation).

Indeed, substituting the expansions (3.9) into the initial conditions (3.4) and (3.5) to leading order we recover formulae (3.10) for the initial conditions, while at $O(\epsilon)$ we obtain d'Alembert-like formulae for the functions $\phi_i(\xi,T)$ and $\psi_i(\eta,T), i=1,2$:

$$\phi_i(\xi,T)=\frac{1}{2}\left[R_{i1}(\xi,T)+\int_{-\infty}^{\xi}R_{i2}(x,T)dx\right],$$
$$\psi_i(\eta,T)=\frac{1}{2}\left[R_{i1}(\eta,T)-\int_{-\infty}^{\eta}R_{i2}(x,T)dx\right], \tag{3.17}$$

where

$$R_{11}(x,T)=\frac{1}{4}\left[2f^-f^+ + f^-_{\xi}\int_{-\infty}^{\eta}f^+d\tilde{\eta}+f^+_{\eta}\int_{-\infty}^{\xi}f^-d\tilde{\xi}\right]_{t=0},$$
$$R_{12}(x,T)=\left[f^-_T+f^+_T+\frac{1}{4}\left(f^+f^-_{\xi}-f^-f^+_{\eta}+f^-_{\xi\xi}\int_{-\infty}^{\eta}f^+d\tilde{\eta}-f^+_{\eta\eta}\int_{-\infty}^{\xi}f^-d\tilde{\xi}\right)\right]_{t=0},$$
$$R_{21}(x,T)=\frac{\alpha}{4}\left[2g^-g^+ + g^-_{\xi}\int_{-\infty}^{\eta}g^+d\tilde{\eta}+g^+_{\eta}\int_{-\infty}^{\xi}g^-d\tilde{\xi}\right]_{t=0},$$
$$R_{22}(x,T)=\left[g^-_T+g^+_T+\frac{\alpha}{4}\left(g^+g^-_{\xi}-g^-g^+_{\eta}+g^-_{\xi\xi}\int_{-\infty}^{\eta}g^+d\tilde{\eta}-g^+_{\eta\eta}\int_{-\infty}^{\xi}g^-d\tilde{\xi}\right)\right]_{t=0}.$$

Within the accuracy of the problem formulation (i.e. $O(\epsilon^2)$), the dependence of functions ϕ and ψ on the characteristic variables is determined, while their dependence on the slow time variable T is inherited from their dependence on the leading order waves, or it may be neglected, at least for sufficiently small values of time. In order to determine the dependence on T one needs to consider higher $O(\epsilon^2)$ terms. This is discussed in Chapter 5.

The leading order systems of coupled Ostrovsky equations for unidirectional waves can be rewritten in a symmetric form if we use the reference frame moving with the average linear speed $\bar{c}=\frac{c+1}{2}$, i.e. we formally change ξ and η in (3.13)–(3.16) to $\bar{\xi}=\xi-\Delta\bar{c}T$ and $\bar{\eta}=\eta+\Delta\bar{c}T$, where $\Delta=\frac{c-1}{2\epsilon}$, which yields

$$\left[2(f^-_T-\Delta\bar{c}f^-_{\bar{\xi}})+f^-f^-_{\bar{\xi}}+f^-_{\bar{\xi}\bar{\xi}\bar{\xi}}\right]_{\bar{\xi}}=\delta(f^--g^-),$$
$$\left[2(g^-_T+\Delta\bar{c}g^-_{\bar{\xi}})+\alpha g^-g^-_{\bar{\xi}}+\beta g^-_{\bar{\xi}\bar{\xi}\bar{\xi}}\right]_{\bar{\xi}}=-\gamma(f^--g^-),$$

and

$$\left[2(f^+_T+\Delta\bar{c}f^+_{\bar{\eta}})-f^+f^+_{\bar{\eta}}-f^+_{\bar{\eta}\bar{\eta}\bar{\eta}}\right]_{\bar{\eta}}=-\delta(f^+-g^+),$$
$$\left[2(g^+_T-\Delta\bar{c}g^+_{\bar{\eta}})-\alpha g^+g^+_{\bar{\eta}}-\beta g^+_{\bar{\eta}\bar{\eta}\bar{\eta}}\right]_{\bar{\eta}}=\gamma(f^+-g^+).$$

Systems of coupled KdV equations have appeared in the literature before (see [41, 45] and references therein). To the best of our knowledge this is the first appearance of the coupled Ostrovsky equations.

3.2.2 Weak interactions: $c - 1 = O(1)$

In this case, we look for the solution in a different form:

$$\begin{aligned} f &= f^-(\xi_1, T) + f^+(\eta_1, T) + \epsilon f^1(\xi_1, \eta_1, T) + O(\epsilon^2), \\ g &= g^-(\xi_2, T) + g^+(\eta_2, T) + \epsilon g^1(\xi_2, \eta_2, T) + O(\epsilon^2), \end{aligned} \tag{3.18}$$

where $\xi_1 = x - t$, $\eta_1 = x + t$, and $\xi_2 = x - ct$, $\eta_2 = x + ct$ are the two pairs of characteristic variables for the two linear wave operators in (3.3), and again, we consider each wave in its own reference frame.

Substituting expansions (3.18) into (3.3) we obtain

$$\begin{aligned} -4f^1_{\xi_1\eta_1} &= (2f^-_T + f^- f^-_{\xi_1} + f^-_{\xi_1\xi_1\xi_1})_{\xi_1} + (-2f^+_T + f^+ f^+_{\eta_1} + f^+_{\eta_1\eta_1\eta_1})_{\eta_1} \\ &+ 2f^-_{\xi_1} f^+_{\eta_1} + f^+ f^-_{\xi_1\xi_1} + f^- f^+_{\eta_1\eta_1} - \delta(f^- + f^+ - g^- - g^+), \end{aligned} \tag{3.19}$$

$$\begin{aligned} -4c^2 g^1_{\xi_2\eta_2} &= (2cg^-_T + \alpha g^- g^-_{\xi_2} + \beta c^2 g^-_{\xi_2\xi_2\xi_2})_{\xi_2} + (-2cg^+_T + \alpha g^+ g^+_{\eta_2} + \beta c^2 g^+_{\eta_2\eta_2\eta_2})_{\eta_2} \\ &+ \alpha(2g^-_{\xi_2} g^+_{\eta_2} + g^+ g^-_{\xi_2\xi_2} + g^- g^+_{\eta_2\eta_2}) + \gamma(f^- + f^+ - g^- - g^+). \end{aligned} \tag{3.20}$$

Under the same assumptions as in the first case, we average (3.19) and (3.20) with respect to t, by taking

$$\lim_{\tau\to\infty} \frac{1}{\tau} \int_0^\tau \dots dt,$$

at constant ξ_1 or η_1, and ξ_2 or η_2, respectively. In this case we obtain the following four uncoupled Ostrovsky equations:

$$(2f^-_T + f^- f^-_{\xi_1} + f^-_{\xi_1\xi_1\xi_1})_{\xi_1} = \delta f^-, \tag{3.21}$$

$$(2f^+_T - f^+ f^+_{\eta_1} - f^+_{\eta_1\eta_1\eta_1})_{\eta_1} = -\delta f^+, \tag{3.22}$$

$$(2cg^-_T + \alpha g^- g^-_{\xi_2} + \beta c^2 g^-_{\xi_2\xi_2\xi_2})_{\xi_2} = \gamma g^-, \tag{3.23}$$

$$(2cg^+_T - \alpha g^+ g^+_{\eta_2} - \beta c^2 g^+_{\eta_2\eta_2\eta_2})_{\eta_2} = -\gamma g^+, \tag{3.24}$$

and equations for the higher order corrections as

$$f^1_{\xi_1\eta_1} = -\frac{1}{4}\left(2f^-_{\xi_1} f^+_{\eta_1} + f^+ f^-_{\xi_1\xi_1} + f^- f^+_{\eta_1\eta_1}\right) - \frac{\delta}{4}(g^- + g^+), \tag{3.25}$$

$$g^1_{\xi_2\eta_2} = -\frac{\alpha}{4c^2}\left(2g^-_{\xi_2} g^+_{\eta_2} + g^+ g^-_{\xi_2\xi_2} + g^- g^+_{\eta_2\eta_2}\right) - \frac{\gamma}{4c^2}(f^- + f^+), \tag{3.26}$$

where in the right-hand sides we have solutions of the leading order Ostrovsky equations

$$g^-(\xi_2,T)=g^-\left(\frac{(1+c)\xi_1+(1-c)\eta_1}{2},T\right),\ \ g^+(\eta_2,T)=g^+\left(\frac{(1-c)\xi_1+(1+c)\eta_1}{2},T\right),$$

and

$$f^-(\xi_1,T)=f^-\left(\frac{(c+1)\xi_2+(c-1)\eta_2}{2c},T\right),\ \ f^+(\eta_1,T)=f^+\left(\frac{(c-1)\xi_2+(c+1)\eta_2}{2c},T\right).$$

Remarkably, the particular solutions of (3.25) and (3.26) are bounded functions, because of the special property of smooth solutions of the Ostrovsky equation, namely

$$\int_{-\infty}^{\infty}f^-d\xi_1=0,\quad \int_{-\infty}^{\infty}f^+d\eta_1=0,\quad \int_{-\infty}^{\infty}g^-d\xi_2=0,\quad \int_{-\infty}^{\infty}g^+d\eta_2=0. \tag{3.27}$$

Indeed, the solution of (3.25) and (3.26) can be found in the form

$$\begin{aligned}
f^1 &= -\frac{1}{4}\left(2f^-f^+ + f^-_{\xi_1}\int_{-\infty}^{\eta_1}f^+d\tilde\eta_1 + f^+_{\eta_1}\int_{-\infty}^{\xi_1}f^-d\tilde\xi_1\right) + f_{p1}(\xi_2,T)+f_{p2}(\eta_2,T)\\
&+ \phi_1(\xi_1,T)+\psi_1(\eta_1,T),\\
g^1 &= -\frac{\alpha}{4c^2}\left(2g^-g^+ + g^-_{\xi_2}\int_{-\infty}^{\eta_2}g^+d\tilde\eta_2 + g^+_{\eta_2}\int_{-\infty}^{\xi_2}g^-d\tilde\xi_2\right) + g_{p1}(\xi_1,T)+g_{p2}(\eta_1,T)\\
&+ \phi_2(\xi_2,T)+\psi_2(\eta_2,T),
\end{aligned}$$

where

$$f_{p1}=\frac{\delta}{c^2-1}\int_{-\infty}^{\xi_2}\int_{-\infty}^{v}g^-(u,T)dudv,\qquad f_{p2}=\frac{\delta}{c^2-1}\int_{-\infty}^{\eta_2}\int_{-\infty}^{v}g^+(u,T)dudv,$$
$$g_{p1}=-\frac{\gamma}{c^2-1}\int_{-\infty}^{\xi_1}\int_{-\infty}^{v}f^-(u,T)dudv,\quad g_{p2}=-\frac{\gamma}{c^2-1}\int_{-\infty}^{\eta_1}\int_{-\infty}^{v}f^+(u,T)dudv.$$

Let us then consider for example the particular solution f_{p1} and note $\int_{-\infty}^{\infty}g^-(u,T)du=0$, because of the aforementioned property of the Ostrovsky equation, immediately obtained by integrating (3.23). Furthermore, using (3.23) and recalling that solutions are decaying at infinity, we obtain

$$\begin{aligned}
\int_{-\infty}^{\infty}\int_{-\infty}^{v}g^-(u,T)dudv &= \frac{1}{\gamma}\int_{-\infty}^{\infty}(2cg^-_T+\alpha g^-g^-_v+\beta c^2g^-_{vvv})dv\\
&= \frac{2c}{\gamma}\frac{d}{dT}\int_{-\infty}^{\infty}g^-(v,T)dv=0.
\end{aligned}$$

Therefore, the particular solution f_{p1} is a bounded function, and $\lim\limits_{\xi_2\to\pm\infty}f_{p1}=0$. Similarly, other particular solutions are also bounded functions and there are no secular terms.

The presence of four arbitrary functions allows us to satisfy the initial conditions with the desired accuracy. Substituting the expansions (3.18) into the initial conditions (3.4) and (3.5), to leading order we again recover formulae (3.10), while at $O(\epsilon)$ we obtain d'Alembert-like formulae for $\phi_i(\xi_i, T)$ and $\psi_i(\eta_i, T), i = 1, 2$:

$$\begin{aligned}
\phi_i(\xi_i, T) &= \frac{1}{2}\left[R_{i1}(\xi_i, T) + \frac{1}{c_i}\int_{-\infty}^{\xi_i} R_{i2}(x, T)dx\right], \\
\psi_i(\eta_i, T) &= \frac{1}{2}\left[R_{i1}(\eta_i, T) - \frac{1}{c_i}\int_{-\infty}^{\eta_i} R_{i2}(x, T)dx\right],
\end{aligned} \tag{3.28}$$

where $c_1 = 1, c_2 = c$ and

$$\begin{aligned}
R_{11}(x,T) &= \frac{1}{4}\left[2f^-f^+ + f^-_{\xi_1}\int_{-\infty}^{\eta_1} f^+ d\tilde{\eta}_1 + f^+_{\eta_1}\int_{-\infty}^{\xi_1} f^- d\tilde{\xi}_1\right]_{t=0} \\
&- \frac{\delta}{c^2-1}\int_{-\infty}^{x}\int_{-\infty}^{v}\left[g^-(u,T) + g^+(u,T)\right]dudv, \\
R_{12}(x,T) &= \left[f^-_T + f^+_T + \frac{1}{4}\left(f^+f^-_{\xi_1} - f^-f^+_{\eta_1} + f^-_{\xi_1\xi_1}\int_{-\infty}^{\eta_1} f^+ d\tilde{\eta}_1 - f^+_{\eta_1\eta_1}\int_{-\infty}^{\xi_1} f^- d\tilde{\xi}_1\right)\right]_{t=0} \\
&- \frac{\delta c}{c^2-1}\int_{-\infty}^{x}\left[g^-(u,T) - g^+(u,T)\right]du, \\
R_{21}(x,T) &= \frac{\alpha}{4c^2}\left[2g^-g^+ + g^-_{\xi_2}\int_{-\infty}^{\eta_2} g^+ d\tilde{\eta}_2 + g^+_{\eta_2}\int_{-\infty}^{\xi_2} g^- d\xi_2\right]_{t=0} \\
&+ \frac{\gamma}{c^2-1}\int_{-\infty}^{x}\int_{-\infty}^{v}\left[f^-(u,T) + f^+(u,T)\right]dudv, \\
R_{22}(x,T) &= \left[g^-_T + g^+_T + \frac{\alpha}{4c}\left(g^+g^-_{\xi_2} - g^-g^+_{\eta_2} + g^-_{\xi_2\xi_2}\int_{-\infty}^{\eta_2} g^+ d\tilde{\eta}_2 - g^+_{\eta_2\eta_2}\int_{-\infty}^{\xi_2} g^- d\tilde{\xi}_2\right)\right]_{t=0} \\
&+ \frac{\gamma}{c^2-1}\int_{-\infty}^{x}\left[f^-(u,T) - f^+(u,T)\right]du.
\end{aligned}$$

In both cases $c - 1 = O(\epsilon)$ and $c - 1 = O(1)$, the asymptotic multiple-scales expansions and the averaging procedure described above have allowed us to construct a nonsecular weakly nonlinear solution of the given IVP for the values of time up to $O(\epsilon^{-1})$, within the accuracy of the problem formulation. To construct a more accurate solution, and for greater values of time, one would need to know higher order terms in the original cRB equations (3.3). However, the derived hierarchy of Ostrovsky equations will still describe the leading order terms in the solutions, hence making the study of the long-time evolution of the solutions interesting.

To finish this section, we would like to make an important comment that although smooth solutions of the Ostrovsky equation must satisfy the 'zero mass' constraints

(3.27) (and similar conditions $\int_{-\infty}^{\infty}(f^- - g^-)\, d\bar{\xi} = 0$ etc., in the case of coupled Ostrovsky equations derived in Section 3.2.1), this does not impose any forbidding restrictions on the choice of the initial conditions (3.4) and (3.5) for the cRB system (3.3). Indeed, initial conditions for the Ostrovsky equation can always be modified by adding a long but very small amplitude (i.e. $O(\epsilon^2)$ or smaller) 'pedestal' (e.g., $O(\epsilon^n)$ constant over the finite $O(\epsilon^{-n})$ interval, $n \geq 2$), so that the composite initial condition has zero mass. This does not lower the accuracy of the asymptotic solution and a transition to the zero mass solution is very fast (see the relevant discussion in [53]). Moreover numerical simulations for the Ostrovsky equation show that if a smooth initial condition has a nonzero mass, numerically the solution adjusts immediately, since this initial condition can be viewed as an approximation to the composite zero mass solution (with any given accuracy). Note that similar issues have appeared in connection with several other equations, for example the Kadomtsev-Petviashvili equation (see [4]) and more recently the short-pulse equation (see [58]), where the notion of the 'initial time layer' has been introduced to describe such transitions [4] (see also [53] and references therein).

3.3 Numerical simulations

In this section we discuss numerical simulations of solutions of system (3.2). We implement a finite difference scheme which is an extension of the scheme developed in [106] for a single regularised Boussinesq equation. Derivations of the finite difference scheme including stability and accuracy discussions are detailed in Appendix A. The emphasis in this section is to compare the numerical solutions for the two cases discussed in the previous section, i.e. when the difference in the characteristic speeds of the system is of $O(1)$ or $O(\epsilon)$.

We let $x \in [-L, L]$, for finite L, and discretise the (x, t) domain into a grid with spacings $\Delta x = h$ and $\Delta t = \kappa$. The solutions $f(x, t)$ and $g(x, t)$ of the cRB equations (3.2) are approximated by the solutions $f(ih, j\kappa)$ and $g(ih, j\kappa)$ (for $i = 0, 1, ..., N$ and $j = 0, 1, ...$) of the difference scheme, denoted $f_{i,j}$ and $g_{i,j}$. We derive the following

difference scheme for system (3.2) (see Appendix A.2):

$$\begin{aligned}-f_{i-1,j+1}+(2+h^2)f_{i,j+1}-f_{i+1,j+1} = {} & (\kappa^2-2)[f_{i-1,j}-2f_{i,j}+f_{i+1,j}]+2h^2 f_{i,j}\\ & +\frac{\kappa^2}{2}[(f_{i-1,j})^2-2(f_{i,j})^2+(f_{i+1,j})^2]\\ & +f_{i-1,j-1}-(2+h^2)f_{i,j-1}+f_{i+1,j-1}\\ & -h^2\kappa^2\delta(f_{i,j}-g_{i,j}),\end{aligned} \tag{3.29}$$

$$\begin{aligned}-\beta g_{i-1,j+1}+(2\beta+h^2)g_{i,j+1}-\beta g_{i+1,j+1} = {} & (\kappa^2c^2-2\beta)[g_{i-1,j}-2g_{i,j}+g_{i+1,j}]+2h^2 g_{i,j}\\ & +\frac{\alpha\kappa^2}{2}[(g_{i-1,j})^2-2(g_{i,j})^2+(g_{i+1,j})^2]\\ & +\beta g_{i-1,j-1}-(2\beta+h^2)g_{i,j-1}+\beta g_{i+1,j-1}\\ & +h^2\kappa^2\gamma(f_{i,j}-g_{i,j}).\end{aligned} \tag{3.30}$$

We impose zero boundary conditions, far enough from the propagating waves, thus:

$$f_{0,j}=f_{N,j}=g_{0,j}=g_{N,j}=0, \quad \forall j. \tag{3.31}$$

The initial conditions are chosen in the form of the co-propagating pure solitary wave solutions of the uncoupled equations (in which case $\delta=\gamma=0$):

$$\begin{aligned} f_{i,0} &= A_1\,\mathrm{sech}^2\left(\frac{ih}{\Lambda_1}\right), \qquad f_{i,1}=A_1\,\mathrm{sech}^2\left(\frac{ih-v_1\kappa}{\Lambda_1}\right),\\ g_{i,0} &= A_2\,\mathrm{sech}^2\left(\frac{ih}{\Lambda_2}\right), \qquad g_{i,1}=A_2\,\mathrm{sech}^2\left(\frac{ih-v_2\kappa}{\Lambda_2}\right), \quad \forall i, \end{aligned} \tag{3.32}$$

where $A_1=3(v_1^2-1)$, $A_2=\frac{3}{\alpha}(v_2^2-c^2)$, $\Lambda_1=2v_1(v_1^2-1)^{-\frac{1}{2}}$ and $\Lambda_2=2v_2\sqrt{\beta}(v_2^2-c^2)^{-\frac{1}{2}}$. The nine point implicit difference schemes (3.29) and (3.30), with tridiagonal matrices of constant coefficients, are solved simultaneously using a Thomas Algorithm (e.g., [6]).

Using a von Neumann stability analysis on the single regularised Boussinesq equation with arbitrary coefficients (i.e. system (3.2) for $\delta=\gamma=0$ and $f=0$), we find to ensure stability we require the step size restriction $\kappa<\kappa_c=\sqrt{\frac{h^2+4\beta}{c^2+\alpha g_0}}$ (see Appendix A.1.3), where g_0 is a constant introduced to linearise $g_{i,j}$ such that $g_0>g_{i,j}\ \forall i,j$. It can also be shown that the principal truncation error of the single regularised Boussinesq equation with arbitrary coefficients is $O(h^2\kappa^4+h^4\kappa^2)$ (see Appendix A.1.2).

Numerical simulations for the symmetric case (scheme (3.29) with $\delta=0$) compared with the known analytical solution (2.30) reveal that the choice of discretisation can

reduce the maximum absolute error, across x for a given time, to as low as $O(10^{-5})$ (for amplitude $O(1)$). This accuracy is within the range which is deemed suitable from previous work on Boussinesq-type equations (e.g. see [18, 37, 38, 54, 61, 89, 93]). The step size $h = \kappa = 0.01$ results in errors of this order and is thus chosen for simulations in this section. We numerically approximate $u(x,t)$ and $w(x,t)$ (the original variables in the cRB equations (3.1)) via Simpson's rule using the relationship $\int_{-L}^{x} f, g \; dx = u, w$, due to the boundary conditions (3.31), and hence utilise the energy conservation law given in Section 2.2 (naturally numerical integration introduces some additional errors). The conserved quantity $\int_{-\infty}^{\infty} A_2 dx$ was monitored and for simulations with $h = \kappa = 0.1$ the energy was conserved, within the chosen time interval, up to 0.021% and 0.006% for the results shown in Figures 3.1 & 3.2, respectively. For smaller step sizes energy conservation computations become very time-consuming, but there is no noticeable difference in the plots of the solutions for $h = \kappa = 0.1$ and $h = \kappa = 0.01$ (useful discussions of the difficulties associated with the accuracy of conservation laws in finite-difference schemes can be found in [24]).

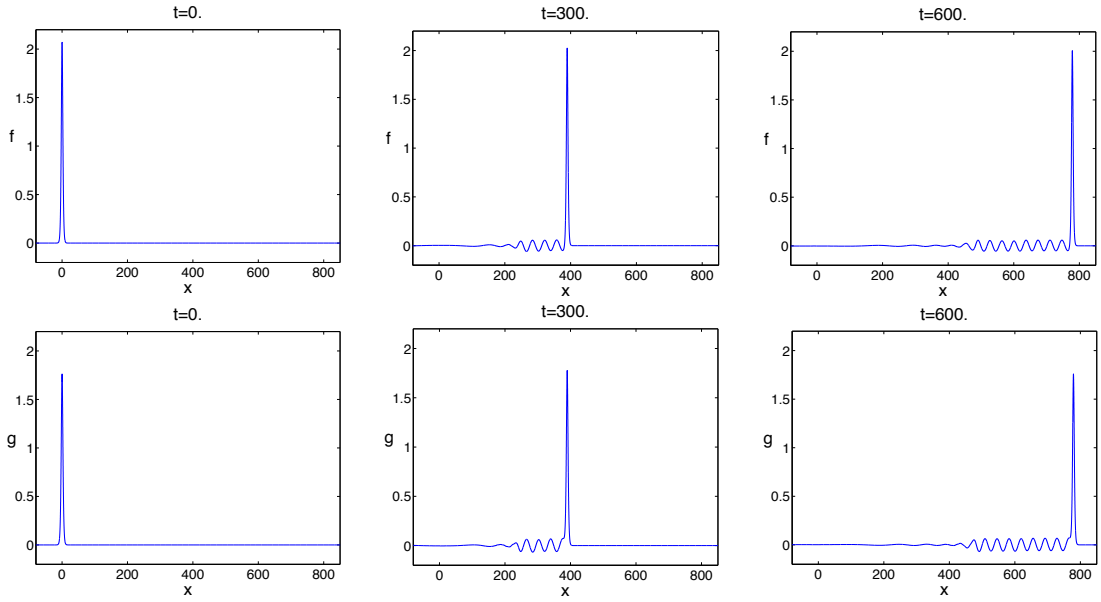

Figure 3.1: Generation of radiating solitary waves for $c = 1.05, \alpha = \beta = 1, \gamma = \delta = 0.01; v_1 = v_2 = 1.3$ from pure solitary waves of the uncoupled equations.

The emergence of radiating solitary waves replacing the initial pure solitary waves

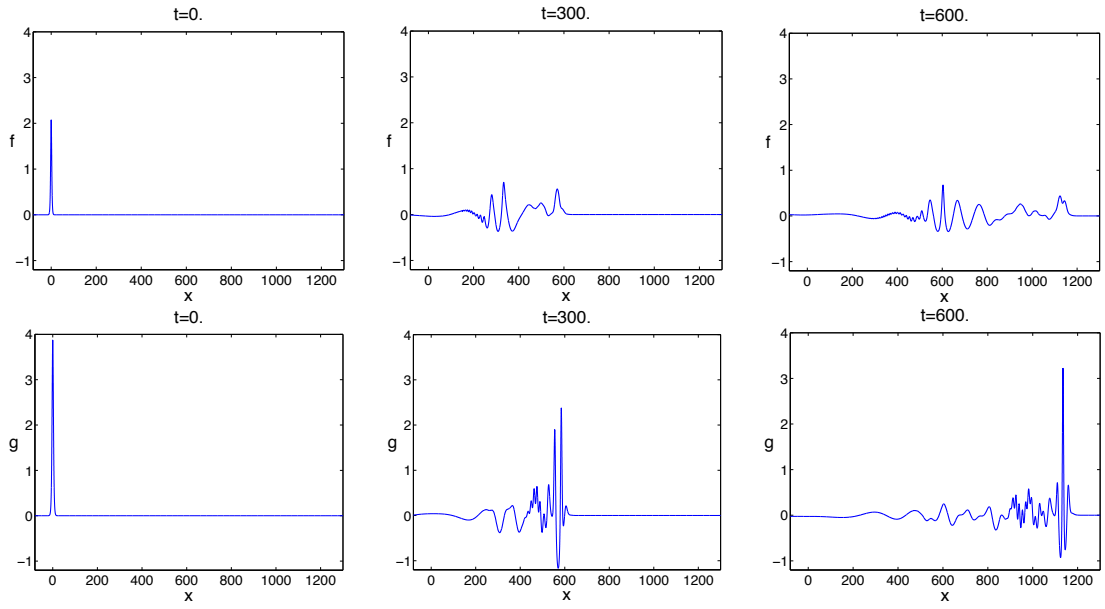

Figure 3.2: Generation of wave packets for $c = 2, \alpha = \beta = 1, \gamma = \delta = 0.01; v_1 = 1.3, v_2 = 2.3$ from pure solitary waves of the uncoupled equations.

in both components of f and g is shown in Figure 3.1 for the case $c = 1.05$, $\alpha = \beta = 1$, $\delta = \gamma = 0.01$; $v_1 = v_2 = 1.3$. These simulations agree with the discussion in Section 2.3 and numerical studies in [76]. The numerically determined wavelength of the oscillatory tail at $t = 300$ is (36.5 ± 0.1) for f and (37.0 ± 0.2) for g, which is close to the theoretical prediction (≈ 36.7) for $p = 1.3$ using the dispersion relation (see Figure 2.7 in Section 2.3).

As the interactions between the waves become weak ($c - 1 = O(1)$), one can see a transition from the radiating solitary wave solutions (as depicted in Figure 3.2) to wave packet type solutions. The amplitude of the leading pure solitary wave in each component starts to decrease and similarly the amplitude of the oscillations in the co-propagating oscillatory tails tend to zero. Once the parameter c is sufficiently increased, the oscillatory tails completely diminish and the leading pure solitary wave in each component forms a stable dominant wave packet.

For the case $c = 2$, $\alpha = \beta = 1$, $\delta = \gamma = 0.01$; $v_1 = 1.3$, $v_2 = 2.3$, the initial solitary waves are replaced by these aforementioned dominant wave packets in both components, shown in Figure 3.2. The emergence of a wave packet in both f and g

can be observed almost instantaneously and for long time appears stable. From the asymptotic analysis for $c-1=O(1)$ in Section 3.2.2 we found that to leading order, the solution for both f and g, for right propagating waves, are the solution to the two Ostrovsky equations (3.21) and (3.23). At $t=600$ in Figure 3.2 the leading wave packet in g qualitatively closely resembles the numerical solution of the Ostrovsky equation studied in [50]. Similarly, at $t=600$ for f a similar but smaller and slower moving wave packet is present at approximately $x=600$. In [50] it is shown that a parameter denoted a_0, equivalent to $a_{f0}=\frac{6(v_1-1)}{\sqrt{\delta}}$ and $a_{g0}=\frac{6(v_2-c)}{\sqrt{\beta\delta}}$ for f and g respectively in the system of cRB equations (3.3), determines whether a distinct wave packet emerges or not. For the simulations shown in Figure 3.2, this aforementioned parameter lies within the range for which the distinctive wave packet will emerge and hence it can be seen in both f and g. As $a_{f0}, a_{g0}\to 0$ there exists a range for which the distinctive wave packet no longer emerges. Alternatively as the parameters a_{f0}, a_{g0} are increased, the faster the wave packet emerges and in the case of g, the faster it will move away from the rest of the solution. The range of a_{f0} and a_{g0} for which this transition occurs is also in very good agreement with the results for the Ostrovsky equation in [50].

The simulations in this section confirm that there is indeed a distinctive difference in the qualitative behaviour of the solution upon varying the difference in the characteristic speeds, and hence support the asymptotic analysis. From the numerics we can conclude that for pure solitary wave initial data in the parameter range $c-1=O(\epsilon)$, stable radiating solitary waves emerge in both components f and g. However as we increase the difference in the characteristic speeds, i.e. let $c-1=O(1)$, we see to leading order the emergence of wave packets in both components f and g, agreeing with the numerical solution of the Ostrovsky equation (for example in [50]).

3.4 Concluding remarks

In this chapter we addressed the question of constructing a weakly nonlinear solution of the IVP for coupled Boussinesq-type equations for localised or sufficiently rapidly decaying initial data, generating sufficiently rapidly decaying right- and left-propagating waves. Crucially, we considered the general case, when the two linear wave operators have different characteristic speeds, which complicates the analysis since in this case the number of characteristic variables (four) is greater than the number of independent

variables (two). Further generalisations to the case of more than two equations (and characteristic speeds) are straightforward.

We introduced two different types of asymptotic multiple-scales expansions for the cases $c-1=O(\epsilon)$ and $c-1=O(1)$ and averaged with respect to the fast time variable, which allowed us to derive, to leading order, a hierarchy of asymptotically exact coupled and uncoupled Ostrovsky equations for unidirectional waves. We then constructed the nonsecular solution of the IVP in terms of solutions of the derived leading order models for the values of time up to $O(\epsilon^{-1})$, within the accuracy of the problem formulation. To construct a more accurate solution, and for greater values of time, one needs to know higher order terms in the original cRB equations (3.3).

We performed numerical simulations of the original unapproximated cRB equations (3.3) for the initial conditions in the form of co-propagating pure solitary waves of the uncoupled equations, and compared the numerical results with known numerical results for the Ostrovsky equation [50], which confirmed predictions of the leading order asymptotic theory. Expanded numerical studies for the cRB system of equations (3.3), and analysis for other types of initial conditions, will follow in subsequent chapters. Later in this thesis we will also directly compare numerical simulations of Ostrovsky-type equations with numerical simulations for the corresponding Boussinesq-type equation, in order to explicitly determine the accuracy of the models as approximations for the corresponding Boussinesq-type equations (see Section 5.3).

The approach developed in this chapter is generic and can be used to construct weakly nonlinear solutions of some other IVPs, and in other physical contexts. In particular the coupled Ostrovsky equations have been recently derived for strongly interacting internal waves in a rotating ocean [5].

For the practical applications of the constructed solution it is useful to remember that within the accuracy of the problem formulation in (3.3) (i.e. $O(\epsilon^2)$), the initial conditions (3.4) and (3.5) can be represented in the form

$$f|_{t=0} = F^0(x) + \epsilon F^1(x) + O(\epsilon^2), \quad g|_{t=0} = G^0(x) + \epsilon G^1(x) + O(\epsilon^2),$$
$$f_t|_{t=0} = V^0(x) + \epsilon V^1(x) + O(\epsilon^2), \quad g_t|_{t=0} = W^0(x) + \epsilon W^1(x) + O(\epsilon^2).$$

This allows one (if needed) to formally satisfy the zero mass constraints for $f_0^{\pm}, g_0^{\pm}$ by adding appropriate $O(\epsilon^2)$ 'pedestal' terms (as explained in Section 3.2). However, it also gives some flexibility with the choice of initial conditions for the auxiliary IVP

problems for unidirectional waves by splitting the functions $F(x), G(x), V(x), W(x)$ into a 'nice' $O(1)$ part (i.e. in the case that the IVP problems have some favourable analytical properties, e.g. from the viewpoint of the IST) and a small $O(\epsilon)$ remainder. This $O(\epsilon)$ remainder can be readily accounted for in the d'Alembert-like formulae (3.17) and (3.28) for the functions ϕ_i and $\psi_i, i = 1, 2$. We expand the weakly nonlinear solution to explicitly include initial conditions of this type in the next chapter.

Finally, we would like to emphasise the importance of the Ostrovsky equation as a canonical asymptotically exact model, similar to the KdV model. The reduced form of the Ostrovsky equation

$$(\eta_t + \nu\eta\eta_x)_x = \lambda\eta$$

was recently shown to be an integrable equation [79, 111], reducible to the Tzitzeica equation [110]. We also believe that the full Ostrovsky equation might have some 'nice' analytical properties (although it is not necessarily integrable in the conventional sense).

Chapter 4

Weakly nonlinear extension of d'Alembert's formula

In this chapter we construct a weakly nonlinear solution of the Cauchy problem for the regularised Boussinesq equation (the case when $\gamma = \delta = 0$ in the cRB equations from the previous chapter), which constitutes an extension of the classical d'Alembert's formula for the linear wave equation. We also generalise the formula in the preceding chapter to account for possible perturbations to 'exactly solvable initial conditions'. The derived weakly nonlinear solution is given by a simple and explicit formula, expressed in terms of two special functions solving the IVPs for two KdV equations, integrable by the IST. We test the formula by considering several examples with exactly solvable initial conditions and also examples with perturbations to these. Explicit analytical solutions are compared directly with the results of numerical simulations of the regularised Boussinesq equation.

The results of this chapter are partially summarised in [73].

4.1 Introduction

The Boussinesq equation and its generalisations, since the original derivation in the context of fluids [15] and reappearance in connection with the famous FPU problem [40, 119], have recently emerged in a vast variety of problems describing nonlinear waves in solids (see, for example, [22, 62, 75, 76, 85, 96, 102]). At the same time, considerable progress has been made in understanding the validity of regularised models and proofs of existence and local well-posedness of the IVP in the context of water waves (see [10, 11, 12, 13, 80] and references therein), while the global well-posedness is known to be a complicated issue [64]. Some progress has also been made in the study of boundary-value problems [42]. Most relevant to the work in this chapter are the results establishing the validity of two KdV equations as a leading order approximation to solutions of Boussinesq-type equations, as well as some results for the higher order corrections [8, 27, 45, 63, 65, 66, 91, 103, 104, 114].

In the previous chapter (see [72] for the full published work) we constructed a weakly nonlinear solution of the IVP for a system of cRB equations on the infinite line, assuming that initial data generates sufficiently rapidly decaying right- and left-propagating waves, in terms of solutions of various Ostrovsky-type equations (see [94] for the original Ostrovsky equation). When coupling parameters are equal to zero, the results yield a simple formula for the weakly nonlinear solution of an IVP for the regularised Boussinesq equation

$$f_{tt} - f_{xx} = \epsilon \left[\frac{1}{2}(f^2)_{xx} + f_{ttxx} \right] + O(\epsilon^2). \tag{4.1}$$

In this chapter we begin in Section 4.2 by generalising the weakly nonlinear solution of the Cauchy problem studied in the previous chapter (see Section 3.2) by considering the case when initial conditions are split into $O(1)$ and $O(\epsilon)$ terms, allowing one to construct explicit analytical solutions for a wider class of initial conditions. We use asymptotic multiple-scales expansions, similar to the type used in the study of oblique interaction of solitary waves [86], and an averaging technique, used for example in [8, 72], to derive asymptotically exact models which describe the leading order terms in the expansions. The leading order terms satisfy the IVP for two KdV equations [78], integrable by the IST [44] (see also [3, 29]). We use two arbitrary functions present in the higher order terms to improve the accuracy of the approximate solution. The

derived formula constitutes a weakly nonlinear extension of the classical d'Alembert's formula for the linear wave equation, and has a similar structure. To the best of our knowledge, such a formula has not been suggested in previous studies. The simple and explicit form of this solution allows one to construct a large class of approximate solutions corresponding to exactly solvable initial conditions (see Section 4.4). The weakly nonlinear approach used in this chapter can be applied to any form of the Boussinesq equation and coupled systems of Boussinesq equations (see [72]) and, in particular, it offers an alternative to implementing the IST to the integrable version of the equation in physically relevant cases.

In Section 4.3 we numerically solve, via the finite difference scheme introduced in Appendix A.1, a scaled version of (4.1), in the form

$$\tilde{f}_{\tilde{t}\tilde{t}} - \tilde{f}_{\tilde{x}\tilde{x}} = \frac{1}{2}(\tilde{f}^2)_{\tilde{x}\tilde{x}} + \tilde{f}_{\tilde{t}\tilde{t}\tilde{x}\tilde{x}}, \tag{4.2}$$

where $\tilde{f} = \epsilon f,\ t = \sqrt{\epsilon}\,\tilde{t},\ x = \sqrt{\epsilon}\,\tilde{x}$. Equation (4.2) has particular solitary wave solutions of the form

$$\tilde{f} = A\ \mathrm{sech}^2\left(\frac{\tilde{x} - v\tilde{t}}{\Lambda}\right), \quad \text{where} \quad A = 3(v^2-1), \quad \Lambda = \frac{2v}{\sqrt{v^2-1}}, \tag{4.3}$$

which we denote f_{sol}. We directly measure the scheme's accuracy by comparing the analytical solution (4.3) to corresponding numerical simulations (denoted f_{num}), at times within the derived asymptotic model's validity, i.e. from $\tilde{t} = 0$ to some point between $\tilde{t} \approx t_a = \frac{1}{\epsilon\sqrt{\epsilon}}$ and $\tilde{t} \approx t_b = \frac{1}{\epsilon^2\sqrt{\epsilon}}$.

In Section 4.4, we explicitly derive the weakly nonlinear solution for exactly solvable initial conditions of the IVP in the form of right-propagating and both right- and left-propagating N-soliton solutions of the KdV equation. Note that these initial conditions do not correspond to the exact soliton solutions of the Boussinesq equation.

In Section 4.5 we consider particular cases of initial conditions, namely one- and two-soliton solutions of the KdV equation, and analyse the absolute error in comparison with relevant numerical simulations. We define the maximum absolute error of the solution at $\tilde{t} = \tau$ as

$$e_\tau^l = \max_{-L\le\tilde{x}\le L} |f_{\mathrm{num}}(\tilde{x},\tau) - \tilde{f}_l(\tilde{x},\tau)|, \quad \text{for} \ \ l = 1, 2,$$

where we restrict $\tilde{x}$ to the finite domain $2L$ and $\tilde{f}_l(\tilde{x},\tilde{t})$ denotes the weakly nonlinear solution up to and including $O(\epsilon^l)$ terms.

In Section 4.6 we consider perturbations to exactly solvable initial conditions of the IVP, in particular for the case of right-propagating N-soliton solutions, and again analyse the error for a specific example. We finish with concluding remarks in Section 4.7.

4.2 Weakly nonlinear solution

We consider the following IVP for a single regularised Boussinesq equation on the infinite line:

$$\begin{aligned} &f_{tt} - f_{xx} = \epsilon\left[\frac{1}{2}(f^2)_{xx} + f_{ttxx}\right] + O(\epsilon^2), \\ &f|_{t=0} = F^0(x) + \epsilon F^1(x) + O(\epsilon^2), \qquad f_t|_{t=0} = V^0(x) + \epsilon V^1(x) + O(\epsilon^2), \end{aligned} \tag{4.4}$$

(or any other asymptotically equivalent form of this equation) for the case when the initial conditions generate sufficiently rapidly decaying right- and left-propagating waves. Therefore to leading order the initial ($t = O(1)$) evolution of the Cauchy data is described by the classical d'Alembert's solution

$$f_0(x,t) = f_0^-(x-t) + f_0^+(x+t) \quad \text{for} \quad f_0^\pm(x \pm t) = \frac{1}{2}\left(F^0(x \pm t) \pm \int_{-\infty}^{x\pm t} V^0(x)dx\right).$$

In general $f_0^\pm$ are some step like functions but in what follows we shall restrict further considerations to the case when these functions are sufficiently rapidly decaying at infinity (in particular, $\int_{-\infty}^{\infty} V^0(x)dx = 0$).

To describe the subsequent ($t = O(\epsilon^{-1})$) evolution of the Cauchy data we introduce the slow time variable $T = \epsilon t$ and seek the following weakly nonlinear solution in the form of asymptotic multiple-scales expansions

$$f = f^-(\xi, T) + f^+(\eta, T) + \epsilon f^1(\xi, \eta, T) + O(\epsilon^2), \tag{4.5}$$

where $\xi = x - t$ and $\eta = x + t$. Substituting (4.5) into the Boussinesq equation (4.4) we find to leading order the equation is satisfied, whilst at $O(\epsilon)$ we obtain

$$\begin{aligned} -4f^1_{\xi\eta} &= (2f^-_T + f^-f^-_\xi + f^-_{\xi\xi\xi})_\xi + (-2f^+_T + f^+f^+_\eta + f^+_{\eta\eta\eta})_\eta \\ &+ 2f^-_\xi f^+_\eta + f^+f^-_{\xi\xi} + f^-f^+_{\eta\eta}. \end{aligned} \tag{4.6}$$

The subsequent derivation can be performed either by integrating (4.6) and requiring that f^1 is nonsecular (see, for example, [45]) or using averaging arguments similar to

the previous chapter (see also [8, 72]). In what follows we use the latter of the two, namely, we average (4.6) with respect to the fast time variable t at constant ξ or η. The left-hand side of (4.6) at constant ξ is averaged as follows

$$\lim_{\tau\to\infty}\frac{1}{\tau}\int_0^\tau f^1_{\xi\eta}dt=\lim_{\tau\to\infty}\frac{1}{2\tau}\int_\xi^{\xi+2\tau} f^1_{\xi\eta}d\eta=\lim_{\tau\to\infty}\frac{1}{2\tau}\left[f^1_\xi\right]_{\eta=\xi}^{\eta=\xi+2\tau}=0,$$

where we assume f^1 and its derivatives remain bounded (required to have a nonsecular expansion (4.5)), and similarly we get zero when averaging the same term at constant η. Averaging entirely over (4.6) at constant ξ and assuming $f^\pm$ and their derivatives remain bounded and are sufficiently rapidly decaying at infinity for any fixed T (consistent with relevant numerical experiments), we obtain

$$\begin{aligned}0 = &\left(2f^-_T+f^-f^-_\xi+f^-_{\xi\xi\xi}\right)_\xi\\ &+\lim_{\tau\to\infty}\frac{1}{2\tau}\left\{\left[-2f^+_T+f^+f^+_\eta+f^+_{\eta\eta\eta}\right]_{\eta=\xi}^{\eta=\xi+2\tau}+\int_\xi^{\xi+2\tau}(2f^-_\xi f^+_\eta+f^+f^-_{\xi\xi}+f^-f^+_{\eta\eta})d\eta\right\}\\ = &\left(2f^-_T+f^-f^-_\xi+f^-_{\xi\xi\xi}\right)_\xi.\end{aligned}$$

Averaging entirely over (4.6) at constant η we derive a similar equation for the function f^+. Integrating each of these equations with respect to their respective characteristic variables, and taking into account the behaviour of $f^\pm$ at infinity, yields the following two KdV equations

$$f^-_T+\frac{1}{2}f^-f^-_\xi+\frac{1}{2}f^-_{\xi\xi\xi}=0,\qquad f^+_T-\frac{1}{2}f^+f^+_\eta-\frac{1}{2}f^+_{\eta\eta\eta}=0. \tag{4.7}$$

The higher order correction f^1 is then obtained by substituting (4.7) into (4.6) to yield

$$f^1=-\frac{1}{4}\left(2f^-f^++f^-_\xi\int_{-\infty}^\eta f^+d\tilde\eta+f^+_\eta\int_{-\infty}^\xi f^-d\tilde\xi\right)+\phi(\xi,T)+\psi(\eta,T), \tag{4.8}$$

where ϕ and ψ are arbitrary functions. Finally, substituting the weakly nonlinear solution (4.5) into the initial conditions of the IVP (4.4), we derive to leading order initial conditions with respect to T, for the leading order terms $f^\pm$

$$f^\pm|_{T=0}=f^\pm_0=\frac{1}{2}\left(F^0(x\pm t)\pm\int_{-\infty}^{x\pm t}V^0(x)dx\right),$$

whilst at $O(\epsilon)$ we obtain, within the accuracy of the problem formulation, the following d'Alembert-like formulae for the functions $\phi(\xi,T)$ and $\psi(\eta,T)$:

$$\phi(\xi,T)=\frac{1}{2}\left[R_1(\xi,T)+\int_{-\infty}^\xi R_2(x,T)dx\right],\quad \psi(\eta,T)=\frac{1}{2}\left[R_1(\eta,T)-\int_{-\infty}^\eta R_2(x,T)dx\right],$$

where

$$R_1(x,T) = \frac{1}{4}\left[2f^-f^+ + f^-_\xi \int_{-\infty}^{\eta} f^+ d\tilde{\eta} + f^+_\eta \int_{-\infty}^{\xi} f^- d\tilde{\xi}\right]_{t=0} + F^1(x), \tag{4.9}$$

$$R_2(x,T) = \left[f^-_T + f^+_T + \frac{1}{4}\left(f^+f^-_\xi - f^-f^+_\eta + f^-_{\xi\xi}\int_{-\infty}^{\eta} f^+ d\tilde{\eta} - f^+_{\eta\eta}\int_{-\infty}^{\xi} f^- d\tilde{\xi}\right)\right]_{t=0} - V^1(x).$$

The dependence of the functions ϕ and ψ on T is either inherited from their dependence on the leading order functions f^- and f^+, or it is neglected, i.e. $R_{1,2}(x,T)$ can be replaced with $R_{1,2}(x,0)$. To construct a more accurate solution, valid for greater values of time, one needs to know higher order terms in the problem formulation (4.4). An alternative way of defining ϕ and ψ's dependence on T is discussed in detail in the next chapter.

4.3 Numerical scheme

We next examine the numerical scheme used to solve the Boussinesq equation (4.2). We implement a finite difference scheme derived in [106] for a regularised Boussinesq equation (see Appendix A.1) or equivalently the scheme used for simulations in Section 3.3 but with the reduction $g = \delta = \gamma = 0$ and $c = \alpha = \beta = 1$.

We let $\tilde{x} \in [-L, L]$, for finite L, and discretise the $(\tilde{x}, \tilde{t})$ domain into a grid with spacings $\Delta\tilde{x} = h$ and $\Delta\tilde{t} = \kappa$. The solution $\tilde{f}(\tilde{x}, \tilde{t})$ of (4.2) is approximated by the solution $f(ih, j\kappa)$ (for $i = 0, 1, ..., N$ and $j = 0, 1, ...$) of the difference scheme, denoted $f_{i,j}$. We consider the following difference scheme for (4.2) (see Appendix A.1):

$$\begin{aligned} -f_{i-1,j+1} + (2+h^2)f_{i,j+1} - f_{i+1,j+1} = {} & (\kappa^2 - 2)[f_{i-1,j} - 2f_{i,j} + f_{i+1,j}] + 2h^2 f_{i,j} \\ & + \frac{\kappa^2}{2}\left[(f_{i-1,j})^2 - 2(f_{i,j})^2 + (f_{i+1,j})^2\right] \\ & + f_{i-1,j-1} - (2+h^2)f_{i,j-1} + f_{i+1,j-1}. \end{aligned} \tag{4.10}$$

We choose zero boundary conditions such that they are sufficiently far away from the propagating waves. Periodic boundary conditions were also considered (see Appendix A.1.1), but for the added complexity and computational effort involved in solving the difference scheme, the difference in the error of the solution was negligible, therefore

$$f_{0,j} = f_{N,j} = 0, \quad \forall j.$$

To directly analyse the error of the difference scheme we choose initial conditions of the IVP (4.4) in the form of the particular Boussinesq soliton solution (4.3), namely

$$f_{i,0} = A\ \mathrm{sech}^2\left(\frac{ih}{\Lambda}\right), \qquad f_{i,1} = A\ \mathrm{sech}^2\left(\frac{ih - v\kappa}{\Lambda}\right), \qquad \forall i,$$

where $A = 3(v^2-1)$, $\Lambda = 2v(v^2-1)^{-\frac{1}{2}}$ and we choose $v \approx \sqrt{\frac{\epsilon}{3}+1}$ to ensure the amplitude is $O(\epsilon)$ (required to make comparisons with the weakly nonlinear solution in the next sections). The nine point implicit difference scheme (4.10), with tridiagonal matrices of constant coefficients, is solved using a Thomas Algorithm (e.g., [6]).

It can be shown from using a von Neumann linear stability analysis (see Appendix A.1.3) that we require the step size restriction $\kappa < \kappa_c = \sqrt{\frac{h^2+4}{1+f_0}}$ to ensure stability of scheme (4.10), where f_0 is a constant introduced to linearise $f_{i,j}$ such that $f_0 > f_{i,j}\ \forall i,j$. It can also be shown that the principal truncation error of scheme (4.10) is $O(h^2\kappa^4 + h^4\kappa^2)$ (see Appendix A.1.2).

For a given h, the step size restriction on κ can be used to determine valid choices of the time discretisation in order to ensure stability. Table 4.1 displays the maximum absolute error across $\tilde{x}$ for different choices of κ for fixed ϵ (and hence fixed v) for two different space step sizes h, and at two different times t_a and t_b (within the asymptotic region of validity of the KdV models (4.7)). The optimal discretisations $h = \kappa = 0.1$ are chosen for subsequent numerical simulations in this chapter, where the maximum absolute error within the time interval considered ranges from $O(10^{-6})$ to $O(10^{-7})$; well within what is considered acceptable in previous numerical studies of such equations.

Figure 4.1 shows the evolution of the numerical solution of scheme (4.10) compared with the particular analytical solution (4.3), along with the respective error plots at each time. It is clear that for this range of time, the numerical solution is in good agreement with the analytical solution.

Table 4.2 depicts the maximum absolute error over $\tilde{x}$ for different ϵ at the corresponding times $\tilde{t} \approx t_a$. This measure of accuracy for the scheme is utilised when analysing the error of the weakly nonlinear solution for particular examples in Sections 4.5 & 4.6.

	Max error at $\tilde{t} = 32$		Max error at $\tilde{t} = 300$	
κ	h=0.1	h=0.01	h=0.1	h=0.01
1	4.4693×10^{-4}	4.5089×10^{-4}	3.3×10^{-3}	3.3×10^{-3}
0.5	8.8851×10^{-5}	1.1299×10^{-4}	7.7082×10^{-4}	4.8012×10^{-4}
0.2	4.4300×10^{-5}	1.8105×10^{-5}	9.7890×10^{-4}	1.2671×10^{-4}
0.1	5.2846×10^{-6}	4.5133×10^{-6}	2.6891×10^{-4}	3.1518×10^{-5}
0.05	2.8857×10^{-6}	1.1439×10^{-6}	2.1081×10^{-5}	8.0360×10^{-6}
0.025	3.7396×10^{-6}	4.3677×10^{-7}	2.7026×10^{-5}	3.2910×10^{-6}
0.0125	3.9559×10^{-6}	9.0239×10^{-7}	2.8532×10^{-5}	1.1751×10^{-6}
0.00625	4.0198×10^{-6}	3.6362×10^{-7}	2.8988×10^{-5}	4.6968×10^{-6}

Table 4.1: Maximum absolute error of the numerical solution compared with the exact solution (4.3) for various time and space discretisations h and κ, with $\epsilon = 0.1$.

ϵ	$\tilde{t}(\approx t_a)$	Max error of $\lvert f_{\text{num}} - f_{\text{sol}} \rvert$
0.1	32	5.2846×10^{-7}
0.075	49	3.6296×10^{-7}
0.05	90	1.3789×10^{-7}
0.025	253	3.4930×10^{-8}
0.0125	716	8.4222×10^{-9}
0.00625	2024	2.3201×10^{-9}

Table 4.2: Maximum absolute error of the numerical solution compared with the exact solution (4.3) at $\tilde{t} \approx t_a$ for $h = \kappa = 0.1$ and various ϵ.

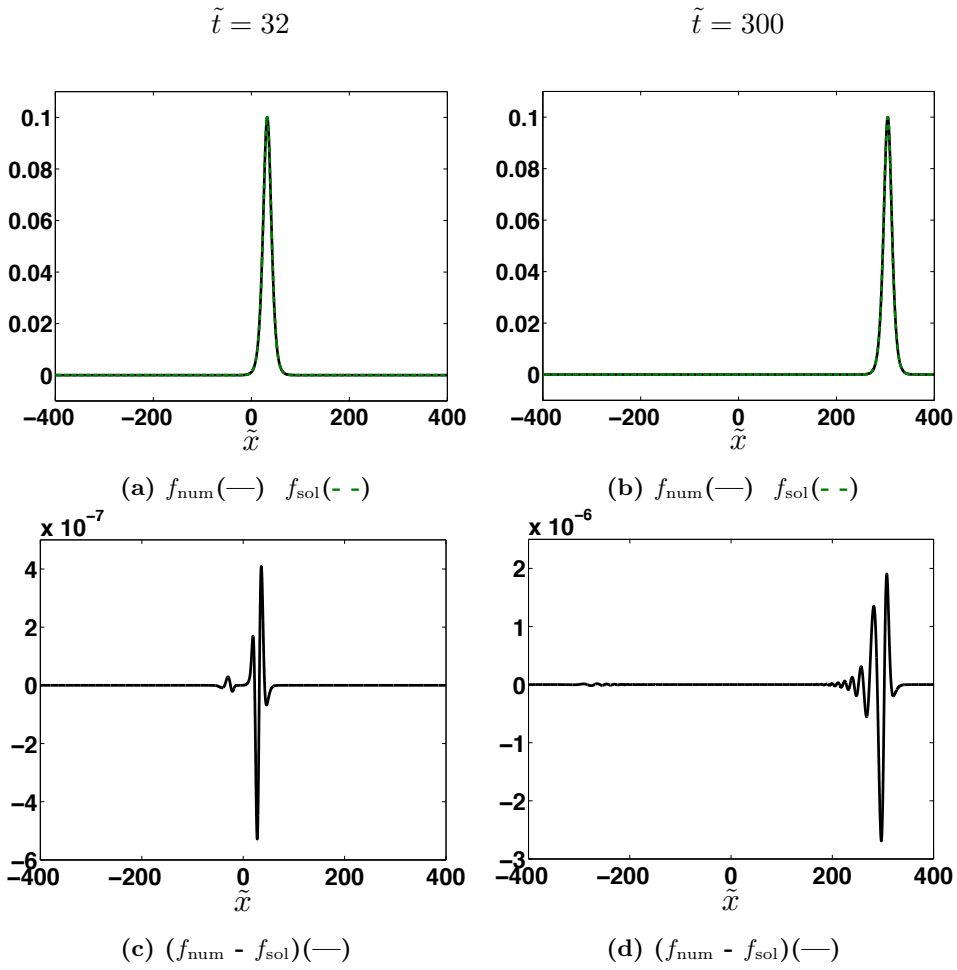

(a) f_{num}(—) f_{sol}(- -) **(b)** f_{num}(—) f_{sol}(- -)

(c) (f_{num} - f_{sol})(—) **(d)** (f_{num} - f_{sol})(—)

Figure 4.1: Evolution of numerical solution and exact solution (4.3) at (a) $\tilde{t} = 32$ ($\approx t_a$) & (b) $\tilde{t} = 300$ ($\approx t_b$), and the absolute errors (c) & (d) at the respective times. Parameter values are $h = \kappa = 0.1$ and $\epsilon = 0.1$.

4.4 Exactly solvable initial conditions

Due to the construction of the weakly nonlinear solution (4.5) it is favourable to split the initial conditions of the IVP (4.4), if possible, into an $O(1)$ 'exactly solvable part' (from the viewpoint of the leading order KdV equations) and an $O(\epsilon)$ perturbation. In this section we consider the case when the perturbations are zero. First we transform the KdV equations (4.7) into the standard form

$$\hat{f}^-_{\hat{T}} - 6\hat{f}^-\hat{f}^-_{\hat{\xi}} + \hat{f}^-_{\hat{\xi}\hat{\xi}\hat{\xi}} = 0, \qquad \hat{f}^+_{\hat{T}^+} - 6\hat{f}^+\hat{f}^+_{\hat{\eta}} + \hat{f}^+_{\hat{\eta}\hat{\eta}\hat{\eta}} = 0, \quad \text{where} \tag{4.11}$$

$$\hat{f}^- = -\frac{1}{6\beta^2}f^-, \quad \hat{f}^+ = -\frac{1}{6\beta^2}f^+, \quad \hat{\xi} = \beta\xi, \quad \hat{\eta} = \beta\eta, \quad \hat{T} = \frac{\beta^3}{2}T, \quad \hat{T}^+ = -\frac{\beta^3}{2}T,$$

and β is a free parameter. We consider the class of N-soliton solutions of equations (4.11) (see [44, 57, 68]), which yields, for the original functions,

$$f^-_N(\xi,T) = 12\frac{\partial^2}{\partial\xi^2}\log[\det M_N(\xi,-T)], \qquad f^+_N(\eta,T) = 12\frac{\partial^2}{\partial\eta^2}\log[\det M_N(\eta,T)],$$

for the N x N matrix $M_N(x,T) = (m_{ij}(x,T))$ with elements

$$m_{ij}(x,T) = \delta_{ij} + \frac{2k_i}{k_i+k_j}e^{(k_ix+\frac{k_i^3T}{2}+\alpha_i)},$$

where α_i and k_i are arbitrary parameters for $i,j = 1...N$ and δ_{ij} is the Kronecker delta function.

4.4.1 Right-propagating initial conditions

Let us first consider the case of initial conditions of the IVP (4.4) in the form of right-propagating N-soliton solutions of the KdV equation, i.e.

$$f|_{t=0} = 12\frac{\partial^2}{\partial x^2}\log[\det M_N(x,0)], \qquad f_t|_{t=0} = -12\frac{\partial^3}{\partial x^3}\log[\det M_N(x,0)]. \tag{4.12}$$

In this case the leading order solutions of the weakly nonlinear solution appear in the form $f^+ = 0$, $f^- = f^-_N(\xi,T)$ and the higher order terms (4.8) reduce to $f^1 = \phi(\xi,T) + \psi(\eta,T)$ where

$$\phi(\xi,T) = \frac{1}{2}\int_{-\infty}^{\xi} R_2(x,T)dx, \qquad \psi(\eta,T) = -\frac{1}{2}\int_{-\infty}^{\eta} R_2(x,T)dx,$$

and $R_2(x,T) = (f_T^-)|_{t=0}$. Therefore we have

$$f^1 \;=\; -\frac{1}{2}\frac{\partial}{\partial T}\int_\xi^\eta f_N^-(x,T)dx \;=\; -6\left[\frac{\partial^2}{\partial x \partial T}\log[\det M_N(x,-T)]\right]_{x=\xi}^{x=\eta},$$

and consequently the weakly nonlinear solution of the IVP (4.4) for KdV N-soliton initial conditions propagating to the right is

$$f = 12\frac{\partial^2}{\partial \xi^2}\log[\det M_N(\xi,-T)] - 6\epsilon\left[\frac{\partial^2}{\partial x \partial T}\log[\det M_N(x,-T)]\right]_{x=\xi}^{x=\eta} + O(\epsilon^2). \quad (4.13)$$

4.4.2 Right- and left-propagating initial conditions

For the case of right- and left-propagating KdV N-soliton initial conditions of the IVP (4.4), we choose the initial conditions in the form

$$f|_{t=0} = 24\frac{\partial^2}{\partial x^2}\log[\det M_N(x,0)], \qquad f_t|_{t=0} = 0. \quad (4.14)$$

The leading order solutions take the form $f^+ = f_N^+(\eta,T)$, $f^- = f_N^-(\xi,T)$. Unlike the previous case, the higher order terms are now more difficult to determine since $f^+ \neq 0$. It is convenient to introduce the notation

$$f^- = 12U_{\xi\xi}(\xi,T), \qquad f^+ = 12V_{\eta\eta}(\eta,T), \quad \text{where}$$

$$U(x,T) = \log[\det M_N(x,-T)] \quad \text{and} \quad V(x,T) = \log[\det M_N(x,T)],$$

and thus we can write the higher order terms of the weakly nonlinear solution as

$$\begin{aligned} f^1 \;&=\; -36\left[2U_{\xi\xi}(\xi,T)V_{\eta\eta}(\eta,T) + U_{\xi\xi\xi}(\xi,T)V_\eta(\eta,T) + V_{\eta\eta\eta}(\eta,T)U_\xi(\xi,T)\right] \\ &+\; \phi(\xi,T) + \psi(\eta,T). \end{aligned}$$

The terms ϕ and ψ are constructed from the functions (4.9), which for this case are

$$\begin{aligned} R_1(x,T) \;&=\; 36\frac{\partial}{\partial x}[U_{xx}(x,T)V_x(x,T) + U_x(x,T)V_{xx}(x,T)], \\ R_2(x,T) \;&=\; 12[U_{xxT}(x,T) + V_{xxT}(x,T)] \\ &+\; 36\frac{\partial}{\partial x}\left[U_{xxx}(x,T)V_x(x,T) - U_x(x,T)V_{xxx}(x,T)\right]. \end{aligned}$$

It therefore follows that

$$\begin{aligned} \int_{-\infty}^x R_2(s,T)ds \;&=\; 12[U_{xT}(x,T) + V_{xT}(x,T)] \\ &+\; 36[U_{xxx}(x,T)V_x(x,T) - U_x(x,T)V_{xxx}(x,T)], \end{aligned}$$

and since we have

$$\begin{aligned}\phi+\psi &= \frac{1}{2}\left[R_1(\xi,T)+R_1(\eta,T)-\int_\xi^\eta R_2(x,T)dx\right]\\ &= 36\Big\{U_{\xi\xi}(\xi,T)V_{\xi\xi}(\xi,T)+U_{\eta\eta}(\eta,T)V_{\eta\eta}(\eta,T)+U_{\xi\xi\xi}(\xi,T)V_\xi(\xi,T)\\ &\quad +V_{\eta\eta\eta}(\eta,T)U_\eta(\eta,T)+\frac{1}{6}\Big[U_{\xi T}(\xi,T)+V_{\xi T}(\xi,T)-U_{\eta T}(\eta,T)-V_{\eta T}(\eta,T)\Big]\Big\},\end{aligned}$$

the weakly nonlinear solution of the IVP (4.4) for KdV N-soliton initial conditions propagating both left and right, can be explicitly expressed in the form

$$\begin{aligned}f &= 12[U_{\xi\xi}(\xi,T)+V_{\eta\eta}(\eta,T)]+36\epsilon\left\{\frac{\partial}{\partial x}\Big[U_{\xi\xi}(\xi,T)\left[V_x(x,T)\right]_{x=\eta}^{x=\xi}\right.\\ &\quad \left.+V_{\eta\eta}(\eta,T)\left[U_x(x,T)\right]_{x=\xi}^{x=\eta}\Big]+\frac{1}{6}\left[U_{xT}(x,T)+V_{xT}(x,T)\right]_{x=\eta}^{x=\xi}\right\}+O(\epsilon^2). \quad (4.15)\end{aligned}$$

4.5 Examples: weakly nonlinear solution and numerical simulations

4.5.1 Right-propagating 1-soliton initial conditions

We now consider particular examples of the two general classes of solutions formulated in the previous section and compare them to numerical simulations of the regularised Boussinesq equation. For the case of initial conditions of the IVP (4.4) in the form of a right-propagating single KdV soliton solution, the leading order terms are

$$f^+=0, \qquad f^- \;=\; f_1^-(\xi,T) \;=\; 12\frac{\partial^2}{\partial\xi^2}\log(1+e^{\theta(\xi,-T)}),$$

where $\theta(x,T)=kx+\frac{k^3}{2}T+\alpha$. From (4.12) the initial conditions of the IVP (4.4) are

$$f|_{t=0}=12\frac{\partial^2}{\partial x^2}\log(1+e^{\theta(x,0)}), \qquad f_t|_{t=0}=-12\frac{\partial^3}{\partial x^3}\log(1+e^{\theta(x,0)}), \quad (4.16)$$

and from (4.13) the weakly nonlinear solution is

$$f=12\frac{\partial^2}{\partial\xi^2}\log(1+e^{\theta(\xi,-T)})-6\epsilon\left[\frac{\partial^2}{\partial x\partial T}\log(1+e^{\theta(x,-T)})\right]_{x=\xi}^{x=\eta}+O(\epsilon^2). \quad (4.17)$$

Explicitly evaluating the derivatives in (4.17) yields

$$\begin{aligned}f &= 3k^2\mathrm{sech}^2\left[\frac{k}{2}\left(\xi-\frac{k^2}{2}T\right)+\frac{\alpha}{2}\right]+\frac{3k^4\epsilon}{4}\left\{-\mathrm{sech}^2\left[\frac{k}{2}\left(\xi-\frac{k^2}{2}T\right)+\frac{\alpha}{2}\right]\right.\\ &+ \left.\mathrm{sech}^2\left[\frac{k}{2}\left(\eta-\frac{k^2}{2}T\right)+\frac{\alpha}{2}\right]\right\}+O(\epsilon^2). \quad (4.18)\end{aligned}$$

To consider the error of the weakly nonlinear solution in this example, we transform (4.18) into the same form used in the numerics:

$$\begin{aligned}\tilde{f} &= 3k^2\epsilon\,\mathrm{sech}^2\left[\frac{k\sqrt{\epsilon}}{2}\left(\tilde{x}-\left[1+\frac{k^2\epsilon}{2}\right]\tilde{t}\right)+\frac{\alpha}{2}\right] \\ &+ \frac{3k^4\epsilon^2}{4}\left\{-\mathrm{sech}^2\left[\frac{k\sqrt{\epsilon}}{2}\left(\tilde{x}-\left[1+\frac{k^2\epsilon}{2}\right]\tilde{t}\right)+\frac{\alpha}{2}\right]\right. \\ &\qquad \left.+\,\mathrm{sech}^2\left[\frac{k\sqrt{\epsilon}}{2}\left(\tilde{x}+\left[1-\frac{k^2\epsilon}{2}\right]\tilde{t}\right)+\frac{\alpha}{2}\right]\right\}+O(\epsilon^3). \qquad (4.19)\end{aligned}$$

The initial conditions for numerical simulations are chosen to coincide with (4.16):

$$f_{i,0}=3k^2\epsilon\,\mathrm{sech}^2\left(\frac{k\sqrt{\epsilon}\,\tilde{x}+\alpha}{2}\right),\quad f_{i,1}=3k^2\epsilon\,\mathrm{sech}^2\left(\frac{k\sqrt{\epsilon}(\tilde{x}-\kappa)+\alpha}{2}\right),\quad \forall i,$$

where we choose k such that the weakly nonlinear solution is applicable.

Figure 4.2 depicts the evolution of the weakly nonlinear solution (4.19) within the time region of its applicability. Figures 4.3(a) & (b) highlight the difference in the numerical solution compared with the weakly nonlinear solution, taken up to leading and second order, for a particular time and choice of ϵ. In Figure 4.3(a) the difference between the solution (4.19) and the numerical solution is almost indistinguishable, whilst a considerable difference can be observed for the leading order solution upon comparison with the numerical solution.

Figure 4.3(c) displays the maximum absolute error compared with ϵ at the corresponding time $\tilde{t}\approx t_a$. It can be seen that higher order corrections significantly reduce the error of the solution. Note that the leading order solution does not capture the left-propagating wave whatsoever. More detailed analysis of errors will be discussed in the next chapter. Each of the errors plotted in Figure 4.3(c) are far greater in magnitude than the corresponding errors of the numerical scheme (for the same parameters but for different initial conditions), given in Table 4.2 of Section 4.3. This confirms the validity of these plots as a true measure of the accuracy of the weakly nonlinear solution and hence are not displaying potential numerical artefacts of the finite difference scheme.

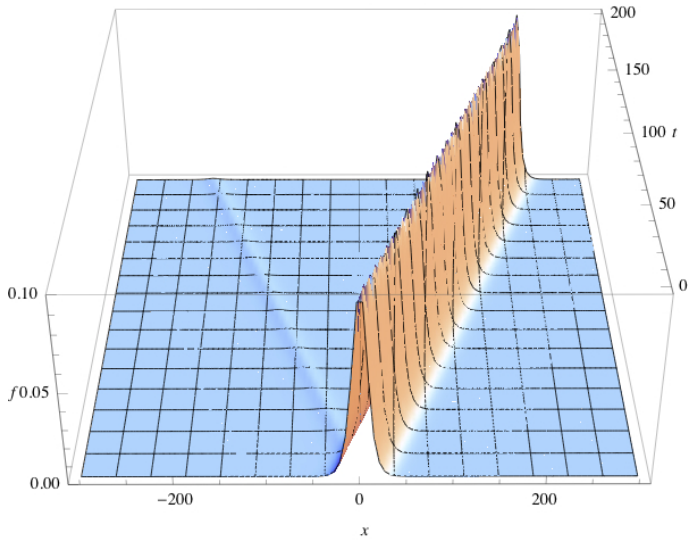

Figure 4.2: Evolution of the weakly nonlinear solution for right-propagating 1-soliton initial conditions, with $\epsilon = 0.1$, $k = \frac{1}{\sqrt{3}}$ and $\alpha = 0$.

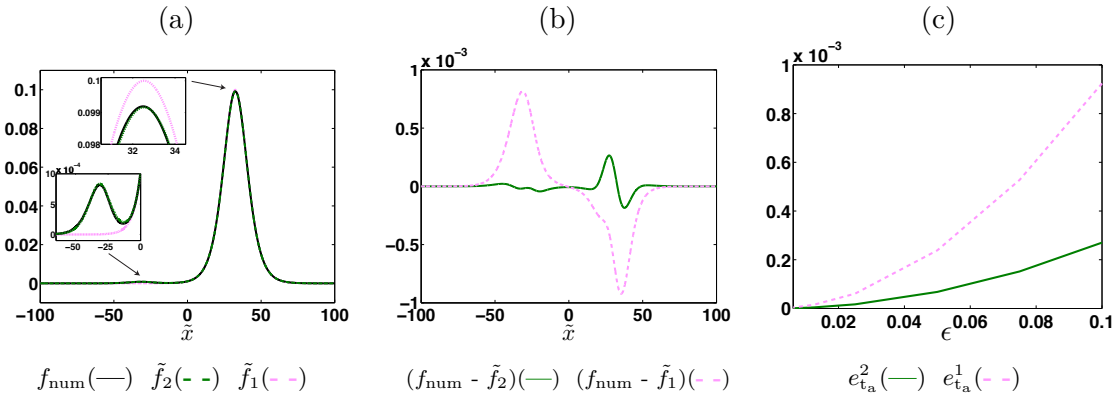

Figure 4.3: Right-propagating 1-soliton initial conditions. (a) Numerical solution compared with the weakly nonlinear solution $\tilde{f}_2$ and $\tilde{f}_1$, and (b) the respective absolute errors, both for $\epsilon = 0.1$ and $\tilde{t} = 32$ ($\approx t_a$). (c) Maximum absolute errors $e^2_{t_a}$ and $e^1_{t_a}$ versus ϵ at $\tilde{t} \approx t_a$. All other parameters are $k = \frac{1}{\sqrt{3}}$ and $\alpha = 0$.

4.5.2 Right- and left-propagating 1-soliton initial conditions

The case of initial conditions of the IVP (4.4) in the form of a right- and left-propagating single KdV soliton solution, yields the leading order solutions

$$f^+ = f_1^+(\eta, T) = 12\frac{\partial^2}{\partial\eta^2}\log(1+e^{\theta(\eta,T)}), \qquad f^- = f_1^-(\xi, T) = 12\frac{\partial^2}{\partial\xi^2}\log(1+e^{\theta(\xi,-T)}).$$

From (4.14) this corresponds to the initial conditions of the IVP (4.4) in the form

$$f|_{t=0} = 24\frac{\partial^2}{\partial x^2}\log(1+e^{\theta(x,0)}), \qquad f_t|_{t=0} = 0. \tag{4.20}$$

The weakly nonlinear solution is therefore in the form (4.15) where in this particular case $U(x,T) = \log(1+e^{\theta(x,-T)})$ and $V(x,T) = \log(1+e^{\theta(x,T)})$. Explicitly evaluating each of the terms in the weakly nonlinear solution yields the solution in the form

$$\begin{aligned} f &= 3k^2\left[\operatorname{sech}^2\theta^{\xi-} + \operatorname{sech}^2\theta^{\eta+}\right] + \frac{9k^4\epsilon}{2}\left\{-\frac{1}{6}\left[\operatorname{sech}^2\theta^{x+} - \operatorname{sech}^2\theta^{x-}\right]_{x=\xi}^{x=\eta}\right. \\ &- \operatorname{sech}^2\theta^{\xi-}\left[\frac{1}{2}\left(\operatorname{sech}^2\theta^{\eta+} + \operatorname{sech}^2\theta^{\xi+}\right) - \tanh\theta^{\xi-}\left(\tanh\theta^{\eta+} + \tanh\theta^{\xi+}\right)\right] \\ &\left.- \operatorname{sech}^2\theta^{\eta+}\left[\frac{1}{2}\left(\operatorname{sech}^2\theta^{\xi-} + \operatorname{sech}^2\theta^{\eta-}\right) - \tanh\theta^{\eta+}\left(\tanh\theta^{\xi-} + \tanh\theta^{\eta-}\right)\right]\right\} \\ &+ O(\epsilon^2), \end{aligned} \tag{4.21}$$

where we introduce the notation $\theta^{x\pm} = \frac{1}{2}\theta(x, \pm T)$.

To investigate the error of the weakly nonlinear solution we transform the variables in (4.21) to the same form used in the numerics, and for numerical simulations we use the following initial conditions to coincide with (4.20):

$$f_{i,0} = 6k^2\epsilon\,\operatorname{sech}^2\left(\frac{\sqrt{\epsilon}k\tilde{x}+\alpha}{2}\right), \quad \text{and} \quad f_{i,1} = \frac{1}{2}\Big(f_{i,0}|_{\tilde{x}=\tilde{x}-\kappa} + f_{i,0}|_{\tilde{x}=\tilde{x}+\kappa}\Big).$$

We again choose suitable k to ensure the validity of the weakly nonlinear solution.

Figure 4.4 depicts the evolution of the weakly nonlinear solution (4.21) but transformed to the same variables used in the numerics. Figures 4.5(a) & (b) display the behaviour of the numerical solution compared with the weakly nonlinear solution, up to leading and second order, for fixed $\tilde{t}$ and ϵ. Figure 4.5(c) displays the maximum of the absolute errors for the weakly nonlinear solution taken up to each order, for various ϵ and at the corresponding times $\tilde{t} \approx t_a$. Similar to the previous example, the weakly nonlinear solution derived for this example becomes more accurate when we account for the higher order corrections.

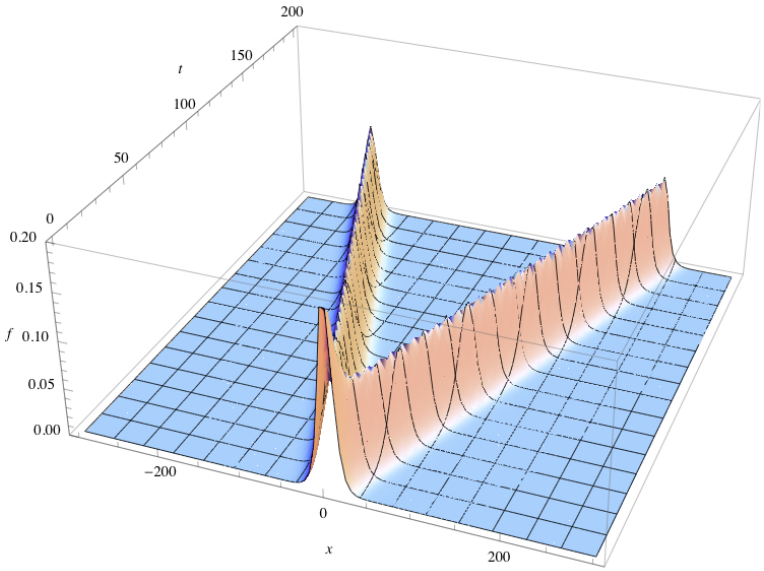

Figure 4.4: Evolution of the weakly nonlinear solution for right- and left-propagating 1-soliton initial conditions, with $\epsilon = 0.1$, $k = \frac{1}{\sqrt{3}}$ and $\alpha = 0$.

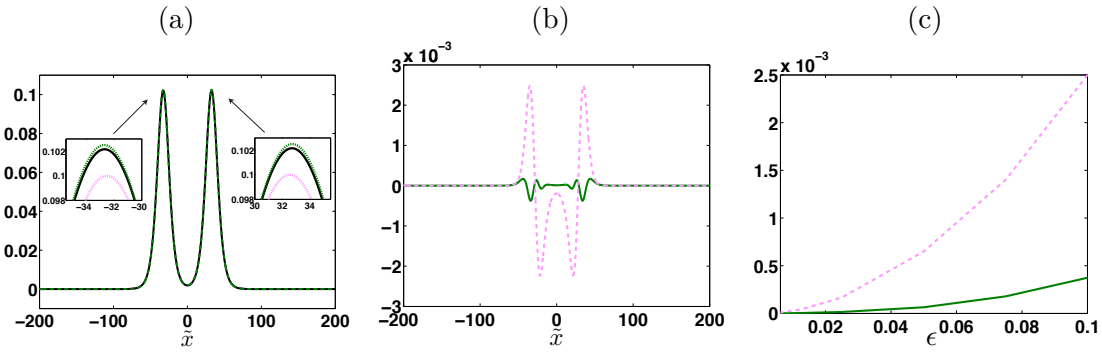

Figure 4.5: Right- and left-propagating 1-soliton initial conditions. (a) Numerical solution compared with the weakly nonlinear solution $\tilde{f}_2$ and $\tilde{f}_1$, and (b) the respective absolute errors, both for $\epsilon = 0.1$ and $\tilde{t} = 32$ ($\approx t_a$). (c) Maximum absolute errors $e^2_{t_a}$ and $e^1_{t_a}$ versus ϵ at $\tilde{t} \approx t_a$. All other parameters are $k = \frac{1}{\sqrt{3}}$ and $\alpha = 0$.

4.5.3 Right-propagating 2-soliton initial conditions

We next examine another particular example of the weakly nonlinear solution derived in Section 4.4.1, namely initial conditions of the IVP (4.4) in the form of a right-propagating 2-soliton solution of the KdV equation. Therefore we have the following leading order solutions

$$f^+ = 0, \quad f^- = f_2^-(\xi, T) = 12\frac{\partial^2}{\partial \xi^2}\log\left(1 + e^{\theta_1(\xi,-T)} + e^{\theta_2(\xi,-T)} + Ce^{\theta_1(\xi,-T)+\theta_2(\xi,-T)}\right),$$

where we denote $C = [(k_1 - k_2)/(k_1 + k_2)]^2$ and $\theta_i(x,T) = k_i x + \frac{k_i^3}{2}T + \alpha_i$ for $i = 1, 2$. From (4.12) the corresponding initial conditions of the IVP (4.4) in this case are

$$f|_{t=0} = 12\frac{\partial^2}{\partial x^2}\log\left(1 + e^{\theta_1(x,0)} + e^{\theta_2(x,0)} + Ce^{\theta_1(x,0)+\theta_2(x,0)}\right), \quad f_t|_{t=0} = -\frac{\partial}{\partial x}f|_{t=0}, \tag{4.22}$$

and from (4.13) the weakly nonlinear solution can be explicitly expressed as

$$\begin{aligned} f &= 6\frac{(k_1-k_2)^2 + \sqrt{C}\left(k_1^2\cosh\theta_2^{\xi-} + k_2^2\cosh\theta_1^{\xi-}\right)}{\left[\cosh\left(\frac{\theta_1^{\xi-}-\theta_2^{\xi-}}{2}\right) + \sqrt{C}\cosh\left(\frac{\theta_1^{\xi-}+\theta_2^{\xi-}}{2}\right)\right]^2} \\ &+ \frac{3\epsilon}{2}\left\{\frac{D + \sqrt{C}\left(k_1^4\cosh\theta_2^s + k_2^4\cosh\theta_1^s\right)}{\left[\cosh\left(\frac{\theta_1^s-\theta_2^s}{2}\right) + \sqrt{C}\cosh\left(\frac{\theta_1^s+\theta_2^s}{2}\right)\right]^2}\right\}_{s=\xi-}^{s=\eta-} + O(\epsilon^2), \end{aligned} \tag{4.23}$$

where $D = (k_1 - k_2)^2(k_1^2 + k_2^2)$ and we use the notation $\theta_i^{x\pm} = k_i x \pm \frac{k_i^3}{2}T + \hat{\alpha}_i$ (where we shift $\alpha_i \to \hat{\alpha}_i - \ln\sqrt{C}$) for $i = 1, 2$. We next examine the error of solution (4.23) by transforming the variables into the same form as used in numerical simulations, and to coincide with (4.22) we implement the following initial conditions:

$$f_{i,0} = 6\epsilon\frac{(k_1-k_2)^2 + \sqrt{C}\left(k_1^2\cosh\tilde{\theta}_2^{x0} + k_2^2\cosh\tilde{\theta}_1^{x0}\right)}{\left[\cosh\left(\frac{\tilde{\theta}_1^{x0}-\tilde{\theta}_2^{x0}}{2}\right) + \sqrt{C}\cosh\left(\frac{\tilde{\theta}_1^{x0}+\tilde{\theta}_2^{x0}}{2}\right)\right]^2}, \qquad f_{i,1} = f_{i,0}|_{\tilde{x}=\tilde{x}-\kappa},$$

where $\tilde{\theta}_i^{x0} = k_i\tilde{x}\sqrt{\epsilon} + \hat{\alpha}_i$ for $i = 1, 2$, and we choose k_1 and k_2 appropriately to ensure applicability of the weakly nonlinear solution.

In Figure 4.6 we consider the case where the amplitudes of the leading order parts of the solution are close ($k_1 = 0.61, k_2 = 0.56$) and their relative positions are initially close together ($\hat{\alpha}_1 = \hat{\alpha}_2 = 0$). The initial conditions of the IVP (4.4) for this example

are shown in Figures 4.6(a) & (d), and the evolution of the weakly nonlinear solution, up to first and second order, and the numerical solution, are displayed in Figures 4.6(b) & (c), all for times within the region of validity of the weakly nonlinear solution. The corresponding absolute errors up to each order are displayed in Figures 4.6(e) & (f) at each of the respective times. It can be seen that there is a noticeable improvement in the agreement of the numerical solution with the weakly nonlinear solution taken up to second order compared to the leading order solution, best emulated at earlier time (i.e. in Figures 4.6(b) & (c).

We also examined each combination for when the two leading order components of the weakly nonlinear solution are initially close or separate and when the amplitudes are similar or essentially different, controlled by the $\hat{\alpha}_i$'s and the k_i's respectively. There were slight alterations to these results from the example presented in Figure 4.6, however the main features remained; that being e_t^2 remained small throughout the same time interval, but $e_t^2 \to e_t^1$ as time increased through the region of the validity of the weakly nonlinear solution.

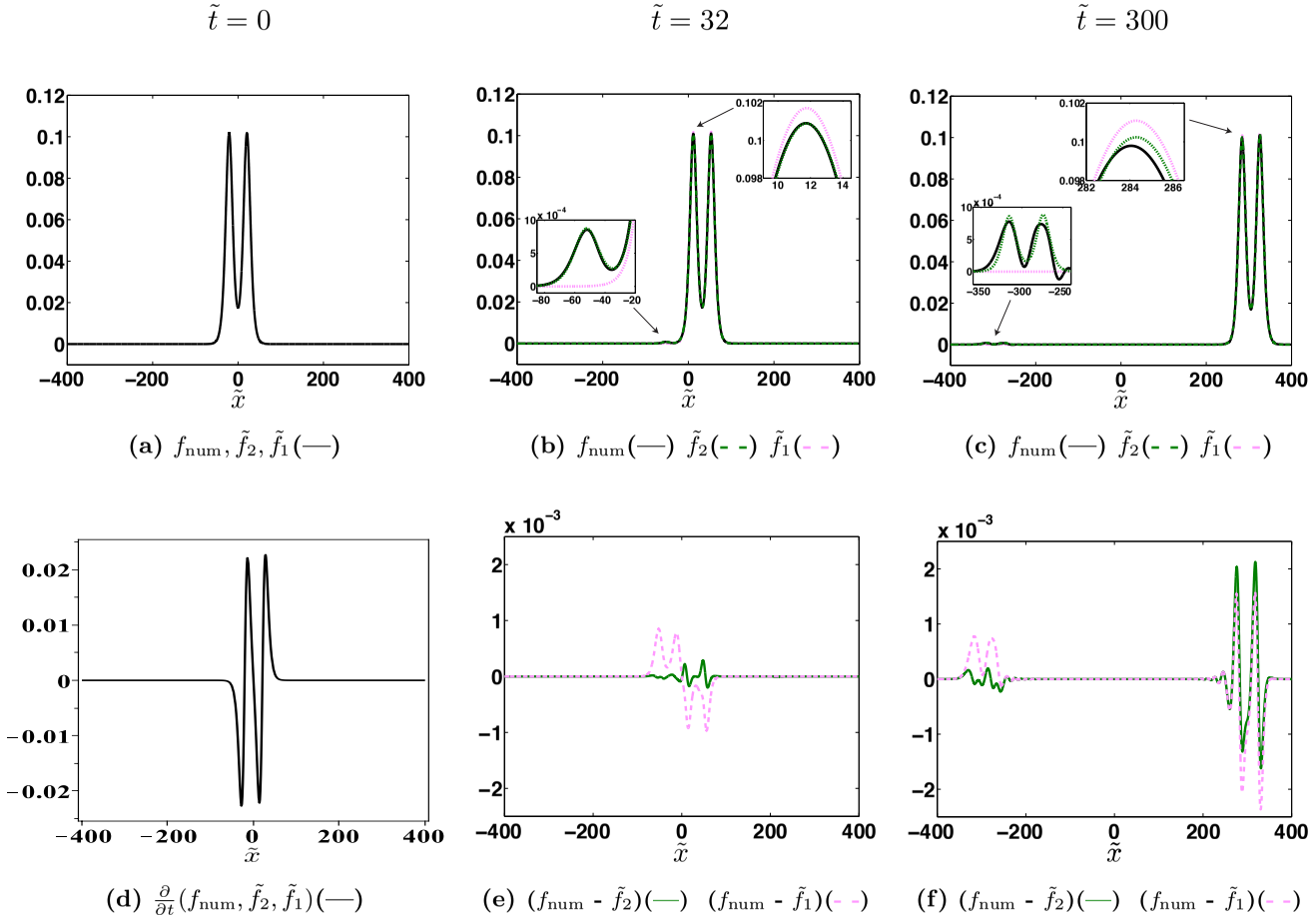

(a) $f_{\text{num}}, \tilde{f}_2, \tilde{f}_1$(—) **(b)** f_{num}(—) $\tilde{f}_2$(- -) $\tilde{f}_1$(- -) **(c)** f_{num}(—) $\tilde{f}_2$(- -) $\tilde{f}_1$(- -)

(d) $\frac{\partial}{\partial t}(f_{\text{num}}, \tilde{f}_2, \tilde{f}_1)$(—) **(e)** ($f_{\text{num}}$ - $\tilde{f}_2$)(—) (f_{num} - $\tilde{f}_1$)(- -) **(f)** (f_{num} - $\tilde{f}_2$)(—) (f_{num} - $\tilde{f}_1$)(- -)

Figure 4.6: Right-propagating 2-soliton initial conditions (a) & (d). Evolution of the numerical solution compared with the weakly nonlinear solution $\tilde{f}_2$ and $\tilde{f}_1$ at (b) $\tilde{t} = 32$ ($\approx t_a$), (c) $\tilde{t} = 300$ ($\approx t_b$), and the absolute errors at each of the respective times (e) & (f). All other parameters are $\epsilon = 0.1, k_1 = 0.61, k_2 = 0.56$ and $\hat{\alpha}_1 = \hat{\alpha}_2 = 0$.

4.5.4 Right- and left-propagating 2-soliton initial conditions

We consider one final particular example of exactly solvable initial conditions, namely initial conditions of the IVP (4.4) in the form of right and left-propagating 2-soliton solutions of the KdV equations. Therefore, the leading order solutions are in the form

$$\begin{aligned} f^+ &= f_2^+(\eta,T) &&= 12\frac{\partial^2}{\partial\eta^2}\log\left(1+e^{\theta_1(\eta,T)}+e^{\theta_2(\eta,T)}+Ce^{\theta_1(\eta,T)+\theta_2(\eta,T)}\right), \\ f^- &= f_2^-(\xi,T) &&= 12\frac{\partial^2}{\partial\xi^2}\log\left(1+e^{\theta_1(\xi,-T)}+e^{\theta_2(\xi,-T)}+Ce^{\theta_1(\xi,-T)+\theta_2(\xi,-T)}\right), \end{aligned} \tag{4.24}$$

and the initial conditions (4.14) for this example are

$$f|_{t=0} = 24\frac{\partial^2}{\partial x^2}\log\left(1+e^{\theta_1(x,0)}+e^{\theta_2(x,0)}+Ce^{\theta_1(x,0)+\theta_2(x,0)}\right), \quad f_t|_{t=0}=0. \tag{4.25}$$

The explicit form of the weakly nonlinear solution for this example is omitted here since the solution is rather lengthy, particularly due to the requirement of third order derivatives of the log terms in (4.24) within the solution (4.15). However, the solution can be easily obtained from (4.15) using any computer algebra package (we use *Maple 14* to determine the solution in subsequent comparisons in this chapter), indeed, the only operations required in determining (4.15) are differentiations.

Once again, we explicitly compare the weakly nonlinear solution in this example with numerical simulations. Transforming the variables into the same form as used in the numerics, we use the following initial conditions for numerical simulations to coincide with (4.25):

$$\begin{aligned} f_{i,0} &= 12\epsilon\frac{(k_1-k_2)^2+\sqrt{C}\left(k_1^2\cosh\tilde{\theta}_2^{x0}+k_2^2\cosh\tilde{\theta}_1^{x0}\right)}{\left[\cosh\left(\frac{\tilde{\theta}_1^{x0}-\tilde{\theta}_2^{x0}}{2}\right)+\sqrt{C}\cosh\left(\frac{\tilde{\theta}_1^{x0}+\tilde{\theta}_2^{x0}}{2}\right)\right]^2}, \\ f_{i,1} &= \frac{1}{2}\left(f_{i,0}|_{\tilde{x}=\tilde{x}-\kappa}+f_{i,0}|_{\tilde{x}=\tilde{x}+\kappa}\right), \end{aligned}$$

where we again choose the k_i's appropriately in order to maintain the applicability of the weakly nonlinear solution.

For the example presented in Figure 4.7 we choose the same $\hat{\alpha}_i$'s and k_i's as chosen in the previous example. The initial conditions of the IVP (4.4) for this example are shown in Figures 4.7(a) & (d), and the evolution of the weakly nonlinear solution, taken up to first and second order, along with the numerical solution, is shown in Figures 4.7(b) & (c). As the solution evolves one can notice qualitatively the resemblance of

the leading order terms in the previous example propagating in both directions. The absolute errors of the weakly nonlinear solution up to each order are shown in Figures 4.7(e) & (f) at each of the respective times and it is again clear that they are small throughout the time interval considered. There is a significant improvement in the accuracy of $\tilde{f}_2$ compared with $\tilde{f}_1$ for this example especially at earlier time, shown in Figure 4.7(e), where e_t^2/e_t^1 is approximately $O(\epsilon)$.

4.6 Perturbations of exactly solvable initial conditions

Finally we consider the weakly nonlinear solution for perturbations to the exactly solvable initial conditions of the IVP (4.4) considered in Section 4.4. More specifically, we examine just one particular case: initial conditions with a perturbation to a right propagating KdV N-soliton solution. We choose the simplest perturbed form to the initial conditions of the IVP (4.4):

$$f|_{t=0} = 12\frac{\partial^2}{\partial x^2}\log[\det M_N(x,0)] + \epsilon F^1(x), \qquad f_t|_{t=0} = -12\frac{\partial^3}{\partial x^3}\log[\det M_N(x,0)].$$

Therefore, the leading order terms are still given in the form considered in Section 4.4.1

$$f^+ = 0, \qquad f^- = f_N^-(\xi, T),$$

but the higher order terms are of the form

$$f^1 = \frac{1}{2}\left[R_1(\xi,T) + R_1(\eta,T) - \int_\xi^\eta R_2(x,T)dx\right], \quad \text{where}$$

$$R_1(x,T) = F^1(x), \qquad R_2(x,T) = \frac{\partial}{\partial T}f_N^-(x,T).$$

The weakly nonlinear solution for a perturbation of the KdV N-soliton initial conditions propagating to the right, is therefore

$$\begin{aligned} f &= 12\frac{\partial^2}{\partial \xi^2}\log[\det M_N(\xi,-T)] \\ &+ \frac{\epsilon}{2}\left\{F^1(\xi) + F^1(\eta) - 12\left[\frac{\partial^2}{\partial x \partial T}\log[\det M_N(x,-T)]\right]_{x=\xi}^{x=\eta}\right\} + O(\epsilon^2). \quad (4.26) \end{aligned}$$

We consider a particular example, namely a perturbation of the single KdV soliton solution, as in Section 4.5.1, with the perturbation defined as

$$F^1(x) = \operatorname{sech}\left(\frac{kx+\alpha}{2}\right).$$

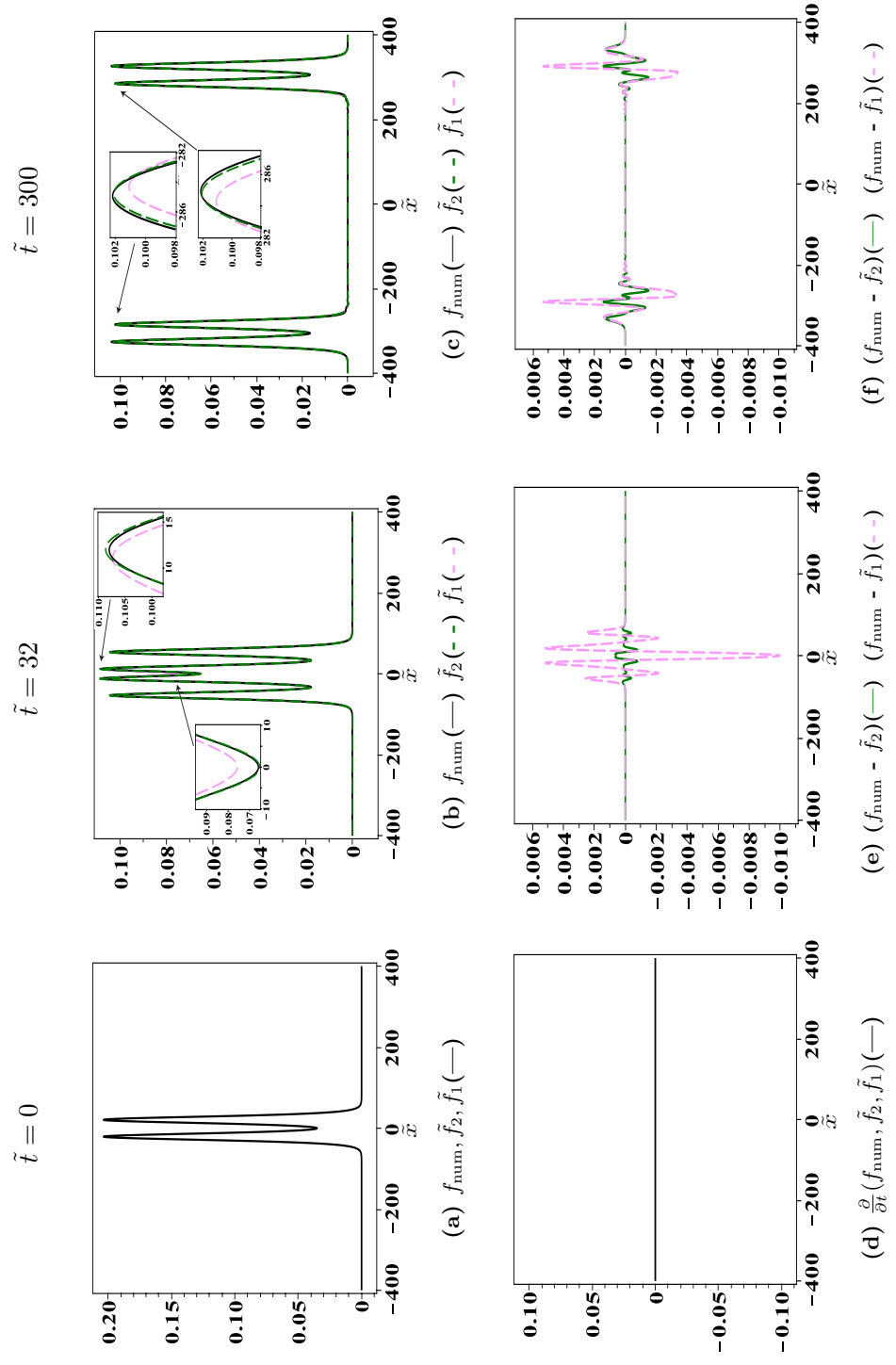

Figure 4.7: Right- and left-propagating 2-soliton initial conditions (a) & (d). Evolution of the numerical solution compared with the weakly nonlinear solution $\tilde{f}_2$ and $\tilde{f}_1$ at (b) $\tilde{t} = 32$ ($\approx t_a$), (c) $\tilde{t} = 300$ ($\approx t_b$), and the absolute errors at each of the respective times (e) & (f). Other parameters are $\epsilon = 0.1, k_1 = 0.61, k_2 = 0.56$ and $\hat{\alpha}_1 = \hat{\alpha}_2 = 0$.

Therefore, the initial conditions of the IVP are

$$\begin{aligned} f|_{t=0} &= 12\frac{\partial^2}{\partial x^2}\log(1+e^{\theta(x,0)}) + \epsilon\ \text{sech}\left(\frac{kx+\alpha}{2}\right), \\ f_t|_{t=0} &= -12\frac{\partial^3}{\partial x^3}\log(1+e^{\theta(x,0)}), \end{aligned} \tag{4.27}$$

and from (4.26) the weakly nonlinear solution is explicitly given by

$$\begin{aligned} f =\ & 3k^2\text{sech}^2\left(\frac{k}{2}\left(\xi-\frac{k^2}{2}T\right)+\frac{\alpha}{2}\right)+\frac{\epsilon}{2}\left\{\text{sech}\left(\frac{k\xi+\alpha}{2}\right)+\text{sech}\left(\frac{k\eta+\alpha}{2}\right)\right. \\ & \left.+\frac{3k^4}{2}\left[-\text{sech}^2\left(\frac{k}{2}\left(\xi-\frac{k^2}{2}T\right)+\frac{\alpha}{2}\right)+\text{sech}^2\left(\frac{k}{2}\left(\eta-\frac{k^2}{2}T\right)+\frac{\alpha}{2}\right)\right]\right\}+O(\epsilon^2). \end{aligned} \tag{4.28}$$

To analyse the error we transform the variables to the form used in the numerics and for simulations we use the following initial conditions in order to comply with (4.27):

$$\begin{aligned} f_{i,0} &= 3k^2\epsilon\ \text{sech}^2\left(\frac{k\sqrt{\epsilon}\tilde{x}+\alpha}{2}\right)+\epsilon^2\text{sech}\left(\frac{k\sqrt{\epsilon}\tilde{x}+\alpha}{2}\right), \\ f_{i,1} &= 3k^2\epsilon\ \text{sech}^2\left(\frac{k\sqrt{\epsilon}(\tilde{x}-\kappa)+\alpha}{2}\right) \\ &+ \frac{\epsilon^2}{2}\left\{\text{sech}\left(\frac{k\sqrt{\epsilon}(\tilde{x}-\kappa)+\alpha}{2}\right)+\text{sech}\left(\frac{k\sqrt{\epsilon}(\tilde{x}+\kappa)+\alpha}{2}\right)\right\}. \end{aligned}$$

The initial conditions of the IVP (4.4), for this example, are shown in Figures 4.8(a) & (d), and the evolution of the weakly nonlinear solution, up to leading and second order, along with the numerical solution are shown in Figures 4.8(b) & (c). Figures 4.8(e) & (f) depict the corresponding errors of the weakly nonlinear solution at each of the respective times. The weakly nonlinear solution (4.28) is significantly more accurate than the leading order solution, most evident for early time (Figure 4.8(e)). However, as time increases beyond the region of validity of the weakly nonlinear solution, we find that $e_t^2 \to e_t^1$.

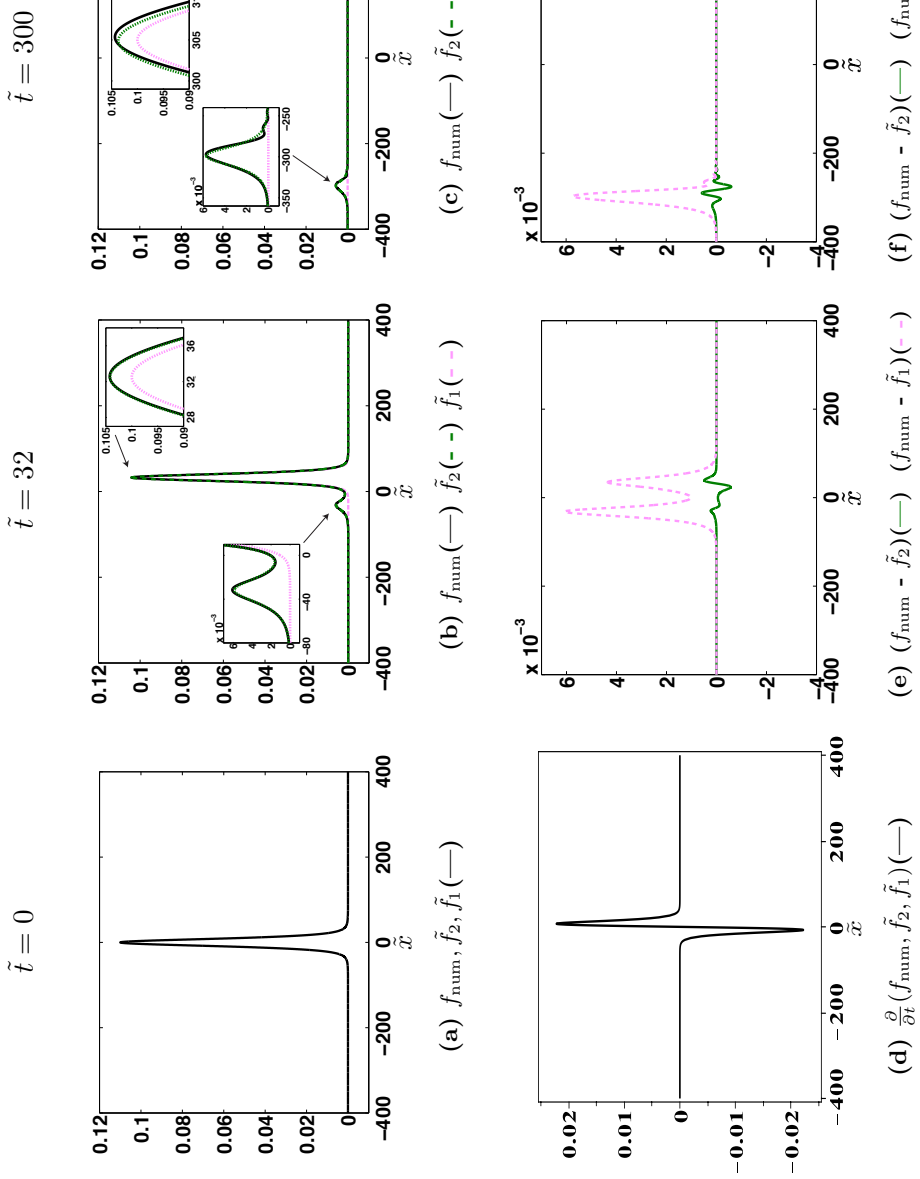

(a) $f_{\text{num}}, \tilde{f}_2, \tilde{f}_1$(—) (b) f_{num}(—) $\tilde{f}_2$(- -) $\tilde{f}_1$(- -) (c) f_{num}(—) $\tilde{f}_2$(- -) $\tilde{f}_1$(- -)

(d) $\frac{\partial}{\partial t}(f_{\text{num}}, \tilde{f}_2, \tilde{f}_1)$(—) (e) ($f_{\text{num}}$ - $\tilde{f}_2$)(—) (f_{num} - $\tilde{f}_1$)(- -) (f) (f_{num} - $\tilde{f}_2$)(—) (f_{num} - $\tilde{f}_1$)(- -)

Figure 4.8: Perturbation of right-propagating 1-soliton initial conditions (a) & (d). Evolution of the numerical solution compared with the weakly nonlinear solution $\tilde{f}_2$ and $\tilde{f}_1$ at (b) $\tilde{t} = 32$ ($\approx t_a$), (c) $\tilde{t} = 300$ ($\approx t_b$), and the absolute errors at each of the respective times (e) & (f). All other parameters are $\epsilon = 0.1$, $k = \frac{1}{\sqrt{3}}$ and $\alpha = 0$.

4.7 Concluding remarks

In this chapter we have constructed a nonsecular weakly nonlinear solution of the IVP for the Boussinesq equation on the infinite line, for initial data generating sufficiently rapidly decaying right- and left-propagating waves. Seeking asymptotic multiple-scales expansions and implementing an averaging procedure with respect to the fast time variable, we derived two KdV equations describing the leading order terms and obtained formulae for the higher order corrections in an explicit and simple form. The initial data was split into $O(1)$ and $O(\epsilon)$ parts, and it was shown, in a case study, that this allows one to obtain explicit approximate solutions of the IVP for exactly solvable initial conditions (from the viewpoint of the IST for the leading order KdV equations).

A finite difference scheme was implemented primarily to check the accuracy of the developed weakly nonlinear solution. We showed through comparisons of the numerical solution with an exact solution of the Boussinesq equation that the scheme's accuracy was well within the required accuracy to measure the weakly nonlinear solution. Albeit that changing the initial conditions in simulations for subsequent examples would undoubtedly alter the magnitude of the error of the numerical scheme determined in the test case in Section 4.3, it remains a good indicator of the scheme's accuracy.

On comparison of the weakly nonlinear solution with relevant numerical simulations there arose two consistent features in each of the examples considered. Firstly, the weakly nonlinear solution remained within its required accuracy throughout the time interval of its validity. For a more accurate solution and applicability for larger time, one must reformulate equation (4.1) to consider higher order terms. Secondly, the maximum absolute error of the weakly nonlinear solution (e_t^2) was significantly lower than for the leading order solution (e_t^1). This was particularly evident for earlier times. As time extended towards the end of the validity region of the weakly nonlinear solution, it can be seen that e_t^2 and e_t^1 become comparable. Improvements to the accuracy of the solution relating to this feature, are accounted for in the next chapter.

In all examples considered in this chapter the constructed weakly nonlinear solution was in excellent agreement with the results of numerical simulations, within the range of the solutions asymptotic validity. It would be interesting to consider other classes of initial conditions for the leading order KdV equations, using the well-developed techniques of the IST.

Chapter 5

Time dependence of higher order solution

In the previous two chapters we have constructed a weakly nonlinear solution of the Cauchy problem for Boussinesq-type equations on the infinite line, with localised and sufficiently rapidly decaying initial conditions, up to the accuracy of the problem formulation. The derived higher order functions denoted ψ and ϕ, which were found at $T = 0$ (where T is the slow time variable), enabled us to satisfy the initial conditions of the Cauchy problem for the Boussinesq-type equations. However, within the accuracy of the problem formulation, there was no way to correctly define the time dependence of ψ and ϕ. The aim of this chapter is to improve the accuracy of the previously constructed weakly nonlinear solution by defining the functions ψ and ϕ's dependence on T, for the more broader 'Boussinesq–type' equation.

We examine the accuracy of the approach by considering a particular example for the regularised Boussinesq equation, corresponding to a right-propagating leading order KdV soliton solution. In this case we derive higher order linearised KdV equations for ψ, ϕ and solve the equations by (i) using a perturbation approach and (ii) using numerical techniques. We compare the accuracy of the two different approaches with numerical simulations of the Boussinesq equation. Lastly, we consider an example for the Boussinesq–type equation modified by the 'Ostrovsky term', which we refer to henceforth as the 'Boussinesq–Ostrovsky' equation. We compare the derived solution with numerical simulations of the Boussinesq–Ostrovsky equation.

The results of this chapter are partially summarised in [74].

5.1 Weakly nonlinear solution

We consider the following Cauchy problem for the truncated Boussinesq–Ostrovsky equation on the infinite line:

$$\begin{aligned} &f_{tt} - f_{xx} = \epsilon \left[\frac{1}{2}(f^2)_{xx} + f_{ttxx} - \gamma f \right], \\ &f|_{t=0} = F(x), \qquad f_t|_{t=0} = -F_x(x), \end{aligned} \tag{5.1}$$

where the initial conditions are assumed to be localised or sufficiently rapidly decaying, and so too is the initial evolution of the solution from the initial conditions. Note, the form of the initial conditions (5.1a) is chosen to simplify derivations in order to best emphasise the subsequent methodology outlined in this chapter. The extension to the more general class of initial conditions constituting left- and right-propagating leading order terms is omitted since derivations become rather lengthy).

Of course, Boussinesq-type models should not be considered 'exact' in the majority of real life applications; from this viewpoint the problem formulation (5.1) can be viewed as a 'toy'-problem. Nevertheless, (5.1) is still a valid mathematical problem. Moreover, the methodology we develop in this chapter can be generalised and extended when the problem formulation of Boussinesq-type equations include higher order terms.

Following the derivation of the weakly nonlinear solutions developed in Sections 3.2 & 4.2, we seek the following solution of the particular configuration (5.1):

$$f = f^-(\xi, T) + \epsilon[\phi(\xi, T) + \psi(\eta, T)] + \epsilon^2 f^2(\xi, \eta, T) + O(\epsilon^3), \tag{5.2}$$

(the initial evolution found from d'Alembert's solution yields $f^+ = 0$), where $\xi = x - t$, $\eta = x + t$ and $T = \epsilon t$. Note we now include further higher order terms in the solution, denoted f^2. However, we do not specify and include these terms in the solution, they appear purely to derive the evolution equations for the terms ψ and ϕ.

Substituting expansions (5.2) into (5.1a) we find the equations at leading order are satisfied and at $O(\epsilon)$ we directly find

$$(2f^-_T + f^- f^-_\xi + f^-_{\xi\xi\xi})_\xi = \gamma f^-, \tag{5.3}$$

which is indeed the Ostrovsky equation. Note, to derive (5.3) it is not required to average the equations at $O(\epsilon)$ (as we did in the previous chapters) due to the construction of the solution (5.2) and the particular configuration of the IVP (5.1). The initial

condition for (5.3) in terms of T, is found from matching with the initial evolution of the Cauchy data (5.1b) (described by the classical d'Alembert's solution), thus we find

$$f^-_{T=0} = F(\xi). \tag{5.4}$$

Next we find at $O(\epsilon^2)$

$$\begin{aligned} -4f^2_{\xi\eta} &= (2\phi_T + (f^-\phi)_\xi + \phi_{\xi\xi\xi})_\xi - \gamma\phi - f^-_{TT} - 2f^-_{\xi\xi\xi T} + (-2\psi_T + \psi_{\eta\eta\eta})_\eta - \gamma\psi \\ &+ 2f^-_\xi\psi_\eta + f^-\psi_{\eta\eta} + f^-_{\xi\xi}\psi, \end{aligned} \tag{5.5}$$

which after averaging with respect to the fast time variable t, at constant ξ and then at constant η (see Chapters 3 & 4, [72], [73]), yields the following linearised Ostrovsky equations respectively (see also [74]):

$$\Big(-2\psi_T + \psi_{\eta\eta\eta}\Big)_\eta = \gamma\psi, \tag{5.6}$$

and

$$\Big(2\phi_T + (f^-\phi)_\xi + \phi_{\xi\xi\xi}\Big)_\xi = \gamma\phi + f^-_{TT} + 2f^-_{\xi\xi\xi T}, \tag{5.7}$$

where we assume (i) f^2 and it's derivatives remain bounded (required in order to have a nonsecular solution) and (ii) f^-, ψ, ϕ and their derivatives remain bounded and are sufficiently rapidly decaying for any fixed T. The initial conditions for (5.6) and (5.7) are obtained in the same way as the solutions obtained in Chapters 3 & 4 (which were previously used to describe ψ and ϕ $\forall T$), namely

$$\psi(\eta,0) = -\frac{1}{2}\Big[\int_{-\infty}^{\eta} f^-_T(s,T)ds\Big]_{T=0}, \qquad \phi(\xi,0) = \frac{1}{2}\Big[\int_{-\infty}^{\xi} f^-_T(s,T)ds\Big]_{T=0}. \tag{5.8}$$

It is important to reiterate that the approach considered here is not implemented to yield a more accurate solution beyond $O(\epsilon)$ and for applicability for larger time. It is considered instead to yield a solution with closer accuracy to $O(\epsilon)$ throughout all times within the solutions applicability. It was noted in Chapters 3 & 4 that although the previously developed weakly nonlinear solution improved the leading order approximation at all times $t \in [0, \epsilon^{-1}]$, the absolute error increased with time. We would like to emphasise that this previously noted characteristic of the solution should be viewed as a deficiency of the problem formulation, not the constructed solution.

5.2 Regularised Boussinesq equation

In this new setting, let us reconsider the Cauchy problem for the single regularised Boussinesq equation with the configuration corresponding to a single right-propagating KdV soliton solution to leading order (previously considered in Section 4.5.1), that is

$$\begin{aligned} f_{tt} - f_{xx} &= \epsilon\left[\frac{1}{2}(f^2)_{xx} + f_{ttxx}\right], \\ f|_{t=0} &= 12\frac{\partial^2}{\partial x^2}\log(1+e^{px}) \quad = 3p^2\ \mathrm{sech}^2(px/2), \\ f_t|_{t=0} &= -12\frac{\partial^3}{\partial x^3}\log(1+e^{px}) = 3p^3\ \mathrm{sech}^2(px/2)\ \tanh(px/2), \end{aligned} \tag{5.9}$$

(note, $\gamma = 0$) on the infinite line. The weakly nonlinear solution is therefore of the form

$$f = f^-(\xi, T) + \epsilon[\phi(\xi, T) + \psi(\eta, T)] + O(\epsilon^2), \tag{5.10}$$

where the leading order solution is given by the single KdV soliton solution

$$f^-(\xi, T) = 3p^2\mathrm{sech}^2(z), \quad z = \frac{p}{2}\left(\xi - \frac{p^2}{2}T\right). \tag{5.11}$$

However, the higher order terms ψ, ϕ, under the configuration (5.9), are now found as solutions to the Cauchy problems for the following linearised KdV equations:

$$\begin{aligned} \Big(-2\psi_T + \psi_{\eta\eta\eta}\Big)_\eta &= 0, \\ \psi|_{T=0} &= \frac{3p^4}{4}\mathrm{sech}^2(p\eta/2), \end{aligned} \tag{5.12}$$

and

$$\begin{aligned} \big(2\phi_T + (f^-\phi)_\xi + \phi_{\xi\xi\xi}\big)_\xi &= f^-_{TT} + 2f^-_{\xi\xi\xi T}, \\ \phi|_{T=0} &= -\frac{3p^4}{4}\mathrm{sech}^2(p\xi/2). \end{aligned} \tag{5.13}$$

The linearised KdV equations have previously appeared in the framework of the regularised Boussinesq equation [114], however in the work contained in this chapter we explicitly construct solutions of the IVP in terms of the leading order solutions.

By noting $f^-_T = -\frac{p^2}{2}f^-_\xi$, we can integrate the nonhomogeneous variable coefficient linearised KdV equation (5.13a), subject to zero boundary conditions, to yield

$$2\phi_T + (f^-\phi)_\xi + \phi_{\xi\xi\xi} = \frac{p^4}{4}f^-_\xi - p^2 f^-_{\xi\xi\xi}. \tag{5.14}$$

It can be shown that (5.14) has a particular solution in the form

$$\phi_{ps}(\xi, T) = -\frac{3}{8}p^4 T f_\xi^- + p^2 f^-, \tag{5.15}$$

and therefore the general solution of (5.13) can be written as

$$\phi(\xi, T) = \tilde{\phi}(\xi, T) + 3p^4 \mathrm{sech}^2(z) + \frac{9p^7 T}{8}\mathrm{sech}^2(z)\tanh(z), \tag{5.16}$$

where $\tilde{\phi}$ is the solution to the following Cauchy problem for the homogeneous linearised KdV equation:

$$\begin{aligned} 2\tilde{\phi}_T + (f^-\tilde{\phi})_\xi + \tilde{\phi}_{\xi\xi\xi} &= 0, \\ \tilde{\phi}|_{T=0} &= -\frac{15p^4}{4}\mathrm{sech}^2\left(\frac{p\xi}{2}\right), \end{aligned} \tag{5.17}$$

(note the slight change to the initial conditions in (5.13b)).

The method of stationary phase is often used to obtain some asymptotic form of solutions for equations of the type (5.12a) (e.g., see [1]). However, approaches of this type require one to consider long time, which contradicts the restrictions on the slow time T for the construction of the weakly nonlinear solution in this work. Cauchy problems of the type (5.17) were studied in [100], for arbitrary initial conditions and with f^- as a general solution of the KdV equation. However, the constructed solutions are not always easily explicitly obtainable in terms of elementary functions. This therefore motivates the consideration of the perturbation approach for the Cauchy problems (5.13) and (5.17), detailed in the next section.

5.2.1 Perturbation solution for higher order left-propagating wave

Integrating the linearised KdV equation for ψ with respect to η, subject to zero boundary conditions, yields the Cauchy problem (5.12) in the form

$$\begin{aligned} -2\psi_T + \psi_{\eta\eta\eta} &= 0, \\ \psi|_{T=0} &= \frac{3p^4}{4}\mathrm{sech}^2\left(\frac{p\eta}{2}\right) = g_1(\eta). \end{aligned} \tag{5.18}$$

Applying the Fourier transform (B.1) to (5.18) yields

$$\begin{aligned} -2\hat{\psi}_T - ik^3\hat{\psi} &= 0, \\ \hat{\psi}(k, 0) &= \int_{-\infty}^{\infty} e^{-ik\eta} g_1(\eta) d\eta, \end{aligned} \tag{5.19}$$

which we can solve in the Fourier space to find

$$\hat{\psi}(k,T) \;=\; \hat{\psi}(k,0)e^{\frac{-ik^3T}{2}}. \tag{5.20}$$

Applying the inverse Fourier transform (B.2), the solution of (5.18) can be written as

$$\psi(\eta,T)=\frac{1}{2\pi}\int_{-\infty}^{\infty}\left[\int_{-\infty}^{\infty}e^{-iky}g_1(y)dy\right]e^{\frac{-ik^3T}{2}}e^{ik\eta}dk, \tag{5.21}$$

where the inner integral can be explicitly found as

$$\int_{-\infty}^{\infty}g_1(y)e^{-iky}dy=\frac{3p^2k\pi}{\sinh\left(\frac{k\pi}{p}\right)}, \tag{5.22}$$

but the full outer integral in (5.21) is not so easy to explicitly obtain.

To yield an easily obtainable solution in terms of elementary functions, we Taylor expand the exponential term involving T in (5.21), about $T=0$ (not only do we in principle require $T\in[0,1]$ but moreover this expansion converges on the entire domain), to find

$$\begin{aligned}\psi(\eta,T) \;&=\; \frac{3p^2}{2}\int_{-\infty}^{\infty}\frac{k[\cos(k\eta)+i\sin(k\eta)]}{\sinh\left(\frac{k\pi}{p}\right)}\left(1-\frac{ik^3T}{2}-\frac{k^6T^2}{8}+...\right)dk\\ &=\; \frac{3p^2}{2}\int_{-\infty}^{\infty}\frac{k\cos(k\eta)}{\sinh\left(\frac{k\pi}{p}\right)}dk+\frac{3p^2T}{4}\int_{-\infty}^{\infty}\frac{k^4\sin(k\eta)}{\sinh\left(\frac{k\pi}{p}\right)}dk-\frac{3p^2T^2}{16}\int_{-\infty}^{\infty}\frac{k^7\cos(k\eta)}{\sinh\left(\frac{k\pi}{p}\right)}dk\\ &+\quad ... \;.\end{aligned} \tag{5.23}$$

Explicitly evaluating the integrals in (5.23) yields

$$\begin{aligned}\psi(\eta,T) \;&=\; \frac{3p^4}{4}\mathrm{sech}^2\left(\frac{p\eta}{2}\right)+\frac{3p^7T}{8}\mathrm{sech}^2\left(\frac{p\eta}{2}\right)\tanh\left(\frac{p\eta}{2}\right)\left[3\mathrm{sech}^2\left(\frac{p\eta}{2}\right)-1\right]\\ &+\; \frac{3p^{10}T^2}{128}\mathrm{sech}^2\left(\frac{p\eta}{2}\right)\left[4-126\mathrm{sech}^2\left(\frac{p\eta}{2}\right)+420\mathrm{sech}^4\left(\frac{p\eta}{2}\right)-315\mathrm{sech}^6\left(\frac{p\eta}{2}\right)\right]\\ &+\quad ... \;.\end{aligned} \tag{5.24}$$

Therefore Taylor expanding in this way, provides an easily obtainable explicit solution for ψ, found up to a chosen order of p. Restricting p^4 to being a small parameter will yield an accurate asymptotic approach to the solution for ψ (this assumption on p is made in the next section in order to make analytical progress with the solution for ϕ).

5.2.2 Perturbation solution for higher order right-propagating wave

Rescaling (5.17) such that $\tilde{\phi} = p^4\bar{\phi}$, we have the following Cauchy problem for $\bar{\phi}$:

$$\begin{aligned} 2\bar{\phi}_T + \bar{\phi}_{\xi\xi\xi} &= -3p^2\bar{\phi}_\xi \operatorname{sech}^2(z) + 3p^3\bar{\phi}\operatorname{sech}^2(z)\tanh(z), \\ \bar{\phi}|_{T=0} &= -\frac{15}{4}\operatorname{sech}^2\left(\frac{p\xi}{2}\right). \end{aligned} \tag{5.25}$$

Assuming $|p| \ll 1$, we seek the following asymptotic solution of (5.25)

$$\bar{\phi} = \bar{\phi}_0 + p\bar{\phi}_1 + p^2\bar{\phi}_2 + p^3\bar{\phi}_3 + p^4\bar{\phi}_4 + p^5\bar{\phi}_5 + p^6\bar{\phi}_6 + \dots . \tag{5.26}$$

Substituting (5.26) into (5.25) yields the following Cauchy problems up to $O(p^3)$:

$$\begin{aligned} O(1): \quad 2\bar{\phi}_{0T} + \bar{\phi}_{0\xi\xi\xi} &= 0, \\ \bar{\phi}_0|_{T=0} &= -\frac{15}{4}\operatorname{sech}^2\left(\frac{p\xi}{2}\right), \end{aligned} \tag{5.27}$$

$$\begin{aligned} O(p): \quad 2\bar{\phi}_{1T} + \bar{\phi}_{1\xi\xi\xi} &= 0, \\ \bar{\phi}_1|_{T=0} &= 0, \end{aligned} \tag{5.28}$$

$$\begin{aligned} O(p^2): \quad 2\bar{\phi}_{2T} + \bar{\phi}_{2\xi\xi\xi} &= -3\bar{\phi}_{0\xi}\operatorname{sech}^2(z), \\ \bar{\phi}_2|_{T=0} &= 0, \end{aligned} \tag{5.29}$$

$$\begin{aligned} O(p^3): \quad 2\bar{\phi}_{3T} + \bar{\phi}_{3\xi\xi\xi} &= -3\bar{\phi}_{1\xi}\operatorname{sech}^2(z) + 3\bar{\phi}_0\operatorname{sech}^2(z)\tanh(z), \\ \bar{\phi}_3|_{T=0} &= 0. \end{aligned} \tag{5.30}$$

To leading order we have a very similar problem to that for ψ. Taking the Fourier transform of (5.27), solving the derived ordinary differential equation (ODE) in the Fourier space and implementing the inverse Fourier transform to get back to the physical space, yields the solution

$$\bar{\phi}_0(\xi, T) = \frac{1}{2\pi}\int_{-\infty}^{\infty}\left[\int_{-\infty}^{\infty} g_2(y)e^{-iky}dy\right]e^{\frac{ik^3T}{2}}e^{ik\xi}dk, \tag{5.31}$$

where we denote $g_2(\xi) = \bar{\phi}_0|_{T=0}$. The inner integral in (5.31) is explicitly found as

$$\int_{-\infty}^{\infty} g_2(y)e^{-iky}dy = -\frac{15k\pi}{p^2\sinh\left(\frac{k\pi}{p}\right)}, \tag{5.32}$$

therefore, Taylor expanding the exponential in (5.31) involving T, about $T = 0$, yields

$$\begin{aligned}\bar{\phi}_0(\xi,T) &= -\frac{15}{2p^2}\int_{-\infty}^{\infty}\frac{k[\cos(k\xi)+i\sin(k\xi)]}{\sinh\left(\frac{k\pi}{p}\right)}\left(1+\frac{ik^3T}{2}-\frac{k^6T^2}{8}+...\right)dk \\ &= -\frac{15}{2p^2}\int_{-\infty}^{\infty}\frac{k\cos(k\xi)}{\sinh\left(\frac{k\pi}{p}\right)}dk+\frac{15T}{4p^2}\int_{-\infty}^{\infty}\frac{k^4\sin(k\xi)}{\sinh\left(\frac{k\pi}{p}\right)}dk+\frac{15T^2}{16p^2}\int_{-\infty}^{\infty}\frac{k^7\cos(k\xi)}{\sinh\left(\frac{k\pi}{p}\right)}dk \\ &+ \quad ... \,. \end{aligned} \tag{5.33}$$

Explicitly evaluating the integrals in (5.33), yields the solution to (5.27) as

$$\begin{aligned}\bar{\phi}_0(\xi,T) &= -\frac{15}{4}\mathrm{sech}^2\left(\frac{p\xi}{2}\right)+\frac{15p^3T}{8}\mathrm{sech}^2\left(\frac{p\xi}{2}\right)\tanh\left(\frac{p\xi}{2}\right)\left[3\mathrm{sech}^2\left(\frac{p\xi}{2}\right)-1\right] \\ &- \frac{15p^6T^2}{128}\mathrm{sech}^2\left(\frac{p\xi}{2}\right)\left[4-126\mathrm{sech}^2\left(\frac{p\xi}{2}\right)+420\mathrm{sech}^4\left(\frac{p\xi}{2}\right)-315\mathrm{sech}^6\left(\frac{p\xi}{2}\right)\right] \\ &+ \quad ... \,. \end{aligned} \tag{5.34}$$

From (5.34) it is now clear that the term $\bar{\phi}_{0\xi}$ in (5.29) is indeed $O(p)$ and so we must shift this term to the next order. As a result, the solution of Cauchy problems (5.28) and (5.29) will be in the same form as (5.31), but with zero initial conditions, and are therefore the trivial solutions

$$\bar{\phi}_1(\xi,T) = \bar{\phi}_2(\xi,T) = 0. \tag{5.35}$$

The Cauchy problem (5.30) is now modified to the following form:

$$\begin{aligned} 2\bar{\phi}_{3T}+\bar{\phi}_{3\xi\xi\xi} &= -\frac{3}{p}\left[\bar{\phi}_0\ \mathrm{sech}^2(z)\right]_\xi, \\ \bar{\phi}_3|_{T=0} &= 0. \end{aligned} \tag{5.36}$$

From Duhamel's principle (see e.g. [43]), the solution of (5.36) can be expressed as

$$\bar{\phi}_3(\xi,T) = \frac{1}{2}\int_0^T \breve{\phi}_3(\xi,T,s)ds, \tag{5.37}$$

where $\breve{\phi}_3$, for fixed $s \geq 0$, is the solution to the homogeneous Cauchy problem

$$\begin{aligned} 2\breve{\phi}_{3T}+\breve{\phi}_{3\xi\xi\xi} &= 0, \\ \breve{\phi}_3|_{T=s} &= -\frac{3}{p}\left\{\bar{\phi}_0(\xi;s)\ \mathrm{sech}^2\left[\frac{p}{2}\left(\xi-\frac{p^2s}{2}\right)\right]\right\}_\xi. \end{aligned} \tag{5.38}$$

Taking the Fourier transform of (5.38), and solving the resulting ODE, one can yield the solution of (5.38) in the original physical space as

$$\breve{\phi}_3(\xi,T,s)=\frac{1}{2\pi}\int_{-\infty}^{\infty}\left[\int_{-\infty}^{\infty}g_3(y;s)e^{-iky}dy\right]e^{\frac{-ik^3(s-T)}{2}}e^{ik\xi}dk, \tag{5.39}$$

where we denote $g_3(\xi;s)=\breve{\phi}_3|_{T=s}$. Integrating the inner integral in (5.39) by parts once, and noting that $\bar{\phi}_0$ is bounded as $\xi\to\pm\infty\ \forall T$, we find

$$\int_{-\infty}^{\infty}g_3(y;s)e^{-iky}dy=-\frac{3ik}{p}\int_{-\infty}^{\infty}\bar{\phi}_0(y;s)\ \mathrm{sech}^2\left[\frac{p}{2}\left(y-\frac{p^2s}{2}\right)\right]e^{-iky}dy. \tag{5.40}$$

We substitute the leading order expression for $\bar{\phi}_0$, given by (5.34), into (5.40), such that the overall solution of $\bar{\phi}$ is accurate up to $O(p^6)$. In order to obtain some explicit form of (5.40), in terms of elementary functions (useful for the subsequent outer integral in (5.39)), we also Taylor expand the non-symmetric hyperbolic term in (5.40) about $s=0$ (s is restricted to the same domain as $T\in[0,1]$, moreover the radius of convergence of this expansion is greater than this domain), to obtain

$$\begin{aligned}\int_{-\infty}^{\infty}g_3(y;s)e^{-iky}dy\ =\ &\frac{45ik}{4p}\int_{-\infty}^{\infty}\mathrm{sech}^4\left(\frac{py}{2}\right)\cos(ky)dy\\ &-\frac{45p^2ks}{8}\int_{-\infty}^{\infty}\mathrm{sech}^4\left(\frac{py}{2}\right)\tanh\left(\frac{py}{2}\right)\left[3\mathrm{sech}^2\left(\frac{py}{2}\right)-2\right]\sin(ky)dy\\ &+\frac{45p^5iks^2}{128}\int_{-\infty}^{\infty}\mathrm{sech}^4\left(\frac{py}{2}\right)\left[16-164\mathrm{sech}^2\left(\frac{py}{2}\right)+444\mathrm{sech}^4\left(\frac{py}{2}\right)\right.\\ &\left.-315\mathrm{sech}^6\left(\frac{py}{2}\right)\right]\cos(ky)dy+\ldots\ .\end{aligned} \tag{5.41}$$

Explicitly evaluating the integrals in (5.41) we find the inner integral of (5.39) is

$$\begin{aligned}\int_{-\infty}^{\infty}g_3(y;s)e^{-iky}dy\ =\ &\frac{30ik^2(k^2+p^2)\pi}{p^5\sinh\left(\frac{k\pi}{p}\right)}-\frac{3sk^3(k^4-p^4)\pi}{p^5\sinh\left(\frac{k\pi}{p}\right)}\\ &+\frac{is^2k^2(k^2+p^2)(35k^6+127k^4p^2+440k^2p^4+288p^6)\pi}{112\ p^5\sinh\left(\frac{k\pi}{p}\right)}+\ldots\ .\end{aligned} \tag{5.42}$$

Taylor expanding the exponential term involving T in (5.39) about $(s-T)=0$; noticing the order of each of the resulting integrals will be $O(p^{n+m+1})$, where n,m are the order of the terms p^nk^m in the resulting integrands; we find $\breve{\phi}_3$ up to $O(p^3)$ as

$$\begin{aligned}\breve{\phi}_3(\xi,T,s)\ =\ &+\frac{15i}{p^5}\int_{-\infty}^{\infty}\frac{k^2(k^2+p^2)\left[\cos(ky)+i\sin(ky)\right]}{\sinh\left(\frac{k\pi}{p}\right)}\left[1-\frac{ik^3(s-T)}{2}+\ldots\right]dk\\ &-\frac{3s}{2p^5}\int_{-\infty}^{\infty}\frac{k^3(k^4-p^4)\left[\cos(ky)+i\sin(ky)\right]}{\sinh\left(\frac{k\pi}{p}\right)}\Big[1+\ldots\Big]dk+\ldots\ .\end{aligned} \tag{5.43}$$

Explicitly evaluating the integrals in (5.43) yields

$$\begin{aligned}\breve{\phi}_3(\xi,T,s) = & -\frac{45}{2}\text{sech}^4\left(\frac{p\xi}{2}\right)\tanh\left(\frac{p\xi}{2}\right) \\ & + \frac{45p^3(s-T)}{16}\text{sech}^4\left(\frac{p\xi}{2}\right)\left[32-130\text{sech}^2\left(\frac{p\xi}{2}\right)+105\text{sech}^4\left(\frac{p\xi}{2}\right)\right] \\ & - \frac{45p^3 s}{16}\text{sech}^4\left(\frac{p\xi}{2}\right)\left[8-28\text{sech}^2\left(\frac{p\xi}{2}\right)+21\text{sech}^4\left(\frac{p\xi}{2}\right)\right]+\ldots\,, \quad (5.44)\end{aligned}$$

where we find from (5.37), the solution to the Cauchy problem (5.36), up to $O(p^3)$, is

$$\begin{aligned}\bar{\phi}_3(\xi,T) = & -\frac{45T}{4}\text{sech}^4\left(\frac{p\xi}{2}\right)\tanh\left(\frac{p\xi}{2}\right) \\ & - \frac{45p^3T^2}{32}\text{sech}^4\left(\frac{p\xi}{2}\right)\left[20-79\text{sech}^2\left(\frac{p\xi}{2}\right)+63\text{sech}^4\left(\frac{p\xi}{2}\right)\right]+\ldots\,. \quad (5.45)\end{aligned}$$

We next consider higher order solutions. From the substitution of (5.26) into (5.25), we find the following higher order Cauchy problems that arise at the next three orders:

$$\begin{aligned} O(p^4): \quad 2\bar{\phi}_{4T}+\bar{\phi}_{4\xi\xi\xi} &= 0, \\ \bar{\phi}_4|_{T=0} &= 0, \quad (5.46) \\ O(p^5): \quad 2\bar{\phi}_{5T}+\bar{\phi}_{5\xi\xi\xi} &= -3\bar{\phi}_{3\xi}\,\text{sech}^2(z), \\ \bar{\phi}_5|_{T=0} &= 0, \quad (5.47) \\ O(p^6): \quad 2\bar{\phi}_{6T}+\bar{\phi}_{6\xi\xi\xi} &= -3\bar{\phi}_{4\xi}\,\text{sech}^2(z)+3\bar{\phi}_3\,\text{sech}^2(z)\tanh(z), \\ \bar{\phi}_6|_{T=0} &= 0. \quad (5.48)\end{aligned}$$

The first thing to note is that from (5.47) the term $\bar{\phi}_{3\xi}$, which can be found from (5.45), is $O(p)$. Therefore we shift this term to the next order, which as a result reduces the Cauchy problem (5.47) to the same form as (5.46) and indeed (5.28), thus

$$\bar{\phi}_4(\xi,T)=\bar{\phi}_5(\xi,T)=0. \quad (5.49)$$

Now from (5.48) we have the following Cauchy problem

$$\begin{aligned} 2\bar{\phi}_{6T}+\bar{\phi}_{6\xi\xi\xi} &= -\frac{3}{p}\left[\bar{\phi}_3\,\text{sech}^2(z)\right]_\xi, \\ \bar{\phi}_6|_{T=0} &= 0, \quad (5.50)\end{aligned}$$

which is analogous to the Cauchy problem for $\bar{\phi}_3$. From Duhamel's principle, the solution of (5.50) can be written as

$$\bar{\phi}_6(\xi,T)=\frac{1}{2}\int_0^T \breve{\phi}_6(\xi,T,s)ds, \tag{5.51}$$

where $\breve{\phi}_6$, for fixed $s\geq 0$, is the solution to the following homogeneous Cauchy problem

$$\begin{aligned} 2\breve{\phi}_{6T}+\breve{\phi}_{6\xi\xi\xi} &= 0, \\ \breve{\phi}_6|_{T=s} &= -\frac{3}{p}\left\{\bar{\phi}_3(\xi;s)\ \mathrm{sech}^2\left[\frac{p}{2}\left(\xi-\frac{p^2 s}{2}\right)\right]\right\}_\xi . \end{aligned} \tag{5.52}$$

Taking the Fourier transform of (5.52), one can obtain the solution of (5.52) as

$$\breve{\phi}_6(\xi,T,s)=\frac{1}{2\pi}\int_{-\infty}^{\infty}\left[\int_{-\infty}^{\infty} g_4(y;s)e^{-iky}dy\right]e^{\frac{-ik^3(s-T)}{2}}e^{ik\xi}dk, \tag{5.53}$$

where we denote $g_4(\xi;s)=\breve{\phi}_6|_{T=s}$. Integrating the inner integral in (5.53) by parts once, and noting that $\bar{\phi}_3$ is bounded as $\xi\to\pm\infty\ \forall T$, we find

$$\int_{-\infty}^{\infty} g_4(y;s)e^{-iky}dy=-\frac{3ik}{p}\int_{-\infty}^{\infty}\bar{\phi}_3(y;s)\ \mathrm{sech}^2\left[\frac{p}{2}\left(y-\frac{p^2 s}{2}\right)\right]e^{-iky}dy. \tag{5.54}$$

Taking the first term in the expression for $\bar{\phi}_3$ and Taylor expanding the non-symmetric hyperbolic term in (5.54), about $s=0$, (both taken such that the overall solution for $\bar{\phi}$ is accurate up to $O(p^6)$), we find the inner integral (5.54) in the form

$$\begin{aligned} \int_{-\infty}^{\infty} g_4(y;s)e^{-iky}dy &= \frac{135sk}{4p}\int_{-\infty}^{\infty}\mathrm{sech}^6\left(\frac{py}{2}\right)\tanh\left(\frac{py}{2}\right)\sin(ky)dy\ +\ ... \\ &= \frac{6sk^3(k^2+p^2)(k^2+4p^2)\pi}{p^8\sinh\left(\frac{k\pi}{p}\right)}\ +\ ... . \end{aligned} \tag{5.55}$$

Substituting (5.55) into (5.53) and Taylor expanding the exponential term involving T in (5.53), about $(s-T)=0$, yields the solution $\breve{\phi}_6$ as follows

$$\begin{aligned} \breve{\phi}_6(\xi,T,s) &= \frac{3s}{p^8}\int_{-\infty}^{\infty}\frac{k^3(k^2+p^2)(k^2+4p^2)\cos(k\xi)}{\sinh\left(\frac{k\pi}{p}\right)}dk\ +\ ... \\ &= \frac{135s}{8}\mathrm{sech}^6\left(\frac{p\xi}{2}\right)\left[7\mathrm{sech}^2\left(\frac{p\xi}{2}\right)-6\right]\ +\ ... . \end{aligned} \tag{5.56}$$

From (5.51) we find the solution to the Cauchy problem (5.50), to leading order, as

$$\bar{\phi}_6(\xi,T)=\frac{135T^2}{32}\mathrm{sech}^6\left(\frac{p\xi}{2}\right)\left[7\mathrm{sech}^2\left(\frac{p\xi}{2}\right)-6\right]\ +\ ... . \tag{5.57}$$

Combining solutions (5.34), (5.35), (5.45), (5.49) and (5.57), each found such that the overall solution for $\bar{\phi}$ is accurate up to $O(p^6)$, yields the following asymptotic solution of the Cauchy problem (5.25):

$$\begin{aligned}\bar{\phi}(\xi,T) \;=\; & -\frac{15}{4}\mathrm{sech}^2\left(\frac{p\xi}{2}\right) - \frac{15p^3T}{8}\mathrm{sech}^2\left(\frac{p\xi}{2}\right)\tanh\left(\frac{p\xi}{2}\right)\left[3\mathrm{sech}^2\left(\frac{p\xi}{2}\right)+1\right] \\ & -\; \frac{15p^6T^2}{128}\mathrm{sech}^2\left(\frac{p\xi}{2}\right)\left[4+114\mathrm{sech}^2\left(\frac{p\xi}{2}\right) - 312\mathrm{sech}^4\left(\frac{p\xi}{2}\right)\right. \\ & +\quad \left. 189\mathrm{sech}^6\left(\frac{p\xi}{2}\right)\right] \;+\; \ldots\,. \end{aligned} \tag{5.58}$$

Therefore the general solution to the original Cauchy problem (5.13), up to $O(p^{10})$, is

$$\begin{aligned}\phi(\xi,T) \;=\; & -\frac{15p^4}{4}\mathrm{sech}^2\left(\frac{p\xi}{2}\right) - \frac{15p^7T}{8}\mathrm{sech}^2\left(\frac{p\xi}{2}\right)\tanh\left(\frac{p\xi}{2}\right)\left[3\mathrm{sech}^2\left(\frac{p\xi}{2}\right)+1\right] \\ & -\; \frac{15p^{10}T^2}{128}\mathrm{sech}^2\left(\frac{p\xi}{2}\right)\left[4+114\mathrm{sech}^2\left(\frac{p\xi}{2}\right) - 312\mathrm{sech}^4\left(\frac{p\xi}{2}\right) + 189\mathrm{sech}^6\left(\frac{p\xi}{2}\right)\right] \\ & +\; 3p^4\mathrm{sech}^2(z) + \frac{9p^7T}{8}\mathrm{sech}^2(z)\tanh(z) \;+\; \ldots\,, \end{aligned} \tag{5.59}$$

where the particular solution comprises of the final two terms in (5.59) (although the particular solution contains different orders of p, it is indeed found exactly).

5.2.3 Numerical solution for higher order corrections

We numerically solve the Cauchy problems for ψ and $\tilde{\phi}$, given by (5.18) and (5.17) respectively. This is considered firstly to directly compare the accuracy of the perturbation solutions developed in the previous sections, but ultimately to further improve the accuracy of the weakly nonlinear solution of the Cauchy problem for the Boussinesq equation (5.9), using the evolution equations for ψ, ϕ.

Both of the homogenous linearised KdV equations governing ψ and $\bar{\phi}$ are solved using spectral methods based on the fast Fourier transform (FFT) algorithm (refer to Appendix B.3.1 & B.3.2 respectively, for full details of the methods). As a result the numerical methods are implemented on a periodic domain, although for simulations comparing the weakly nonlinear solution on the infinite line we simply adjust the spatial boundaries such that they are suitably far enough from the propagating waves. We let $\eta, \xi \in [-L, L]$, for finite L, and discretise the (η, T), (ξ, T) domains into grids with constant spacings $\Delta\eta$, ΔT and $\Delta\xi$, ΔT respectively. The solutions $\psi(\eta, T)$ and $\phi(\xi, T)$

of the linearised KdV equations (5.12) and (5.13) are approximated by the solutions $\psi(i\Delta\eta, j\Delta T) = \psi_{\text{num}}$ and $\phi(i\Delta\xi, j\Delta T) = \phi_{\text{num}}$ for $i = 1, 2, ..., N$ and $j = 0, 1, ...,$ found via the solutions of spectral methods (B.20) and (B.26) plus the particular solution (5.15), respectively. For later comparisons with numerical simulations of the Boussinesq equation (5.9), we shift the spatial domains from the moving reference frames η and ξ to the x domain. This is simply done provided t is completely divisible by $\Delta\eta$ and $\Delta\xi$.

If we note that $\bar{\phi}$ has an exact solution in the form:

$$\bar{\phi}_{\text{sol}}(\xi, T) \;=\; -3p^3\text{sech}^2(z)\,\tanh(z), \tag{5.60}$$

(which is indeed the first order derivative of $f^-(\xi, T)$), the accuracy of ϕ_{num} can be tested with the following exact solution of the nonhomogeneous equation for ϕ:

$$\phi_{\text{sol}}(\xi, T) \;=\; -3p^3\text{sech}^2(z)\,\tanh(z) + 3p^4\text{sech}^2(z) + \frac{9p^7T}{8}\text{sech}^2(z)\tanh(z). \tag{5.61}$$

Setting the initial condition in the spectral method (B.26) in Appendix B.3.2, as

$$\hat{\bar{\phi}}_{\text{sol}}(k, 0) \;=\; -3p^3\,\mathscr{F}\left[\text{sech}^2\left(\frac{p\xi}{2}\right)\,\tanh\left(\frac{p\xi}{2}\right)\right], \tag{5.62}$$

we compare the difference between ϕ_{num} and the particular solution for ϕ, given by (5.61). One can see from Table 5.1 that as the time step size is reduced by a factor of 2, the maximum absolute error in ϕ_{num} improves by almost exactly the same factor. One can continue to improve the accuracy of ϕ_{num} by further reducing the time step, although as $\Delta T \to 0$ the length of computational time will start to compromise the value in the improvement of error (this is of course a question of how accurate one requires the solution to be). To make comparisons with the developed perturbation solution for ϕ and subsequently with the weakly nonlinear solution of the Cauchy problem for the Boussinesq equation (5.9) (at least for times up to $T = O(1)$), the magnitude of the maximum absolute error in the latter entries of Table 5.1 already far exceed the necessary accuracy required. Figure 5.1 illustrates ϕ_{num} and the exact solution ϕ_{sol} for specific parameters at times $T = \epsilon$ and $T = 1$.

We define the perturbation solutions derived in Sections 5.2.1 & 5.2.2 for the Cauchy problems (5.12) and (5.13) as

$$\begin{aligned} \phi^{3i+1}_{\text{pert}} &= \phi \qquad \text{up to } O(p^{3i+1}), \\ \psi^{3i+1}_{\text{pert}} &= \psi \qquad \text{up to } O(p^{3i+1}), \quad \text{for } i = 1, 2, 3, .., \end{aligned} \tag{5.63}$$

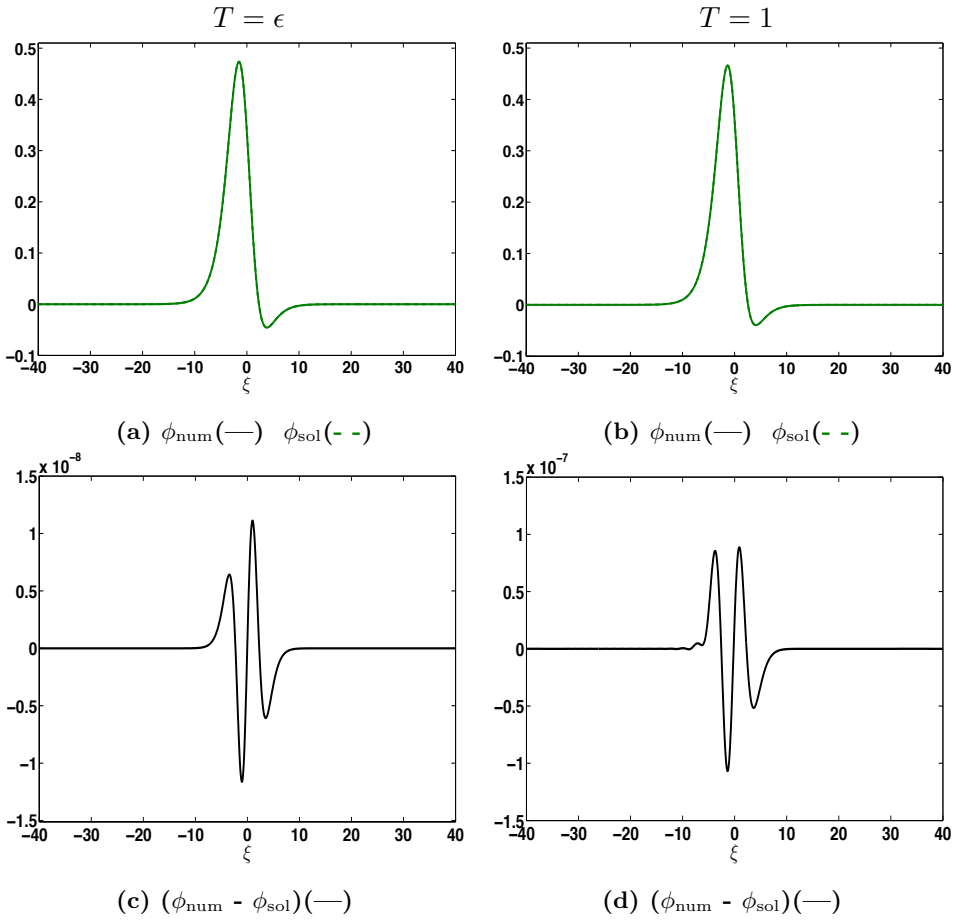

(a) ϕ_{num}(—) ϕ_{sol}(- -) **(b)** ϕ_{num}(—) ϕ_{sol}(- -)

(c) (ϕ_{num} - ϕ_{sol})(—) **(d)** (ϕ_{num} - ϕ_{sol})(—)

Figure 5.1: Evolution of numerical solution ϕ_{num} and exact solution (5.61) at (a) $T = \epsilon$ & (b) $T = 1$, and the absolute errors (c) & (d) at the respective times, with $p = 1/\sqrt{3}$, $\epsilon = 0.1$. Numerical parameters: $L = 10^3$, $N = 20000$ and $\Delta T = 7.8125 \times 10^{-5}$.

	Maximum absolute error	
ΔT	$T = \epsilon$	$T = 1$
0.01	1.4883 x 10^{-6}	1.3674 x 10^{-5}
0.005	7.4393 x 10^{-7}	6.8372 x 10^{-6}
0.0025	3.7191 x 10^{-7}	3.4186 x 10^{-6}
0.00125	1.8594 x 10^{-7}	1.7093 x 10^{-6}
6.25 x 10^{-4}	9.2967 x 10^{-8}	8.5466 x 10^{-7}
3.125 x 10^{-4}	4.6483 x 10^{-8}	4.2733 x 10^{-7}
1.5625 x 10^{-4}	2.3241 x 10^{-8}	2.1367 x 10^{-7}
7.8125 x 10^{-5}	1.1621 x 10^{-8}	1.0683 x 10^{-7}
3.90625 x 10^{-5}	5.8103 x 10^{-9}	5.3416 x 10^{-8}
1.95313 x 10^{-5}	2.9051 x 10^{-9}	2.6708 x 10^{-8}

Table 5.1: Maximum absolute error of the numerical solution ϕ_{num} compared to the exact solution (5.61) at $T = \epsilon$ and $T = 1$, for various time discretisations ΔT, with $p = 1/\sqrt{3}$ and $\epsilon = 0.1$. Numerical parameters: $L = 10^3$, $N = 20000$.

where ψ and ϕ are given by (5.24) and (5.59) respectively. Figures 5.2 & 5.3 illustrate the difference in the perturbation solutions (5.63) compared with their respective numerical solutions ψ_{num} and ϕ_{num}. As we increase the number of terms in (5.63), we see the perturbation solutions ψ_{pert} and ϕ_{pert} tending towards ψ_{num} and ϕ_{num} respectively (at least for times up to $T = O(1)$). One can also notice a worse approximation of the numerical solution ϕ_{num} from the perturbation solution ϕ_{pert}, than for ψ_{num} from ψ_{pert}, particularly for the perturbation solutions up to $O(p^4)$ and $O(p^7)$. This is perhaps due to more approximations being used in the derivation of ϕ_{pert}, namely the extra Taylor expansion of the non-symmetric hyperbolic term in (5.40) and (5.54). Nonetheless, in both comparisons there is a clear convergence of the perturbation solutions to the numerical solutions as more terms are added, thus encouraging the use of (5.24) and (5.59) as accurate asymptotic representations of the solutions to the Cauchy problems (5.12) and (5.13) respectively.

5.2.4 Numerical simulations

We now compare direct numerical simulations of the Cauchy problem for the Boussinesq equation (5.9) with: (i) the weakly nonlinear solution found from the perturbation

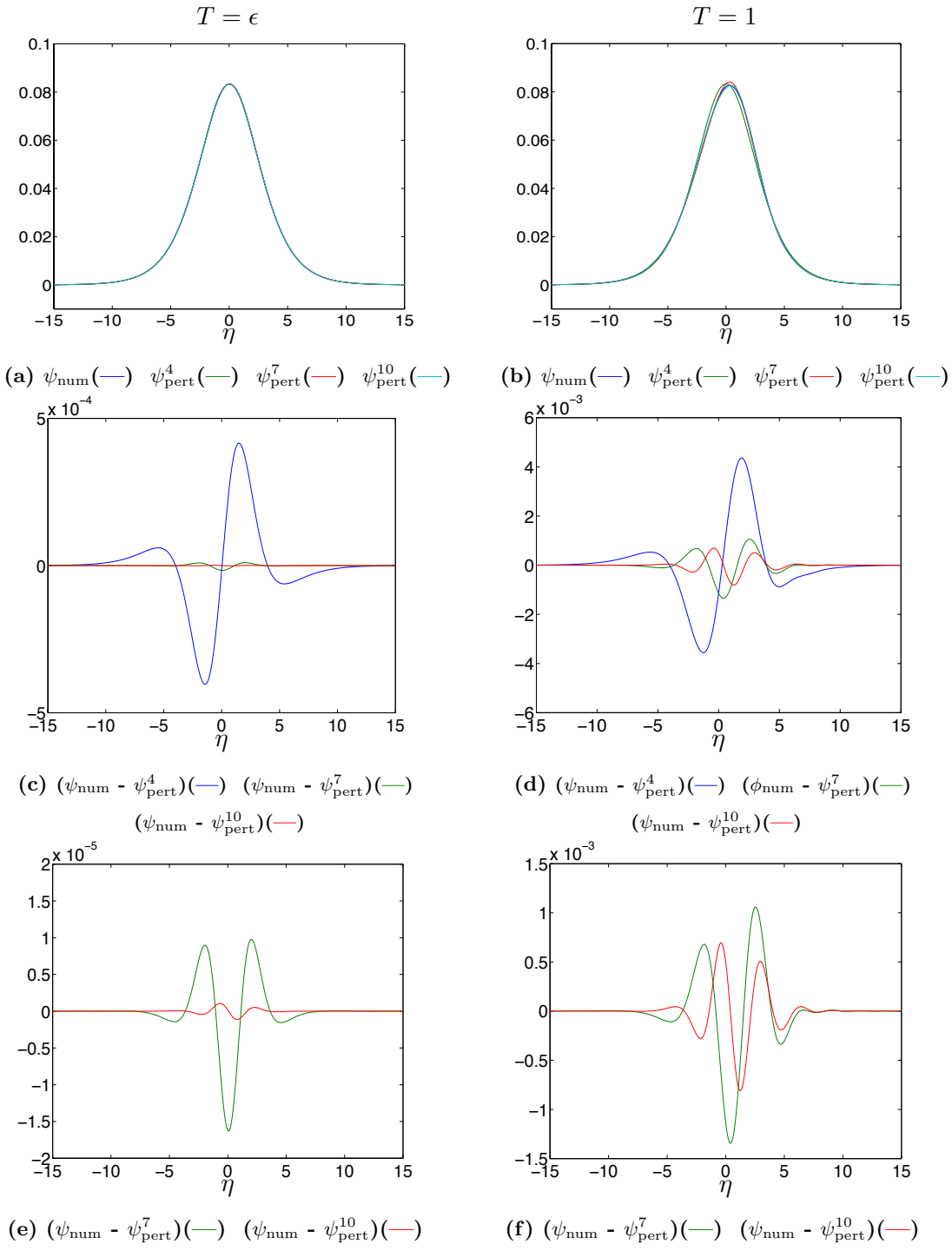

(a) ψ_{num}(—) ψ^4_{pert}(—) ψ^7_{pert}(—) ψ^{10}_{pert}(—)

(b) ψ_{num}(—) ψ^4_{pert}(—) ψ^7_{pert}(—) ψ^{10}_{pert}(—)

(c) (ψ_{num} - ψ^4_{pert})(—) (ψ_{num} - ψ^7_{pert})(—) (ψ_{num} - ψ^{10}_{pert})(—)

(d) (ψ_{num} - ψ^4_{pert})(—) (ϕ_{num} - ψ^7_{pert})(—) (ψ_{num} - ψ^{10}_{pert})(—)

(e) (ψ_{num} - ψ^7_{pert})(—) (ψ_{num} - ψ^{10}_{pert})(—)

(f) (ψ_{num} - ψ^7_{pert})(—) (ψ_{num} - ψ^{10}_{pert})(—)

Figure 5.2: Evolution of ψ_{num} and perturbation solutions (5.63a), with $p = 1/\sqrt{3}$, $\epsilon = 0.1$, at (a) $T = \epsilon$ & (b) $T = 1$, and the absolute errors (c) & (d) at the respective times, (e) & (f) are close ups of the errors. Numerical parameters: $L = 10^3$, $N = 20000$, $\Delta T = 0.00125$.

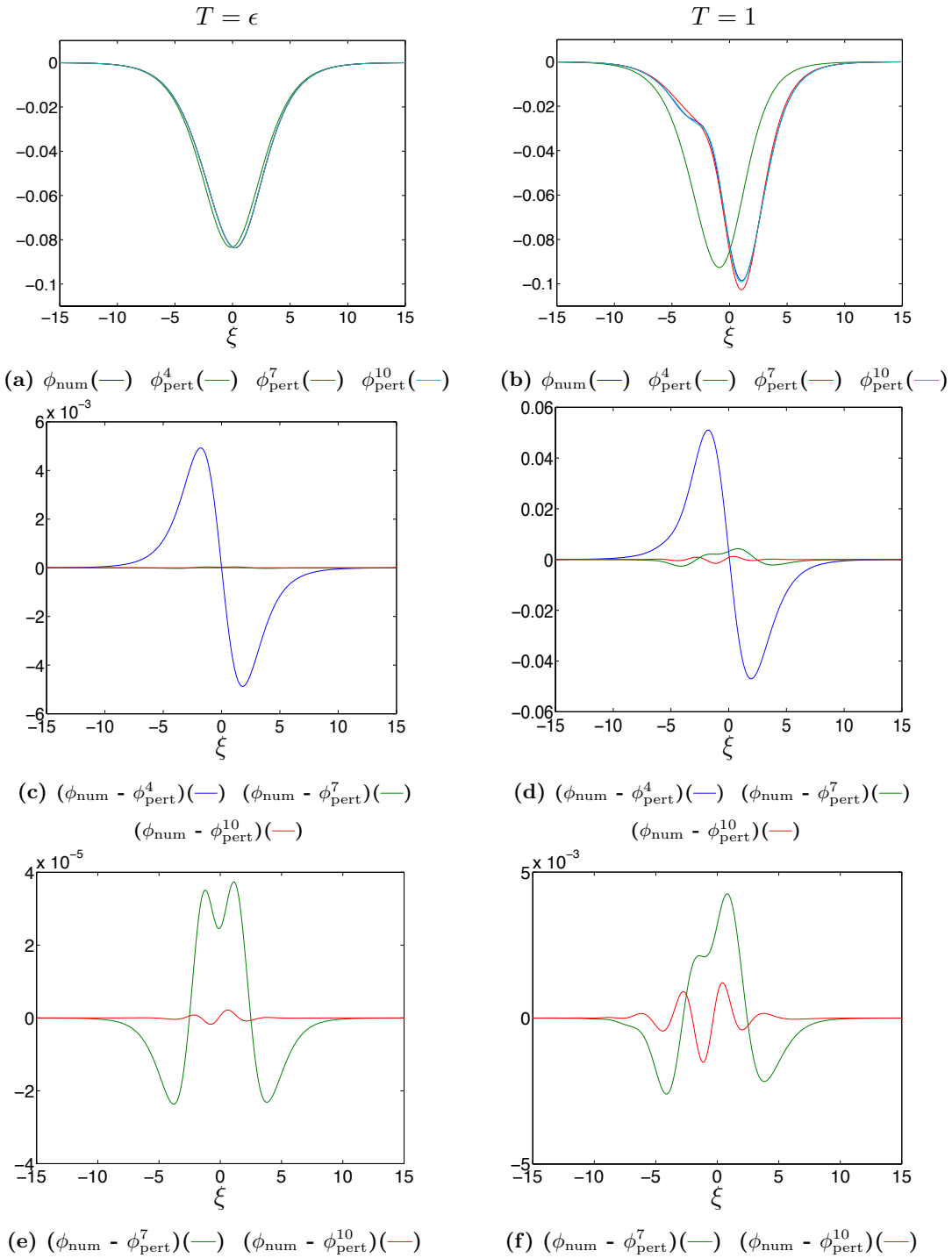

(a) ϕ_{num}(—) ϕ^4_{pert}(—) ϕ^7_{pert}(—) ϕ^{10}_{pert}(—)

(b) ϕ_{num}(—) ϕ^4_{pert}(—) ϕ^7_{pert}(—) ϕ^{10}_{pert}(—)

(c) (ϕ_{num} - ϕ^4_{pert})(—) (ϕ_{num} - ϕ^7_{pert})(—) (ϕ_{num} - ϕ^{10}_{pert})(—)

(d) (ϕ_{num} - ϕ^4_{pert})(—) (ϕ_{num} - ϕ^7_{pert})(—) (ϕ_{num} - ϕ^{10}_{pert})(—)

(e) (ϕ_{num} - ϕ^7_{pert})(—) (ϕ_{num} - ϕ^{10}_{pert})(—)

(f) (ϕ_{num} - ϕ^7_{pert})(—) (ϕ_{num} - ϕ^{10}_{pert})(—)

Figure 5.3: Evolution of ϕ_{num} and perturbation solutions (5.63b), with $p = 1/\sqrt{3}$, $\epsilon = 0.1$, at (a) $T = \epsilon$ & (b) $T = 1$, and the absolute errors (c) & (d) at the respective times, (e) & (f) are close ups of the errors. Numerical parameters: $L = 10^3$, $N = 20000$, $\Delta T = 0.00125$.

solutions for the higher order evolution problems; (ii) the weakly nonlinear solution found with the numerical solutions for the higher order evolution problems; (iii) the weakly nonlinear solution originally developed in Chapter 4.

The Boussinesq equation is solved using a pseudo-spectral method, based on the FFT algorithm (details of the method are outlined in Appendix B.2, along with discussions regarding the accuracy of the method). We let $x \in [-L, L]$, for finite L, and discretise the (x, t) domain into a grid with constant spacings Δx and Δt. The solution $f(x, t)$ of the Boussinesq equation (5.9a) is approximated by the solution $f(i\Delta x, j\Delta t) = f_{\text{num}}$ for $i = 1, 2, ..., N$ and $j = 0, 1, ...$, found via the solution of the spectral method (B.15) (with $\gamma = 0$). The accuracy of the numerical method is far in excess of what is required for comparisons with the weakly nonlinear solution derived in this chapter, nevertheless, extensions for further more accurate requirements are trivially achieved by further decreasing the time step and/or increasing the number of harmonics in the FFT.

To consider the errors of the different weakly nonlinear solutions we first introduce some notation. We define the weakly nonlinear solution of the Cauchy problem for the Boussinesq equation (5.9), with the perturbation solutions ψ and ϕ, as

$$f^l_{\text{pert}} = f_1 + \epsilon[\psi^l_{\text{pert}} + \phi^l_{\text{pert}}], \tag{5.64}$$

where ψ^l_{pert} and ϕ^l_{pert} up to $O(p^l)$, are defined by (5.63), and f_1 is the leading order term in the weakly nonlinear solution (for the configuration (5.9), $f_1 = f^-$). We define the weakly nonlinear solution of the Cauchy problem for the Boussinesq equation (5.9), with the numerical solutions for ψ and ϕ, as

$$f^{\text{num}}_2 = f_1 + \epsilon[\psi_{\text{num}} + \phi_{\text{num}}], \tag{5.65}$$

where the numerical methods for ψ_{num} and ϕ_{num} are developed in Appendix B.3.1 & B.3.2 respectively.

Figure 5.4(a) depicts the weakly nonlinear solutions (5.72) and (5.64) for $l = 4, 7, 10$, and the weakly nonlinear solution originally developed in Chapter 4, all in comparison with the numerical solution f_{num}. Figures 5.4(b) & (c) depict the absolute errors of each of the weakly nonlinear solutions with respect to f_{num}. The first thing one can notice from Figure 5.4 is that f^{num}_2 and all but the lowest order perturbation solution improve the accuracy of the weakly nonlinear solution previously developed in Chapter 4. As seen in Figures 5.2 & 5.3, one can also notice the weakly nonlinear solution

for the perturbation solutions converging towards $f_{\rm num}$ as more terms are taken in the perturbation solutions for ψ and ϕ. The most accurate solution is indeed $f_2^{\rm num}$, significantly better than all but the highest order perturbation solution we consider, which is $f_{\rm pert}^{10}$.

We now analyse the errors of the weakly nonlinear solutions (5.64) and (5.72) in more detail, by first defining the maximum absolute error over x at $t=\tau$, as

$$\begin{aligned} e_\tau^m &= \max_{-L\le x\le L}|f_{\rm num}(x,\tau)-f_m(x,\tau)|, \qquad \text{for } \ m=1,2,\\ e_\tau^{Pi} &= \max_{-L\le x\le L}|f_{\rm num}(x,\tau)-f_{\rm pert}^{(3i+1)}(x,\tau)|, \quad \text{for } \ i=1,2,3,\dots,\\ e_\tau^N &= \max_{-L\le x\le L}|f_{\rm num}(x,\tau)-f_2^{\rm num}(x,\tau)|, \end{aligned} \tag{5.66}$$

where e_τ^2 corresponds to the maximum absolute error of the weakly nonlinear solution without the evolution equations describing the higher order problems (i.e. the solution developed in Chapter 4). We use a least squares power fit to determine how the maximum absolute error of each of the weakly nonlinear solutions vary with the small parameter ϵ. Let us write the errors defined in (5.66) as

$$\begin{aligned} e_\tau^m &= C_m\epsilon^{\alpha_m} \qquad \text{for} \quad m=1,2,\\ e_\tau^{Pi} &= C_{Pi}\epsilon^{\alpha_{Pi}} \qquad \text{for} \quad i=1,2,3,\dots,\\ e_\tau^N &= C_N\epsilon^{\alpha_N}. \end{aligned} \tag{5.67}$$

Taking logs of the errors in this form and considering a range of ϵ, one can find the coefficients C and α, with the latter revealing how the maximum absolute errors scale with ϵ. We find the coefficients using *Matlab*'s 'polyfit' command.

Figures 5.5 & 5.6 display double log plots of the maximum absolute errors we find explicitly from numerical simulations compared with the log of the errors defined in (5.67), both against $\ln(\epsilon)$. Figure 5.5 illustrates the error scaling of the weakly nonlinear solution developed previously without the higher order evolution equations, compared with the most accurate weakly nonlinear solution which includes the solution of the higher order evolution equations developed in this chapter; which is the solution with ψ, ϕ solved numerically. The error scaling of the leading order approximation is also included. As one can see from Figure 5.5, the weakly nonlinear solution $f_{\rm num}^2$ dramatically improves the scaling of the maximum absolute error with ϵ, in comparison with the previously developed solution f_2. To be precise, the maximum absolute error

of f^2_{num} scales almost precisely as $O(\epsilon^2)$ as opposed to f_2 which scales almost as $O(\epsilon)$; a complete order of ϵ larger.

The scalings of the errors found here coincide very accurately with that derived in [74], where rigorous error estimates of the weakly nonlinear solution are developed for the Cauchy problem for the Boussinesq–Ostrovsky equation.

Since analysis of error using a least squares power fit was not undertaken in Chapters 3 & 4, this similarity of scaling with ϵ between both orders of the previously developed weakly nonlinear solution was not observed. Upon direct comparison of each order of the previously found solution, it was shown that the maximum absolute error of f_2 was significantly smaller than f_1. This is because the constant C_2 in the definition of the higher order error (5.67) is substantially smaller than C_1, corresponding to the leading order error.

Figure 5.6 displays the scaling of the maximum absolute error with ϵ, for the weakly nonlinear solution found using the perturbation solutions for the higher order evolution problems, compared with f_2 and f_2^{num}. One can see that the error scaling is improved from the previously developed solution at all orders of the perturbation solution. One can also see an increasing improvement of the error scaling as the order of the perturbation solutions for ψ_{pert}, ϕ_{pert} is increased. This further cements the validity of the developed perturbation approach outlined in Sections 5.2.1 & 5.2.2 as a valid and effective methodology for solving the higher order evolution problems in the weakly nonlinear solution of the Cauchy problem for the Boussinesq equation (5.9). Although the errors of the weakly nonlinear solution found from the numerically obtained solutions for ψ and ϕ, scale significantly closer to $O(\epsilon^2)$, the developed perturbation approach has the scope to be continued to obtain f_{pert} up to arbitrary orders of p, and subsequently the accuracy can be continually improved. Moreover, if one wants to extend the weakly nonlinear solution of the Cauchy problem (5.9) beyond $O(\epsilon)$ accuracy (indeed one needs to also extend the derivation of the Boussinesq equation to the same order), it can be very useful to have ψ, ϕ in some analytical form.

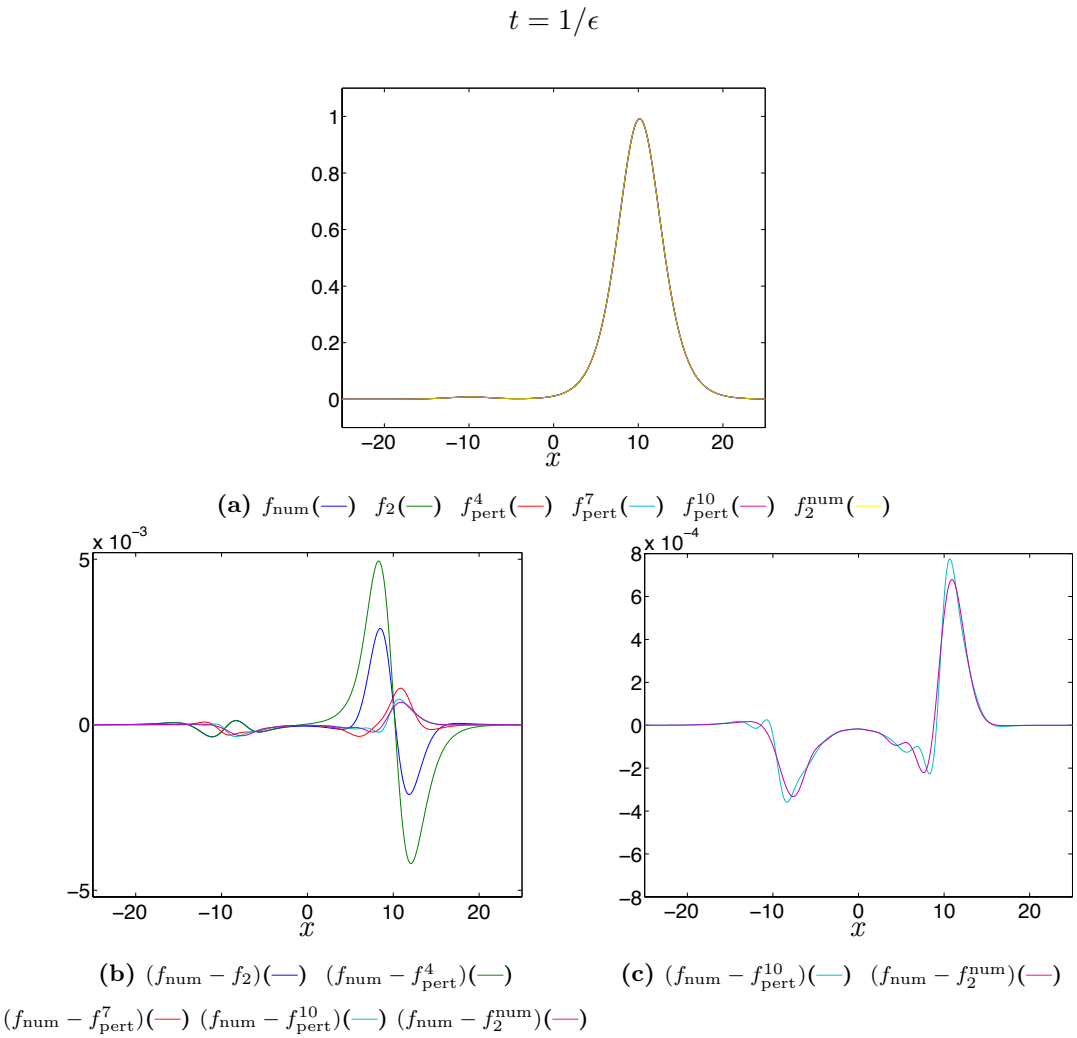

(a) $f_{\rm num}$(—) f_2(—) $f^4_{\rm pert}$(—) $f^7_{\rm pert}$(—) $f^{10}_{\rm pert}$(—) $f^{\rm num}_2$(—)

(b) $(f_{\rm num} - f_2)$(—) $(f_{\rm num} - f^4_{\rm pert})$(—) $(f_{\rm num} - f^7_{\rm pert})$(—) $(f_{\rm num} - f^{10}_{\rm pert})$(—) $(f_{\rm num} - f^{\rm num}_2)$(—)

(c) $(f_{\rm num} - f^{10}_{\rm pert})$(—) $(f_{\rm num} - f^{\rm num}_2)$(—)

Figure 5.4: (a) Comparison of numerical solution $f_{\rm num}$ with the weakly nonlinear solution using the higher order: (i) perturbation solutions; (ii) numerical solutions; (iii) solution f_2; all for $p = 1/\sqrt{3}$, $\epsilon = 0.1$, at $t = 1/\epsilon$, with (b) the absolute errors and (c) a close up of the errors. Numerical parameters: $L = 10^3$, $N = 20000$, $\Delta T = 0.00125$, $\Delta t = 0.01$.

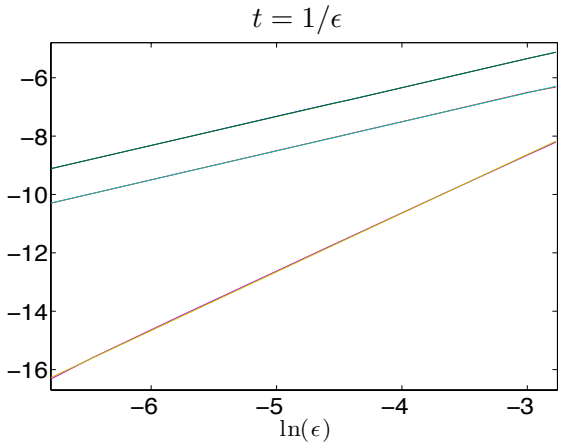

$\ln(e^1_{ta})$(—) $\alpha_1 \ln(\epsilon) + \ln(C_1)$(—) $\ln(e^2_{ta})$(—) $\alpha_2 \ln(\epsilon) + \ln(C_2)$(—) $\ln(e^N_{ta})$(—) $\alpha_N \ln(\epsilon) + \ln(C_N)$(—)

Figure 5.5: Double log plot of absolute errors of the weakly nonlinear solution, at $t = t_a = 1/\epsilon$ ($T = 1$), for $p = 1/\sqrt{3}$ and varying ϵ. Coefficients are $\alpha_1 = 0.9906$, $\alpha_2 = 0.9928$, $\alpha_N = 2.0103$ and $C_1 = 0.09281$, $C_2 = 0.02896$, $C_N = 0.07417$. Numerical parameters: $\Delta t = 0.01$, $\Delta T = 0.00125$ and $L = 2000$, $N = 2 \times 10^4$.

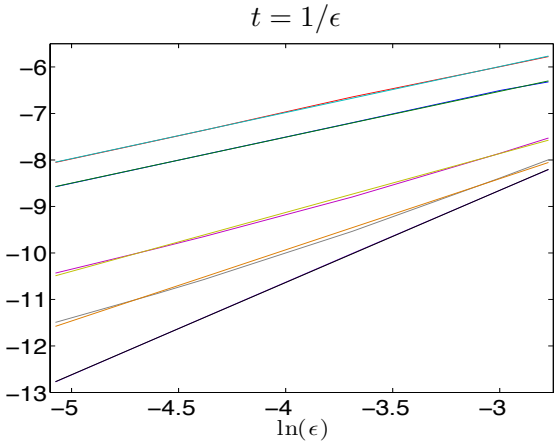

$\ln(e^2_{ta})$(—) $\alpha_2 \ln(\epsilon) + \ln(C_2)$(—) $\ln(e^{P1}_{ta})$(—) $\alpha_{P1} \ln(\epsilon) + \ln(C_{P1})$(—)
$\ln(e^{P2}_{ta})$(—) $\alpha_{P2} \ln(\epsilon) + \ln(C_{P2})$(—) $\ln(e^{P3}_{ta})$(—) $\alpha_{P3} \ln(\epsilon) + \ln(C_{P3})$(—)
$\ln(e^N_{ta})$(—) $\alpha_N \ln(\epsilon) + \ln(C_N)$(—)

Figure 5.6: Double log plot of absolute errors of the weakly nonlinear solution, at $t = t_a = 1/\epsilon$ ($T = 1$), for $p = 1/\sqrt{3}$ and varying ϵ. Coefficients are $\alpha_2 = 0.9865$, $\alpha_{P1} = 0.9906$, $\alpha_{P2} = 1.2669$, $\alpha_{P3} = 1.5308$, $\alpha_N = 1.9827$ and $C_2 = 0.02830$, $C_{P1} = 0.04885$, $C_{P2} = 0.01722$, $C_{P3} = 0.0221$, $C_N = 0.0668$. Numerical parameters: $\Delta t = 0.01$, $\Delta T = 0.00125$ and $L = 2000$, $N = 2 \times 10^4$.

5.3 Regularised Boussinesq–Ostrovsky equation

We now consider an initial configuration for the Boussinesq–Ostrovsky equation (5.1):

$$\begin{aligned} f_{tt} - f_{xx} &= \epsilon\left(\frac{1}{2}(f^2)_{xx} + f_{ttxx} - \gamma f\right), \\ f|_{t=0} &= 3p^2\ \mathrm{sech}^2(px/2) - \hat{\alpha}[\mathrm{sech}^2(p(x+x_0)/2) + \mathrm{sech}^2(p(x-x_0)/2)], \\ f_t|_{t=0} &= 3p^3\ \mathrm{sech}^2(px/2)\ \tanh(px/2) - p\hat{\alpha}\Big[\mathrm{sech}^2(p(x+x_0)/2)\ \tanh(p(x+x_0)/2) \\ &+ \mathrm{sech}^2(p(x-x_0)/2)\ \tanh(p(x-x_0)/2)\Big], \end{aligned} \tag{5.68}$$

where x_0 is an arbitrary shift along x. Note we choose the constant $\hat{\alpha}$ in the initial conditions of (5.68) to satisfy the zero mass property of the subsequent leading order Ostrovsky equation. For the particular configuration (5.68) this yields

$$\hat{\alpha} = \frac{3p^2\ \tanh(pL/2)}{\tanh(p(L+x_0)/2) + \tanh(p(L-x_0)/2)},$$

(note, $\hat{\alpha} \to 3p^2/2$ in the limit $L \to \infty$).

The weakly nonlinear solution of the Cauchy problem (5.68) is of the form

$$f = f^-(\xi, T) + \epsilon[\phi(\xi, T) + \psi(\eta, T)] + O(\epsilon^2)\ ,$$

where the leading order term f^- is the solution to the Ostrovsky Cauchy problem:

$$\begin{aligned} \left(2f^-_T + f^-f^-_\xi + f^-_{\xi\xi\xi}\right)_\xi &= \gamma f^-, \\ f^-|_{T=0} &= 3p^2\ \mathrm{sech}^2(p\xi/2) - \hat{\alpha}\Big[\mathrm{sech}^2(p(\xi+x_0)/2) \\ &+ \mathrm{sech}^2(p(\xi-x_0)/2)\Big]. \end{aligned} \tag{5.69}$$

From the particular configuration (5.68), the higher order terms ψ, ϕ are given as solutions of the following linearised Ostrovsky Cauchy problems:

$$\begin{aligned} \left(-2\psi_T + \psi_{\eta\eta\eta}\right)_\eta &= \gamma\psi, \\ \psi|_{T=0} &= -\frac{1}{2}\left[\int_{-L}^{\eta} f^-_T(s)ds\right]_{T=0} \end{aligned} \tag{5.70}$$

and

$$\begin{aligned} \left(2\phi_T + (f^-\phi)_\xi + \phi_{\xi\xi\xi}\right)_\xi &= \gamma\phi + f^-_{TT} + 2f^-_{\xi\xi\xi T}, \\ \phi|_{T=0} &= \frac{1}{2}\left[\int_{-L}^{\xi} f^-_T(s)ds\right]_{T=0}. \end{aligned} \tag{5.71}$$

The Cauchy problems (5.69), (5.70) and (5.71) are solved numerically and simultaneously at each time step; details of the numerical methods are outlined in Appendix B.4, B.5.1 & B.5.2 respectively. We let $\eta, \xi \in [-L, L]$, for finite L, and discretise the (η, T), (ξ, T) domains into grids with constant spacings $\Delta\eta$, ΔT and $\Delta\xi$, ΔT respectively. The solutions $f^-(\xi, T)$, $\psi(\eta, T)$ and $\phi(\xi, T)$ of the Ostrovsky-type equations (5.69), (5.70) and (5.71) are approximated by the solutions $f^-(i\Delta\xi, j\Delta T) = f^-_{\text{num}}$, $\psi(i\Delta\eta, j\Delta T) = \psi_{\text{num}}$ and $\phi(i\Delta\xi, j\Delta T) = \phi_{\text{num}}$ for $i = 1, 2, ..., N$ and $j = 0, 1, ...$, found via the solutions of the spectral methods (B.31), (B.35) and (B.42), respectively.

We now compare direct numerical simulations of the Cauchy problem for the Boussinesq–Ostrovsky equation (5.68) denoted f_{num}, found via the spectral method outlined in Appendix B.2, with the weakly nonlinear solution at each order. We define the weakly nonlinear solution of the Cauchy problem for the Boussinesq–Ostrovsky equation (5.68), with the numerical solutions for ψ and ϕ, as

$$f_2^{\text{num}} = f_1 + \epsilon[\psi_{\text{num}} + \phi_{\text{num}}], \tag{5.72}$$

where f_1 denotes the leading order approximation (in this case $f_1 = f^-$) and the numerical solutions ψ_{num} and ϕ_{num} are developed in Appendix B.5. Figures 5.7(a) & (b) illustrate the evolution of f_{num}, with the weakly nonlinear solution at each order, for a particular choice of ϵ. Figures 5.7(c) & (d) depict a magnification of the aforementioned figures. One can notice a distinct improvement in the absolute error (Figures 5.7(e) & (f)) of the weakly nonlinear solution with the higher order correction terms included.

Note, the terms we choose in the initial conditions for (5.68) to satisfy zero mass are chosen in the form of localised functions. Since the initial conditions of ψ, ϕ are dependent on the integral of the term f^-_T, it transpires that choosing a localised zero mass term in the problem for f^- (for instance, as opposed to a nonlocal constant pedestal term), enables the initial conditions of ψ, ϕ to be localised and not too large.

5.4 Concluding remarks

In this chapter we have extended the weakly nonlinear solution of the Cauchy problem for Boussinesq-type equations, originally constructed in Chapters 3 & 4 (see also [72], [73]), to include time dependence within the higher order solutions. We considered the so-called Boussinesq–Ostrovsky equation (reducible to the regularised Boussinesq

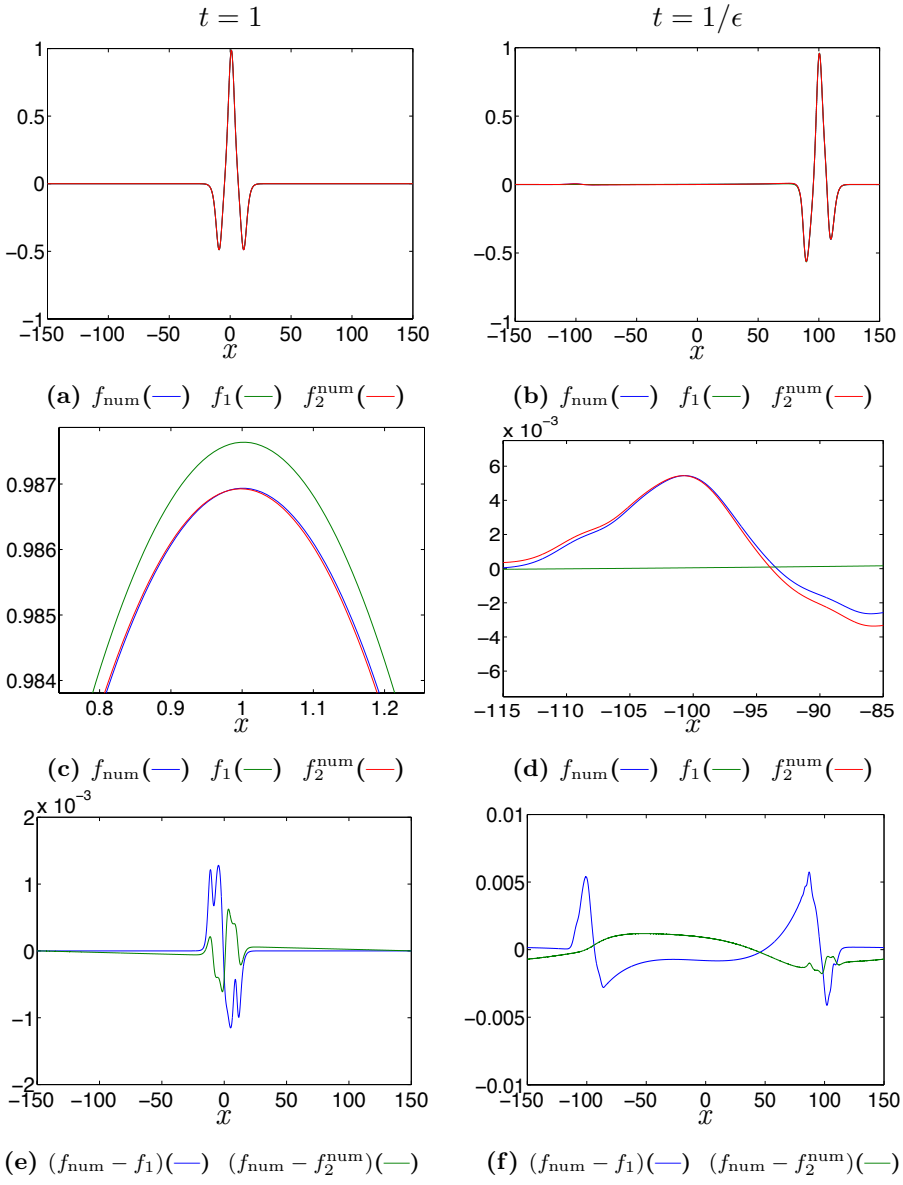

(a) f_{num}(—) f_1(—) f_2^{num}(—)

(b) f_{num}(—) f_1(—) f_2^{num}(—)

(c) f_{num}(—) f_1(—) f_2^{num}(—)

(d) f_{num}(—) f_1(—) f_2^{num}(—)

(e) $(f_{\text{num}} - f_1)$(—) $(f_{\text{num}} - f_2^{\text{num}})$(—)

(f) $(f_{\text{num}} - f_1)$(—) $(f_{\text{num}} - f_2^{\text{num}})$(—)

Figure 5.7: Comparison of the weakly nonlinear solution with respect to the numerical solution f_{num}, for $p = 1/\sqrt{3}$, $\epsilon = 0.01$, $\gamma = 0.1$, $x_0 = 10$, at (a) $t = 1$ & (b) $t = 1/\epsilon$, with close ups (c) & (d), and the absolute errors (e) & (f), at the respective times. Numerical parameters: $\Delta t = 0.01$, $\Delta T = 0.0000125$ and $L = 150$, $N = 4 \times 10^4$.

equation under one parameter choice) as an exact model, in order to simplify the analysis. The weakly nonlinear solution from the previous approach is extended to include a further higher order term, which is not included in the solution but rather introduced in order to derive the evolution equations at the previous order.

We derived the weakly nonlinear solution for the Cauchy problem with initial conditions which eliminated the left-propagating leading order solutions. For the case of the regularised Boussinesq equation we derived the KdV equation to leading order and two linearised KdV equations describing the higher order terms. Similarly, for the Cauchy problem for the Boussinesq–Ostrovsky equation we derived the Ostrovsky equation to leading order and two linearised Ostrovsky equations describing the higher order correction terms.

First, by considering a particular configuration of the Cauchy problem for the regularised Boussinesq equation we: (i) numerically solved the higher order evolution equations; (ii) developed an accurate perturbation theory for solving the higher order evolution equations; (iii) compared (i) and (ii) with numerical simulations of the Boussinesq Cauchy problem, along with the weakly nonlinear solutions previously considered in Chapter 4. We found the weakly nonlinear solution with the higher order terms, found via the numerical solution and perturbation solution, both improved the previously constructed weakly nonlinear solution developed in Chapter 4. The weakly nonlinear solution with the numerical solution at higher order produced the most accurate approximation and by considering a least squares power fit, the maximum absolute error of this solution was shown to scale almost precisely as $O(\epsilon^2)$. On the contrary, the corresponding error from the previous approach in Chapter 4 was found to scale as $O(\epsilon)$ at $T = 1$. We would like to stress that this should be viewed as a deficiency of the problem formulation, not the constructed solution in the previous approach.

Finally, we considered a particular configuration of the Cauchy problem for the Boussinesq–Ostrovsky equation by numerically solving both the leading order Ostrovsky and higher order linearised Ostrovsky problems. On comparison with numerical simulations of the Cauchy problem for the Boussinesq–Ostrovsky equation we found that the constructed solution up to $O(\epsilon)$ significantly improved the leading order approximation.

All numerical methods used throughout this chapter are implemented using pseudo-spectral methods, derived and discussed in Appendix B.

Chapter 6

Radiating solitary wave solutions of coupled Boussinesq equations

In this chapter we are concerned with the construction of a theoretical description for radiating solitary wave solutions of the coupled system of cRB equations (3.2) (see Section 2.3 for details regarding radiating solitary waves). This type of solution, comprising of a leading pure solitary wave with a linear co-propagating oscillatory tail, emerges from a pure solitary wave solution when the parameters c, α, β are slightly perturbed from the symmetric case ($c = \alpha = \beta = 1$); seen in particular for the parameter c in Section 3.2.1 (in the case of strong interactions).

We construct an asymptotic procedure to yield the solution of the cRB equations, where the leading order approximation in both components f and g is given in terms of the particular solution (2.30) of the regularised Boussinesq equation in the symmetric case. At higher order, the system uncouples into two linear nonhomogeneous ODEs with variable coefficient terms, one correcting the localised part of the solution, for which we solve analytically, and the other describing the co-propagating oscillatory tail. We solve the latter of these higher order problems by: (i) making an assumption on some of the small localised terms in the governing equation and subsequently determining key features in the far spatial limits; (ii) implementing an asymptotic approach and similarly investigating the solution in the far spatial limits.

The derived theoretical radiating solitary wave solutions of the cRB equations are compared with corresponding numerical simulations (this is already considered for some parameter choices in Chapter 3) to examine the accuracy of the developed approach.

6.1 Weak perturbation from the symmetric case

Let us rewrite the system of cRB equations (3.2) as

$$\begin{aligned} f_{tt} - f_{xx} &= \frac{1}{2}(f^2)_{xx} + f_{ttxx} - \delta(f-g), \\ g_{tt} - g_{xx} &= \frac{1}{2}(g^2)_{xx} + g_{ttxx} + \gamma(f-g) + \mu\left[Ag + \frac{1}{2}Bg^2 + Cg_{tt}\right]_{xx}, \end{aligned} \tag{6.1}$$

where $(c^2-1) = A\mu$, $(\alpha-1) = B\mu$, $(\beta-1) = C\mu$, for $A, B, C = O(1)$ and $|\mu| \ll 1$. Seeking travelling wave solutions of the form $f = f(\xi)$, $g = g(\xi)$ for $\xi = x - vt$, we have from (6.1)

$$\begin{aligned} (v^2-1)f_{\xi\xi} &= \frac{1}{2}(f^2)_{\xi\xi} + v^2 f_{\xi\xi\xi\xi} - \delta(f-g), \\ (v^2-1)g_{\xi\xi} &= \frac{1}{2}(g^2)_{\xi\xi} + v^2 g_{\xi\xi\xi\xi} + \gamma(f-g) + \mu\left[Ag + \frac{1}{2}Bg^2 + v^2 Cg_{\xi\xi}\right]_{\xi\xi}. \end{aligned} \tag{6.2}$$

We look for a solution of (6.2) in the form of the following asymptotic expansions:

$$f = f_0 + \mu f_1 + O(\mu^2)\,, \quad g = g_0 + \mu g_1 + O(\mu^2), \quad v^2 = v_0^2(1 + \mu v_1 + O(\mu^2))\,. \tag{6.3}$$

Substituting (6.3) into (6.2), we derive the particular solution of the single regularised Boussinesq equation, as discussed in Section 2.3 (given by (2.30)), as the leading order terms for f and g:

$$f_0 = g_0 = A_0\ \mathrm{sech}^2\left(\frac{\xi}{\Lambda}\right), \quad \text{where} \quad A_0 = 3(v_0^2-1), \quad \Lambda = \frac{2v_0}{\sqrt{v_0^2-1}}, \tag{6.4}$$

and at $O(\mu)$ we find

$$\begin{aligned} (v_0^2-1)f_{1\xi\xi} &= (f_0 f_1)_{\xi\xi} + v_0^2 f_{1\xi\xi\xi\xi} - \delta(f_1 - g_1) + v_0^2 v_1 (f_{0\xi\xi} - f_0)_{\xi\xi}, \\ (v_0^2-1)g_{1\xi\xi} &= (f_0 g_1)_{\xi\xi} + v_0^2 g_{1\xi\xi\xi\xi} + \gamma(f_1 - g_1) + v_0^2 v_1 (f_{0\xi\xi} - f_0)_{\xi\xi} + \\ &\qquad \left[Af_0 + \frac{1}{2}Bf_0^2 + v_0^2 Cf_{0\xi\xi}\right]_{\xi\xi}. \end{aligned} \tag{6.5}$$

Introducing the variables $\phi = f_1 - g_1$ and $\psi = f_1 + \frac{\delta}{\gamma}g_1$, system (6.5) uncouples into

$$(v_0^2-1)\phi_{\xi\xi} = (f_0\phi)_{\xi\xi} + v_0^2\phi_{\xi\xi\xi\xi} - (\delta+\gamma)\phi - P(f_0)_{\xi\xi}, \tag{6.6}$$

$$(v_0^2-1)\psi_{\xi\xi} = (f_0\psi)_{\xi\xi} + v_0^2\psi_{\xi\xi\xi\xi} + \frac{\delta}{\gamma}P(f_0)_{\xi\xi} + v_0^2 v_1(1+\frac{\delta}{\gamma})(f_{0\xi\xi} - f_0)_{\xi\xi}, \tag{6.7}$$

where we denote

$$P(f_0) = Af_0 + \frac{1}{2}Bf_0^2 + v_0^2 Cf_{0\xi\xi} = [A + (v_0^2-1)C]f_0 + \frac{1}{2}(B-C)f_0^2.$$

6.2 Non-oscillating higher order part of the solution

Introducing the variable $\chi = \frac{\sqrt{v_0^2-1}}{2v_0}\xi$ and integrating (6.7) twice yields

$$\psi_{\chi\chi} + 4(3\text{sech}^2\chi - 1)\psi = L(\chi) + C_1\chi + C_2, \tag{6.8}$$

for the arbitrary constants $C_{1,2}$, and we denote the term

$$L = -\frac{4\delta}{\gamma(v_0^2-1)}P(f_0) + \frac{2v_1(1+\frac{\delta}{\gamma})}{v_0^2-1}[2f_0(\chi) + f_0^2(\chi)].$$

We choose the constants of integration $C_1, C_2 = 0$ since we seek solutions of ψ which are localised as $\chi \to \pm\infty$. The homogeneous part of (6.8):

$$\psi_{\chi\chi} + 4(3\text{sech}^2\chi - 1)\psi = 0, \tag{6.9}$$

has a bounded solution of the form

$$\psi_1(\chi) = \tanh(\chi)\ \text{sech}^2(\chi), \tag{6.10}$$

(see for example [29]) which is proportional to $f_{0\chi}$, since (6.9) is the linearisation of the solitary wave equation for f_0. A second linearly independent solution of (6.9), denoted ψ_2, can be found using the Wronskian

$$\psi_1\psi_{2\chi} - \psi_2\psi_{1\chi} = W, \tag{6.11}$$

where W is a constant. Solving (6.11) for ψ_2 yields

$$\psi_2(\chi) = \frac{W}{32}\Big[60\chi - 32\ \coth(\chi) + 16\ \sinh(2\chi) + \sinh(4\chi)\Big]\ \tanh(\chi)\text{sech}^2(\chi), \tag{6.12}$$

and note, ψ_2 is unbounded as $\chi \to \pm\infty$. Using the method of variation of parameters, the general solution of (6.8) can be written in the form

$$\psi = \alpha_1\psi_1 + \alpha_2\psi_2 - \frac{\psi_1(\chi)}{W}\int_0^\chi L(\hat{\chi})\psi_2(\hat{\chi})d\hat{\chi} + \frac{\psi_2(\chi)}{W}\int_0^\chi L(\hat{\chi})\psi_1(\hat{\chi})d\hat{\chi}, \tag{6.13}$$

for the arbitrary constants $\alpha_{1,2}$. Since we have $\psi_1 \sim \exp(\mp 2\chi)$ and $\psi_2 \sim \exp(\pm 2\chi)$ as $\chi \to \pm\infty$, we must set $\alpha_2 = 0$. Also the first term in the particular solution will contain a secular term proportional to $\chi\exp(\mp 2\chi)$. This term arises from the term in L proportional to $f_0 \sim \exp(\mp 2\chi)$ but can be removed by the choice of v_1, namely

$$v_1 = \frac{\delta}{\gamma+\delta}[A + (v_0^2-1)C]\,. \tag{6.14}$$

Therefore we derive the following nonsecular general solution of (6.8), for $W = 32$:

$$\psi(\chi) = \alpha_1\tanh(\chi)\text{sech}^2(\chi) + \frac{3\delta(v_0^2-1)}{\gamma}(A - B + v_0^2C)\text{sech}^2(\chi)[1 - \tanh(\chi)]. \tag{6.15}$$

6.3 Oscillating higher order part of the solution

The equation for ϕ is more difficult to solve since we cannot simply begin by integrating the problem to reduce it to a 2nd order ODE. Let us first write (6.6) in the form

$$L(\phi) \equiv \phi_{\xi\xi\xi\xi} + (3\hat{\varepsilon}^2 \mathrm{sech}^2(\hat{\varepsilon}\xi/2)\phi)_{\xi\xi} - \hat{\varepsilon}^2\phi_{\xi\xi} - k^4\phi = Q_{\xi\xi}\,, \quad Q = \frac{P(f_0)}{v_0^2}\,, \tag{6.16}$$

where we denote $\hat{\varepsilon} = \sqrt{v_0^2 - 1}/v_0$ and $k^4 = (\delta + \gamma)/v_0^2$. The homogeneous form of (6.16) has four linearly independent solutions, which can be uniquely defined by their behaviour as $\xi \to \pm\infty$, as

$$\phi_1 \sim \cos m\xi\,, \quad \phi_2 \sim \sin m\xi\,, \quad \phi_3 \sim \cosh M\xi\,, \quad \phi_4 \sim \sinh M\xi\,, \quad \xi \to \infty\,, \tag{6.17}$$

$$\hat{\phi}_1 \sim \cos m\xi\,, \quad \hat{\phi}_2 \sim \sin m\xi\,, \quad \hat{\phi}_3 \sim \cosh M\xi\,, \quad \hat{\phi}_4 \sim \sinh M\xi\,, \quad \xi \to -\infty\,. \tag{6.18}$$

$$\text{where} \quad m^2, M^2 = (k^4 + \frac{\hat{\varepsilon}^4}{4})^{1/2} \mp \frac{\hat{\varepsilon}^2}{2}\,,$$

and note, in the limit as $\hat{\varepsilon} \to 0$, we have $m, M \to k$. Exploiting the symmetry in the operator L; namely if $\phi(\xi)$ is a solution, so too is $\phi(-\xi)$; we can write

$$\hat{\phi}_1(\xi) = \phi_1(-\xi)\,, \quad \hat{\phi}_2(\xi) = -\phi_2(-\xi)\,, \quad \hat{\phi}_3(\xi) = \phi_3(-\xi)\,, \quad \hat{\phi}_4(\xi) = -\phi_4(-\xi)\,.$$

Also, we note the solutions

$$\phi_5 = \phi_3 - \phi_4 \sim \exp(-M\xi), \quad \xi \to \infty\,; \quad \phi_6 = \hat{\phi}_3 + \hat{\phi}_4 \sim \exp(M\xi), \quad \xi \to \infty\,. \tag{6.19}$$

Let us write the fourth order equation (6.16) as the following 4×4 system

$$\mathbf{U}_\xi = \mathbf{A}\mathbf{U} + \mathbf{F}\,, \quad \text{where} \quad \mathbf{U} = (\phi, \phi_\xi, \phi_{\xi\xi}, \phi_{\xi\xi\xi})^{\mathbf{T}}\,, \quad \mathbf{F} = (0, 0, 0, Q_{\xi\xi})^{\mathbf{T}}\,, \tag{6.20}$$

and $\mathbf{A}$ is a 4×4 matrix with rows $(0,1,0,0), (0,0,1,0), (0,0,0,1), ((k^4 - S_{\xi\xi}), -2S_\xi, (\hat{\varepsilon}^2 - S), 0)$, where $S = 3\hat{\varepsilon}^2\mathrm{sech}^2(\hat{\varepsilon}\xi/2)$. Using the method of variation of parameters we seek a solution of (6.20) in the form

$$\mathbf{U} = B_1\mathbf{U}_1 + B_2\mathbf{U}_2 + B_3\mathbf{U}_3 + B_4\mathbf{U}_4 = \mathbf{G}\mathbf{B}\,, \quad \mathbf{B} = (B_1, B_2, B_3, B_4)^{\mathbf{T}}\,, \tag{6.21}$$

where the vectors $\mathbf{U}_i$ for $i = 1, 2, 3, 4$ are solutions of the homogeneous part of equation (6.20) corresponding to ϕ_i, and $\mathbf{G}$ is the fundamental matrix whose columns are $\mathbf{U}_1, \mathbf{U}_2, \mathbf{U}_3, \mathbf{U}_4$, namely

$$\mathbf{G}(\xi) = \begin{pmatrix} \phi_1 & \phi_2 & \phi_3 & \phi_4 \\ \phi_{1\xi} & \phi_{2\xi} & \phi_{3\xi} & \phi_{4\xi} \\ \phi_{1\xi\xi} & \phi_{2\xi\xi} & \phi_{3\xi\xi} & \phi_{4\xi\xi} \\ \phi_{1\xi\xi\xi} & \phi_{2\xi\xi\xi} & \phi_{3\xi\xi\xi} & \phi_{4\xi\xi\xi} \end{pmatrix}. \tag{6.22}$$

Substituting (6.21) into (6.20) yields

$$\begin{aligned} \mathbf{G}_\xi\mathbf{B} + \mathbf{G}\mathbf{B}_\xi - \mathbf{A}\mathbf{G}\mathbf{B} &= \mathbf{F}, \\ (\mathbf{G}_\xi - \mathbf{A}\mathbf{G})\mathbf{B} + \mathbf{G}\mathbf{B}_\xi &= \mathbf{F}, \\ \mathbf{B}_\xi &= \mathbf{G}^{-1}\mathbf{F}\,, \end{aligned} \tag{6.23}$$

since $\mathbf{G}$ (more specifically each column in $\mathbf{G}$) satisfies the homogeneous equation. Integrating (6.23) enables us to deduce the general solution of (6.20):

$$\mathbf{U} = \mathbf{G}(\xi)\{\mathbf{C} + \int_0^\xi \mathbf{G}^{-1}(\eta)\mathbf{F}(\eta)\,d\eta\}\,, \tag{6.24}$$

where $\mathbf{C} = (C_1, C_2, C_3, C_4)^{\mathbf{T}}$ is an arbitrary constant vector. In what follows, two of these arbitrary constants are chosen to ensure ϕ is bounded as $\xi \to \pm\infty$. Then, we impose an asymmetric condition on the oscillatory part of the solution (supported by relevant numerical simulations or equivalently from relevant group velocity arguments), in order to specify the final two arbitrary constants.

6.3.1 Approximation to the variable coefficient term

To make further analytical progress we let $\hat{\varepsilon} \to 0$ but only in the variable coefficient term in the left-hand side of (6.16). This yields approximate solutions of the homogeneous equation in the form

$$\phi_1 \to \cos(m\xi)\,, \quad \phi_2 \to \sin(m\xi)\,, \quad \phi_3 \to \cosh(M\xi)\,, \quad \phi_4 \to \sinh(M\xi)\,. \tag{6.25}$$

This approximation is inaccurate $\forall\xi$ but since the variable coefficient term is localised and small we maintain the correct behaviour of ϕ as $\xi \to \pm\infty$ (in what follows we seek the solution of ϕ in the far spatial region only). Under this approximation we find

$$\mathbf{G}^{-1}(\xi) = \frac{1}{m^2+M^2}\begin{pmatrix} M^2\phi_1 & -\frac{M^2}{m}\phi_2 & -\phi_1 & \frac{1}{m}\phi_2 \\ M^2\phi_2 & \frac{M^2}{m}\phi_1 & -\phi_2 & -\frac{1}{m}\phi_1 \\ m^2\phi_3 & -\frac{m^2}{M}\phi_4 & \phi_3 & -\frac{1}{M}\phi_4 \\ -m^2\phi_4 & \frac{m^2}{M}\phi_3 & -\phi_4 & \frac{1}{M}\phi_3 \end{pmatrix}. \tag{6.26}$$

With the variable coefficient term neglected in (6.16), the matrix $\mathbf{A}$ in equation (6.20) is now a constant coefficient matrix. Therefore, if $\mathbf{U}(\xi)$ is a solution of the homogeneous equation, so is $\mathbf{U}(\xi+\xi_0)$ for any constant ξ_0. Let us define $\mathbf{K}(\xi,\eta) = \mathbf{G}(\xi)\mathbf{G}^{-1}(\eta)$ as the unique matrix solution of the homogeneous equation, such that $\mathbf{K}(\eta,\eta) = \mathbf{I}$ where

I is the unit matrix. It then follows that we have $\mathbf{K}(\xi,\eta) = \mathbf{E}(\xi-\eta)$, where $\mathbf{E}(\hat{\xi})$ (we denote $\hat{\xi} = \xi - \eta$) is the unique matrix solution of the homogeneous equation, such that $\mathbf{E}(0) = \mathbf{I}$. One can write the unique matrix solution in the form

$$\mathbf{E}(\hat{\xi}) = \frac{1}{m^2+M^2}(\mathbf{\Phi}_1, \mathbf{\Phi}_2, \mathbf{\Phi}_3, \mathbf{\Phi}_4)\,,$$

where the column vectors $\mathbf{\Phi}_i = (\Phi_i, \Phi_{i\xi}, \Phi_{i\xi\xi}, \Phi_{i\xi\xi\xi})^{\mathbf{T}}$, for $i = 1,2,3,4$, are generated from the approximate solutions (6.25), corresponding to the homogeneous part of (6.6), where the first element of each vector is of the form

$$\begin{aligned}
\Phi_1 &= M^2\cos(m\hat{\xi}) + m^2\cosh(M\hat{\xi})\,, \quad \Phi_2 = \frac{1}{mM}[M^3\sin(m\hat{\xi}) + m^3\sinh(M\hat{\xi})]\,,\\
\Phi_3 &= -\cos(m\hat{\xi}) + \cosh(M\hat{\xi})\,, \qquad\quad \Phi_4 = \frac{1}{mM}[-M\sin(m\hat{\xi}) + m\sinh(M\hat{\xi})]\,. \quad (6.27)
\end{aligned}$$

It then follows from (6.24), with the aforementioned approximation on the variable coefficient term, that the general solution of (6.20) is

$$\begin{aligned}
\mathbf{U} &= \mathbf{G}(\xi)\mathbf{C} + \int_0^{\xi}\mathbf{E}(\hat{\xi})\mathbf{F}(\eta)\,d\eta\,,\\
&= \mathbf{G}(\xi)\mathbf{C} + \frac{1}{m^2+M^2}\int_0^{\xi}\mathbf{\Phi_4}(\hat{\xi})Q_{\eta\eta}\,d\eta. \qquad (6.28)
\end{aligned}$$

Taking the first equation from (6.28), yields the solution of (6.6), with the variable coefficient term neglected, as follows

$$\begin{aligned}
\phi &= C_1\cos(m\xi) + C_2\sin(m\xi) + C_3\cosh(M\xi) + C_4\sinh(M\xi)\\
&+ \frac{1}{m^2+M^2}\int_0^{\xi}\Phi_4(\xi-\eta)Q_{\eta\eta}(\eta)\,d\eta\,. \qquad (6.29)
\end{aligned}$$

Evaluating the integral term in (6.29) by integrating twice by parts, and noting that Q is a symmetric function in η, we can rewrite (6.29) in the alternative form

$$\begin{aligned}
\phi &= \tilde{C}_1\cos(m\xi) + C_2\sin(m\xi) + \tilde{C}_3\cosh(M\xi) + C_4\sinh(M\xi)\\
&+\frac{1}{m^2+M^2}\int_0^{\xi}[m\sin(m\hat{\xi}) + M\sinh(M\hat{\xi})]Q(\eta)\,d\eta, \qquad (6.30)
\end{aligned}$$

where $\tilde{C}_1 = C_1 + \frac{1}{m^2+M^2}Q(0)$ and $\tilde{C}_3 = C_3 - \frac{1}{m^2+M^2}Q(0)$. Writing (6.30) as

$$\begin{aligned}
\phi &= \tilde{C}_1\cos(m\xi) + C_2\sin(m\xi) + \frac{1}{2}\tilde{C}_3(e^{M\xi}+e^{-M\xi}) + \frac{1}{2}C_4(e^{M\xi}-e^{-M\xi})\\
&+ \frac{1}{m^2+M^2}\int_0^{\xi}\left\{m\sin[m(\xi-\eta)] + \frac{M}{2}\left[e^{M(\xi-\eta)} - e^{-M(\xi-\eta)}\right]\right\}Q(\eta)\,d\eta\,, \qquad (6.31)
\end{aligned}$$

and recalling that Q is symmetric and exponentially small in the limit $\xi \to \pm\infty$, yields

$$\phi \sim \left(\frac{1}{2}\tilde{C}_3 \pm \frac{1}{2}C_4 + D\right)\exp\left(\pm M\xi\right), \qquad \text{as} \qquad \xi \to \pm\infty, \tag{6.32}$$

$$\text{where} \quad D = \frac{M}{2(m^2+M^2)}\int_0^\infty \exp(-M\eta)Q(\eta)\,d\eta\,.$$

Since these terms are secular, we require $\frac{1}{2}\tilde{C}_3 \pm \frac{1}{2}C_4 + D = 0$, which implies $C_4 = 0,\ \tilde{C}_3 = -2D$. Now in the limit $\xi \to \pm\infty$ we find the following oscillatory terms

$$\phi \sim (\tilde{C}_1 + E_3)\cos\left(m\xi\right) + (C_2 \pm E_4)\sin\left(m\xi\right) \qquad \text{as} \qquad \xi \to \pm\infty, \tag{6.33}$$

$$\text{for} \quad E_3 = -\frac{m}{m^2+M^2}\int_0^\infty \sin\left(m\eta\right)Q(\eta)\,d\eta\,, \quad E_4 = \frac{m}{m^2+M^2}\int_0^\infty \cos\left(m\eta\right)Q(\eta)\,d\eta\,,$$

where in particular,

$$E_4 \;=\; \frac{6m^2\pi[A + Bv_0^2(\hat{\varepsilon}^2+m^2) - Cv_0^2m^2]}{(m^2+M^2)\sinh\left(\frac{m\pi}{\hat{\varepsilon}}\right)}. \tag{6.34}$$

Finally, we impose an asymmetric condition on ϕ, namely that we have one-sided oscillating solutions in the region $\xi < 0$ only. This implies from (6.33) that we require $\tilde{C}_1 = -E_3$ and $C_2 = -E_4$, and thus yields

$$\begin{aligned} \phi &\sim 0 && \text{as} \qquad \xi \to +\infty, \\ \phi &\sim -2E_4\sin\left(m\xi\right) && \text{as} \qquad \xi \to -\infty. \end{aligned} \tag{6.35}$$

The one-sided oscillating asymptotic solution for ϕ depends only upon the original parameters in the cRB problem (6.1) without the presence of any arbitrary parameters. From (6.34) it is clear that the amplitude of oscillations is dependent upon all three perturbations of c^2, α and β from 1. Also we note as $\hat{\varepsilon} \to 0$, the amplitude of oscillations tend to zero, which we expect since the same follows for the rest of the solution (amplitude of f_0).

We next consider an alternative approach to neglecting the variable coefficient term in the governing equation for ϕ.

6.3.2 Asymptotic solution

If we assume the speed of the solitary wave solution at leading order is sufficiently close to 1 (which is natural since we require it to be close to the characteristic speed c), this implies we have the small parameter $|\hat{\varepsilon}| \ll 1$. Let us rewrite (6.16) in the form

$$\begin{aligned}\phi'''' - k^4\phi &= \hat{\varepsilon}^2\phi''(1-3\,\mathrm{sech}^2\chi) + 6\hat{\varepsilon}^3\phi'\,\mathrm{sech}^2\chi\tanh\chi \\ &+ \frac{3}{2}\hat{\varepsilon}^4(A-\phi)\,\mathrm{sech}^2\chi\left(2-3\,\mathrm{sech}^2\chi\right) + \frac{3v_0^2}{2}\hat{\varepsilon}^6\,\mathrm{sech}^2\chi\Big[2C \\ &+ 15C\,\mathrm{sech}^2\chi(\,\mathrm{sech}^2\chi - 1) + 3B\,\mathrm{sech}^2\chi(4-5\,\mathrm{sech}^2\chi)\Big]. \quad (6.36)\end{aligned}$$

For $\hat{\varepsilon} = 0$ the solution of (6.36) will exhibit simple harmonic motion (at least sufficiently far away from the origin; that is as $\xi \to \pm\infty$) with period $2\pi/\omega$, for some frequency ω. We therefore follow the Lindstedt–Poincaŕe method (e.g. [28]) by introducing $\tau = \omega\xi$ and seeking an asymptotic solution for $\phi(\tau)$, as well as expanding the frequency ω.

Under this change of variable in ξ, we find (6.36) in the following form

$$\begin{aligned}\omega^4\phi(\tau)'''' - k^4\phi(\tau) &= \hat{\varepsilon}^2\omega^2\phi''(\tau)(1-3\,\mathrm{sech}^2\chi) + 6\hat{\varepsilon}^3\omega\phi'(\tau)\,\mathrm{sech}^2\chi\tanh\chi \\ &+ \frac{3}{2}\hat{\varepsilon}^4(A-\phi(\tau))\,\mathrm{sech}^2\chi\left(2-3\,\mathrm{sech}^2\chi\right) + \frac{3v_0^2}{2}\hat{\varepsilon}^6\,\mathrm{sech}^2\chi\Big[2C \\ &+ 15C\,\mathrm{sech}^2\chi(\,\mathrm{sech}^2\chi - 1) + 3B\,\mathrm{sech}^2\chi(4-5\,\mathrm{sech}^2\chi)\Big], \quad (6.37)\end{aligned}$$

where $\chi(\tau) = \hat{\varepsilon}\tau/2\omega$. We seek an asymptotic solution of (6.37) as follows

$$\phi(\tau) = \phi_0 + \hat{\varepsilon}\phi_{01} + \hat{\varepsilon}^2\phi_1 + \hat{\varepsilon}^3\phi_2 + \hat{\varepsilon}^4\phi_3 + \hat{\varepsilon}^5\phi_4 + \hat{\varepsilon}^6\phi_5 + \ldots\,, \quad (6.38)$$

and also expand the frequency as

$$\omega = \omega_0 + \hat{\varepsilon}\omega_{01} + \hat{\varepsilon}^2\omega_1 + \hat{\varepsilon}^3\omega_2 + \hat{\varepsilon}^4\omega_3 + \hat{\varepsilon}^5\omega_4 + \hat{\varepsilon}^6\omega_5 + \ldots\,. \quad (6.39)$$

Substituting (6.38) and (6.39) into (6.37) yields the following equations up to $O(\hat{\varepsilon}^3)$

$$O(1): \quad \omega_0^4\phi_0'''' - k^4\phi_0 = 0, \quad (6.40)$$

$$O(\hat{\varepsilon}): \quad \omega_0^4\phi_{01}'''' - k^4\phi_{01} = -4\omega_0^3\omega_{01}\phi_0'''', \quad (6.41)$$

$$\begin{aligned}O(\hat{\varepsilon}^2): \quad \omega_0^4\phi_1'''' - k^4\phi_1 &= -4\omega_0^3\omega_{01}\phi_{01}'''' - (4\omega_0^3\omega_1 + 6\omega_0^2\omega_{01}^2)\phi_0'''' \\ &+ \omega_0^2\phi_0''(1-3\,\mathrm{sech}^2\chi), \quad (6.42)\end{aligned}$$

$$\begin{aligned}O(\hat{\varepsilon}^3): \quad \omega_0^4\phi_2'''' - k^4\phi_2 &= -4\omega_0^3\omega_{01}\phi_1'''' - (4\omega_0^3\omega_1 + 6\omega_0^2\omega_{01}^2)\phi_{01}'''' \\ &- (12\omega_0^2\omega_{01}\omega_1 + 4\omega_0\omega_{01}^3 + 4\omega_0^3\omega_2)\phi_0'''' + 6\omega_0\phi_0'\,\mathrm{sech}^2\chi\,\tanh\chi \\ &+ (\omega_0^2\phi_{01}'' + 4\omega_0^3\omega_{01}\phi_0'')(1-3\,\mathrm{sech}^2\chi)\,. \quad (6.43)\end{aligned}$$

From the leading order equation (6.40), the general solution is

$$\phi_0 = C_{01}\cos(\hat{k}\tau) + C_{02}\sin(\hat{k}\tau) + C_{03}\cosh(\hat{k}\tau) + C_{04}\sinh(\hat{k}\tau), \tag{6.44}$$

where C_{0i}, for $i = 1, 2, 3, 4$, are arbitrary constants and we denote $\hat{k} = k/\omega_0$. To ensure ϕ_0 remains bounded as $\tau \to \pm\infty$, and imposing an asymmetric condition on ϕ (namely that we have one-sided oscillating solutions in the region $\xi < 0$ only), we must choose $C_{0i} = 0\ \forall i$, and hence

$$\phi_0 = 0.$$

Consequently, equations (6.41)–(6.43) systematically reduce to the same form as (6.40), and similarly

$$\phi_{01} = \phi_1 = \phi_2 = 0.$$

The first nonhomogeneous equations appear at and beyond $O(\hat{\varepsilon}^4)$, where we have

$$O(\hat{\varepsilon}^4): \quad \omega_0^4\phi_3'''' - k^4\phi_3 = \frac{3A}{2}\operatorname{sech}^2\chi\ \left(2 - 3\operatorname{sech}^2\chi\right), \tag{6.45}$$

$$O(\hat{\varepsilon}^5): \quad \omega_0^4\phi_4'''' - k^4\phi_4 = -4\omega_0^3\omega_{01}\phi_3'''', \tag{6.46}$$

$$\begin{aligned} O(\hat{\varepsilon}^6): \quad \omega_0^4\phi_5'''' - k^4\phi_5 = &-(4\omega_0^3\omega_1 + 6\omega_0^2\omega_{01}^2)\phi_3'''' + \omega_0^2\phi_3''(1 - 3\operatorname{sech}^2\chi) \\ &- 4\omega_0^3\omega_{01}\phi_4'''' + \frac{3v_0^2}{2}\operatorname{sech}^2\chi\Big[2C + 15C\operatorname{sech}^2\chi(\operatorname{sech}^2\chi - 1) \\ &+ 3B\operatorname{sech}^2\chi(4 - 5\operatorname{sech}^2\chi)\Big], \end{aligned} \tag{6.47}$$

and therefore ϕ_3 will constitute the leading order solution for ϕ. It turns out that non-zero higher order correction terms appear only at subsequent even powers of $\hat{\varepsilon}$ (after imposing boundedness and asymmetry conditions on the solution).

6.3.2.1 Leading order solution

Using variation of parameters, the general solution for the leading order term ϕ_3 is

$$\begin{aligned} \phi_3 = &\ C_{31}\cos(\hat{k}\tau) + C_{32}\sin(\hat{k}\tau) + C_{33}\cosh(\hat{k}\tau) + C_{34}\sinh(\hat{k}\tau) \\ &+ \frac{\omega_0^3}{2k^3}\Bigg\{\cos(\hat{k}\tau)\int_0^\tau L_3(s)\,\sin(\hat{k}s)\,ds - \sin(\hat{k}\tau)\int_0^\tau L_3(s)\,\cos(\hat{k}s)\,ds \\ &+ \frac{e^{\hat{k}\tau}}{2}\int_0^\tau L_3(s)e^{-\hat{k}s}\,ds - \frac{e^{-\hat{k}\tau}}{2}\int_0^\tau L_3(s)e^{\hat{k}s}\,ds\Bigg\}, \end{aligned} \tag{6.48}$$

where $L_3(\tau) = (3A/2\omega_0^4)\ \mathrm{sech}^2\chi\left(2 - 3\ \mathrm{sech}^2\chi\right)$. If we consider the limit as $\tau \to \pm\infty$, noting L_3 is localised and symmetric, we find

$$\phi_3 \sim \left(\frac{1}{2}C_{33} \pm \frac{1}{2}C_{34} + F_1\right)\exp\left(\pm\hat{k}\tau\right), \qquad \text{as} \qquad \tau \to \pm\infty, \tag{6.49}$$

$$\text{where} \qquad F_1 = \frac{\omega_0^3}{4k^3}\int_0^\infty L_3(s)e^{-\hat{k}s}\,ds\,, \tag{6.50}$$

and thus for ϕ_3 to be nonsecular we require $C_{33} = -2F_1$ and $C_{34} = 0$. Therefore,

$$\phi_3 \sim (C_{31} + F_3)\cos\left(\hat{k}\tau\right) + (C_{32} \pm F_4)\sin\left(\hat{k}\tau\right) \qquad \text{as} \qquad \tau \to \pm\infty, \tag{6.51}$$

$$\text{for} \quad F_3 = \frac{\omega_0^3}{2k^3}\int_0^\infty L_3(s)\sin\left(\hat{k}s\right)ds\,, \quad F_4 = -\frac{\omega_0^3}{2k^3}\int_0^\infty L_3(s)\cos\left(\hat{k}s\right)ds\,, \tag{6.52}$$

where in particular

$$F_4 \;=\; \frac{3A\pi\omega^4}{\hat{\varepsilon}^4\omega_0^4\ \sinh\left(\frac{k\omega\pi}{\omega_0\hat{\varepsilon}}\right)}. \tag{6.53}$$

Finally, imposing an asymmetric condition on ϕ (namely that ϕ has one-sided oscillations only in the region $\xi < 0$), requires $C_{31} = -F_3$ and $C_{32} = -F_4$. This yields (6.51) in the form

$$\begin{aligned} \phi_3 &\sim 0 && \text{as} \qquad \tau \to +\infty, \\ \phi_3 &\sim -2F_4\sin\left(\hat{k}\tau\right) && \text{as} \qquad \tau \to -\infty. \end{aligned} \tag{6.54}$$

Notice the leading order asymptotic solution for ϕ developed here (up to $O(\hat{\varepsilon}^4)$, and at leading order for ω) coincides with solution (6.35) (at leading order for m and M), with $B = C = 0$, found from the alternative approach outlined in Section 6.3.1. It follows that ϕ's dependence on perturbations via B and C are found at higher order, subject to a constraint on the magnitude of the three perturbation terms A, B and C.

6.3.2.2 Higher order correction terms

It is clear that the terms in the right-hand side of the higher order equations (6.46) and (6.47), which do not tend to zero in the limit $\tau \to \pm\infty$, will contain secular terms. If we follow the same approach used for solving the leading order equations, we find in order to impose an asymmetric solution, some of these secular terms are nonremovable

from the choice of the arbitrary constants alone (these arbitrary constants arise from the solutions of the homogeneous equations). We therefore utilise the higher order correction terms in the expansion of the frequency ω.

At $O(\hat{\varepsilon}^5)$ we can easily remove these so-called 'nonremovable' secular terms by choosing $\omega_{01} = 0$, and as a result, (6.46) reduces to a homogeneous equation in the same form as (6.40), which means

$$\phi_4 = 0.$$

With this choice of ω_{01}, the equation (6.47) at $O(\hat{\varepsilon}^6)$, reduces to

$$\phi_5'''' - \frac{k^4}{\omega_0^4}\phi_5 = -\frac{3}{\omega_0^2}\phi_3'' \operatorname{sech}^2\chi + P(\tau) + \frac{1}{\omega_0^2}L_{5BC}(\tau), \tag{6.55}$$

where these nonremovable secular terms arise within the term we denote

$$P(\tau) = \frac{\phi_3''}{\omega_0^2} - \frac{4\omega_1\phi_3''''}{\omega_0}, \tag{6.56}$$

and we also denote the term which contains the perturbations B and C by

$$L_{5BC}(\tau) = \frac{3v_0^2}{2}\operatorname{sech}^2\chi\left[2C + 15C\operatorname{sech}^2\chi(\operatorname{sech}^2\chi - 1) + 3B\ \operatorname{sech}^2\chi(4 - 5\ \operatorname{sech}^2\chi)\right]. \tag{6.57}$$

We note the 2nd and 4th order derivatives of the leading order solution ϕ_3, which appear in the term denoted $P(\tau)$, are of the form

$$\begin{aligned}\phi_3'' &= \frac{k^2}{\omega_0^2}\left[F_3\cos(\hat{k}\tau) + F_4\sin(\hat{k}\tau) - F_1(e^{\hat{k}\tau} + e^{-\hat{k}\tau})\right] \\ &+ \frac{\omega_0}{2k}\Bigg\{-\cos(\hat{k}\tau)\int_0^\tau L_3(s)\ \sin(\hat{k}s)\ ds + \sin(\hat{k}\tau)\int_0^\tau L_3(s)\ \cos(\hat{k}s)\ ds \\ &+ \frac{e^{\hat{k}\tau}}{2}\int_0^\tau L_3(s)e^{-\hat{k}s}\ ds - \frac{e^{-\hat{k}\tau}}{2}\int_0^\tau L_3(s)e^{\hat{k}s}\ ds\Bigg\},\end{aligned} \tag{6.58}$$

and

$$\begin{aligned}\phi_3'''' &= -\frac{k^4}{\omega_0^4}\left[F_3\cos(\hat{k}\tau) + F_4\sin(\hat{k}\tau) + F_1(e^{\hat{k}\tau} + e^{-\hat{k}\tau})\right] \\ &+ \frac{k}{2}\Bigg\{\cos(\hat{k}\tau)\int_0^\tau L_3(s)\ \sin(\hat{k}s)\ ds - \sin(\hat{k}\tau)\int_0^\tau L_3(s)\ \cos(\hat{k}s)\ ds \\ &+ \frac{e^{\hat{k}\tau}}{2}\int_0^\tau L_3(s)e^{-\hat{k}s}\ ds - \frac{e^{-\hat{k}\tau}}{2}\int_0^\tau L_3(s)e^{\hat{k}s}\ ds\Bigg\} + \frac{L_3(\tau)}{2},\end{aligned} \tag{6.59}$$

where $F_{1,3,4}$ are constants defined by (6.50), (6.52) and (6.53). It transpires that these secular terms which are nonremovable from the choice of the arbitrary constants alone (in order to still impose an asymmetric solution), arise only from the trigonometric terms in (6.56). Therefore, choosing $\omega_1 = -\omega_0/4k^2$ removes these terms, thus

$$\phi_5'''' - \frac{k^4}{\omega_0^4}\phi_5 = -\frac{3}{\omega_0^2}\phi_3'' \operatorname{sech}^2\chi + \hat{P}(\tau) + \frac{1}{\omega_0^2}L_{5BC}, \tag{6.60}$$

where

$$\begin{aligned}\hat{P}(\tau) &= -\frac{2k^2F_1}{\omega_0^2}\left(e^{\hat{k}\tau} + e^{-\hat{k}\tau}\right) + \frac{\omega_0}{2k}\left[e^{\hat{k}\tau}\int_0^\tau L_3(s)e^{-\hat{k}s}\,ds - e^{-\hat{k}\tau}\int_0^\tau L_3(s)e^{\hat{k}s}\,ds\right] \\ &- \frac{\omega_0^2}{2k^2}L_3(\tau).\end{aligned} \tag{6.61}$$

The general solution of (6.60), using variation of parameters, can be written as

$$\begin{aligned}\phi_5 &= C_{51}\cos(\hat{k}\tau) + C_{52}\sin(\hat{k}\tau) + C_{53}e^{\hat{k}\tau} + C_{54}e^{-\hat{k}\tau} \\ &+ \frac{\omega_0^3}{2k^3}\left\{\cos(\hat{k}\tau)\int_0^\tau L_5(s)\,\sin(\hat{k}s)\,ds - \sin(\hat{k}\tau)\int_0^\tau L_5(s)\,\cos(\hat{k}s)\,ds\right. \\ &+ \left.\frac{e^{\hat{k}\tau}}{2}\int_0^\tau L_5(s)e^{-\hat{k}s}\,ds - \frac{e^{-\hat{k}\tau}}{2}\int_0^\tau L_5(s)e^{\hat{k}s}\,ds\right\},\end{aligned} \tag{6.62}$$

for the arbitrary constants C_{5i}, $i = 1, 2, 3, 4$, and where we denote

$$L_5(\tau) = -\frac{3}{\omega_0^2}\phi_3'' \operatorname{sech}^2\chi + \hat{P}(\tau) + \frac{1}{\omega_0^2}L_{5BC}.$$

Using (6.58) and (6.59) we can write (6.62) as $\phi_5 = \sum_{i=1}^4 C_{5i}\hat{\phi}_i(\tau) + \phi_5^{ps}$, for

$$\begin{aligned}\phi_5^{ps} &= \frac{\omega_0}{2k^3}\sum_{i=1}^4 \frac{(-1)^{i+1}\hat{\phi}_i(\tau)}{b_i}\left\{-\frac{3k^2}{\omega_0^2}\int_0^\tau S^2\hat{\phi}_{(i+a)}(s)\left[F_3\hat{\phi}_1(s) + F_4\hat{\phi}_2(s)\right.\right. \\ &- \left.\left. F_1[\hat{\phi}_3(s) + \hat{\phi}_4(s)]\right]ds + \int_0^\tau \hat{\phi}_{(i+a)}(s)L_{5BC}(s)ds \\ &+ \frac{3\omega_0}{2k}\int_0^\tau S^2\hat{\phi}_{(i+a)}(s)\left(\hat{\phi}_1(s)\left[\int_0^s L_3(y)\hat{\phi}_2(y)dy\right] - \hat{\phi}_2(s)\left[\int_0^s L_3(y)\hat{\phi}_1(y)dy\right]\right)ds \\ &- \frac{3\omega_0}{4k}\int_0^\tau S^2\hat{\phi}_{(i+a)}(s)\left(\hat{\phi}_3(s)\left[\int_0^s L_3(y)\hat{\phi}_4(y)dy\right] - \hat{\phi}_4(s)\left[\int_0^s L_3(y)\hat{\phi}_3(y)dy\right]\right)ds \\ &+ \frac{\omega_0^3}{2k}\int_0^\tau \hat{\phi}_{(i+a)}(s)\left(\hat{\phi}_3(s)\left[\int_0^s L_3(y)\hat{\phi}_4(y)dy\right] - \hat{\phi}_4(s)\left[\int_0^s L_3(y)\hat{\phi}_3(y)dy\right]\right)ds \\ &- 2k^2F_1\int_0^\tau \hat{\phi}_{(i+a)}(s)\left[\hat{\phi}_3(s) + \hat{\phi}_4(s)\right]ds - \frac{\omega_0^4}{2k^2}\int_0^\tau \hat{\phi}_{(i+a)}(s)L_3(s)ds\Bigg\},\end{aligned} \tag{6.63}$$

where we denote $S = \text{sech}(\chi(s))$, $a = (-1)^{i+1}$, $b_{1,2} = 1$, $b_{3,4} = 2$, and

$$\hat{\phi}_1(\tau) = \cos(\hat{k}\tau), \qquad \hat{\phi}_2(\tau) = \sin(\hat{k}\tau), \qquad \hat{\phi}_3(\tau) = e^{\hat{k}\tau}, \qquad \hat{\phi}_4(\tau) = e^{-\hat{k}\tau},$$

(see Appendix C for the summation in (6.63) written explicitly).

Taking the limit as $\tau \to \infty$ we find

$$\phi_5 \sim \frac{\omega_0 I_2^+ \cos(\hat{k}\tau)}{2k^3} - \frac{\omega_0 I_1^+ \sin(\hat{k}\tau)}{2k^3} - \frac{\omega_0 I_3^+ e^{-\hat{k}\tau}}{4k^3} + \left(\frac{1}{2}C_{53} + \frac{1}{2}C_{54} + J_1\right) e^{\hat{k}\tau}\,, \quad (6.64)$$

where we define

$$\begin{aligned} I_j^+ &= \frac{3k^2 F_1}{\omega_0^2}\int_0^\infty S^2\hat{\phi}_j(s)e^{\hat{k}s}ds - \frac{3\omega_0}{4k}\int_0^\infty S^2\hat{\phi}_j(s)e^{\hat{k}s}\left[\int_0^s L_3(y)e^{-\hat{k}y}dy\right]ds \\ &- 2k^2F_1\int_0^\infty \hat{\phi}_j(s)e^{\hat{k}s}ds + \frac{\omega_0^3}{2k}\int_0^\infty \hat{\phi}_j(s)e^{\hat{k}s}\left[\int_0^s L_3(y)e^{-\hat{k}y}dy\right]ds, \end{aligned} \quad (6.65)$$

for $j = 1, 2, 3$, and the bounded term J_1 is defined as the integral coefficients of $\hat{\phi}_3(\tau)$ in (6.63) for $i = 3$, with $\tau \to \infty$. Unlike the asymptotics for ϕ_3, it appears we have unbounded terms within the coefficients of the other three solutions of the homogeneous equation for ϕ_5 as $\tau \to +\infty$ (each separate integral within I_j^+ is unbounded $\forall j$), which is problematic in removing secular terms whilst also later requiring asymmetry of the solution. However writing (6.65) with F_1 explicitly

$$\begin{aligned} I_j^+ = -\frac{\omega_0^3}{2k}\Bigg\{ &\int_0^\infty L_3(s)e^{-\hat{k}s}ds\int_0^\infty\left[1 - \frac{3}{2\omega_0^2}\text{sech}^2(\chi(s))\right]\hat{\phi}_j(s)e^{\hat{k}s}ds \\ &- \int_0^\infty\left[1 - \frac{3}{2\omega_0^2}\text{sech}^2(\chi(s))\right]\hat{\phi}_j(s)e^{\hat{k}s}\left[\int_0^s L_3(y)e^{-\hat{k}y}dy\right]ds\Bigg\}, \end{aligned} \quad (6.66)$$

for $j = 1, 2, 3$, and noting the following general property of definite integrals:

$$\int_0^{x^*} I_a(s)ds\int_0^{x^*} I_b(s)ds - \int_0^{x^*} I_b(s)\left[\int_0^s I_a(y)dy\right]ds = \int_0^{x^*} I_a(s)\left[\int_0^s I_b(y)dy\right]ds, \quad (6.67)$$

for any functions $I_{a,b}$ and some fixed point x^*, we find the combined terms within each I_j^+ $\forall j$ are in fact bounded. Therefore from (6.64) we actually have

$$\phi_5 \sim \left(\frac{1}{2}C_{53} + \frac{1}{2}C_{54} + J_1\right)e^{\hat{k}\tau} \quad \text{as} \quad \tau \to +\infty. \quad (6.68)$$

Similarly as $\tau \to -\infty$ we have

$$\phi_5 \sim \frac{\omega_0 I_2^- \cos(\hat{k}\tau)}{2k^3} - \frac{\omega_0 I_1^- \sin(\hat{k}\tau)}{2k^3} + \frac{\omega_0 I_4^- e^{\hat{k}\tau}}{4k^3} + \left(\frac{1}{2}C_{53} - \frac{1}{2}C_{54} + J_2\right)e^{-\hat{k}\tau}\,, \quad (6.69)$$

where we define

$$\begin{aligned} I_j^- &= \frac{3k^2F_1}{\omega_0^2}\int_0^{-\infty} S^2\hat{\phi}_j(s)e^{-\hat{k}s}ds + \frac{3\omega_0}{4k}\int_0^{-\infty} S^2\hat{\phi}_j(s)e^{-\hat{k}s}\left[\int_0^s L_3(y)e^{\hat{k}y}dy\right]ds \\ &- 2k^2F_1\int_0^{-\infty}\hat{\phi}_j(s)e^{-\hat{k}s}ds - \frac{\omega_0^3}{2k}\int_0^{-\infty}\hat{\phi}_j(s)e^{-\hat{k}s}\left[\int_0^s L_3(y)e^{\hat{k}y}dy\right]ds, \quad (6.70) \end{aligned}$$

for $j = 1, 2, 4$, and the bounded term J_2 is defined as the integral coefficients of $\hat{\phi}_4(\tau)$ in (6.63) for $i = 4$, with $\tau \to -\infty$. Writing F_1 explicitly and changing the signs of the integration variable in (6.70) yields

$$\begin{aligned} I_j^- = \frac{\omega_0^3}{2k}\Bigg\{ &\int_0^{\infty} L_3(s)e^{-\hat{k}s}ds\int_0^{\infty}\left[1 - \frac{3}{2\omega_0^2}\mathrm{sech}^2(\chi(s))\right]\hat{\phi}_j(-s)e^{\hat{k}s}ds \\ &- \int_0^{\infty}\left[1 - \frac{3}{2\omega_0^2}\mathrm{sech}^2(\chi(s))\right]\hat{\phi}_j(-s)e^{\hat{k}s}\left[\int_0^s L_3(y)e^{-\hat{k}y}dy\right]ds\Bigg\}, \quad (6.71) \end{aligned}$$

for $j = 1, 2, 4$. Noting the general property (6.67), we find the combined terms within each I_j^-, for $j = 1, 2, 4$, are indeed bounded. Therefore from (6.69) we actually have

$$\phi_5 \sim \left(\frac{1}{2}C_{53} - \frac{1}{2}C_{54} + J_2\right)e^{-\hat{k}\tau} \quad \text{as} \quad \tau \to -\infty. \quad (6.72)$$

Denoting $J_1 = J_{11} + J_{12}$, we find $J_2 = J_{11} - J_{12}$, where we define

$$J_{12} = -\frac{-3F_4}{4k\omega_0}\int_0^{\infty}\mathrm{sech}^2(\chi(s))\; e^{-\hat{k}s}\sin(\hat{k}s)ds, \quad (6.73)$$

$$\begin{aligned} J_{11} = \frac{\omega_0}{4k^3}\Bigg\{ &-\frac{3k^2}{\omega_0^2}\int_0^{\infty} S^2e^{-\hat{k}s}\left[F_3\cos(\hat{k}s) - F_1\left(e^{\hat{k}s} + e^{-\hat{k}s}\right)\right]ds \\ &+ \frac{3\omega_0}{2k}\int_0^{\infty} S^2e^{-\hat{k}s}\left(\cos(\hat{k}s)\left[\int_0^s L_3(y)\sin(\hat{k}y)dy\right] - \sin(\hat{k}s)\left[\int_0^s L_3(y)\cos(\hat{k}y)dy\right]\right)ds \\ &- \frac{3\omega_0}{4k}\int_0^{\infty} S^2\left(\left[\int_0^s L_3(y)e^{-\hat{k}y}dy\right] - e^{-2\hat{k}s}\left[\int_0^s L_3(y)e^{\hat{k}y}dy\right]\right)ds \\ &+ \frac{\omega_0^3}{2k}\int_0^{\infty}\left(\left[\int_0^s L_3(y)e^{-\hat{k}y}dy\right] - e^{-2\hat{k}s}\left[\int_0^s L_3(y)e^{\hat{k}y}dy\right]\right)ds \\ &- 2k^2F_1\int_0^{\infty} e^{-\hat{k}s}\left[e^{\hat{k}s} + e^{-\hat{k}s}\right]ds - \frac{\omega_0^4}{2k^2}\int_0^{\infty} e^{-\hat{k}s}L_3(s)ds + \int_0^{\infty} e^{-\hat{k}s}L_{5BC}(s)ds\Bigg\}, \end{aligned}$$

and thus from (6.68) and (6.72), the solution of ϕ_5 as $\tau \to \pm\infty$ is of the form

$$\phi_5 \sim \left(\frac{1}{2}C_{53} \pm \frac{1}{2}C_{54} + J_{11} \pm J_{12}\right)e^{\pm\hat{k}\tau} \quad \text{as} \quad \tau \to \pm\infty. \quad (6.74)$$

Therefore, to remove secular terms we require $C_{53} = -2J_{11}$ and $C_{54} = -2J_{12}$.

Now in the limit as $\tau \to \pm\infty$ we find the following oscillatory terms

$$\begin{aligned} \phi_5 &\sim (C_{51} + K_1)\cos(\hat{k}\tau) + (C_{52} + K_3)\sin(\hat{k}\tau) \quad \text{as} \quad \tau \to +\infty, \\ \phi_5 &\sim (C_{51} + K_2)\cos(\hat{k}\tau) + (C_{52} + K_4)\sin(\hat{k}\tau) \quad \text{as} \quad \tau \to -\infty, \end{aligned} \tag{6.75}$$

where we denote $K_1 = K_{11} + K_{12}$, and it can be shown $K_2 = K_{11} - K_{12}$, for

$$K_{12} = -\frac{3F_4}{2k\omega_0}\int_0^\infty \operatorname{sech}^2(\chi(s))\sin^2(\hat{k}s)ds, \tag{6.76}$$

$$\begin{aligned} K_{11} = \frac{\omega_0}{2k^3}\Bigg\{ & \frac{-3k^2}{\omega_0^2}\int_0^\infty S^2\sin(\hat{k}s)\left[F_3\cos(\hat{k}s) - F_1 e^{-\hat{k}s}\right]ds \\ & + \frac{3\omega_0}{2k}\int_0^\infty S^2\sin(\hat{k}s)\left(\cos(\hat{k}s)\left[\int_0^s L_3(y)\sin(\hat{k}y)dy\right] - \sin(\hat{k}s)\left[\int_0^s L_3(y)\cos(\hat{k}y)dy\right]\right)ds \\ & + \frac{\omega_0}{4k}\int_0^\infty L_3(s)e^{-\hat{k}s}\left(\int_0^s \left[3\operatorname{sech}^2(\chi(y)) - 2\omega_0^2\right]\sin(\hat{k}y)e^{\hat{k}y}dy\right)ds \\ & + \frac{\omega_0}{4k}\int_0^\infty \left[3S^2 - 2\omega_0^2\right]\sin(\hat{k}s)e^{-\hat{k}s}\left[\int_0^s L_3(y)e^{\hat{k}y}dy\right]ds \\ & - 2k^2F_1\int_0^\infty \sin(\hat{k}s)e^{-\hat{k}s}ds - \frac{\omega_0^4}{2k^2}\int_0^\infty \sin(\hat{k}s)L_3(s)ds + \int_0^\infty \sin(\hat{k}s)L_{5BC}(s)ds\Bigg\}. \end{aligned} \tag{6.77}$$

Similarly we denote $K_3 = K_{31} + K_{32}$, and it can be shown $K_4 = K_{31} - K_{32}$, where

$$K_{31} = \frac{3F_4}{2k\omega_0}\int_0^\infty \operatorname{sech}^2(\chi(s))\cos(\hat{k}s)\sin(\hat{k}s)ds, \tag{6.78}$$

$$\begin{aligned} K_{32} = -\frac{\omega_0}{2k^3}\Bigg\{ & \frac{-3k^2}{\omega_0^2}\int_0^\infty S^2\cos(\hat{k}s)\left[F_3\cos(\hat{k}s) - F_1 e^{-\hat{k}s}\right]ds \\ & + \frac{3\omega_0}{2k}\int_0^\infty S^2\cos(\hat{k}s)\left(\cos(\hat{k}s)\left[\int_0^s L_3(y)\sin(\hat{k}y)dy\right] - \sin(\hat{k}s)\left[\int_0^s L_3(y)\cos(\hat{k}y)dy\right]\right)ds \\ & + \frac{\omega_0}{4k}\int_0^\infty L_3(s)e^{-\hat{k}s}\left(\int_0^s \left[3\operatorname{sech}^2(\chi(y)) - 2\omega_0^2\right]\cos(\hat{k}y)e^{\hat{k}y}dy\right)ds \\ & + \frac{\omega_0}{4k}\int_0^\infty \left[3S^2 - 2\omega_0^2\right]\cos(\hat{k}s)e^{-\hat{k}s}\left[\int_0^s L_3(y)e^{\hat{k}y}dy\right]ds \\ & - 2k^2F_1\int_0^\infty \cos(\hat{k}s)e^{-\hat{k}s}ds - \frac{\omega_0^4}{2k^2}\int_0^\infty \cos(\hat{k}s)L_3(s)ds + \int_0^\infty \cos(\hat{k}s)L_{5BC}(s)ds\Bigg\}. \end{aligned} \tag{6.79}$$

Therefore, we can write (6.75) as

$$\phi_5 \sim (C_{51}+K_{11}+K_{12})\cos(\hat{k}\tau)+(C_{52}+K_{31}+K_{32})\sin(\hat{k}\tau) \quad \text{as} \quad \tau\to+\infty,$$
$$\phi_5 \sim (C_{51}+K_{11}-K_{12})\cos(\hat{k}\tau)+(C_{52}+K_{31}-K_{32})\sin(\hat{k}\tau) \quad \text{as} \quad \tau\to-\infty. \quad (6.80)$$

Imposing the asymmetric condition on ϕ (that is, we have one-sided oscillating solutions in the region $\xi<0$ only), we must choose $C_{51}=-(K_{11}+K_{12})$ and $C_{52}=-(K_{31}+K_{32})$, thus yielding the asymptotic asymmetric solution for ϕ_5 as

$$\begin{aligned}\phi_5 &\sim 0 && \text{as} \quad \tau\to+\infty,\\ \phi_5 &\sim -2K_{12}\cos(\hat{k}\tau)-2K_{32}\sin(\hat{k}\tau) && \text{as} \quad \tau\to-\infty. \end{aligned} \quad (6.81)$$

Therefore, the asymptotic solution of (6.37) as $\tau\to\pm\infty$, up to $O(\hat{\varepsilon}^6)$, is

$$\begin{aligned}\phi(\tau) &\sim 0 && \text{as} \quad \tau\to+\infty,\\ \phi(\tau) &\sim -2\hat{\varepsilon}^4F_4\sin(\hat{k}\tau)-2\hat{\varepsilon}^6[K_{12}\cos(\hat{k}\tau)+K_{32}\sin(\hat{k}\tau)] && \text{as} \quad \tau\to-\infty. \end{aligned} \quad (6.82)$$

The leading order term ω_0 in the frequency expansion factors out of the solution, thus we set $\omega_0=1$ (any other choice results in an unnecessary trivial change in ξ), yielding

$$\omega = 1-\frac{\hat{\varepsilon}^2}{4k^2}+O(\hat{\varepsilon}^3). \quad (6.83)$$

Further corrections to the asymptotic solution for ϕ can be obtained by deriving equations beyond $O(\hat{\varepsilon}^6)$. Similarly the frequency ω is systematically corrected by choosing the suitable higher order terms ω_i for $i=2,3,4,...$, in order to remove secular terms that arise in the derived equations for ϕ.

Lastly we comment on a constraint between the perturbation parameters A, B and C. If we explicitly evaluate the final integral in (6.79), containing the B, C terms, we find the contribution to the asymptotic solution (6.82) as $\tau\to-\infty$ is

$$\frac{\hat{\varepsilon}^6\sin(k\tau)}{k^3}\int_0^\infty \cos(\hat{k}s)L_{5BC}(s)ds = -\frac{6v_0^2\pi[B(\hat{\varepsilon}^2+k^2)-Ck^2]}{\sinh\left(\frac{k\pi}{\hat{\varepsilon}}\right)}\sin(k\tau). \quad (6.84)$$

It is now clear that this term will be comparable to the leading order terms which involve perturbations via A. Therefore, to maintain asymptotic validity we must either consider perturbations via B and C separately from perturbations via A, or alternatively for all three perturbations A, B and C to coexist, we must impose that perturbations via

B and C are at least $O(\hat{\varepsilon}^2)$ smaller than via A. It is apparent that the leading order solution of ϕ for perturbations in B, C arise at $O(\hat{\varepsilon}^6)$. Indeed, to find higher order corrections to the solution in this case, as we did for perturbations via the parameter A, we must again seek further higher order equations in ϕ and repeat the procedure outlined in this section.

Finally, we note that if $A = 0$, the asymptotic solution (6.82) reduces to

$$\begin{aligned} \phi(\tau) &\sim 0 && \text{as} \quad \tau \to +\infty, \\ \phi(\tau) &\sim -\frac{6v_0^2\pi[B(\hat{\varepsilon}^2+k^2)-Ck^2]}{\sinh\left(\frac{k\pi}{\hat{\varepsilon}}\right)}\sin(k\tau) && \text{as} \quad \tau \to -\infty, \end{aligned} \tag{6.85}$$

which if we take ω to leading order, coincides with the asymptotic solution derived from the previous approach in Section 6.3.1, given by (6.35) with $A = 0$ (also taking m and M to leading order). We can view the approach developed in the previous section as an alternative way to derive the leading order solution of ϕ from this approach. The systematic methodology outlined in this section has the scope to extend the solution to arbitrary orders of $\hat{\varepsilon}$.

Later in this chapter we compare the developed asymptotic solution for ϕ with corresponding numerical simulations for the system of cRB equations, in order to analyse the methodology. More specifically, we examine the solution with and without the inclusion of the higher order corrections, in order to determine the effectiveness of this approach in describing radiating solitary wave solutions of cRB equations.

6.4 Analytical description of radiating solitary waves

Returning to the original variables f and g, we have the following asymptotic solution of the system of cRB equations (3.2):

$$f{=}A_0\,\mathrm{sech}^2(\chi)+\frac{\mu}{\delta+\gamma}(\gamma\psi+\delta\phi)+O(\mu^2), \quad g{=}A_0\,\mathrm{sech}^2(\chi)+\frac{\mu\gamma}{\delta+\gamma}(\psi-\phi)+O(\mu^2).$$

Using the particular solution for ψ, given by (6.15), and the asymptotic solution for ϕ from Section 6.3.2, given by (6.35) (under the approximation to the variable coefficient

term in the governing equation for ϕ), we have the following solution:

$$\begin{aligned} f &= A_0\,\mathrm{sech}^2(\chi) + \frac{\mu}{\delta+\gamma}\Big\{\delta A_0(A - B + v_0^2 C)\mathrm{sech}^2(\chi)[1-\tanh(\chi)] \\ &- 2\delta E_4 H(-\xi)\sin(m\xi)\Big\} + \dots\,, \\ g &= A_0\,\mathrm{sech}^2(\chi) + \frac{\mu}{\delta+\gamma}\Big\{\delta A_0(A - B + v_0^2 C)\mathrm{sech}^2(\chi)[1-\tanh(\chi)] \\ &+ 2\gamma E_4 H(-\xi)\sin(m\xi)\Big\} + \dots\,, \end{aligned} \tag{6.86}$$

where $\chi = \hat{\varepsilon}\xi/2$, $H(\cdot)$ is the Heaviside function and E_4 is given by (6.34).

Alternatively, using the asymptotic solution for ϕ from Section 6.3.2 taken up to $O(\hat{\varepsilon}^6)$, given by (6.82), we instead have the solution of the system of cRB equations (3.2) as

$$\begin{aligned} f &= A_0\,\mathrm{sech}^2(\chi) + \frac{\mu}{\delta+\gamma}\Big\{\delta A_0(A - B + v_0^2 C)\mathrm{sech}^2(\chi)[1-\tanh(\chi)] \\ &- 2\hat{\varepsilon}^4\delta H(-\xi)\Big(F_4\sin(k\omega\xi) + \hat{\varepsilon}^2[K_{12}\cos(k\omega\xi) + K_{32}\sin(k\omega\xi)]\Big)\Big\} + \dots, \\ g &= A_0\,\mathrm{sech}^2(\chi) + \frac{\mu}{\delta+\gamma}\Big\{\delta A_0(A - B + v_0^2 C)\mathrm{sech}^2(\chi)[1-\tanh(\chi)] \\ &+ 2\hat{\varepsilon}^4\gamma H(-\xi)\Big(F_4\sin(k\omega\xi) + \hat{\varepsilon}^2[K_{12}\cos(k\omega\xi) + K_{32}\sin(k\omega\xi)]\Big)\Big\} + \dots, \end{aligned} \tag{6.87}$$

where the frequency ω is given by (6.83) and the constants F_4, K_{12} and K_{32} are defined by (6.53), (6.76) and (6.79) respectively.

We next compare direct numerical simulations of the system cRB equations (3.2) with each of the corresponding analytical approximations (6.86) and (6.87).

6.5 Numerical Simulations

In this section we compare the theoretically derived radiating solitary wave solutions of the cRB equations (3.2) with corresponding numerical simulations, using a pseudo-spectral method which is extended from the work in [36] for a single regularised Boussinesq equation. Details of the spectral method for the cRB equations are described in Appendix B.6. Alternatively, one can implement the finite difference scheme used in Section 3.3, however the spectral methods we consider generally outperform the finite difference schemes and hence we choose the former of the two approaches.

We let $x \in [-L, L]$, for finite L, and discretise the (x,t) domain into a grid with constant spacings Δx and Δt. The solutions $f(x,t)$ and $g(x,t)$ of the cRB equations

(3.2) are approximated by the solutions $f(i\Delta x, j\Delta t) = f_{\text{num}}$ and $g(i\Delta x, j\Delta t) = g_{\text{num}}$ for $i = 1, 2, ..., N$ and $j = 0, 1, ...$, found via the spectral method (B.54).

Since we implement a spectral method, we impose periodic boundary conditions, but in order to simulate the solutions propagating on the infinite line, we choose L to be sufficiently large. To compare the numerical and theoretical solutions we choose the initial conditions in numerical simulations to coincide with the localised part of the theoretical solutions (6.86) and (6.87). This comprises of the leading order solitary wave solution and the higher order correction terms given by ψ, in Section 6.2, namely:

$$\begin{aligned} f|_{t=0} = g|_{t=0} &= A_0 \operatorname{sech}^2\left(\frac{\hat{\varepsilon}x}{2}\right) + \frac{\mu\delta A_0}{\delta+\gamma}\left(A - B + v_0^2 C\right)\operatorname{sech}^2\left(\frac{\hat{\varepsilon}x}{2}\right)\left[1 - \tanh\left(\frac{\hat{\varepsilon}x}{2}\right)\right], \\ f_t|_{t=0} = g_t|_{t=0} &= \hat{\varepsilon}vA_0 \operatorname{sech}^2\left(\frac{\hat{\varepsilon}x}{2}\right)\tanh\left(\frac{\hat{\varepsilon}x}{2}\right) + \frac{\mu\delta A_0\hat{\varepsilon}v}{\delta+\gamma}\left(A - B + v_0^2 C\right)\operatorname{sech}^2\left(\frac{\hat{\varepsilon}x}{2}\right) \\ &\times \quad \left[\tanh\left(\frac{\hat{\varepsilon}x}{2}\right) - 1 + \frac{3}{2}\operatorname{sech}^2\left(\frac{\hat{\varepsilon}x}{2}\right)\right]. \end{aligned} \tag{6.88}$$

6.5.1 Simulations using the approach in Section 6.3.1

We first consider the radiating solitary wave solutions derived from the first approach, given by (6.86), which we denote as f_{theory} and g_{theory}. Figures 6.1 & 6.2 depict the comparison of the theoretical and numerical radiating solitary wave solutions propagating in each component f and g, for perturbations in the parameters c and β respectively. In both figures we find the leading order solitary wave solution is indeed significantly improved by the localised higher order correction term ψ. However, as one can see from the close up plots of the oscillating tail region, there is significant discrepancies in the amplitude of oscillations; more evident in Figure 6.1, which corresponds to perturbations in c.

On the contrary, the wavenumber of oscillations from the theoretical (m) and numerical solution are in good agreement, as well as with predictions found via the dispersion relation (see Table 6.1). From both Figures 6.1 & 6.2 it also appears that the phase of oscillations are well described from the theoretical description, however this is only by chance since we do not expect to capture the phase of ϕ as it is found in the limit $\xi \to -\infty$.

	Wavenumber	Wavelength
Dispersion Relation	0.8110	7.747
Numerical	0.81 ± 0.1	7.75 ± 0.1
k	0.85	7.392
m	0.8147	7.712
$k\omega$	0.8139	7.719

Table 6.1: Comparison of wavenumbers/wavelengths of the numerical solution (averaged readings), m, k and that predicted from the linear dispersion relation. All parameter values correspond to Figure 6.1.

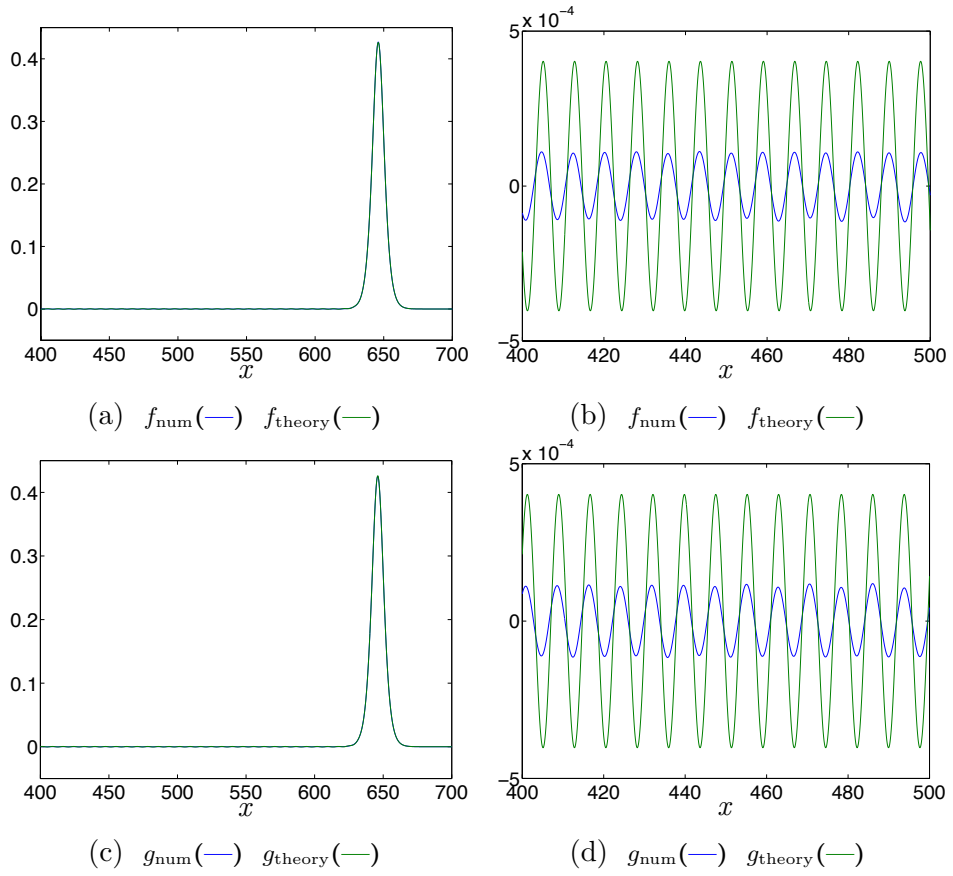

Figure 6.1: Numerical solution and theoretical solution (6.86), at $t = 600$ and a magnification of the oscillating tail. Parameter values: $\hat{\varepsilon} = 0.35$, $k = 0.85$, $\mu = 0.005$ and $A = 7$, $B = C = 0$, which implies $m = 0.8147$, $M = 0.8868$, $\omega = 0.9576$, $c = 1.017$, $\alpha = \beta = 1$, $\gamma = \delta = 0.297$, $v = 1.077$, $v_0 = 1.068$. Numerical parameters: $\Delta t = 0.01$, $L = 2000$, $N = 4 \times 10^5$.

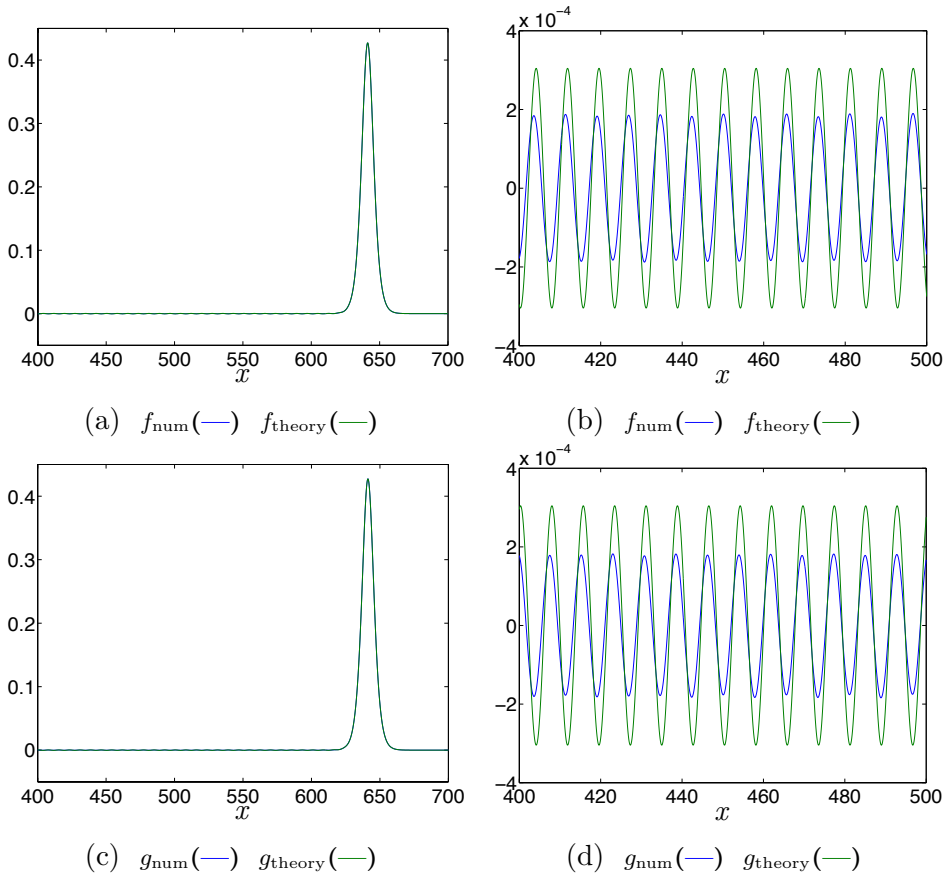

(a) f_{num}(—) f_{theory}(—) (b) f_{num}(—) f_{theory}(—)

(c) g_{num}(—) g_{theory}(—) (d) g_{num}(—) g_{theory}(—)

Figure 6.2: Numerical solution and theoretical solution (6.86), at $t = 600$ and a magnification of the oscillating tail. Parameter values: $\hat{\varepsilon} = 0.35$, $k = 0.85$, $\mu = 0.005$ and $C = 7$, $A = B = 0$, which implies $m = 0.8147$, $M = 0.8868$, $\omega = 0.9576$, $c = \alpha = 1$, $\beta = 1.035$, $\gamma = \delta = 0.297$, $v = 1.069$, $v_0 = 1.068$. Numerical parameters: $\Delta t = 0.01$, $L = 2000$, $N = 4 \times 10^5$.

Although the tail region of the radiating solitary waves shown in Figures 6.1 & 6.2 are rather small, they are still considerably greater in magnitude than $O(\mu^2)$, which rules out the discrepancies are due to higher order terms in the expansions for f and g (6.3) not being included.

6.5.2 Simulations using the approach in Section 6.3.2

We next consider the alternative asymptotic approach for finding ϕ, derived up to $O(\hat{\varepsilon}^6)$, given by (6.87). Figure 6.3 depicts numerical simulations and the solution (6.87) for the same perturbation in the parameter c as in the simulations illustrated in Figure 6.1, which is reincluded in Figure 6.3 for comparison purposes. We denote the solutions f and g from (6.87) with the perturbation solution for ϕ (6.82) as f^i_{pert} and g^i_{pert}, where ϕ is taken up to $O(\hat{\varepsilon}^{2(i+1)})$, for $i = 1, 2, \ldots$.

One can see that the solutions for f and g with the higher order terms for ϕ included indeed correct the leading order approximations f^1_{pert} and g^1_{pert}. This supports the approach outlined in Section 6.3.2 as a valid perturbation method for obtaining the oscillatory part of radiating solitary wave solutions of cRB equations.

Moreover, it is clear that this alternative asymptotic approach for finding the oscillatory part of radiating solitary wave solutions of cRB equations is more effective. The solutions for f and g with ϕ taken up to $O(\hat{\varepsilon}^6)$ significantly improves the discrepancy in the amplitude of oscillations from the numerics, compared with the solutions for f and g using ϕ from the previous approach in Section 6.3.1

Furthermore, we also see an improvement in the amplitude of oscillations in the solutions f^1_{pert} and g^1_{pert}, compared with the solutions using ϕ from the previous approach denoted, f_{theory} and g_{theory}. It was previously noted that the leading order perturbation solution in ϕ, in the case for $B = C = 0$, is equivalent to the solution for ϕ from the previous approach, however this is only for leading order ω, m and M. Since ω appears explicitly in the coefficient of the leading order term, denoted F_4 (6.53), taking higher order terms in ϕ and subsequently ω, will improve the amplitude of oscillations even for the leading order solution. This is evident in Figure 6.3, which displays the solutions $f^{1,2}_{\text{pert}}$, $g^{1,2}_{\text{pert}}$ with the asymptotic solution ϕ found with the first non-zero correction term in ω (and with m and M taken exactly in the first approach for finding ϕ), where one can already notice a distinct improvement in the accuracy of the leading order solutions f^1_{pert}, g^1_{pert} from the solutions using the previous approach in finding ϕ.

The same follows for perturbations in the parameter β as depicted in Figure 6.4. In this case $A = 0$, and so the leading order asymptotic solution for ϕ appears at $O(\hat{\varepsilon}^6)$, thus the solutions denoted f^2_{pert}, g^2_{pert} indeed correspond to the leading order approximations for ϕ. Since the oscillating part of the solutions in this case are already relatively close to the numerical solution, finding the next order correction in ϕ, which will appear at $O(\hat{\varepsilon}^8)$, should yield a very accurate theoretical solution for radiating solitary waves of the cRB equations (3.2).

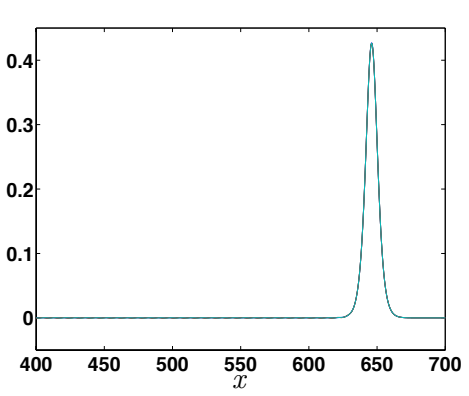

(a) f_{num}(—) f_{theory}(—) f^1_{pert}(—) f^2_{pert}(—)

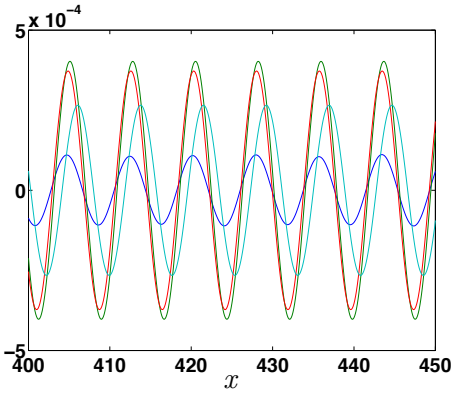

(b) f_{num}(—) f_{theory}(—) f^1_{pert}(—) f^2_{pert}(—)

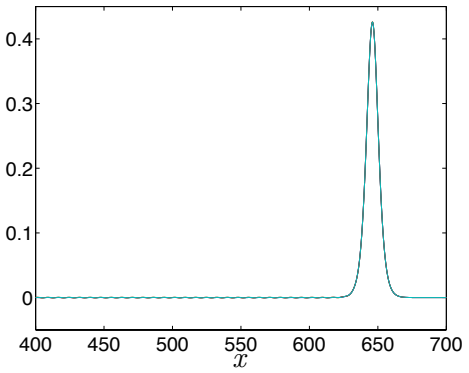

(c) g_{num}(—) g_{theory}(—) g^1_{pert}(—) g^2_{pert}(—)

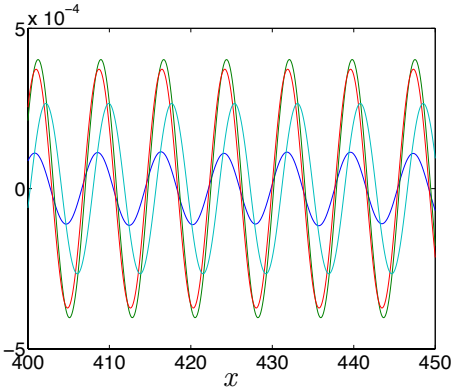

(c) g_{num}(—) g_{theory}(—) g^1_{pert}(—) g^2_{pert}(—)

Figure 6.3: Numerical solution and both theoretical solutions (6.86) and (6.87), at $t = 600$. Parameter values: $\hat{\varepsilon} = 0.35$, $k = 0.85$, $\mu = 0.005$ and $A = 7$, $B = C = 0$, which implies $m = 0.8147$, $M = 0.8868$, $\omega = 0.9576$, $c = 1.017$, $\alpha = \beta = 1$, $\gamma = \delta = 0.297$, $v = 1.077$, $v_0 = 1.068$. Numerical parameters: $\Delta t = 0.01$, $L = 2000$, $N = 4 \times 10^5$.

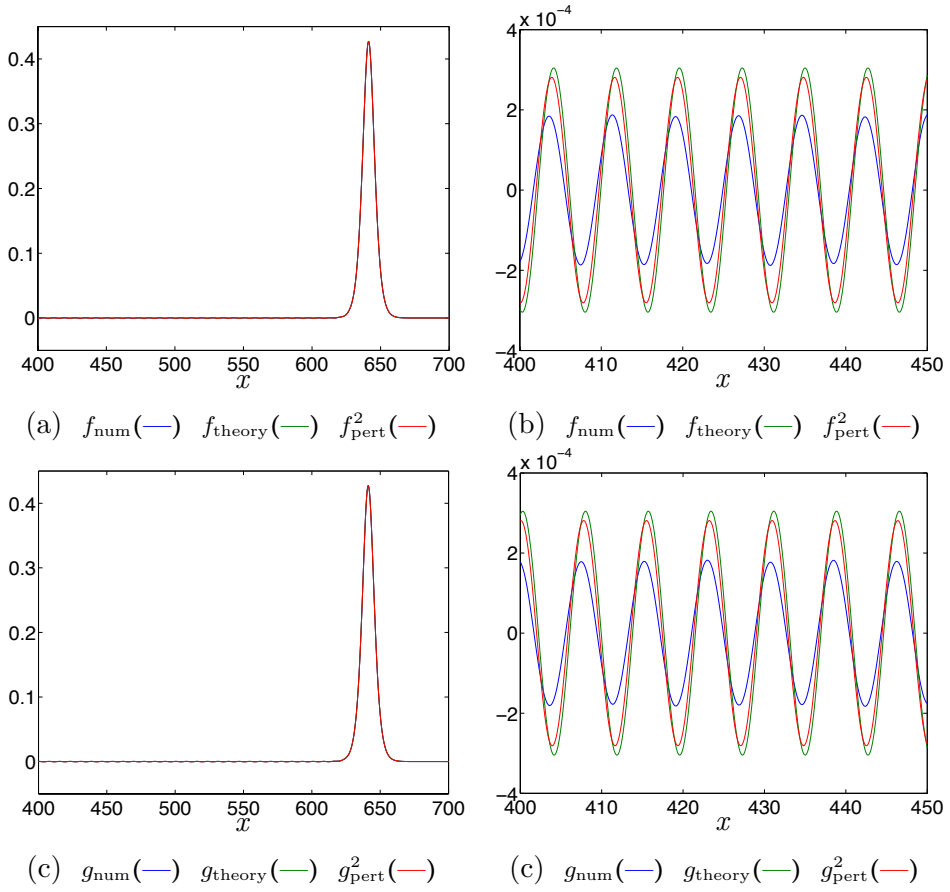

(a) f_{num}(—) f_{theory}(—) f^2_{pert}(—)

(b) f_{num}(—) f_{theory}(—) f^2_{pert}(—)

(c) g_{num}(—) g_{theory}(—) g^2_{pert}(—)

(c) g_{num}(—) g_{theory}(—) g^2_{pert}(—)

Figure 6.4: Numerical solution and both theoretical solutions (6.86) and (6.87), at $t = 600$. Parameter values: $\hat{\varepsilon} = 0.35$, $k = 0.85$, $\mu = 0.005$ and $A = B = 0$, $C = 7$, which implies $m = 0.8147$, $M = 0.8868$, $\omega = 0.9576$, $c = \alpha = 1$, $\beta = 1.035$, $\gamma = \delta = 0.297$, $v = 1.069$, $v_0 = 1.068$. Numerical parameters: $\Delta t = 0.01$, $L = 2000$, $N = 4 \times 10^5$.

6.6 Concluding remarks

In this chapter we have developed an asymptotic approach to describing radiating solitary wave solutions inherent in systems of cRB equations, in the case when the parameters in the system are slightly perturbed from the symmetric case. Using asymptotic expansions similar to the type used in the Lindstedt–Poincaŕe method, we find the leading order approximation is characterised by the pure solitary wave solutions of the symmetric case. To higher order, the equations uncouple into two linear problems, with the solution of one of them correcting the localised part of the radiating solitary wave solutions, and the other describing the co-propagating oscillatory tail. We have developed and implemented a pseudo-spectral method to solve the system of cRB equations primarily in order to test the validity of the derived solutions (details of the method are provided in Appendix B.6).

The derived problem involving the localised higher order term was solved exactly and on comparison with numerical simulations was shown to indeed accurately correct the leading order pure solitary wave approximation. The higher order problem characterising the oscillating terms could not be solved exactly and so we begun by making an assumption on a particular term in the governing equation. This then allowed us to determine the key features of the radiating solitary waves oscillating tails, in the far limits of the spatial domain (see Section 6.3.1). However, on comparison with numerical simulations, this approximation proved slightly too strong and clear discrepancies were apparent in the amplitude of oscillations between numerics and the theory.

This led to the consideration of an alternative asymptotic approach for the higher order problem describing the oscillatory part of the radiating solitary wave solutions (see Section 6.3.2). We found good agreement of the oscillating part of the solutions from the two different approaches, when the latter asymptotic approach was taken to leading order (under a slight ordering constraint to the parameters in the cRB equations). Crucially, the latter approach enables one to improve the solution by taking arbitrary higher order corrections. We found that taking the asymptotic solution of the latter approach to include the first higher order terms significantly improved the noted discrepancy in the amplitude of oscillations between the numerics and the theory, and furthermore corrected the wavelength (in comparison with the numerics and the linear dispersion relation, see Table 6.1). The phase was the only feature of the oscillating

part of the radiating solitary waves solution for which the asymptotic approach fails to capture. This is due to the solution being found in the far limits of the spatial domain.

Chapter 7

Conclusions and future work

In this work we were concerned with the study of nonlinear longitudinal wave propagation in layered elastic waveguides, motivated mainly from the demand to investigate mechanical properties of layered structures.

An accurate asymptotic model, containing all the essential degrees of freedom of a real layered elastic waveguide, was derived in [76] using a complex nonlinear layered lattice model, under the assumption that the bonding between layers is sufficiently 'soft'. For the problem of a two layered waveguide, the model is in the form of two cRB equations; the approach is reviewed in Chapter 2, along with the derivation of the system from a simpler model consisting of two weakly coupled FPU chains.

Throughout this thesis the following four main problems were considered:

(i) The construction of a nonsecular weakly nonlinear solution of the Cauchy problem for cRB equations on the infinite line, for localised or sufficiently rapidly decaying initial conditions.

(ii) The construction of a nonsecular weakly nonlinear solution of a similar Cauchy problem for a single regularised Boussinesq equation on the infinite line, with initial conditions extended to include perturbations to 'exactly solvable' ones.

(iii) Further development and improvement of the weakly nonlinear solution of the Cauchy problem for single regularised Boussinesq and Boussinesq–Ostrovsky equations, in order to make further analytical progress with the higher order terms in the original Cauchy problem.

(iv) Development of an asymptotic methodology to describe the particular class of solutions known as radiating solitary waves, inherent in coupled Boussinesq-type equations.

Problem (i)

The weakly nonlinear solution in the first problem is considered in the general case when the two linear wave operators of the cRB equations have different characteristic speeds, namely for (a) $c-1=O(\epsilon)$ and (b) $c-1=O(1)$.

Introducing two different asymptotic multiple-scales expansions for each of the two cases and implementing an averaging procedure with respect to the fast time variable, we derived to leading order a hierarchy of asymptotically exact coupled and uncoupled Ostrovsky equations in cases (a) and (b) respectively (see [72] for the full published work). Higher order terms were then constructed from the solutions of the leading order problems, and the weakly nonlinear solution up to the accuracy of the problem formulation was shown to be nonsecular. Accurate numerical simulations using a finite difference scheme (see Appendix A.2) were implemented to solve the cRB equations. From pure solitary wave initial conditions, in case (a) the solution in both components was shown to evolve into so-called radiating solitary waves; a pure solitary wave accompanied with a co-propagating oscillatory tail. The dispersion relation was shown to capture the wavelength of the oscillating tail observed from numerical simulations. In case (b) the pure solitary wave solutions in both components were destroyed and to leading order replaced with stable localised wave packets (a well know feature of the Ostrovsky equation [50]). From comparisons with previous numerical studies of the Ostrovsky equation, it was shown that the numerics of the cRB equations qualitatively supported the theory.

The approach developed for the Cauchy problem of the cRB equations is generic and can be used to construct weakly nonlinear solutions of Cauchy problems for other similar models.

Problem (ii)

We then considered the Cauchy problem for a single regularised Boussinesq equation (see [73] for the full published work). We again sought asymptotic multiple-scales expansions and implemented the same averaging procedure as we did in the first problem.

However in this case, to leading order we derived two KdV equations which describe the leading order right- and left-propagating waves. The higher order correction terms were again derived in an explicit simple form, given entirely in terms of the leading order solutions.

The initial conditions in this problem were extended from the first problem by allowing them to be split into $O(1)$ and $O(\epsilon)$ parts, enabling one to implement a broader class of initial conditions. In doing this one can then explicitly obtain solutions of the Cauchy problem for exactly solvable initial conditions (from the viewpoint of the leading order KdV equations being solved via the IST) and also initial conditions with $O(\epsilon)$ perturbations to these.

Explicit examples of the weakly nonlinear solution of the Cauchy problem, in the form of both right-propagating and right- & left-propagating N KdV soliton solutions were developed, and also an example to allow for an arbitrary $O(\epsilon)$ perturbation. Specific examples of these ($N = 1, 2$) were examined with direct numerical simulations of the single regularised Boussinesq equation using a finite difference scheme (see Appendix A.1). It was shown in all examples that the higher order correction terms significantly improved the leading order KdV approximation throughout the times within the validity of the solution.

Problem (iii)

In the previous problem it was noted that although the developed weakly nonlinear solution improved the KdV approximation within the time interval of validity of solutions, the absolute errors of the higher order solution increased with time. This observation is due to a deficiency in the problem formulation and not the constructed solution.

The weakly nonlinear solution constructed for both the single and coupled Boussinesq equations, were found up to the accuracy of the problem formulation in the derivations of the models. However, as a result, there was no way to determine the slow time dependence of the d'Alembert-like functions derived at higher order (instead these solutions were fixed at $T = 0$). To make further analytical progress we reconstructed the weakly nonlinear solution of the Cauchy problem for a single 'Boussinesq–Ostrovsky' equation (reducible to the regularised Boussinesq equation under one parameter choice) on the infinite line, but instead treated the equation as an exact mathematical model (see [74]). We included a further higher $O(\epsilon^2)$ term in the construction of the solution,

although crucially we did not specify and include this term in the solution, instead it was used in order to derive time dependent problems for the terms at the previous order (the ones originally fixed at $T = 0$).

Two particular configurations of this Cauchy problem were examined to assess the accuracy of the derived evolution equations. Firstly (a) the initial conditions were chosen in the form of a right-propagating exactly solvable initial condition of the Boussinesq equation. In this case the higher order terms were found to now be characterised by two linearised KdV Cauchy problems (see also [114]). Secondly (b) we chose a particular configuration corresponding to right-propagating initial conditions of the Boussinesq–Ostrovsky equation, where to leading order we derived a Cauchy problem for the Ostrovsky equation and to higher order, two linearised Ostrovsky Cauchy problems were derived.

The higher order problems in case (a) were solved numerically and also solved using a perturbation approach. The original Boussinesq Cauchy problem was solved numerically and from direct comparison between numerical simulations of the Boussinesq equation and the weakly nonlinear solution, it was shown the accuracy of the solution with the new evolution equations, solved from both the numerical and perturbation approach, was significantly improved from the previously constructed solution. It was shown that the maximum absolute error throughout all times within the region of the solutions applicability, scaled as $O(\epsilon^2)$, as opposed to the solution without the evolution equations which scaled as $O(\epsilon)$ at $T = 1$.

Similar accuracy improvements were obtained in case (b). The leading and higher order Ostrovsky-type problems were solved numerically in this case, and upon solving the Boussinesq–Ostrovsky equation numerically, the accuracy of the weakly nonlinear solution with the higher order evolution equations was shown to significantly improve the leading order approximation.

All numerical simulations in this problem were performed using pseudo-spectral methods, details of which are enclosed in Appendix B .

Problem (iv)

The analytical description of radiating solitary wave solutions in each component of the cRB equations, which evolve from pure solitary wave solutions when the parameters in the system of cRB equations are slightly perturbed from the symmetric case (as

noted in case (a) in Problem (i)), were developed using an asymptotic procedure of Lindstedt-Poincaŕe type. Assuming the parameters in the system were sufficiently close to the symmetric case, and seeking travelling wave solutions, the leading order approximation in both components was found as the exact pure solitary wave solutions of the symmetric case. To higher order it was shown that the system uncoupled into two linear ODEs, the first problem corresponding to correcting the localised region of the solution (where the leading order pure solitary wave is present), and the other problem corresponding to describing the oscillatory tail of the solution.

The problem for the localised higher order component was solved exactly and the higher order problem corresponding to the oscillating part of the solution was solved using two different approaches. In the first approach a particular localised term in the governing equation was neglected and subsequently this enabled us to determine an exact form of the solution in the far spatial regions. In the second approach an accurate asymptotic procedure of the exact form of the governing equation was obtained to describe the solution in the far spatial regions, assuming the oscillations were sufficiently small (and depending on a slight constraint in the order of the parameters).

Upon comparisons with numerical simulations of the cRB equations, for several different examples of perturbations in the parameters, it was shown that the two alternative solutions were found to accurately correct the pure solitary wave approximation and give a relatively good approximation to the oscillatory component of the solution. The first approach coincided with the second asymptotic approach taken to leading order. However taking further higher order terms in the second asymptotic approach, it was shown that the amplitude of the oscillatory part of the solution was significantly improved. As a result the latter asymptotic approach was considered more favourable since it has the scope to be continually extended up to an arbitrary order of accuracy.

Future work

It was previously commented that the weakly nonlinear solution of the Cauchy problem of the cRB equations, developed in Chapter 3, should be straightforward to extend to the problem of N-cRB equations, corresponding to an N layered waveguide with N-1 intermediate soft bonding layers. It would be interesting (and indeed useful from an applications viewpoint) to derive a general solution of the Cauchy problem for an

N-coupled system of Boussinesq equations. One could first consider the problem of a three layered waveguide and examine what happens to the different asymptotic regimes of the derived equations, similar to the ones developed for the difference between the characteristic speeds in the two cRB equations.

In terms of analysing different models, it would be interesting to consider more complicated waveguides. For example, one could consider a waveguide with multiple regions of perfect and imperfect horizontal bonding across the interface of layers. It would then be interesting to observe what would happen to the localised solutions obtained for the waveguides considered in this work as they enter and exit the different regions.

In terms of examining how the current solutions developed here would behave in other waveguides, one could consider the two different developed asymptotic regimes in a two layered waveguide with complete delamination between the layers. More specifically, allowing each one of the radiating solitary wave solutions and wave packet solutions (solved numerically) initially propagating in an imperfectly bonded layered waveguide to enter a region of complete delamination. As a first step, one could take the radiating solitary wave and wave packet solutions as initial conditions of the Cauchy problem for the derived equations in this delamination problem. This would constitute an extension to work in [75], where it was shown, in particular, that a phenomenon known as fission occurs when a pure solitary wave solution propagating in a homogeneous waveguide enters such a region of delamination. Thus it would be interesting to see how delamination of layered waveguides effects the qualitative features of waves propagating in imperfectly bonded layered waveguides. This could first be done numerically and then one could try to develop an analytical solution.

An example of a direct extension to the work contained in this thesis, is to develop the weakly nonlinear solution of the Cauchy problem with the evolution equations describing higher order terms, to allow for more general initial conditions. So far we have considered the configuration which yield right-propagating leading order solutions only. The developed methodology can be extended to include the configuration corresponding to right- and left-propagating leading order solutions, but this is omitted in this work as derivations become rather lengthy. Furthermore, explicit examples for more initial conditions which are in the form of the configuration used in this work can be considered. In particular for the Boussinesq case, one could consider both right- & right- and

left-propagating N KdV soliton solutions as initial conditions. If possible, one could also extend the perturbation approach used to solve the higher order linearised KdV equations to include N KdV soliton solutions of the leading order problem.

Of course, one could also extend the derivation of the Boussinesq equations to incorporate $O(\epsilon^2)$ terms and hence construct the weakly nonlinear solution to higher order (which as a result increases the time validity of the solutions). Computations in derivations using the complex lattice model outlined in Section 2.1.2 would become increasingly more complicated, however this could first be done using the simpler model, explained in Section 2.1.1.

There are indeed many model extensions and alternative problem formulations one can consider to improve the current solutions and to inevitably apply the ideas to a broader area of real life problems. Similarly, there are a vast amount of interesting different mathematical applications for the derived and developed techniques and solutions of the Boussinesq-type problems contained in this thesis.

Appendix A

Finite difference methods for Boussinesq-type equations

A.1 Regularised Boussinesq equation

Using a finite difference scheme originally derived in [106], we numerically solve the Cauchy problem for the following regularised Boussinesq equation on the infinite line:

$$f_{tt} - c^2 f_{xx} = \frac{1}{2}\alpha(f^2)_{xx} + \beta f_{ttxx}, \tag{A.1}$$

$$f|_{t=0} = F(x,0), \tag{A.2}$$

$$f_t|_{t=0} = G(x,0), \tag{A.3}$$

thus we restrict x to the finite interval $x \in [-L, L]$ and discretise the (x,t) domain into a grid with equal spacings $\Delta x = h$ and $\Delta t = \kappa$. The continuous analytical solution $f(x,t)$ is approximated by the exact solution of the difference scheme $f(ih, j\kappa)$ denoted $f_{i,j}$, which lies on the discrete grid at the points $(ih, j\kappa)$ (for $i = 0, 1, ..., N$ and $j = 0, 1, ...$). Approximating the derivatives in (A.1) by the central difference approximations

$$\begin{aligned}(f_{i,j})_{xx} &= \frac{f_{i-1,j} - 2f_{i,j} + f_{i+1,j}}{h^2} + ..., \\ (f_{i,j})_{tt} &= \frac{f_{i,j-1} - 2u_{i,j} + f_{i,j+1}}{\kappa^2} + ...,\end{aligned} \tag{A.4}$$

the regularised Boussinesq equation (A.1) is approximated as

$$\frac{f_{i,j-1} - 2f_{i,j} + f_{i,j+1}}{\kappa^2} - c^2\frac{f_{i-1,j} - 2f_{i,j} + f_{i+1,j}}{h^2} - \frac{\alpha}{2}\left[\frac{(f_{i-1,j})^2 - 2(f_{i,j})^2 + (f_{i+1,j})^2}{h^2}\right]$$
$$-\beta\left[\frac{(\frac{f_{i-1,j-1}-2f_{i-1,j}+f_{i-1,j+1}}{\kappa^2}) - 2(\frac{f_{i,j-1}-2f_{i,j}+f_{i,j+1}}{\kappa^2}) + \frac{f_{i+1,j-1}-2f_{i+1,j}+f_{i+1,j+1}}{\kappa^2}}{h^2}\right] = 0.$$

Multiplying through by $h^2\kappa^2$ and rearranging to separate the unknown $j+1$ terms, we derive the following nine point implicit difference scheme

$$\begin{aligned}-\beta f_{i-1,j+1} + (2\beta + h^2) f_{i,j+1} - \beta f_{i+1,j+1} = {} & (\kappa^2 c^2 - 2\beta)[f_{i-1,j} - 2f_{i,j} + f_{i+1,j}] + 2h^2 f_{i,j} \\ & + \frac{\alpha\kappa^2}{2}[(f_{i-1,j})^2 - 2(f_{i,j})^2 + (f_{i+1,j})^2] \\ & + \beta f_{i-1,j-1} - (2\beta + h^2) f_{i,j-1} + \beta f_{i+1,j-1}.\end{aligned} \tag{A.5}$$

To solve scheme (A.5) for $f_{i,j+1}$ $\forall i$ one requires boundary conditions and since it is a three time-level scheme, two initial conditions. Throughout this work we deal mainly with localised solutions of the Boussinesq-type equations considered. In this case, provided the boundaries are sufficiently large, we can choose zero boundary conditions:

$$f_{0,j} = f_{N,j} = 0 \quad \forall j. \tag{A.6}$$

If the initial condition (A.2) is given analytically then we can simply choose the initial conditions for scheme (A.5) as follows

$$f_{i,0} = F(ih, 0), \qquad f_{i,1} = F(ih, \kappa) \qquad \forall i. \tag{A.7}$$

Alternatively if the initial conditions (A.2) and (A.3) are not analytical then one can deduce the second initial condition for scheme (A.5) by implementing the forward difference approximation (simulations have proved either choice are sufficiently accurate).

Writing the difference scheme (A.5) in matrix form, excluding the zero boundary terms, highlights in particular the system's tridiagonal nature

$$\begin{pmatrix} b & c & 0 & . & . & . & . & . & 0 \\ a & b & c & 0 & . & . & . & . & 0 \\ 0 & a & b & c & 0 & . & . & . & 0 \\ . & & . & & & & & & . \\ . & & & . & & & & & . \\ . & & & & . & & & & . \\ . & & & & & . & & & 0 \\ 0 & . & . & . & . & 0 & a & b & c \\ 0 & . & . & . & . & . & 0 & a & b \end{pmatrix} \begin{pmatrix} f_{1,j+1} \\ f_{2,j+1} \\ . \\ . \\ . \\ . \\ . \\ . \\ f_{n-1,j+1} \end{pmatrix} = \begin{pmatrix} X_1 \\ X_2 \\ . \\ . \\ . \\ . \\ . \\ . \\ X_{n-1} \end{pmatrix}, \tag{A.8}$$

where $a = c = 1$, $b = 2 + h^2$ and X_i $\forall i$ denotes the known terms in the right-hand side of (A.5). We solve the system of equations (A.8) using a Thomas Algorithm (e.g.,

[6]); essentially an optimised Gaussian elimination which utilises the tridiagonal characteristic of the matrix to minimise computational effort. Furthermore, computational storage is also minimised since we solve for a constant coefficient matrix.

A.1.1 Periodic Boundary conditions

As opposed to the zero boundary conditions implemented in the previous section, one may require the case of periodic boundary conditions (e.g. if one wishes to solve the Cauchy problem (A.1)–(A.3) on the periodic domain).

In this case the boundary conditions are

$$f_{0,j} = f_{N,j} \quad \forall j, \tag{A.9}$$

and the system of equations which must be solved at each time step, denoted by the matrix form $AF = X$, is now

$$\begin{pmatrix} b & c & 0 & . & . & . & . & 0 & a \\ a & b & c & 0 & . & . & . & . & 0 \\ 0 & a & b & c & 0 & . & . & . & 0 \\ . & & . & & & & & & . \\ . & & & . & & & & & . \\ . & & & & . & & & & . \\ . & & & & & . & & & 0 \\ 0 & . & . & . & . & 0 & a & b & c \\ c & 0 & . & . & . & . & 0 & a & b \end{pmatrix} \begin{pmatrix} f_{1,j+1} \\ f_{2,j+1} \\ . \\ . \\ . \\ . \\ . \\ f_{n-1,j+1} \\ f_{n,j+1} \end{pmatrix} = \begin{pmatrix} X_1 \\ X_2 \\ . \\ . \\ . \\ . \\ . \\ X_{n-1} \\ X_n \end{pmatrix}, \tag{A.10}$$

where $a = c = 1$, $b = 2 + h^2$ and the vectors X and F denote the known right-hand side of (A.5) and the unknown $j + 1$ solutions respectively.

Essentially, the difference from the zero boundary condition problem is that an extra row and column is introduced to the matrix A. However, crucially the banded tridiagonal structure is no longer present and hence the Thomas algorithm used in the zero boundary condition problem is no longer applicable.

Therefore, we rewrite the non-diagonally dominant $n \times n$ matrix A as $A = \bar{A} + uv^T$

where

$$\bar{A} = \begin{pmatrix} 0 & c & 0 & . & . & . & . & 0 & 0 \\ a & b & c & 0 & . & . & . & . & 0 \\ 0 & a & b & c & 0 & . & . & . & 0 \\ . & & . & & & & & & . \\ . & & & . & & & & & . \\ . & & & & . & & & & . \\ . & & & & & . & & & 0 \\ 0 & . & . & . & . & 0 & a & b & c \\ 0 & 0 & . & . & . & . & 0 & a & \bar{b} \end{pmatrix}, \quad u = \begin{pmatrix} b \\ 0 \\ . \\ . \\ . \\ . \\ . \\ 0 \\ c \end{pmatrix}, \quad v = \begin{pmatrix} 1 \\ 0 \\ . \\ . \\ . \\ . \\ . \\ 0 \\ \frac{a}{b} \end{pmatrix}. \tag{A.11}$$

The term $\bar{b} = (b^2 - ca)/b$ and we now note the matrix $\bar{A}$ is indeed tridiagonal. Using the Sherman–Morrison formula (see [105]) we can write

$$(\bar{A} + uv^T)^{-1} = \bar{A}^{-1} - \frac{\bar{A}^{-1}uv^T\bar{A}^{-1}}{1 + v^T\bar{A}u}, \tag{A.12}$$

and therefore the j+1 solutions of the system of equations (A.10) can be expressed as

$$F = \bar{A}^{-1}X - \frac{\bar{A}^{-1}uv^T\bar{A}^{-1}}{1 + v^T\bar{A}u}X. \tag{A.13}$$

If we denote $Q_1 = \bar{A}^{-1}X$, $Q_2 = \bar{A}^{-1}u$ and $\eta = \frac{v^TQ_1}{1+v^TQ_2}$ we can re-write (A.13) as

$$F = Q_1 - \eta\, Q_2. \tag{A.14}$$

Since $\bar{A}$ is tridiagonal and u and X are known, we can solve for the vectors Q_1 and Q_2 simultaneously at each time step using a Thomas Algorithm. It then remains to calculate the parameter η at each time step and hence one can determine F, yielding the solutions $f_{i,j+1}\ \forall\ i$.

A.1.2 Local truncation error

Let $D_{i,j}$ denote the difference scheme operator approximating the solution of (A.1) at the discrete (i,j)th mesh points where $D_{i,j}(f_{i,j}) = 0$. If we denote the exact solution of (A.1) as $\bar{f}$ then we have the expression

$$\begin{aligned} D_{i,j}(\bar{f}) &= -\beta\bar{f}_{i-1,j+1} + (2\beta + h^2)\bar{f}_{i,j+1} - \beta\bar{f}_{i+1,j+1} - (k^2c^2 - 2\beta)\left[\bar{f}_{i-1,j} - 2\bar{f}_{i,j}\right. \\ &\quad \left. + \bar{f}_{i+1,j}\right] - 2h^2\bar{f}_{i,j} - \frac{\alpha\kappa^2}{2}\left[(\bar{f}_{i-1,j})^2 - 2(\bar{f}_{i,j})^2 + (\bar{f}_{i+1,j})^2\right] \\ &\quad -\beta\bar{f}_{i-1,j-1} + (2\beta + h^2)\bar{f}_{i,j-1} - \beta\bar{f}_{i+1,j-1} \\ &= T_{i,j}, \end{aligned} \tag{A.15}$$

where $T_{i,j}$, the local truncation error, measures the amount in which the exact solution of (A.1) does not satisfy the solution of the difference scheme (A.5), at the point $(ih, j\kappa)$.

We determine the magnitude of $T_{i,j}$ in terms of the discretisations h and κ by approximating the terms in (A.15) with Taylor series expansions. It transpires that the magnitude of the principal part of the local truncation error is unchanged if we include terms in the expansions $O(h^n\kappa^m)$ or beyond, where $n+m=5$. Hence, we approximate the terms

$$\begin{aligned}
\bar{f}_{i\pm1,j} &= \bar{f}_{i,j} \pm h(\bar{f}_x)|_{i,j} + \frac{h^2}{2}(\bar{f}_{xx})|_{i,j} \pm \frac{h^3}{6}(\bar{f}_{xxx})|_{i,j} + \frac{h^4}{24}(\bar{f}_{xxxx})|_{i,j} + O(h^5),\\
\bar{f}_{i,j\pm1} &= \bar{f}_{i,j} \pm \kappa(\bar{f}_t)|_{i,j} + \frac{\kappa^2}{2}(\bar{f}_{tt})|_{i,j} \pm \frac{\kappa^3}{6}(\bar{f}_{ttt})|_{i,j} + \frac{\kappa^4}{24}(\bar{f}_{tttt})|_{i,j} + O(\kappa^5),\\
\bar{f}_{i+1,j\pm1} &= \bar{f}_{i,j} + h(\bar{f}_x)|_{i,j} \pm \kappa(\bar{f}_t)|_{i,j} + \frac{1}{2}\Big[h^2(\bar{f}_{xx})|_{i,j} \pm 2h\kappa(\bar{f}_{xt})|_{i,j} + \kappa^2(\bar{f}_{tt})|_{i,j}\Big]\\
&\quad +\frac{1}{6}\Big[h^3(\bar{f}_{xxx})|_{i,j} \pm 3h^2\kappa(\bar{f}_{xxt})|_{i,j} + 3h\kappa^2(\bar{f}_{xtt})|_{i,j} \pm \kappa^3 3h^2\kappa(\bar{f}_{ttt})|_{i,j}\Big]\\
&\quad +\frac{1}{24}\Big[h^4(\bar{f}_{xxxx})|_{i,j} \pm 4h^3\kappa(\bar{f}_{xxxt})|_{i,j} + 6h^2\kappa^2(\bar{f}_{xxtt})|_{i,j} \pm 4h\kappa^3(\bar{f}_{xttt})|_{i,j}\\
&\quad +\kappa^4(\bar{f}_{tttt})|_{i,j}\Big] + O(h^5 + h^4\kappa + h^3\kappa^2 + h^2\kappa^3 + h\kappa^4 + \kappa^5),\\
\bar{f}_{i-1,j\pm1} &= \bar{f}_{i,j} - h(\bar{f}_x)|_{i,j} \pm \kappa(\bar{f}_t)|_{i,j} + \frac{1}{2}\Big[h^2(\bar{f}_{xx})|_{i,j} \mp 2h\kappa(\bar{f}_{xt})|_{i,j} + \kappa^2(\bar{f}_{tt})|_{i,j}\Big]\\
&\quad +\frac{1}{6}\Big[-h^3(\bar{f}_{xxx})|_{i,j} \pm 3h^2\kappa(\bar{f}_{xxt})|_{i,j} - 3h\kappa^2(\bar{f}_{xtt})|_{i,j} \pm \kappa^3 3h^2\kappa(\bar{f}_{ttt})|_{i,j}\Big]\\
&\quad +\frac{1}{24}\Big[h^4(\bar{f}_{xxxx})|_{i,j} \mp 4h^3\kappa(\bar{f}_{xxxt})|_{i,j} + 6h^2\kappa^2(\bar{f}_{xxtt})|_{i,j} \mp 4h\kappa^3(\bar{f}_{xttt})|_{i,j}\\
&\quad +\kappa^4(\bar{f}_{tttt})|_{i,j}\Big] + O(h^5 + h^4\kappa + h^3\kappa^2 + h^2\kappa^3 + h\kappa^4 + \kappa^5),
\end{aligned}$$

and the nonlinear terms in (A.15) are then approximated as

$$\begin{aligned}
(\bar{f}_{i-1,j})^2 - 2(\bar{f}_{i,j})^2 + (\bar{f}_{i+1})^2 &= 2\left[h^2(\bar{f}_x^2)|_{i,j} + \frac{h^4}{4}(\bar{f}_{xx}^2)|_{i,j}\right] + 4\left[\frac{h^2}{2}\bar{f}_{i,j}(\bar{f}_{xx})|_{i,j}\right.\\
&\quad \left.+\frac{h^4}{24}\bar{f}_{i,j}(\bar{f}_{xxxx})|_{i,j} + \frac{h^4}{6}(\bar{f}_x)|_{i,j}(\bar{f}_{xxx})|_{i,j}\right] + O(h^5).
\end{aligned}$$

Substituting the Taylor expansions into (A.15) yields

$$\begin{aligned}
T_{i,j} &= h^2\kappa^2\left[(\bar{f}_{tt})_{i,j} - c^2(\bar{f}_{xx})_{i,j} - \alpha\frac{1}{2}\Big((\bar{f}^2)_{xx}\Big)_{i,j} - \beta(\bar{f}_{xxtt})_{i,j}\right] + h^2\kappa^4\left[\frac{1}{12}(\bar{f}_{tttt})_{i,j}\right]\\
&\quad +h^4\kappa^2\left[-\frac{c^2}{12}\bar{f}_{xxxx} - \alpha(\frac{1}{24}\bar{f}\bar{f}_{xxxx} + \frac{1}{3}\bar{f}_x\bar{f}_{xxx} + \frac{1}{4}\bar{f}_{xx}^2)\right] + \dots\,, \qquad \text{(A.16)}
\end{aligned}$$

where to leading order the discrete form of the regularised Boussinesq equation (A.1) has emerged. Since $\bar{f}$ is the exact solution of (A.1), $T_{i,j}$ reduces to the following form

$$\begin{aligned} T_{i,j} &= h^2\kappa^4\left[\frac{1}{12}(\bar{f}_{tttt})_{i,j}\right] + h^4\kappa^2\left[-\frac{c^2}{12}\bar{f}_{xxxx} - \alpha(\frac{1}{24}\bar{f}\bar{f}_{xxxx} + \frac{1}{3}\bar{f}_x\bar{f}_{xxx} + \frac{1}{4}\bar{f}_{xx}^2)\right] \\ &\quad + O(h^5 + h^4\kappa + h^3\kappa^2 + h^2\kappa^3 + h\kappa^4 + \kappa^5). \end{aligned} \tag{A.17}$$

The principal part of the local truncation error is therefore $O(h^2\kappa^4 + h^4\kappa^2)$. One can easily show that taking higher order terms in the Taylor series expansions, namely beyond $O(h^n\kappa^m)$ where $n + m = 4$, will not effect the leading order form of $T_{i,j}$. One can also notice that only terms of even powers of h and κ appear in the truncation error.

A.1.3 Stability

We examine the stability of the difference scheme (A.5) using a von Neumann linear stability analysis. First we linearise the scheme by setting $f_{i,j} = f_0 + \hat{f}_{i,j}$, where f_0 is constant such that $f_0 > f_{ij}\ \forall i, j$. Hence, from (A.5) we have

$$\begin{aligned} -\beta\hat{f}_{i-1,j+1} + (2\beta + h^2)\hat{f}_{i,j+1} - \beta\hat{f}_{i+1,j+1} &= [\kappa^2(c^2 + \alpha f_0) - 2\beta][\hat{f}_{i-1,j} - 2\hat{f}_{i,j} + \hat{f}_{i+1,j}] \\ &\quad + 2h^2\hat{f}_{i,j} \\ &\quad + \beta\hat{f}_{i-1,j-1} - (2\beta + h^2)\hat{f}_{i,j-1} + \beta\hat{f}_{i+1,j-1}, \end{aligned} \tag{A.18}$$

where essentially the nonlinear terms $f_{i,j}^2$ in (A.5) have been replaced with $2f_0\hat{f}_{i,j}$. We are concerned with the growth of error in (A.18) as $t \to \infty$. Let us define round off error at the (i, j)th point as $\xi_{i,j} = N_{i,j} - \hat{f}_{i,j}$, where $N_{i,j}$ is the numerical solution we compute from simulations for scheme (A.18). Since the difference scheme is now linear, the error $\hat{\xi}_{i,j}$ will also satisfy (A.18) and so the numerical solution and the round off error will both have the same decay/growth behaviour with respect to time. Furthermore we can express the error in the interval $2L$ as

$$\xi(x, t) = \Sigma_{n=0}^{N} A_i e^{\mathrm{i}\theta x}, \tag{A.19}$$

where $\theta \geq 0$ (and $\mathrm{i}^2 = -1$), but since it satisfies the linear scheme (A.18) we can examine just a single term in the series (A.19) to understand the decay/growth rate of the entire error (all other terms will be additive).

Writing the error at the (i,j)th point as

$$\xi_{i,j} = e^{aj\kappa}e^{\mathrm{i}\theta_i ih} = G^j e^{\mathrm{i}\theta_i ih} \tag{A.20}$$

where $G = e^{a\kappa}$ (often denoted the amplification factor) and G is generally complex, it is clear the error will grow without bound if $|\xi_{i,j+1}| > |\xi_{i,j}|$ as $j \to \infty$. Therefore for the difference scheme (A.18) to remain stable we require

$$\left|\frac{\xi_{i,j+1}}{\xi_{i,j}}\right| = \left|\frac{e^{a(j+1)\kappa}e^{\mathrm{i}\theta_i ih}}{e^{aj\kappa}e^{\mathrm{i}\theta_i ih}}\right| = |G| \leq 1 \quad \forall\theta \text{ and arbitrary } \mathrm{h}, \kappa. \tag{A.21}$$

Substituting the error (A.20) into scheme (A.18) we find the following quadratic expression for G:

$$G^2 - 2\mu G + 1 = 0 \quad \text{where} \quad \mu = 1 - \frac{2\kappa^2(c^2+\alpha f_0)\sin^2(\frac{\theta h}{2})}{h^2 + 4\beta\sin^2(\frac{\theta h}{2})}. \tag{A.22}$$

Since $\mu \leq 1\ \forall\theta, h, \kappa$, the roots of (A.22) are $G_{1,2} = \mu \pm \sqrt{\mu^2 - 1}$.

If G is real ($\mu^2 \geq 1$), and in particular $\mu^2 > 1$ then $|G_1| > 1$ and we have instability. Alternatively if $\mu^2 = 1$, we have stability, although this particular case is not of much use or interest (this case corresponds to the wave number being zero and hence there is no propagation through space). Therefore to ensure stability is maintained, G cannot be real. If G is complex ($\mu^2 < 1$) this implies $|G| = 1$ and hence the scheme is indeed stable $\forall\theta$ and arbitrary h, κ provided $|\mu| < 1$, which implies

$$0 < \frac{\kappa^2(c^2+\alpha f_0)\sin^2(\frac{\theta h}{2})}{h^2 + 4\beta\sin^2(\frac{\theta h}{2})} < 1. \tag{A.23}$$

The left-hand side of (A.23) is unconditionally satisfied $\forall\theta$ and arbitrary h, κ and the right-hand side is also satisfied provided

$$\kappa = \kappa_c < \sqrt{\frac{h^2 + 4\beta}{c^2 + \alpha f_0}}. \tag{A.24}$$

Therefore if (A.24) holds true, difference scheme (A.18) is stable. For simulations of the original nonlinear scheme (A.5), we implement the stricter condition $\kappa < \frac{1}{2}\kappa_c$, to help accommodate for the effects of nonlinearity. We also choose f_0 to be the largest positive value which is the most restrictive choice on the criteria (A.24).

A.2 Coupled regularised Boussinesq equations

We extend the numerical method outlined in Section A.1 to the case of cRB equations. In particular let us consider the IVP for two cRB equations on the infinite line:

$$\begin{aligned} f_{tt} - f_{xx} &= \frac{1}{2}(f^2)_{xx} + f_{ttxx} - \delta(f-g), \\ g_{tt} - c^2 g_{xx} &= \frac{1}{2}\alpha(g^2)_{xx} + \beta g_{ttxx} + \gamma(f-g), \end{aligned} \tag{A.25}$$

imposing the following initial conditions:

$$f|_{t=0} = F_1(x,0), \quad g|_{t=0} = G_1(x,0), \tag{A.26}$$

$$f_t|_{t=0} = G_1(x,0), \quad g_t|_{t=0} = G_2(x,0). \tag{A.27}$$

Analogous to the single Boussinesq equation, we let $x \in [-L, L]$, for finite L, and discretise the (x,t) domain into a grid with spacings $\Delta x = h$ and $\Delta t = \kappa$. The solutions $f(x,t)$ and $g(x,t)$ of (A.25) are approximated by the solutions $f(ih, j\kappa)$ and $g(ih, j\kappa)$ (for $i = 0, 1, ..., N$ and $j = 0, 1, ...$) of the difference scheme, denoted $f_{i,j}$ and $g_{i,j}$. Substituting central difference approximations of the form (A.4) into system (A.25) we derive the following coupled difference scheme:

$$\begin{aligned} -f_{i-1,j+1} + (2+h^2)f_{i,j+1} - f_{i+1,j+1} = {} & (\kappa^2 - 2)[f_{i-1,j} - 2f_{i,j} + f_{i+1,j}] + 2h^2 f_{i,j} \\ & + \frac{\kappa^2}{2}[(f_{i-1,j})^2 - 2(f_{i,j})^2 + (f_{i+1,j})^2] \\ & + f_{i-1,j-1} - (2+h^2)f_{i,j-1} + f_{i+1,j-1} \\ & - h^2\kappa^2\delta(f_{i,j} - g_{i,j}), \end{aligned} \tag{A.28}$$

$$\begin{aligned} -\beta g_{i-1,j+1} + (2\beta+h^2)g_{i,j+1} - \beta g_{i+1,j+1} = {} & (\kappa^2 c^2 - 2\beta)[g_{i-1,j} - 2g_{i,j} + g_{i+1,j}] + 2h^2 g_{i,j} \\ & + \frac{\alpha\kappa^2}{2}[(g_{i-1,j})^2 - 2(g_{i,j})^2 + (g_{i+1,j})^2] \\ & + \beta g_{i-1,j-1} - (2\beta+h^2)g_{i,j-1} + \beta g_{i+1,j-1} \\ & + h^2\kappa^2\gamma(f_{i,j} - g_{i,j}). \end{aligned} \tag{A.29}$$

We now have two coupled nine point implicit difference schemes, both with tridiagonal matrices of constant coefficients, which we solve simultaneously at each time step for $f_{i,j+1}$ and $g_{i,j+1}$, using two Thomas algorithms.

Periodic boundary conditions can be implemented analogous to the approach implemented for the single Boussinesq equation in Section A.1.1. However, since we consider localised solutions of (A.25) for the majority of the work in this thesis, we implement zero boundary conditions

$$f_{0,j} = f_{N,j} = g_{0,j} = g_{N,j} = 0, \quad \forall j, \tag{A.30}$$

provided we set L to be sufficiently large. If the initial conditions (A.26) and (A.27) are given analytically we can choose the initial conditions of scheme (A.29) as

$$\begin{aligned} f_{i,0} &= F_1(ih, 0) \qquad f_{i,1} = F_1(ih, \kappa), \\ g_{i,0} &= F_2(ih, 0), \qquad g_{i,1} = F_2(ih, \kappa), \quad \forall i, \end{aligned} \tag{A.31}$$

alternatively we can utilise the forward difference approximation and make use of the two derivative initial conditions $G_{1,2}$.

The numerical scheme for N cRB equations is easily extended by solving N difference schemes of the form (A.28) and (A.29) in the same way, simultaneously at each time step.

Conservation laws inherent in the system of cRB equations (A.25) are utilised in the numerics in order to test the accuracy of the coupled difference scheme (A.28) and (A.29). See Section 2.2 for more details concerning the conservation laws.

A. FINITE DIFFERENCE METHODS FOR BOUSSINESQ-TYPE EQUATIONS

Appendix B

Pseudo-spectral methods and the Fourier transform

B.1 Introduction

Spectral methods have come to the forefront of numerical approaches for solving PDEs, initialising in the early 1970's (naturally some of the underlying ideas were developed prior to this). As was the case with the once leading preceding techniques in finite difference methods and then with finite element methods, a newer more effective and efficient approach has come into prominence (of course this depends on the specific nature of the problem). Generally if one wants to solve an ODE or PDE on a simple domain with smooth data, spectral methods will usually offer the best accuracy and computational efficiency.

The underlying concept behind spectral methods is to write the solution of a differential equation as a sum of basis functions. Then by implementing the FFT algorithm, one can determine the coefficients of the sum to yield the best approximation of the solution to the differential equation. The FFT is an algorithm developed in 1965 by Cooley and Tukey [26] (although it has been suggested, e.g. in [55], that it was originally deduced in unpublished work by Gauss with a presumed year of composition dating back to 1805), which is used to efficiently compute the discrete Fourier transform (DFT), and similarly the inverse fast Fourier transform (IFFT) is used for calculating the inverse discrete Fourier transform (IDFT).

The DFT's are analogues of the Fourier transforms on the continuous domain. We

define the Fourier transform of a function $u(x,t)$ for $x \in \mathbb{R}$, denoted by the operator $\mathscr{F}\{u(x,t)\} = \hat{u}(k,t)$, as

$$\hat{u}(k,t) = \int_{-\infty}^{\infty} e^{-ikx} u(x,t) dx, \tag{B.1}$$

where $k \in \mathbb{R}$ is known as the transform variable. Conversely the inverse Fourier transform, denoted $\mathscr{F}^{-1}\{\hat{u}(k,t)\} = u(x,t)$, is defined as

$$u(x,t) = \frac{1}{2\pi} \int_{-\infty}^{\infty} e^{ikx} \hat{u}(k,t) dk. \tag{B.2}$$

Considering the spatial derivative for the function $u(x,t)$, we find from (B.1) that

$$\mathscr{F}\left\{\frac{\partial u}{\partial x}\right\} = \int_{-\infty}^{\infty} e^{-ikx} \frac{\partial u}{\partial x} dx, \tag{B.3}$$

which after integrating by parts and assuming $u(x,t) \to 0$ as $|x| \to \infty$ yields

$$\begin{aligned} \mathscr{F}\left\{\frac{\partial u}{\partial x}\right\} &= \left[e^{-ikx} u\right]_{-\infty}^{\infty} + ik \int_{-\infty}^{\infty} e^{-ikx} u(x,t) dx \\ &= ik\hat{u}(k,t). \end{aligned} \tag{B.4}$$

Therefore it follows if $u(x,t)$ is continuously n times differentiable and $\frac{\partial^n u}{\partial x^n} \to 0$ as $|x| \to \infty$, for $k = 1, 2, ..., (n-1)$, then

$$\mathscr{F}\left\{\frac{\partial^n u}{\partial x^n}\right\} = (ik)^n \hat{u}(k,t). \tag{B.5}$$

For the DFT let us consider the function $v(x,t)$ on the finite domain $x \in [-L, L]$ and discretise the domain into N equally spaced points, which yields the spacing $\Delta x = 2L/N$. Denoting the discrete form of the function $v(x,t) = v_j(x_j,t)$ where $x_j = j\Delta x$ for $j = 1, .., N$, we define the DFT for the function $v_j(x_j,t)$ as

$$\hat{v}_k = \Delta x \sum_{j=1}^{N} e^{-ikx_j} v_j(x_j,t), \quad \text{for} \quad k = -\frac{N}{2} + 1, ..., \frac{N}{2}, \tag{B.6}$$

and similarly, the IDFT is defined as

$$v_j = \frac{1}{2\pi} \sum_{k=-N/2+1}^{N/2} e^{ikx_j} \hat{v}_k(k,t), \quad \text{for} \quad j = 1, ..., N, \tag{B.7}$$

where $k \in \mathbb{Z}$, is now the discrete transform variable.

We implement the FFT and IFFT in *Matlab* using the built-in algorithms denoted 'ftt' and 'iftt' respectively. Unlike the definitions for the DFT (B.6) and IDFT (B.7), *Matlab* requires the transform variable k to be ordered as $k = 0, 1, ..., \frac{N}{2}, -\frac{N}{2}+1, -\frac{N}{2}+2, ..., -1$. Note we have only considered even N, although naturally this is not a restriction and the algorithms we use introduced throughout this work can be easily modified to accommodate odd choices of N. In terms of computational duration of simulations: if one discretises the spatial domain of a function into N equally spaced points, the usual number of arithmetical operations of determining the DFT is $O(N^2)$, however the FFT can compute the DFT in as few as $O(N \log N)$ operations (this requires N to be highly composite).

For the purpose of implementing the spectral methods outlined in this appendix, we scale the periodic spatial domain from $x \in [-L, L]$ to $x \in [0, 2\pi]$ (this formally corresponds to multiplying the Fourier domain by $s = \pi/L$).

B.2 Boussinesq–Ostrovsky equation

We first outline a pseudo-spectral method used to solve the Cauchy problem for the following Boussinesq–Ostrovsky equation:

$$\begin{aligned} U_{tt} - c^2 U_{xx} &= \epsilon \left(\frac{\alpha}{2} (U^2)_{xx} + \beta U_{ttxx} - \gamma U \right), \\ U|_{t=0} &= F(x), \\ U_t|_{t=0} &= V(x), \end{aligned} \tag{B.8}$$

on the periodic domain $-L \leq x \leq L$. This method is an extension to the approach outlined in [36] which solves the regularised Boussinesq equation in the context of microstructured solids.

Introducing

$$W = U - \epsilon \beta U_{xx}, \tag{B.9}$$

we find from (B.8a)

$$W_{tt} = c^2 U_{xx} + \epsilon \left(\frac{\alpha}{2} (U^2)_{xx} - \gamma U \right). \tag{B.10}$$

Taking the Fourier transform of (B.9) yields

$$\hat{W} = (1 + \epsilon \beta k^2) \hat{U}, \tag{B.11}$$

where k is the Fourier transform variable, and thus the solution to (B.8) in the Fourier space is as follows

$$\hat{U} = \frac{\hat{W}}{(1+\epsilon\beta k^2)}. \tag{B.12}$$

Taking the Fourier transform of (B.10) and substituting (B.12) into the resulting ODE yields the following ODE for $\hat{W}$:

$$\begin{aligned} \hat{W}_{tt} &= -\frac{(\epsilon\gamma + k^2c^2)}{(1+\epsilon k^2\beta)}\hat{W} - \frac{\epsilon k^2\alpha}{2}\,\mathscr{F}\left\{ \mathscr{F}^{-1}\left[\frac{\hat{W}}{(1+\epsilon k^2\beta)}\right]^2 \right\} \\ &= \hat{H}(\hat{W}). \end{aligned} \tag{B.13}$$

We solve the second order ODE (B.13) by reducing it to two first order ODE's and simultaneously implementing a Runge–Kutta fourth-order (RK4) method to solve in time. We therefore define

$$\begin{aligned} \hat{W}_t &= \hat{G}, \\ \hat{G}_t &= \hat{H}(\hat{W}), \end{aligned} \tag{B.14}$$

and discretise $t = t_n$, $\hat{W}(k,t_n) = \hat{W}_n$, $\hat{G}(k,t_n) = \hat{G}_n$ for $n = 0, 1, 2, ...$, where $t_n = n\Delta t$ and k now denotes the discrete Fourier space. Taking the Fourier transform of the initial conditions (B.8b,c) yields the initial conditions $\hat{W}_0$ and $\hat{G}_0$ and thus we implement the following RK4 method:

$$\begin{aligned} \hat{W}_{n+1} &= \hat{W}_n + \frac{1}{6}\left[k_1 + 2(k_2+k_3) + k_4\right], \quad \hat{G}_{n+1} = \hat{G}_n + \frac{1}{6}\left[l_1 + 2(l_2+l_3) + l_4\right], \\ \text{where} \quad k_1 &= \Delta t\hat{G}_n, & l_1 &= \Delta t\hat{H}(\hat{W}_n), \\ k_2 &= \Delta t(\hat{G}_n + l_1/2), & l_2 &= \Delta t\hat{H}(\hat{W}_n + k_1/2), \\ k_3 &= \Delta t(\hat{G}_n + l_2/2), & l_3 &= \Delta t\hat{H}(\hat{W}_n + k_2/2), \\ k_4 &= \Delta t(\hat{G}_n + l_3), & l_4 &= \Delta t\hat{H}(\hat{W}_n + k_3). \end{aligned} \tag{B.15}$$

Once (B.15) is solved up to a given time, we substitute the solution $\hat{W}$ into (B.12) and implement the inverse fast Fourier transform to find U in the original physical space.

We now test the accuracy of scheme (B.15) by considering the case $\gamma = 0$ in (B.8a), corresponding to the Cauchy problem of the regularised Boussinesq equation. This equation has exact solitary wave solutions of the form:

$$U_{\text{sol}}(x,t) = A\ \text{sech}^2\left(\frac{x-vt}{\Lambda}\right), \quad \text{where} \quad A = \frac{3(v^2-c^2)}{\alpha}, \quad \Lambda = 2v\sqrt{\frac{\beta}{v^2-c^2}}, \tag{B.16}$$

therefore we choose the following initial conditions to coincide with the exact solution:

$$\begin{aligned} \hat{W}_0 &= (1+\epsilon\beta k^2)\,\mathscr{F}\{U_{\rm sol}(x,0)\}, \\ \hat{G}_0 &= (1+\epsilon\beta k^2)\,\mathscr{F}\left\{\left[\frac{\partial}{\partial t}U_{\rm sol}(x,t)\right]|_{t=0}\right\}, \end{aligned} \tag{B.17}$$

and illustrate in Table B.1 the accuracy of scheme (B.15), for $\gamma = 0$ with initial conditions (B.17), compared with the corresponding exact solution (B.16). As one can see, simulations of scheme (B.15) are extremely accurate for the time region we are concerned with in this problem. As the time step is decreased we find the accuracy of the scheme is bound only by the accuracy of the FFT algorithms used to compute the DFT and IDFT in (B.13) and (B.17). Increasing the number of harmonics and further decreasing the time step would yield even better results.

	Maximum absolute error	
ΔT	$T = \epsilon$	$T = 1$
0.01	7.1767 x 10^{-12}	7.2886 x 10^{-11}
0.005	4.4853 x 10^{-13}	4.5370 x 10^{-12}
0.0025	2.7978 x 10^{-14}	2.8366 x 10^{-13}
0.00125	1.9984 x 10^{-15}	1.7653 x 10^{-14}
6.25 x 10^{-4}	4.4409 x 10^{-16}	1.4433 x 10^{-15}
3.125 x 10^{-4}	9.6936 x 10^{-16}	9.6936 x 10^{-16}

Table B.1: Maximum absolute error of the numerical solution (B.15) for $c = \alpha = \beta = 1$, $\epsilon = 0.1$, $v = 1.016$ & $\gamma = 0$, compared with the exact solution (B.16), for various time discretisations ΔT. Numerical parameters: $L = 2000$, $N = 2^{14}$.

B.3 Linearised Korteweg–de Vries equation

B.3.1 Linearised Korteweg–de Vries equation on zero background

We next outline the spectral method used to solve the Cauchy problem for the homogeneous linearised KdV equation, linearised on a zero background, namely

$$\begin{aligned} -2\psi_T + \psi_{\eta\eta\eta} &= 0, \\ \psi|_{T=0} &= \frac{3p^4}{4}\mathrm{sech}^2\left(\frac{p\eta}{2}\right). \end{aligned} \tag{B.18}$$

on the periodic domain $-L \leq x \leq L$. Taking the Fourier transform of (B.18) yields

$$\begin{aligned} -2\hat{\psi}_T - ik^3\hat{\psi} &= 0, \\ \hat{\psi}(k,0) &= \frac{3p^4}{4}\mathscr{F}\left\{\operatorname{sech}^2\left(\frac{p\xi}{2}\right)\right\}. \end{aligned} \tag{B.19}$$

and solving the Cauchy problem for the ODE (B.19) yields

$$\psi(\eta,T) = \mathscr{F}^{-1}\left\{\hat{\psi}(k,0)e^{\frac{-ik^3T}{2}}\right\}. \tag{B.20}$$

Discretising $\hat{\psi}(k,T_n) = \hat{\psi}_n$ with $T = \Delta T = T_n$ for $n = 0,1,2,...$, where k now denotes the discrete Fourier space, the solution (B.20) is obtained from applying the FFT algorithms.

B.3.2 Linearised Korteweg–de Vries equation on nonzero background

We next outline the spectral method used to solve the Cauchy problem for the homogeneous linearised KdV equation, linearised on a non-zero background, namely

$$\begin{aligned} 2\phi_T + (f^-\phi)_\xi + \phi_{\xi\xi\xi} &= 0, \\ \phi|_{T=0} &= -\frac{15p^4}{4}\operatorname{sech}^2\left(\frac{p\xi}{2}\right). \end{aligned} \tag{B.21}$$

on the periodic domain $-L \leq x \leq L$. Taking the Fourier transform of (B.21) yields

$$\begin{aligned} 2\hat{\phi}_T + ik\widehat{(f^-\phi)} - ik^3\hat{\phi} &= 0, \\ \hat{\phi}(k,0) &= -\frac{15p^4}{4}\mathscr{F}\left\{\operatorname{sech}^2\left(\frac{p\xi}{2}\right)\right\}. \end{aligned} \tag{B.22}$$

Analogous to the approach in [109] used to solve the KdV equation, we remove the stiff-term by multiplying (B.22a) by the integrating factor $\exp(-ik^3T/2)$ and introduce

$$\hat{\Phi} = e^{-\frac{ik^3T}{2}}\ \hat{\phi}, \tag{B.23}$$

which after noting $\hat{\Phi}_T = \exp(-ik^3T/2)\ \hat{\phi}_T - ik^3/2\ \hat{\phi}$, yields (B.22a) in the form

$$\hat{\Phi}_T = -\frac{ik}{2}e^{-\frac{ik^3T}{2}}\widehat{f^-\phi}. \tag{B.24}$$

Therefore we have the following ODE for $\hat{\Phi}$, in the Fourier space:

$$\begin{aligned} \hat{\Phi}_T &= -\frac{ik}{2}e^{-\frac{ik^3T}{2}}\mathscr{F}\left\{f^-\mathscr{F}^{-1}\left[e^{\frac{ik^3T}{2}}\hat{\Phi}\right]\right\} \\ &= A(T,\hat{\Phi}). \end{aligned} \tag{B.25}$$

We discretise $\hat{\Phi}(k,T_n)=\hat{\Phi}_n$ with $T=\Delta T=T_n$ for $n=0,1,2,...$, where k now denotes the discrete Fourier space, and with $\hat{\Phi}_0$ obtainable from the initial conditions (B.22b), we implement the following optimised RK4 method (see [109]):

$$\begin{aligned}
\hat{\phi}_{n+1} &= E^2\hat{\phi}_n+\frac{1}{6}\left[E^2h_1+2E(h_2+h_3)+h_4\right],\\
\text{where}\quad h_1 &= -\frac{ikdt}{2}\mathscr{F}\left\{f^-\,\mathscr{F}^{-1}\left[\phi_n\right]\right\},\\
h_2 &= -\frac{ikdt}{2}\mathscr{F}\left\{f^-\,\mathscr{F}^{-1}\left[E\left(\phi_n+\frac{h_1}{2}\right)\right]\right\},\\
h_3 &= -\frac{ikdt}{2}\mathscr{F}\left\{f^-\,\mathscr{F}^{-1}\left[E\phi_n+\frac{h_2}{2}\right]\right\},\\
h_4 &= -\frac{ikdt}{2}\mathscr{F}\left\{f^-\,\mathscr{F}^{-1}\left[E^2\phi_n+Eh_3\right]\right\},
\end{aligned}\tag{B.26}$$

for $E=\exp(ik^3dt/4)$ (note, for convenience we have returned to the original variable $\hat{\phi}$). Once $\hat{\phi}_n$ is obtained up to a given n, we apply the inverse Fourier transform to find the solution ϕ in the original physical space, and thus obtain the solution to the Cauchy problem (B.21).

B.4 Ostrovsky equation

The Ostrovsky equation has recently been solved numerically using both pseudo-spectral and finite difference methods (e.g., [50, 88, 92, 117]). We extend the spectral method described in [109], used to solve the KdV equation, to now solve the Cauchy problem for the Ostrovsky equation:

$$\begin{aligned}
\left(\alpha_0 f^-_T+\frac{\nu_0}{2}((f^-)^2)_{\xi_-}+\lambda_0 f^-_{\xi_-\xi_-\xi_-}\right)_{\xi_-} &= \gamma f^-,\\
f^-|_{T=0} &= 3k^2\,\mathrm{sech}^2(k\xi^-/2)-c_0,
\end{aligned}\tag{B.27}$$

on the periodic domain $-L\le x\le L$. The constant 'pedestal' term denoted c_0 is introduced to satisfy the zero mass property inherent in the Ostrovsky equation (alternatively one can choose a variable term to satisfy zero mass).

Taking the Fourier transform of (B.27a) yields

$$\hat{f}^-_T=\frac{i}{\alpha_0}\left(\lambda_0k^3-\frac{\gamma}{k}\right)\hat{f}^--\frac{ik\nu_0}{2\alpha_0}\widehat{(f^-)^2}.\tag{B.28}$$

Multiplying (B.28) by the integrating factor $\exp[-i/\alpha_0\left(\lambda_0k^3-\gamma/k\right)T]$ and introducing

$$\hat{\tilde{f}}^-_T=e^{-\frac{i}{\alpha_0}(\lambda_0k^3-\frac{\gamma}{k})T}\hat{f}^-,\tag{B.29}$$

yields from (B.28) the following ODE for $\hat{\hat{f}}^-$:

$$\hat{\hat{f}}^-_T = -\frac{ik\nu_0}{2\alpha_0} e^{-\frac{i}{\alpha_0}\left(\lambda_0 k^3 - \frac{\gamma}{k}\right)T} \mathscr{F}\left\{ \mathscr{F}^{-1}\left[e^{\frac{i}{\alpha_0}\left(\lambda_0 k^3 - \frac{\gamma}{k}\right)} \hat{\hat{f}}^- \right]^2 \right\}. \tag{B.30}$$

We discretise $\hat{\hat{f}}^-(k, T_n) = \hat{\hat{f}}^-_n$ with $T = n\Delta T = T_n$ for $n = 0, 1, 2, ...$, where k now denotes the discrete Fourier space, and implement the following optimised RK4 method:

$$\begin{aligned}
\hat{f}^-_{n+1} &= E^2 \hat{f}^-_n + \frac{1}{6}\left[E^2 h_1 + 2E(h_2 + h_3) + h_4\right], \\
\text{where} \quad h_1 &= -\frac{ik\nu_0 \Delta T}{2\alpha_0} \mathscr{F}\left\{ \mathscr{F}^{-1}\left[\hat{f}^-_n\right]^2 \right\}, \\
h_2 &= -\frac{ik\nu_0 \Delta T}{2\alpha_0} \mathscr{F}\left\{ \mathscr{F}^{-1}\left[E\left(\hat{f}^-_n + \frac{h_1}{2} \right) \right]^2 \right\}, \\
h_3 &= -\frac{ik\nu_0 \Delta T}{2\alpha_0} \mathscr{F}\left\{ \mathscr{F}^{-1}\left[E\hat{f}^-_n + \frac{h_2}{2} \right]^2 \right\}, \\
h_4 &= -\frac{ik\nu_0 \Delta T}{2\alpha_0} \mathscr{F}\left\{ \mathscr{F}^{-1}\left[E^2 \hat{f}^-_n + E h_3 \right]^2 \right\},
\end{aligned} \tag{B.31}$$

for $E = \exp[i/2\alpha_0 \left(\lambda_0 k^3 - \gamma/k\right) \Delta T]$ (note, for convenience we have returned to the original variable $\hat{f}^-$). Once $\hat{f}^-_n$ is obtained up to a given n, we simply apply the inverse Fourier transform to find the solution f^- in the original physical space, and thus obtain the solution to the Cauchy problem (B.27).

As previously mentioned, the DFT and IDFT in (B.31) are computed using the FFT algorithms via *Matlab*'s build in 'fft' commands. To avoid having problems computing the zero harmonic (due to terms in (B.31) containing $1/k$ coefficients) we simply alter the zero harmonic from precisely zero to something close to zero. Since the Ostrovsky equation satisfies zero mass, the Fourier coefficient at $k = 0$ is indeed zero, thus there will be no contribution from this term anyway. In doing this, one can still utilise the built in FFT algorithms.

B.5 Linearised Ostrovsky equations

B.5.1 Linearised Ostrovsky equation on zero background

First we consider the Cauchy problem for ϕ^+; a homogeneous linearised Ostrovsky equation, linearised on a zero background:

$$\begin{aligned}\left(\alpha_1\phi_T^+ + \lambda_1\phi^+_{\xi_+\xi_+\xi_+}\right)_{\xi_+} &= \gamma\phi^+,\\ \phi^+|_{T=0} &= -\frac{1}{2}\left[\int_{-L}^{\xi_+} f_T^-(s)ds\right]_{T=0}\end{aligned} \tag{B.32}$$

on the periodic domain $-L \leq x \leq L$. Taking the Fourier transform of (B.32a) yields

$$\hat{\phi}_T^+ = \frac{i}{\alpha_1}\left(\lambda_1 k^3 - \frac{\gamma}{k}\right)\hat{\phi}^+, \tag{B.33}$$

which given the initial condition, can be solved to yield the general solution

$$\hat{\phi}^+(k,T) = \hat{\phi}^+(k,0)e^{\frac{i}{\alpha_1}\left(\lambda_1 k^3 - \frac{\gamma}{k}\right)T}. \tag{B.34}$$

Taking the inverse Fourier transform yields the following general solution to the Cauchy problem (B.32):

$$\phi^+(\xi^+,T) = \mathscr{F}^{-1}\left\{\hat{\phi}^+(k,0)e^{\frac{i}{\alpha_1}\left(\lambda_1 k^3 - \frac{\gamma}{k}\right)T}\right\}. \tag{B.35}$$

Since the initial condition (B.32b) is given in terms of the solution of the leading order Cauchy problem for the Ostrovsky equation, which is solved numerically, we do not have it in an analytical form. We therefore find the initial condition by differentiating with respect to ξ^+ and taking the Fourier transform to yield

$$\hat{\phi}^+|_{T=0} = -\frac{i}{2k}\left[\hat{f}_T^-(k,T)\right]_{T=0}. \tag{B.36}$$

Substituting (B.28) into (B.36) yields the initial condition (B.32b), in the Fourier space, as follows:

$$\hat{\phi}^+(k,0) = -\frac{1}{2\alpha_0 k}\left[\left(\lambda_0 k^3 - \frac{\gamma}{k}\right)\hat{f}^-(k,0) - \frac{k\nu_0}{2\alpha_0}\mathscr{F}([f^-(k,0)]^2)\right].$$

The general solution (B.35) is now easily obtained from the initial conditions in this form. Alternatively one could reach the same result by numerically integrating the initial conditions.

B.5.2 Linearised Ostrovsky equation on non-zero background

Next we consider the Cauchy problem for the non-homogeneous linearised Ostrovsky equation for ϕ^- on a non-zero background; in this case, on the background of the solution of the leading order Ostrovsky equation f^-:

$$\left(\alpha_2\phi^-_T + \nu_2(f^-\phi^-)_{\xi_-} + \lambda_2\phi^-_{\xi_-\xi_-\xi_-}\right)_{\xi^-} = \gamma\phi^- + S(f^-,\xi^-,T),$$
$$\phi^-|_{T=0} = \frac{1}{2}\left[\int_{-L}^{\xi_-} f^-_T(s)ds\right]_{T=0}, \tag{B.37}$$

on the periodic domain $-L \le x \le L$, where the non-homogeneous forcing term is

$$S = f^-_{TT} + 2f^-_{T\xi^-\xi^-\xi^-}. \tag{B.38}$$

Taking the Fourier transform of (B.37a) yields

$$\hat{\phi}^-_T = \frac{i}{\alpha_2}\left(\lambda_2 k^3 - \frac{\gamma}{k}\right)\hat{\phi}^- - \frac{ik\nu_2}{\alpha_2}\widehat{f^-\phi^-} - \frac{i}{\alpha_2 k}\hat{S}. \tag{B.39}$$

Again, following the approach in [109] for removing the stiff-term, we multiply (B.39) by $\exp[-i/\alpha_2\left(\lambda_2 k^3 - \gamma/k\right)T]$ and introduce

$$\hat{\Phi}^-_T = e^{-\frac{i}{\alpha_2}(\lambda_2 k^3 - \frac{\gamma}{k})T}\hat{\phi}^-, \tag{B.40}$$

to yield (B.39) in the following form

$$\begin{aligned}\hat{\Phi}^-_T &= -\frac{ik\nu_2}{\alpha_2}e^{-\frac{i}{\alpha_2}(\lambda_2 k^3 - \frac{\gamma}{k})T}\mathscr{F}\left\{f^-\,\mathscr{F}^{-1}\left[e^{\frac{i}{\alpha_2}(\lambda_2 k^3 - \frac{\gamma}{k})}\hat{\Phi}^-\right]\right\}\\ &- \frac{i}{\alpha_2 k}e^{-\frac{i}{\alpha_2}(\lambda_2 k^3 - \frac{\gamma}{k})T}\hat{S}.\end{aligned} \tag{B.41}$$

We discretise $\hat{\Phi}^-(k,T_n) = \hat{\Phi}^-_n$ and $\hat{f}^-(k,T_n) = \hat{f}^-_n$ with $T = n\Delta T = T_n$ for $n = 0,1,2,...$, and implement the following optimised RK4 method:

$$\begin{aligned}\hat{\phi}^-_{n+1} &= E^2\hat{\phi}^-_n + \frac{1}{6}\left[E^2h_1 + 2E(h_2+h_3) + h_4\right],\\ \text{where}\quad h_1 &= -\frac{ik\nu_2\Delta T}{\alpha_2}\mathscr{F}\left\{f^-_n\,\mathscr{F}^{-1}\left[\hat{\phi}^-_n\right]\right\} - \frac{i\Delta T}{\alpha_2 k}\hat{S},\\ h_2 &= -\frac{ik\nu_2\Delta T}{\alpha_2}\mathscr{F}\left\{f^-_n\,\mathscr{F}^{-1}\left[E\left(\hat{\phi}^-_n + \frac{h_1}{2}\right)\right]\right\} - \frac{i\Delta T}{\alpha_2 k}\hat{S},\\ h_3 &= -\frac{ik\nu_2\Delta T}{\alpha_2}\mathscr{F}\left\{f^-_n\,\mathscr{F}^{-1}\left[E\hat{\phi}^-_n + \frac{h_2}{2}\right]\right\} - \frac{i\Delta T}{\alpha_2 k}\hat{S},\\ h_4 &= -\frac{ik\nu_2\Delta T}{\alpha_2}\mathscr{F}\left\{f^-_n\,\mathscr{F}^{-1}\left[E^2\hat{\phi}^-_n + Eh_3\right]\right\} - \frac{i\Delta T}{\alpha_2 k}\hat{S},\end{aligned} \tag{B.42}$$

for $E = \exp\left[i/2\alpha_2\left(\lambda_2 k^3 - \gamma/k\right)\Delta T\right]$, where again note we have returned to the original variable ϕ^-. In order to optimise computational storage we solve algorithms (B.31) and (B.42) simultaneously with the solution of the Ostrovsky Cauchy problem f^- feeding into (B.42) at each time step. To avoid any problems computing the FFT algorithms in (B.42), due to the $1/k$ terms, we alter the zero harmonic from precisely zero to something close to zero (this is previously discussed in Section B.4).

The non-homogeneous forcing term S, which involves derivatives of the solution of the Cauchy problem for the Ostrovsky equation f^-, must also be computed at each time step. Since we do not have an analytic expression for f^- we construct these terms from the governing equation for f^-; namely the Ostrovsky equation in the Fourier space written in the form (B.28). Thus we can write the term

$$\hat{f}^-_{T\xi^-\xi^-\xi^-} = \frac{k^2}{\alpha_0}\left[\left(\lambda_0 k^4 - \gamma\right)\hat{f}^- - \frac{k^2\nu_0}{2}\widehat{(f^-)^2}\right], \tag{B.43}$$

and similarly

$$\begin{aligned}\hat{f}^-_{TT} = {} & \frac{1}{\alpha_0^2}\left(\frac{\gamma}{k} - \lambda_0 k^3\right)\left[\left(\lambda_0 k^3 - \frac{\gamma}{k}\right)\hat{f}^- - \frac{\nu_0 k}{2}\widehat{(f^-)^2}\right] \\ & + \frac{i\nu_0 k}{\alpha_0^2}\mathscr{F}\left\{f^-\left[\gamma\,\mathscr{F}^{-1}\left(\frac{i}{k}\hat{f}^-\right) - \lambda_0\,\mathscr{F}^{-1}\left(ik^3\hat{f}^-\right) + \frac{\nu_0}{2}\mathscr{F}^{-1}\left(ik\widehat{(f^-)^2}\right)\right]\right\}.\end{aligned} \tag{B.44}$$

Finally to compute the initial condition (B.37b), we follow the same approach used to solve the linearised Ostrovsky problem, linearised on a zero background (see Section B.5.1). Thus we differentiate the initial condition with respect to ξ^- and take the Fourier transform to yield

$$\hat{\phi}^-|_{T=0} = \frac{i}{2k}\left[\hat{f}^-_T(k,T)\right]_{T=0}. \tag{B.45}$$

Substituting (B.28) into (B.45) yields the initial condition of $\hat{\phi}^-$ as:

$$\hat{\phi}^-(k,0) = \frac{1}{2\alpha_0 k}\left[\left(\lambda_0 k^3 - \frac{\gamma}{k}\right)\hat{f}^-(k,0) - \frac{k\nu_0}{2}\mathscr{F}([f^-(k,0)]^2])\right],$$

Finally, we note one potential drawback for the numerical scheme given here for ϕ^-. The term $\hat{f}_{TT}$, which appears within the forcing term $\hat{S}$, for nonzero γ and large enough L will become very large (see equation (B.44)). This is because we scale the spatial domain in all the spectral methods given in the appendices from $x \in [-L, L]$ to $x \in [0, 2\pi]$, which formally corresponds to k being multiplied by $s = \pi/L$. As a

result, the lowest order of k contains the highest order of L, in the case of (B.44) this is L^3. This stiff term will clearly cause the solution to become unbounded for significantly large enough L. To counteract this, significantly smaller time steps must be implemented.

B.6 Coupled regularised Boussinesq equations

We extend the pseudo spectral method used to solve the Cauchy problem for the Boussinesq–Ostrovsky equation in Section B.2 to now solve the Cauchy problem for the cRB equations:

$$\begin{aligned} U_{tt} - c_a^2 U_{xx} &= \epsilon\left[\frac{\alpha_a}{2}(U^2)_{xx} + \beta_a U_{ttxx} - \delta_a(U-V)\right], \\ V_{tt} - c_b^2 V_{xx} &= \epsilon\left[\frac{\alpha_b}{2}(V^2)_{xx} + \beta_b V_{ttxx} + \delta_b(U-V)\right], \\ U|_{t=0} &= F_1(x), \qquad V|_{t=0} = F_2(x), \\ U_t|_{t=0} &= F_3(x), \qquad V_t|_{t=0} = F_4(x). \end{aligned} \tag{B.46}$$

The methodology of the scheme developed in Section B.2 was extended from the work in [36], used to solve a single regularised Boussinesq equation in the context of microstructured solids.

Introducing

$$W^1 = U - \epsilon\beta_a U_{xx}, \qquad W^2 = V - \epsilon\beta_b V_{xx}, \tag{B.47}$$

we can write (B.46b) and (B.46c) in the form

$$\begin{aligned} W^1_{tt} &= c_a^2 U_{xx} + \epsilon\left[\frac{\alpha_a}{2}(U^2)_{xx} - \delta_a(U-V)\right], \\ W^2_{tt} &= c_b^2 V_{xx} + \epsilon\left[\frac{\alpha_b}{2}(V^2)_{xx} + \delta_b(U-V)\right]. \end{aligned} \tag{B.48}$$

Taking the Fourier transforms of (B.47) yields

$$\hat{W}^1 = (1+\epsilon\beta_a k^2)\hat{U}, \qquad \hat{W}^2 = (1+\epsilon\beta_b k^2)\hat{V}, \tag{B.49}$$

where k is the Fourier transform variable, and equivalently we have

$$\hat{U} = \frac{\hat{W}^1}{(1+\epsilon\beta_a k^2)}, \qquad \hat{V} = \frac{\hat{W}^2}{(1+\epsilon\beta_b k^2)}. \tag{B.50}$$

Taking the Fourier transforms of (B.48) and substituting (B.50) into the resulting ODEs, yields the following ODEs for $\hat{W}^{1,2}$:

$$\begin{aligned}\hat{W}^1_{tt} &= -\frac{(\epsilon\delta_a + k^2c_a^2)}{(1+\epsilon k^2\beta_a)}\hat{W}^1 - \frac{\epsilon k^2\alpha_a}{2}\,\mathscr{F}\left\{\mathscr{F}^{-1}\left[\frac{\hat{W}^1}{(1+\epsilon k^2\beta_a)}\right]^2\right\} + \frac{\epsilon\delta_a}{(1+\epsilon k^2\beta_b)}\hat{W}^2 \\ &= \hat{H}^1(\hat{W}^1), \end{aligned} \tag{B.51}$$

$$\begin{aligned}\hat{W}^2_{tt} &= -\frac{(\epsilon\delta_b + k^2c_b^2)}{(1+\epsilon k^2\beta_b)}\hat{W}^2 - \frac{\epsilon k^2\alpha_b}{2}\,\mathscr{F}\left\{\mathscr{F}^{-1}\left[\frac{\hat{W}^2}{(1+\epsilon k^2\beta_b)}\right]^2\right\} + \frac{\epsilon\delta_b}{(1+\epsilon k^2\beta_a)}\hat{W}^1 \\ &= \hat{H}^2(\hat{W}^2). \end{aligned} \tag{B.52}$$

We solve the second order ODEs (B.51) and (B.52) by reducing each of them to two first order ODE's and subsequently implementing a RK4 method on each of the four ODEs, simultaneously at each time step. Therefore we define

$$\begin{aligned}\hat{W}^1_t &= \hat{G}^1, & \hat{W}^2_t &= \hat{G}^2, \\ \hat{G}^2_t &= \hat{H}^2(\hat{W}^1,\hat{W}^2), & \hat{G}^2_t &= \hat{H}^2(\hat{W}^1,\hat{W}^2), \end{aligned} \tag{B.53}$$

and discretise $t = n\Delta t = t_n$, $\hat{W}^{1,2}(k,t_n) = \hat{W}^{1,2}_n$, $\hat{G}(k,t_n) = \hat{G}^{1,2}_n$ for $n = 0,1,2,...,$ where k now denotes the discrete Fourier space. Noting the initial conditions $\hat{W}^{1,2}_0$ and $\hat{G}^{1,2}_0$ are given by (B.46b,c), we implement the following RK4 method:

$$\begin{aligned}\hat{W}^1_{n+1} &= \hat{W}^1_n + \frac{1}{6}\left[k_1 + 2(k_2+k_3) + k_4\right], & \hat{G}^1_{n+1} &= \hat{G}^1_n + \frac{1}{6}\left[l_1 + 2(l_2+l_3) + l_4\right], \\ \hat{W}^2_{n+1} &= \hat{W}^2_n + \frac{1}{6}\left[m_1 + 2(m_2+m_3) + m_4\right], & \hat{G}^1_{n+1} &= \hat{G}^2_n + \frac{1}{6}\left[n_1 + 2(n_2+n_3) + n_4\right], \end{aligned}$$

$$
\begin{aligned}
\text{where} \quad k_1 &= \Delta t \hat{G}_n^1, & l_1 &= \Delta t \hat{H}^1(\hat{W}_n^1, \hat{W}_n^2), \\
m_1 &= \Delta t \hat{G}_n^2, & n_1 &= \Delta t \hat{H}^2(\hat{W}_n^1, \hat{W}_n^2), \\
\\
k_2 &= \Delta t(\hat{G}_n^1 + l_1/2), & l_2 &= \Delta t \hat{H}^1(\hat{W}_n^1 + k_1/2, \hat{W}_n^2 + m_1/2), \\
m_2 &= \Delta t(\hat{G}_n^2 + n_1/2), & n_2 &= \Delta t \hat{H}^2(\hat{W}_n^1 + k_1/2, \hat{W}_n^2 + m_1/2), \\
\\
k_3 &= \Delta t(\hat{G}_n^1 + l_2/2), & l_3 &= \Delta t \hat{H}^1(\hat{W}_n^1 + k_2/2, \hat{W}_n^2 + m_2/2), \\
m_3 &= \Delta t(\hat{G}_n^2 + n_2/2), & n_3 &= \Delta t \hat{H}^2(\hat{W}_n^1 + k_2/2, \hat{W}_n^2 + m_2/2), \\
\\
k_4 &= \Delta t(\hat{G}_n^1 + l_3), & l_4 &= \Delta t \hat{H}^1(\hat{W}_n^1 + k_3, \hat{W}_n^2 + m_3), \\
m_4 &= \Delta t(\hat{G}_n^2 + n_3), & n_4 &= \Delta t \hat{H}^2(\hat{W}_n^1 + k_3, \hat{W}_n^2 + m_3). \qquad \text{(B.54)}
\end{aligned}
$$

Once (B.54) is solved up to a given time, we substitute the solutions $\hat{W}^{1,2}$ back into (B.50), which after implementing the inverse fast Fourier transform, yields U and V in the original physical space.

Appendix C

Miscellaneous equations

As stated in Section 6.3.2.2, equation (6.63) can be expressed fully as

$$
\begin{aligned}
\phi_5^{ps} = \frac{\cos(m\tau)}{m(m^2+M^2)} \Bigg\{ & -3\int_0^\tau S^2 \sin(ms)\Big[m^2F_3\cos(ms) + m^2F_4\sin(ms) \\
& - M^2F_1(e^{Ms}+e^{-Ms})\Big]ds + \int_0^\tau L_{5b}(s)\sin(ms)ds \\
& + \frac{3m}{(m^2+M^2)}\int_0^\tau S^2\sin(ms)\cos(ms)\left[\int_0^s L_3(y)\sin(my)dy\right]ds \\
& - \frac{3m}{(m^2+M^2)}\int_0^\tau S^2\sin^2(ms)\left[\int_0^s L_3(y)\cos(my)dy\right]ds \\
& - \frac{3M}{2(m^2+M^2)}\int_0^\tau S^2\sin(ms)e^{Ms}\left[\int_0^s L_3(y)e^{-My}dy\right]ds \\
& + \frac{3M}{2(m^2+M^2)}\int_0^\tau S^2\sin(ms)e^{-Ms}\left[\int_0^s L_3(y)e^{My}dy\right]ds\Bigg\} \\
-\frac{\sin(m\tau)}{m(m^2+M^2)} \Bigg\{ & -3\int_0^\tau S^2 \cos(ms)\Big[m^2F_3\cos(ms) + m^2F_4\sin(ms) \\
& - M^2F_1(e^{Ms}+e^{-Ms})\Big]ds + \int_0^\tau L_{5b}(s)\cos(ms)ds \\
& + \frac{3m}{(m^2+M^2)}\int_0^\tau S^2\cos^2(ms)\left[\int_0^s L_3(y)\sin(my)dy\right]ds \\
& - \frac{3m}{(m^2+M^2)}\int_0^\tau S^2\cos(ms)\sin(ms)\left[\int_0^s L_3(y)\cos(my)dy\right]ds \\
& - \frac{3M}{2(m^2+M^2)}\int_0^\tau S^2\cos(ms)e^{Ms}\left[\int_0^s L_3(y)e^{-My}dy\right]ds \\
& + \frac{3M}{2(m^2+M^2)}\int_0^\tau S^2\cos(ms)e^{-Ms}\left[\int_0^s L_3(y)e^{My}dy\right]ds\Bigg\}
\end{aligned}
$$

$$
\begin{aligned}
+\frac{e^{M\tau}}{2M(m^2+M^2)}\Bigg\{ & -3\int_0^\tau S^2 e^{-Ms}\Big[m^2F_3\cos(ms)+m^2F_4\sin(ms) \\
& - M^2F_1(e^{Ms}+e^{-Ms})\Big]ds+\int_0^\tau L_{5b}(s)e^{-Ms}ds \\
& + \frac{3m}{(m^2+M^2)}\int_0^\tau S^2e^{-Ms}\cos(ms)\left[\int_0^s L_3(y)\sin(my)dy\right]ds \\
& - \frac{3m}{(m^2+M^2)}\int_0^\tau S^2e^{-Ms}\sin(ms)\left[\int_0^s L_3(y)\cos(my)dy\right]ds \\
& - \frac{3M}{2(m^2+M^2)}\int_0^\tau S^2\left[\int_0^s L_3(y)e^{-My}dy\right]ds \\
& + \frac{3M}{2(m^2+M^2)}\int_0^\tau S^2e^{-2Ms}\left[\int_0^s L_3(y)e^{My}dy\right]ds\Bigg\} \\
-\frac{e^{-M\tau}}{2M(m^2+M^2)}\Bigg\{ & -3\int_0^\tau S^2 e^{Ms}\Big[m^2F_3\cos(ms)+m^2F_4\sin(ms)ds \\
& - M^2F_1(e^{Ms}+e^{-Ms})\Big]+\int_0^\tau L_{5b}(s)e^{Ms}ds \\
& + \frac{3m}{(m^2+M^2)}\int_0^\tau S^2e^{Ms}\cos(ms)\left[\int_0^s L_3(y)\sin(my)dy\right]ds \\
& - \frac{3m}{(m^2+M^2)}\int_0^\tau S^2e^{Ms}\sin(ms)\left[\int_0^s L_3(y)\cos(my)dy\right]ds \\
& - \frac{3M}{2(m^2+M^2)}\int_0^\tau S^2e^{2Ms}\left[\int_0^s L_3(y)e^{-My}dy\right]ds \\
& + \frac{3M}{2(m^2+M^2)}\int_0^\tau S^2\left[\int_0^s L_3(y)e^{My}dy\right]ds\Bigg\}, \qquad \text{(C.1)}
\end{aligned}
$$

where we denote $S=\operatorname{sech}(\hat{\varepsilon}s/2)$.

Bibliography

[1] ABLOWITZ, M.J. (2011) *Nonlinear Dispersive Waves: Asymptotic Analysis and Solitons*. Cambridge University Press, New York.

[2] ABLOWITZ, M.J., KAUP, D.J., NEWELL, A.C. & SEGUR, H. (1974) Inverse scattering transform - Fourier analysis for nonlinear problems. *Stud. Appl. Math.*, **53**, 249-315.

[3] ABLOWITZ, M.J. & SEGUR, H. (1981) *Solitons and the Inverse Scattering Transform*. SIAM Philadelphia.

[4] ABLOWITZ, M.J. & WANG, X.-P. (1997) Initial time layers and Kadomtsev-Petviashvili-type equations. *Stud. Appl. Math.*, **98**, 121-137.

[5] ALIAS, A., GRIMSHAW, R.H.J. & KHUSNUTDINOVA, K.R. (2013) On strongly interacting internal waves in a rotating ocean and coupled Ostrovsky equations. *Chaos*, **23**, 023121.

[6] AMES, W.F. (1979) *Numerical Methods for Partial Differential Equations*. Academic Press, Inc, Thomas Nelson and Sons Ltd.

[7] ASKAR, A. (1985) *Lattice dynamical foundations of continuum theories*. World Scientific, Singapore.

[8] BEN YOUSSEF, W. & COLIN, T. (2000) Rigorous derivation of Korteweg-de Vries-type systems from a general class of nonlinear hyperbolic systems. *M2AN Math. Model. Numer. Anal.*, **34**, 873-911.

[9] BENILOV, E.S., GRIMSHAW, R. & KUZNETSOVA, E.P. (1993) The generation of radiating waves in a singularly perturbed Korteweg-de Vries equation. *Phys. D*, **69**, 270-278.

[10] BENJAMIN, T.B., BONA, J.L. & MAHONY, J.J. (1972) Model equations for long waves in nonlinear dispersive systems. *Philos. Trans. R. Soc. Lond. A*, **272**, 47-48.

[11] BONA, J.L., CHEN, M. & SAUT, J.-C. (2002) Boussinesq equations and other systems for small-amplitude long waves in nonlinear dispersive media. I: Derivation and linear theory. *J. Nonlinear Sci.*, **12**, 283-318.

[12] BONA, J.L., CHEN, M. & SAUT, J.-C. (2004) Boussinesq equations and other systems for small-amplitude long waves in nonlinear dispersive media. II: The nonlinear theory. *Nonlinearity*, **17**, 925-952.

[13] BONA, J.L., COLIN, T. & LANNES, D. (2005) Long wave approximations for water waves. *Arch. Rational Mech. Anal.*, **178**, 373-410.

[14] BONA, J.L., DOUGALIS, V.A. & MITSOTAKIS, D.E. (2008) Numerical solution of Boussinesq systems of KdV-KdV type: II. Evolution of radiating solitary waves. *Nonlinearity*, **21**, 2825-2848.

[15] BOUSSINESQ, J.V. (1872) Théorie des ondes et des remous qui se propagent le long d'un canal rectangulaire horizontal, en communiquant au liquide contenu dans ce canal des vitesses sensiblement pareilles de la surface au fond. *J. Math. Pures Appl., ser. (2)*, **17**, 55-108.

[16] BOUSSINESQ, J.V. (1877) Essai sur la théorie des eaux courantes. Mémoires présentés par divers savants á l'Académie des Sciences, Inst. NAT. France, **XXIII**, 1-660.

[17] BOYD, J.P. (1998) *Weakly Nonlinear Solitary Waves and Beyond-All-Orders Asymptotics*. Kluwer, Boston.

[18] BRATOS, A.G. (2009) A predictor-corrector scheme for the improved Boussinesq equation. *Chaos, Solitons and Fractals*, **40**, 2083-2094.

[19] BRAUN, O.M. & KIVSHAR, Y.S. (2004) *The Frenkel-Kontorova model. Concepts, methods, and applications*. Springer, Berlin.

[20] BRILLOUIN, L. (1953) *Wave propagation in periodic structures*. Dover, Toronto and London.

[21] CHAMPNEYS, A.R., MALOMED, B.A., YANG, J. & KAUP, D.J. (2001) Embedded solitons: solitary waves in resonance with the linear spectrum. *Phys. D*, **152-153**, 340-354.

[22] CHRISTOU, M.A. & CHRISTOV, C.I. (2005) Interacting localized waves for the regularized long wave equation via a Galerkin spectral method. *Math. Comp. Sim.*, **69**, 257-268.

[23] CHRISTOV, C.I., MARINOV, T.T. & MARINOVA, R.S. (2009) Identification of solitary-wave solutions as an inverse problem: Application to shapes with oscillatory tails. *Math. Comp. Sim.*, **80**, 56-65.

[24] CHRISTOV, C.I. & MAUGIN, G.A. (1995) An implicit difference scheme for the long-time evolution of localized solutions of a generalized Boussinesq system. *J. Comp. Phys.*, **116**, 39-51.

[25] CHRISTOV, C.I., MAUGIN, G.A. & VELARDE, M.G. (1996) Well-posed Boussinesq paradigm with purely spatial higher-order derivatives. *Phys. Rev. E*, **54**, 3621-3638.

[26] COOLEY, J.W. & TUKEY, J.W. (1965) An algorithm for the machine calculation of complex Fourier series. *Math. Comput.*, **19, 2**, 297-301.

[27] CRAIG, W. (1985) An existence theory for water waves and the Boussinesq and Korteweg–de Vries scaling limits. *Comm. Part. Diff. Eqs*, **10**, 787-1003.

[28] DRAZIN, P.G. (1992) *Nonlinear Systems*. Cambridge University Press, Bell and Bain Ltd.

[29] DRAZIN, P.G. & JOHNSON, R.S. (1989) *Solitons: an introduction*. Cambridge University Press, Cambridge.

[30] DREIDEN, G.V., KHUSNUTDINOVA, K.R., SAMSONOV, A.M. & SEMENOVA, I.V. (2010) Splitting induced generation of soliton trains in layered waveguides. *J. Appl. Phys.*, **107**, 034909.

[31] DREIDEN, G.V., KHUSNUTDINOVA, K.R., SAMSONOV, A.M. & SEMENOVA, I.V. (2012) Bulk strain solitary waves in bonded layered polymeric bars with delamination. *J.Appl. Phys.*, **112**, 063516.

[32] DREIDEN, G.V., OSTROVSKY, Y.I., SAMSONOV, A.M., SEMENOVA, I.V. & SOKURINSKAYA, E.V. (1988) Formation and propagation of strain solitons in nonlinearly elastic solids. *Sov. Phys.-Tech. Phys.*, **33**, 1237-1241.

[33] DREIDEN, G.V., SAMSONOV, A.M., SEMENOVA, I.V. & KHUSNUTDINOVA, K.R. (2011) Observation of a radiating bulk strain solitary wave in a solid waveguide. *Techn. Phys.*, **81**, 145-149.

[34] DURUK, N., ERBAY, H.A. & ERKIP, A. (2011) Blow-up and global existence for a general class of nonlocal nonlinear coupled wave equations. *J. Diff. Eqs.*, **250**, 1448-1459.

[35] ENGELBRECHT, J. (1981) *Nonlinear Wave Processes of Deformation in Solids.* Pitman, London.

[36] ENGELBRECHT, J., SALUPERE, A. & TAMM, K. (2011) Waves in microstructured solids and the Boussinesq paradigm. *Wave Motion*, **48**, 717-726.

[37] EL-ZOHEIRY, H. (2002) Numerical study of the improved Boussinesq equation. *Chaos, Solitons & Fractals*, **14**, 377-384.

[38] EL-ZOHEIRY, H. (2003) Numerical investigation for the solitary waves interaction of the "good" Boussinesq equation. *Appl. Numer. Math.*, **45**, 161-173.

[39] ERBAY, H.A. (2011) Private communication.

[40] FERMI, E., PASTA, J. & ULAM, S. (1955) Studies on nonlinear problems, I. *Los Alamos Scientific Laboratory Report No. LA-1940.*
NEWELL, A.C. (ed.) (1974) Nonlinear Wave Motion. *AMS Lect. Appl. Math.*, **15**, 143-156.

[41] FOCHESATO, C., DIAS, F. & GRIMSHAW, R. (2005) Generalized solitary waves and fronts in coupled Korteweg-de Vries systems. *Physica D*, **210**, 96-117.

[42] FOKAS, A.S. & PELLONI, B. (2005) Boundary value problems for Boussinesq type systems. *Math. Phys. Anal. Geom.*, **8**, 59-96.

[43] FRITZ, J. (1982) *Partial Differential Equations*. Fourth edition. Applied Mathematical Sciences; 1. Springer-Verlag, New York Inc.

[44] GARDNER, C.S., GREENE, J.M., KRUSKAL, M.D. & MIURA, R.M. (1967) Method for solving the Korteweg-de Vries equation. *Phys. Rev. Lett.*, **19**, 1095-1097.

[45] GEAR, J. & GRIMSHAW, R. (1984) Weak and strong interactions between internal solitary waves. *Stud. Appl. Math.*, **70**, 235-258.

[46] GERKEMA, T. (1996) A unified model for the generation and fission of internal tides in a rotating ocean. *J. Mar. Res.*, **54**, 421-450.

[47] GRIFFITHS, S.D., GRIMSHAW, R.H.J., & KHUSNUTDINOVA, K.R. (2006) Modulational instability of two pairs of counter-propagating waves and energy exchange in a two-component system. *Phys. D*, **214**, 1-24.

[48] GRIMSHAW R.H.J. (2007) *Solitary Waves in Fluids*. Ed., WIT Press, Southampton.

[49] GRIMSHAW, R.H.J., HE, J.-M. & OSTROVSKY, L.A. (1998) Terminal damping of a solitary wave due to radiation in rotational systems. *Stud. Appl. Math.*, **101**, 197-210.

[50] GRIMSHAW, R. & HELFRICH, K. (2008) Long-time solutions of the Ostrovsky Equation. *Stud. Appl. Math.*, **121**, 71-88.

[51] GRIMSHAW, R. & IOOSS, G. (2003) Solitary waves of a coupled Korteweg-de Vries system. *Math. Comp. Sim.*, **62**, 31-40.

[52] GRIMSHAW, R. & JOSHI, N. (1995) Weakly nonlocal solitary waves in a singularly perturbed Korteweg-de Vries equation. *SIAM J. Appl. Math.*, **55**, 124-135.

[53] GRIMSHAW, R. & MELVILLE, W.K. (1989) On the derivation of the modified Kadomtsev- Petviashvili equation. *Stud. Appl. Math.*, **80**, 183-202.

[54] HAJJI, M.A. & AL-KHALED, K. (2007) Analytic studies and numerical simulations of the generalized Boussinesq equation. *Appl. Math. and Comp.*, **191**, 320-333.

[55] HEIDEMAN, M.T., JOHNSON, D.H. & BURRUS, C.S. (1985) Gauss and the history of the Fast Fourier Transform. *Arch. Hist. Exact Sci.*, **34**, 265-277.

[56] HELFRICH, K.R. (2007) Decay and return of internal solitary waves with rotation. *Phys. Fluids*, **19**, 026601.

[57] HIROTA, R. (1971) Exact solution of the Korteweg-de Vries equation for multiple collisions of solitons. *Phys. Rev. Lett.*, **27**, 1192-1194.

[58] HORIKIS, T.P. (2009) The short-pulse equation and associated constraints. *J. Phys. A: Math. Theor.*, 442004.

[59] IBRAGIMOV, N.H. (1994) *CRC Handbook of Lie group analysis of differential equations*. V. 1, Ed. CRC Press, Boca Raton.

[60] IL'YUSHINA, E.A. (1976) Towards formulation of elasticity theory of inhomogenious solids with microstructure. *PhD Thesis, Lomonosov Moscow State University*, (in Russian).

[61] IRK, D. & DAG, I. (2009) Numerical simulations of the improved Boussinesq equation. *Numer. Meth. for Partial Diff. Equations*, **26**, 1316-1327.

[62] JANNO, J. & ENGELBRECHT, J. (2005) Solitary waves in nonlinear microstructured materials. *J. Phys. A: Math. Gen.*, **38**, 5159-5172.

[63] JOHNSON, R.S. (1997) *A Modern Introduction to the Mathematical Theory of Water Waves*. Cambridge University Press, Cambridge.

[64] KALANTAROV, V.K. & LADYZHENSKAYA, O.A. (1978) The occurrence of collapse for quasilinear equations of parabolic and hyperbolic types. *J. Sov. Math.*, **10**, 53-70.

[65] KALYAKIN, L.A. (1989) Long-wave asymptotics. Integrable equations as the asymptotic limit of nonlinear systems. *Uspekhi Mat. Nauk*, **44**, 5-34.

[66] KANO, T. & NISHIDA, T. (1986) A mathematical justification for Korteweg-de Vries equation and Boussinesq equation of water surface waves. *Osaka J. Math.*, **23**, 389-413.

[67] KARPMAN, V.I. (1993) Radiation by solitons due to higher-order dispersion. *Phys. Rev. E*, **47**, 2073-2082.

[68] KAY, I. & MOSES, H.E. (1956) Reflectionless transmission through dielectrics and scattering potentials. *J. Appl. Phys.*, **27**, 1503-1508.

[69] KHUSNUTDINOVA, K.R. (1992) Nonlinear waves in a two-row system of particles. *Vestnik Moskov. Univ. Ser. I Mat. Mekh.*, **2**, 71 -76 (in Russian).

[70] KHUSNUTDINOVA, K.R. (1993) Wave dynamics of a medium constructed on the basis of a two-row system of particles. *"Deep refinement of hydrocarbon material", V. 2, Moscow: TsNIITEneftekhim*, 136-145 (in Russian).

[71] KHUSNUTDINOVA, K.R. (2007) Coupled Klein-Gordon equations and energy exchange in two-component systems. *Eur. Phys. J. - Special Topics*, **147**, 45-72.

[72] KHUSNUTDINOVA, K.R. & MOORE, K.R. (2011) Initial-value problem for coupled Boussinesq equations and a hierarchy of Ostrovsky equations. *Wave Motion*, **48**, 738-752.

[73] KHUSNUTDINOVA, K.R. & MOORE, K.R. (2012) Weakly non-linear extension of d'Alembert's formula. *IMA J. Appl. Math.*, **77**, 361-381.

[74] KHUSNUTDINOVA, K.R., MOORE, K.R. & PELINOVSKY, D.E. (2013) Validity of the weakly-nonlinear solution of the Cauchy problem for the Boussinesq–type equation. To appear in *Stud. Appl. Math.*.

[75] KHUSNUTDINOVA, K.R. & SAMSONOV, A.M. (2008) Fission of a longitudinal strain solitary wave in a delaminated bar. *Phys. Rev. E*, **77**, 066603.

[76] KHUSNUTDINOVA, K.R., SAMSONOV, A.M. & ZAKHAROV, A.S. (2009) Nonlinear layered lattice model and generalized solitary waves in layered elastic structures. *Phys. Rev. E*, **79**, 056606.

[77] KONTOROVA, T.A. & FRENKEL, Y.I. (1938) On the theory of plastic deformation and twinning, I, II. *Zh. Eksp. Teor. Fiz.*, **8**, 89-95, 1340-1348.

[78] KORTEWEG, D.J. & DE VRIES, G. (1895) On the change of form of long waves advancing in a rectangular canal, and on a new type of long stationary waves. *Philos. Mag. (5)*, **39**, 422-443.

[79] KRAENKEL, R., LEBLOND, H. & MANNA, M.A. (2011) An integrable evolution equation for surface waves in deep water. *arXiv: 1101.5773v1 [nlin.SI].*

[80] LANNES, D. (2005) Well-Posedness of the Water Waves Equations. *J. Am. Math. Soc.*, **18**, 605-654.

[81] LAX, P.D. (1968) Integrals of nonlinear equations of evolution and solitary waves. *Comm. Pure Appl. Math.*, **21**, 467-490.

[82] LEONOV, A.I. (1981) The effect of the earth's rotation on the propagation of weak nonlinear surface and internal long oceanic waves. *Ann. NY Acad. Sci.*, **373**, 150-159.

[83] LOMBARDI, E. (2000) *Oscillatory Integrals and Phenomena Beyond all Algebraic Orders*. Lecture Notes in Mathematics 1741, Springer, Berlin.

[84] MARTIN, P.A. (1990) Thin interface layers: adhesives, approximations and analysis. *In: Elastic waves and ultrasonic nondestructive evaluation, North-Holland, Amsterdam*, 217-222.

[85] MAUGIN, G.A. (1999) *Nonlinear Waves in Elastic Crystals*. Oxford University Press, Oxford.

[86] MILES, J.W. (1977) Obliquely interacting solitary waves. *J. Fluid Mech.*, **79**, 157-169.

[87] MILES, J.W. (1977) Resonantly interacting solitary waves. *J. Fluid Mech.* **79**, 171-179.

[88] MIYATAKE, Y., YAGUCHI, T. & MATSUO, T. (2012) Numerical integration of the Ostrovsky equation based on its geometric structures. *J. Comput. Appl. Math.*, **231**, 4542-4559.

[89] MOHSEN, A., EL-ZOHEIRY, H. & ISKANDAR, L. (1993) A highly accurate finite-difference scheme for a Boussinesq-type equation. *Appl. Math. and Comp.*, **55**, 201-212.

[90] NARIBOLI, G.A. & SEDOV, A. (1970) Burgers - KdV equation for viscoelastic rods and plates. *J. Math. Anal. Appl.*, **32** , 661-677.

[91] NEWELL, A.C. (1985) *Solitons in Mathematics and Physics*. SIAM, Philadelphia.

[92] OBREGON, M. & STEPANYANTS, Y. (2012) On numerical solution of the Gardner - Ostrovsky equation. *Math. Model. Nat. Phenom.*, **7**, 113-130.

[93] ORTEGA, T. & SANZ-SERNA, J.M. (1990) Nonlinear stability and convergence of the finite-difference methods for the "good" Boussinesq equation. *Numer. Math.*, **58**, 215-229.

[94] OSTROVSKY, L.A. (1978) Nonlinear internal waves in a rotating ocean. *Oceanology*, **18**, 119-125.

[95] OSTROVSKY, L.A. & SUTIN, A.M. (1977) Nonlinear elastic waves in rods. *Appl. Math. Mech.*, **41**, 543-549.

[96] PORUBOV, A.V. (2003) *Amplification of Nonlinear Strain Waves in Solids*. World Scientific, Singapore.

[97] PORUBOV, A.V. & SAMSONOV, A.M. (1993) Refinement of longitudinal strain wave propagation in non-linearly elastic rod. *Sov. Technic. Phys. Lett.*, **19**, 365-366.

[98] RAYLEIGH, Lord J.W.S. (1876) On waves. *Phil. Mag.*, **1**, 257-279.

[99] RUSSELL, J.S. (1844) Report on Waves: *Report of the fourteenth meeting of the British Association for the Advancement of Science*, London, 311-390.

[100] SACHS R.L. (1983) Completeness of derivatives of squared Schrödinger eigenfunctions and explicit solutions of the linearized KdV equation. *SIAM J. Math. Anal.*, **14-4**, 674-683.

[101] SAMSONOV, A.M. (1984) Soliton evolution in a rod with variable cross section. *Sov. Phys. Dokl.*, **29**, 586-588.

[102] SAMSONOV, A. M. (2001) *Strain Solitons in Solids and How to Construct Them.* Chapman and Hall/CRC, Boca Raton.

[103] SCHNEIDER, G. (1998) The long wave limit for a Boussinesq equation. *SIAM J. Appl. Math.*, **58**, 1237-1245.

[104] SCHNEIDER, G. & WAYNE, C.E. (2000) The long-wave limit for the water wave problem. I. The case of zero surface tension. *Comm. Pure Appl. Math.*, **53**, 1475-1535.

[105] SHERMAN, J. & MORRISON, W.J. (1950) Adjustment of an inverse matrix corresponding to a change in one element of a given matrix. *Ann. Math. Statist.*, **21**, (1), 124-127.

[106] SOERENSEN, M.P., CHRISTIANSEN, P.L. & LOMDAHL, P.S. (1984) Solitary waves on nonlinear elastic rods.I. *J. Acoust. Soc. Am.*, **76**, 871-879.

[107] TAKENO, S., DMITRIEV, S.V., KEVREKIDIS, P.G. & BISHOP, A.R. (2005) Nonlinear lattices generated from harmonic lattices with geometric constraints. *Phys. Rev. B*, **71**, 014304.

[108] TODA, M. (1967) Vibration of a chain with nonlinear interaction. *J. Phys. Soc. Japan*, **22**, 431-436.

[109] TREFETHEN, L.N. (2000) *Spectral Methods in MATLAB.* SIAM, Philadelphia, PA 19104-2688.

[110] TZITZEICA, M. (1910) Sur une nouvelle classe de surfaces. *Comptes Rendus hebd. Seances l'Acad. Sciences Paris*, **150**, 955, 1227.

[111] VAKHNENKO, V.O. & PARKES, E.J. (1998) The two loop soliton solution of the Vakhnenko equation. *Nonlinearity*, **11**, 1457-1464.

[112] VANDEN-BROECK, J.-M. (1991) Elevation solitary waves with surface tension. *Phys. Fluids*, **A3**, 2659-2663.

[113] VORONOVICH, V.V., SAZONOV, I.A. & SHRIRA, V.I. (2006) On radiating solitons in a model of the internal wave-shear flow resonance. *J. Fluid Mech.*, **568**, 273-301.

[114] WAYNE, C.E. & WRIGHT, J.D. (2002) Higher order modulation equations for a Boussinesq equation. *SIAM J. Appl. Dyn. Syst.*, **1**, 271-302.

[115] WHITHAM, G.B. (1974) *Linear and Nonlinear Waves*. Wiley, New York.

[116] YAGI, D. & KAWAHARA, T. (2001) Strongly nonlinear envelope soliton in a lattice model for periodic structure. *Wave Motion*, **34**, 97-107.

[117] YAGUCHI, T., MATSUO, T. & SUGIHARA, M. (2010) Conservative numerical schemes for the Ostrovsky equation. *J. Comput. Appl. Math.*, **234**, 1036-1048.

[118] YANG, J. (2003) Stable Embedded Solitons. *Phys. Rev. Lett.*, **91**, 143903.

[119] ZABUSKY, N.J. & KRUSKAL, M.D. (1965) Interaction of solitons in a collisionless plasma and the recurrence of initial states. *Phys. Rev. Lett.*, **15**, 240-243.

[120] ZAKHAROV, V.E. (1974) On stochastisation of one-dimensional chains of nonlinear oscillators. *Sov. Phys. JETP*, **38**, 108-110.

[121] ZAKHAROV, V.E. & SHABAT, A.B. (1972) Exact theory of two-dimensional self-focusing and one-dimensional self-modulation of waves in a non-linear media, *Sov. Phys. JETP*, **34**, 62-69.